

Design of Viscous and Friction Damper Systems for the Optimal Control of the Seismic Response of Structures

by

DAVID JOHN ALBERT DOWDELL
B.A.Sc., University of Waterloo, 1985
M.A.Sc., University of Waterloo, 1987

A THESIS SUBMITTED IN PARTIAL FULFILMENT OF
THE REQUIREMENTS FOR THE DEGREE OF
DOCTOR OF PHILOSOPHY

In

THE FACULTY OF GRADUATE STUDIES

(CIVIL ENGINEERING)

THE UNIVERSITY OF BRITISH COLUMBIA

May, 2005

© David J.A. Dowdell, 2005

Abstract

The objective of this study was to propose methods for the optimal design of viscous or friction/hysteretic dampers in structures subjected to seismic and other dynamic loads. The systems investigated to control the dynamic response of the structure included passive linear viscous dampers, constant slip force friction dampers, and semi-active variable slip force friction dampers of the Off-On type. This work was primarily concerned with sizing of the viscous damper damping coefficients or the friction damper slip loads of the dampers at pre-selected locations within the structure. The dampers were considered to act in series with a flexible brace, as brace flexibility is an undesirable and often unavoidable characteristic. Two primary methodologies for the design were developed; one for the design of dampers in single degree of freedom (SDOF) structures using the transfer function concept, and one for the design of dampers in general multi degree of freedom (MDOF) structures based on linear quadratic control theory.

It was found that the transfer function based technique proposed for the selection of optimal friction damper slip loads in SDOF structures provided insight into their design. While it was found that SDOF method could be extended to deal with MDOF structures, this process is limited to structures for which the distribution of dampers is known and calibrated to the SDOF design. As a basis for comparison, optimal friction damper slip loads and their distributions in a uniform 4-story structure were studied using an optimization procedure known as level set programming (LSP).

The more general design method proposed based on structural control utilised the peak cycle control force and response quantities to estimate the optimal viscous damper damping coefficients approximating that of the fully active control. Then, considering the amount of energy dissipated in this peak cycle, estimates of the corresponding friction damper slip loads were obtained. Response spectral analysis (RSA) procedures, derived in state-space form, were used to incorporate the effects of earthquake excitation, while permitting the rapid evaluation of estimates of the peak cycle response quantities of non-classically damped structures. Reasonable agreement was obtained between the two methods.

Three examples were provided to demonstrate the control theory based design method for MDOF structures; a uniform 4-story shear structure, a 2-D regular steel moment frame and an 18DOF, 3-D eccentric building structure.

Table of Contents

Abstract	ii
Table of Contents	iv
List of Tables	xi
List of Figures	xii
Preface	xix
Acknowledgements	xxii
Chapter 1: Structural Design and Retrofit – Research Objectives and Methods1	
1.1 Objectives	1
1.2 SDOF and MDOF Structures	2
1.3 Dynamic Loading Characteristics	4
1.4 Seismic Design and Retrofit.....	6
1.5 Structural Control	7
1.5.1 Classical Control Theory and Modern Structural Control Theory	7
1.5.2 Passive Structural Control	8
1.5.2.1 Tuned Mass Dampers	9
1.5.2.2 Friction Dampers	9
1.5.2.3 Hysteretic Dampers.....	13
1.5.2.4 Viscous and Viscoelastic Dampers.....	13
1.5.3 Semi-Active Control	16
1.5.4 Hybrid Systems.....	18
1.6 General Discussion and Thesis Organization	18
Chapter 2: Control Theory Background	21
2.1 Modern vs. Classical Control Theory	21
2.2 Classical Control Algorithms.....	22
2.2.1 Minimum Time Problem – Bang-Bang Control	22
2.2.2 Minimum Fuel Problems	25
2.3 State Space Formulation of the Equations of Motion	26
2.4 Optimal Linear Quadratic (LQ) Regulator: Active Control.....	28
2.5 System Response	32
2.6 Observer Design.....	33

2.7	Direct Output Feedback Control	35
2.8	Sub-Optimal Control	35
2.9	Semi-Active Systems	36
2.10	Passive Structural Control.....	37
2.11	Conclusion.....	37
Chapter 3: Analysis and Design of Dampers in SDOF Structures		39
3.1	Linear and Non-Linear Analysis	41
3.2	Analysis of Linear SDOF Structures.....	41
3.2.1	Response Spectrum Analysis.....	41
3.2.2	Frequency Domain Analysis: Fourier Transforms	43
3.2.2.1	Fourier Transform and Random Vibrations.....	44
3.2.2.2	The Dynamic Amplification Function (DAF)	45
3.2.2.3	The Inverse Fourier Transform.....	45
3.2.2.4	RMS Response of a Random Process.....	45
3.2.2.5	Band Limited Gaussian White Noise.....	46
3.2.2.6	Fourier Transform and Earthquakes	46
3.2.2.7	The Fast Fourier Transform.....	47
3.2.2.8	RMS Estimate from FFT	47
3.2.2.9	RMS of a White Noise	47
3.2.2.10	Energy Concepts	47
3.3	Nonlinear SDOF System Analysis.....	48
3.3.1	Modelling Friction/Hysteretic Damped Structures.....	48
3.3.2	Bilinear Hysteresis	49
3.3.3	Modelling One-Step Memory in State-Space.....	51
3.3.4	Variable Slip Force Semi-Active Friction Damper	53
3.3.5	Off-On Friction Damper	54
3.3.6	Phase Plane Analysis of Off-On and CSFD Damped Structures	55
3.4	Design of SDOF Viscous Damped Structures	60
3.4.1	The Ideal Viscous Damped Structure	60
3.4.1.1	Evaluation of RMS Response	63
3.5	Design of SDOF Friction Damped Structures.....	64
3.5.1	Sinusoidal Input	65
3.5.2	Frequency Response for Equivalent Viscous Damping	65
3.5.2.1	Theoretical Derivation	66
3.5.2.2	Results.....	68

3.5.2.3	Optimal Slip Load Prediction	74
3.5.3	Fourier Transform of Time Histories	75
3.5.3.1	Frequency Domain Analysis Procedure	76
3.5.3.2	White Noise Input Slip Load Optimization	83
3.6	Semi-Active Off-On Friction Dampers	83
3.7	General Discussion	85
Chapter 4:	Extension of SDOF procedures to MDOF Structures	90
4.1	Dynamic Properties of MDOF Structures	91
4.2	Level Set Programming	95
4.2.1	General Description	95
4.2.2	Chosen Objective Functions	96
4.2.3	General Results	97
4.3	Suggested Distribution of CSFD Slip Loads	99
4.4	Prediction of MDOF Slip Loads using the Transfer Function Method	100
4.5	Need for a General Procedure for MDOF Structures	102
Chapter 5:	A General Procedure for Design of Passive Dampers in MDOF Structures	104
5.1	Theoretical Derivation Including Observer	105
5.1.1	Modified Potter's Algorithm	108
5.1.2	The Gain Matrix	109
5.1.3	Deriving Passive Damping Coefficients from the Gain Matrix	110
5.1.3.1	Truncation	110
5.1.3.2	Response Spectrum Analysis	110
5.2	Response Spectrum Analysis Procedure	111
5.2.1	Modal Superposition	113
5.2.2	SRSS Modal Combination	115
5.3	Worked Example: Uniform 4 Story Structure	116
5.3.1	Solution	117
5.4	Extension to Friction Dampers	124
5.4.1	Rigid Brace	124
5.4.2	Flexible Brace	125
5.5	Summary of the Proposed RSA Procedure	126
5.6	Discussion	128

Chapter 6:	Example Application of the General Procedure for Design of Passive Viscous and Friction Damped Structures	130
6.1	Example 1: 4-Story Frame Structure.....	132
6.1.1	Control Objective.....	132
6.1.2	Step 1: Structure definition	133
6.1.3	Step 2: Select damper locations	135
6.1.4	Step 3: Choose weighting matrices; control strength	136
6.1.5	Step 4: Solve the control problem.....	136
6.1.6	Step 5: Estimate peak cycle RSA quantities.....	138
6.1.7	Step 6: Estimate peak cycle displacements, velocities and control forces using RSA	139
6.1.8	Step 7: Estimate SRSS damping coefficients	143
6.1.9	Step 8: Evaluate slip load.....	144
6.1.10	Viscous and Friction/Hysteretic Dampers for $R_{factor} = 0.06$	148
6.1.11	Friction Damper Analysis Results	149
6.2	Example 2: Burbank 6-Story Office Building.....	152
6.2.1	Consideration for Control Loss.....	152
6.2.2	Structural Modeling	153
6.2.2.1	Frequency Comparison	154
6.2.2.2	Structural Damping.....	155
6.2.3	LQ Gains, System Poles and Characteristic Damping	156
6.2.4	Computation of Passive Viscous Damping Coefficients	157
6.2.5	Comparison of Performance, Active vs Passive Viscous and Friction Dampers.....	164
6.2.5.1	Observations	164
6.2.5.2	Comparison of the Performance	165
6.3	Example 3: 18 DOF Eccentric Building Structure.....	177
6.3.1	Structural Modeling	179
6.3.1.1	Configuration 1	184
6.3.1.2	Configuration 2	185
6.3.1.3	Configuration 3	185
6.3.2	Formulation of the Control Problem: Observer Matrices.....	185
6.3.3	Results Configuration 1	187
6.3.3.1	Control Design	187
6.3.3.2	Configuration 1 Damper Stiffness and Friction Damper Slip Loads	191

6.3.4	Results Configuration 2	198
6.3.4.1	Control Design	198
6.3.5	Results - Configuration 3	202
6.3.6	Notes on Modal Combinations	202
6.4	General Discussion.....	206
6.4.1	4-Story Structure.....	207
6.4.2	Burbank 6-Story Structure	208
6.4.3	18-DOF Eccentric Building Structure	209
Chapter 7:	Summary, Conclusions and Recommendations	210
7.1	Summary	210
7.1.1	General	210
7.1.2	SDOF Structures	210
7.1.3	MDOF Structures.....	212
7.2	Conclusions	214
7.2.1	General	214
7.2.2	SDOF structures.....	215
7.2.3	MDOF structures	215
7.3	Recommendations	217
7.3.1	SDOF Structures	217
7.3.1.1	Steady State vs. Transient Response.....	217
7.3.1.2	RMS vs. Peak Response	217
7.3.1.3	Hysteretic vs. Friction Damping.....	217
7.3.2	MDOF Structures.....	218
7.3.2.1	Input Spectra for State-Space RSA.....	218
7.3.2.2	Investigation of Alternative Modal Combination Procedures	218
7.3.2.3	Investigation of Alternative Control Algorithms.....	219
7.3.2.4	Investigate Optimal Design of Viscous Dampers with Flexible Brace	219
7.4	Thesis Contributions	219
7.4.1	SDOF structures.....	219
7.4.2	MDOF structures	220
References	221

Appendix A: Solution of the Ricatti Matrix	230
Appendix A: Solution of the Ricatti Matrix	231
A.1 The Time Variant vs. the Time Invariant Ricatti Matrix	231
A.2 Linearized Solution of the Ricatti matrix	232
A.3 Potter's Algorithm	234
A.4 Example Solution of the Time Invariant Ricatti Matrix	236
A.4.1 Solution	239
A.4.1.1 Reverse Integration	239
A.4.1.2 Potters Algorithm	241
A.5 Significance of the Results	243
Appendix B: Performance Index Study	245
Appendix B: Performance Index Study	246
B.1 Control Structure	246
B.2 Findings	248
B.3 Conclusions	249
Appendix C: 3-D Earthquake Response Spectra	252
Appendix C: 3-D Response Spectra	253
C.1 Background	253
C.2 General Observations	254
C.3 Conclusions and Recommendations	255
Appendix D: MathCad Worksheet: Transfer Functions of a Uniform 4-Story Structure	267
Appendix E: Band Limited White Noise.....	277
Appendix E: Band Limited Gaussian White Noise.....	278
E.1 White Noise	278
E.2 Alternate Band Limited White Noise Procedure	280
Appendix F: Level Set Programming and Optimal Slip Load Distribution in MDOF Structures	281
Appendix F: Level Set Programming and Optimal Slip Load Distribution in MDOF Structures.....	282
F.1 Level Set Programming	282
F.1.1 Objective Functions, Level Sets and Scatter Plots	282
F.2 Problem Formulation	284

F.2.1	Coordinate Transformations	285
F.2.2	Objective Functions	287
F.2.3	Excitation	288
F.2.4	Modeling Considerations	289
F.2.5	Sample LSP Analysis.....	291
F.2.5.1	Example Using El Centro Input – Min RMS Drift.....	291
F.2.6	LSP Results.....	296
F.2.6.1	Impulse.....	296
F.2.6.2	Whote Noise.....	299
F.2.6.3	Earthquake	303
F.2.7	Note on Off-On Damped Structures	306
F.2.8	General Observations and Implication to Designers	309

List of Tables

Table 6.1.	Uniform 4-story structure undamped response frequencies	134
Table 6.2.	Comparison of response of 4DOF structure to varying levels of control strength.	146
Table 6.3.	Burbank 6-Story Office Building. Comparison of ADINA and MATLAB model obtained frequencies with those obtained by Bakhtavar (2000)	154
Table 6.4.	Comparison of system poles and associated modal damping with “weak” and “strong” control.....	159
Table 6.5.	Detailed evaluation of damping coefficients based on peak cycle energy	162
Table 6.6.	Detailed evaluation of friction damper slip loads based on peak cycle energy	163
Table 6.7.	Comparison of control performance – “weak” control.....	175
Table 6.8.	Comparison of control performance – “Strong” control.	176
Table 6.9.	18DOF structure story mass and stiffness parameters: Imperial units	179
Table 6.10.	18DOF structure modal analysis results.	181
Table 6.11.	Damper configuration 1, comparison of response obtained with various levels of control	188
Table 6.12.	Configuration 1 comparison of friction damper design considering brace flexibility.	196
Table 6.13.	Configuration 2 comparison of controlled and uncontrolled response with Rfactor=0.000015.	201
Table 6.14.	Configuration 2 comparison of friction damper design considering brace flexibility.....	201
Table 6.15.	Configuration 2 comparison of controlled and uncontrolled response with Rfactor=0.000015.	203
Table 6.16.	Configuration 3 comparison of friction damper design considering brace flexibility.	203
Table 6.17.	Comparison of envelope state vector computed using a reduced number of modes.	206
Table C.1:	Selected Earthquakes for Evaluation of 3-D State-Space Response Spectra	257
Table F.1.	Comparison of the performance of the Off-On friction damper controlled structure.	307

List of Figures

Figure 1.1. Single degree of freedom structures with viscous and friction damping elements.	3
Figure 1.2. Four degree of freedom semi-active friction damped structure.	4
Figure 1.3. Comparison of selected dynamic loadings in terms of duration and frequency content.	5
Figure 1.4. Pall friction device and Sumitomo friction device shown with associated hysteresis loops.	11
Figure 1.5. Cross-Section of friction pendulum device from Zayas and Low (1989).	12
Figure 1.6. Examples of hysteretic devices.	14
Figure 1.7. Typical hysteretic behaviour of a steel component.	15
Figure 1.8. Best fit of curvilinear stress-strain function using bilinear hysteresis.	15
Figure 1.9. Examples of viscoelastic devices.	16
Figure 1.10. Semi-active viscous damper (SAVD) From Patten et al (1994a).	17
Figure 1.11. Variable friction slip force friction damper, from Feng (1993).	17
Figure 1.12. Hybrid passive and active systems – example from Yang et al (1991).	18
Figure 2.1. Phase plane trajectory of the response of a SDOF structure.	24
Figure 2.2. Bang-bang control phase plane trajectories.	24
Figure 2.3. Bang-off-bang control example.	26
Figure 2.4. Block Diagram of state space equation of motion (Equation 2.3).	27
Figure 2.5. Block Diagram of an observer of a dynamic system.	34
Figure 3.1. Comparison of SDOF structures analyzed.	40
Figure 3.2. Displacement transfer function for structure with ideal viscous damper.	43
Figure 3.3. PSD function for band limited white noise.	46
Figure 3.4. Bilinear hysteresis.	50

Figure 3.5. Decision tree for analysing bilinear hysteretic system in state-space.	52
Figure 3.6. Decision tree for evaluating slip load in a variable slip force friction damper.	54
Figure 3.7. Comparison of time history traces and hysteresis loops produced by (a) friction damper; (b) Off-on friction damper, and (c) variable slip force friction damper (SAFD).	56
Figure 3.8. Models for the sliding and non-sliding phases of response of a bilinear hysteretic damper.	57
Figure 3.9. Phase plane plot of a structure excited by an impulse with a weak control.	59
Figure 3.10. Phase plane plot of a structure excited by an impulse with a strong control.	59
Figure 3.11. Family of transfer functions for viscous damped structure with flexible brace.	62
Figure 3.12. Normalized RMS displacement for viscous damped structure with flexible brace.	63
Figure 3.13. Steady state frequency response function friction damped structure $\alpha=0.5$	69
Figure 3.14. Steady state frequency response function friction damped structure $\alpha=1.0$	69
Figure 3.15. Steady state frequency response function friction damped structure $\alpha=2.0$	70
Figure 3.16. Steady state frequency response function friction damped structure $\alpha=3.0$	71
Figure 3.17. Steady state frequency response function friction damped structure $\alpha=5.0$	71
Figure 3.18. Comparison of steady state displacements amplitudes of a fiction damped structure obtained from simulation data – sinusoidal input.	72
Figure 3.19. Steady state base shear data obtained from numerical simulation sinusoidal input.	73
Figure 3.20. Prediction of optimal slip load based on steady-state transfer function.	75
Figure 3.21. Transfer function derived from friction damped structure response to white-noise, $\alpha=0.5$	77

Figure 3.22. Transfer function derived from friction damped structure response to white-noise, $\alpha=1.0$.	77
Figure 3.23. Transfer function derived from friction damped structure response to white-noise, $\alpha=2.0$.	78
Figure 3.24. Transfer function derived from friction damped structure response to white-noise, $\alpha=3.0$.	79
Figure 3.25. Transfer function derived from friction damped structure response to white-noise, $\alpha=5.0$.	79
Figure 3.26. Smoothed white-noise response transfer function, $\alpha=0.5$.	80
Figure 3.27. Smoothed white-noise response transfer function, $\alpha=1.0$.	80
Figure 3.28. Smoothed white-noise response transfer function, $\alpha=2.0$.	81
Figure 3.29. Smoothed white-noise response transfer function, $\alpha=3.0$.	82
Figure 3.30. Smoothed white-noise response transfer function, $\alpha=5.0$.	82
Figure 3.31. Prediction of optimal slip load – white noise input, $\alpha=2$.	83
Figure 3.32. Raw data transfer function – Off-On semi-active friction damped structure, $\alpha=2.0$.	84
Figure 3.33. Smoothed transfer function – Off-On semi-active friction damped structure, $\alpha=2.0$.	85
Figure 3.34. Comparison of peak and RMS drift vs. slip load	87
Figure 3.35. Comparison of RMS drift and dissipated energy vs. slip load	89
Figure 4.1. 4-Story regular moment frame structure.	92
Figure 4.2. (a). Gain and phase of transfer function of displacement response of 4-story structure	93
(b). Gain and phase of transfer function of displacement response of SDOF system representing 4-story structure.	94
Figure 4.3. LSP optimal slip load comparison – earthquake input – min energy, min drift, $\alpha=1$.	97
Figure 4.4. LSP optimal slip load comparison – earthquake input – min energy, min drift, $\alpha=2$.	98
Figure 4.5. LSP optimal slip load comparison – earthquake input – min energy, min drift, $\alpha=3$.	98

Figure 4.6. LSP optimal slip load comparison – earthquake input – min energy, min drift, $\alpha=5$	99
Figure 4.7. Normalized RMS drift vs slip load ratio, γ , El Centro and San Fernando input records.	101
Figure 4.8. Transfer function based predicted slip loads for El Centro and San Fernando earthquake record input.	101
Figure 4.9. Comparison of Power Spectral Density functions for the two input time histories.	103
Figure 5.1. Assumed peak cycle hysteresis loops.	126
Figure 6.1. Comparison of displacements and velocities for an active, and passively damped 4DOF structure.	145
Figure 6.2. Comparison of slip load distributions obtained using LSP and the proposed control method with El Centro record input.	151
Figure 6.3. Comparison of slip load distributions obtained using LSP and the proposed control procedure with San Fernando record input.	151
Figure 6.4. Uncontrolled Burbank 6-story office building perimeter frame (imperial and metric units).	152
Figure 6.5. Rayleigh damping assumed for Burbank 6-story office building.	155
Figure 6.6. Pole locations, weak and strong control.	158
Figure 6.7. Implementation of control using diagonal braces in the perimeter frame.	159
Figure 6.8. Distribution of viscous dampers – weak control.	161
Figure 6.9. Distribution of viscous dampers – strong control.	161
Figure 6.10. Undamped and controlled displacement response data obtained for the Burbank 6-story office building for the “weak” control having $R_{factor}=0.006$	167
Figure 6.11. Undamped and “weak” controlled response data obtained for the Burbank 6-story office building.	168
Figure 6.12. Undamped and “strong” controlled displacement response data obtained for the Burbank 6-story office building.	171
Figure 6.13. Undamped and “strong” controlled velocity response data obtained for the Burbank 6-story office building.	173

Figure 6.14. 3D eccentric structure and extraction of 18DOF model.	177
Figure 6.15. Damper Configuration 1 (23 dampers).	183
Figure 6.16. Damper Configuration 2 (3 dampers).	183
Figure 6.17. Damper Configuration 3 (17 dampers).	184
Figure 6.18. Comparison of Pole Locations – 4 different control strengths.	192
Figure 6.19. Configuration 1 viscous damping coefficients in kip-sec/ft corresponding to Rfactor = 0.00005.	193
Figure 6.20. Configuration 1 ideal Friction damper slip loads in kips for Rfactor=0.00005.	194
Figure 6.21. Variation of slip force with brace stiffness.	195
Figure 6.22. Configuration 2 viscous damping coefficients in kip-sec/ft for Rfactor = 0.000015.	199
Figure 6.23. Configuration 2 – friction damping slip loads in kips for Rfactor=0.000015.	200
Figure 6.24. Configuration 3 viscous damping coefficients in kip-sec/ft for Rfactor = 0.00005.	204
Figure 6.25. Configuration 3 – friction damping slip loads in kips for Rfactor=0.00005.	205
Figure A.1. 2DOF structure used to illustrate the solution of the time varying Ricatti matrix.	232
Figure A.2. Computation of the Ricatti matrix by backward integration.	233
Figure A.3. 4-Story regular moment frame structure.	237
Figure A.4. Evolution of Ricatti matrix main diagonal terms under backward integration.	240
Figure B.1. Three artificial time histories used to simulate control response.	250
Figure B.2. Values of performance index obtained for (1) Full state feedback; (2) Observer feedback, and (3) Truncated observer feedback.	251
Figure C.1. El Centro N00E.....	258

Figure C.2. San Fernando N21E.....	259
Figure C.3. Hachinohe Harbour NS record.....	260
Figure C.4. UCSC Los Gatos Presentation Center record.....	261
Figure C.5. Ofunato Bochi N41E record.....	262
Figure C.6. Taft 21.....	263
Figure C.7. Sylmar 00.....	264
Figure C.8. Olympia Seattle Army Base record 182.....	265
Figure C.9. Relationship of traditional response spectra basis to the 3-D pole based spectra basis.....	266
Figure E.1. Segment of random time history.....	279
Figure E.2. Probability density function and smoothed randomly generated PDF.....	279
Figure E.3. Error in cumulative probability distribution.....	280
Figure F.1. 4-Story regular moment frame structure.....	285
Figure F.2. Earthquake input time histories with identified strong motion duration.....	290
Figure F.3. Comparison of Power Spectral Density functions for the two input time histories. “El Centro” and “San Fernando”.....	291
Figure F.4. LSP Initial Distribution Scatter Plot – El Centro record, Objective Function: max RMS(d _i). Initial search space:.....	293
Figure F.5. LSP Iteration 6 – note that the search space is beginning to be reduced substantially.....	293
Figure F.6. LSP Iteration 8.....	294
Figure F.7. LSP Iteration 13.....	294
Figure F.8. Convergence – LSP Iteration 17.....	295
Figure F.9. Optimization progress to iteration 17:.....	295
Figure F.10. LSP optimal slip load – Impulse input – minimum total energy, $\alpha=1$	297
Figure F.11. LSP optimal slip load – Impulse input – minimum total energy, $\alpha=2$	297

Figure F.12. LSP optimal slip load – Impulse input – minimum total energy, $\alpha=3$	298
Figure F.13. LSP optimal slip load – Impulse input – minimum total energy, $\alpha=5$	298
Figure F.14. LSP optimal slip load – impulse input – minimum total energy, comparison of all α	299
Figure F.15. LSP optimal slip load – white noise input – minimum energy, minimum RMS drift, $\alpha = 1$	300
Figure F.16. LSP optimal slip load – white noise input – minimum energy, minimum RMS drift, $\alpha = 2$	301
Figure F.17. LSP optimal slip load – white noise input – minimum energy, minimum RMS drift, $\alpha = 3$	301
Figure F.18. LSP optimal slip load – white noise input – minimum energy, minimum RMS drift, $\alpha = 5$	302
Figure F.19. LSP optimal slip load – white noise input – minimum energy – compare all α	302
Figure F.20. LSP optimal slip load – white noise input – minimum RMS drift – compare all α	303
Figure F.21. LSP optimal slip load comparison – earthquake input – min energy, min drift, $\alpha=1$	304
Figure F.22. LSP optimal slip load comparison – earthquake input – min energy, min drift, $\alpha=2$	305
Figure F.23. LSP optimal slip load comparison – earthquake input – min energy, min drift, $\alpha=3$	305
Figure F.24. LSP optimal slip load comparison – earthquake input – min energy, min drift, $\alpha=5$	306
Figure F.25. LSP Scatter plot $\alpha=1$, minimum total energy, El Centro record input.	308
Figure F.26. Comparison of CSFD minimum level set with 8 iterations Off-On level set, $\alpha=1$	309

Preface

Design and Retrofit

Many structures are at risk of being subjected to large environmental loads resulting from winds, earthquakes, floods, waves, landslides, impacts, etc. The aim of a structural engineer is to ensure that the performance of a structure under such loadings provides an acceptably low risk of failure. Adhering to standards in design and construction that are generally accepted in engineering practice and have been proven over time is usually satisfactory. However, as the reliance on performance based standards increase, more responsibility is placed on the engineer to show that the expected design or retrofit of a structure satisfies its performance objectives.

Loads that are dynamic in nature are challenging in that the dynamic characteristics of the structure play a significant role in determining how the structure will respond. More challenging still are non-linear structures for which the magnitude of the loading and its relationship with the non-linear phenomena affects the response of the structure.

Large earthquakes give rise to dynamic loads that often produce non-linear structural response. Extreme loads result as the earthquake acts to impose displacements on a structure. Adding strength alone is often insufficient to improve the performance of the structure as other properties such as ductility and energy dissipation (or absorption) become critical. To this end, high damping devices of a variety of types have been shown to be beneficial.

This thesis investigates the design of structures fitted with linear and non-linear high damping devices. The aim of this study is to find methods with which to optimally design damping systems. Whereas viscous damped structures are linear in nature, alternative energy absorbing systems such as friction/hysteretic dampers are generally not. The precise analysis of structures having non-linear response requires extensive time history analyses that are expensive and can often provide conflicting results, particularly in the case of earthquake analysis where the response is strongly dependant on the character of the chosen input records.

Often it is more desirable to use simplified or approximate analyses such as Response Spectral Analysis (RSA) that provide direct estimates of design quantities. These methods are strictly

linear in nature, and suffer from having to pre-determine the system damping. Borrowing from the theory of structural control, an alternative basis for the analysis of structures outfitted with semi-active and passive dampers is provided. In doing so, some of the shortcomings of RSA are overcome and typical analyses can be extended to structures with high damping and non-classical damping.

Structural control is a specialized field of structural engineering that has evolved over the last 30 years. Although it was originally envisioned that active control systems would be used to directly apply forces that improve the safety and stability of existing structures, for many reasons this has been found to be impractical. Active control systems require the use of sensors, central processing capability to determine the appropriate control response, the input of external energy and the operation of equipment that may or may not behave as intended during critical moments. Passive systems on the other hand need no sensors, do not require any energy input, are inert at times when not in use and therefore can provide a robust dependable control when needed. As will be shown in the course of this thesis, a high level of control can still be obtained with a properly designed passive system. The theoretical concepts of active control are quite powerful and can under certain conditions also be applied to passive structural systems to provide a basis for the optimal design of linear-viscous and non-linear friction and hysteretic dampers.

In Chapter 1, the design problem is introduced. Chapter 2 lays down the theoretical basis for the design of active control systems and sets out the mathematical tools necessary to analyse the dynamic response of a structure. Chapter 3 proposes the design of viscous and friction dampers in a SDOF structure by using a proposed transfer function technique.

Chapter 4 considers the extension of the SDOF analysis method of Chapter 3 to MDOF structures. An example of a 4-story structure in two different earthquake events is used as an example.

In Chapter 5, a method is derived for determining the optimal magnitudes of viscous dampers in a general structural system based on the linear quadratic (LQ) control problem. In order to introduce the effect of the earthquake excitation, a response spectral analysis procedure for non-classically damped structures was developed. With response quantities estimated using this technique, viscous damper damping coefficients approximating that of the LQ control are determined. Then, using the concept of equal peak-cycle energy dissipation, the corresponding

friction damper slip forces (or hysteretic damper yield loads) are estimated. The inclusion of damper brace flexibility is discussed, as it introduces a limitation in the energy that can be dissipated in friction and leads to an alternate concept of an optimally friction damped structure.

Chapter 6 provides three worked examples of the proposed MDOF control theory based damper design method. The first example is the 4-story structure used for the LSP analysis in Chapter 4. The next example considers a steel moment-frame structure extracted from an existing 6-story office building in California, and typical of many steel moment frame structures. In the final example, a 3-D eccentric structure is used to illustrate the capability of the proposed method in dealing with a 3-D structure having simultaneous loading in two directions, over and under specified damper sets and reduced number of modes used in the modal analysis.

Chapter 7 provides a summary and closure to the current study while recommending topics for further study.

Dedication

This thesis is dedicated to the memory of A.G. Dowdell 1929-1994.

Acknowledgement

I would like to acknowledge the patience and encouragement of Dr. C. E. Ventura, without which I could not have picked up and continued with the thread of earlier work. I would also like to acknowledge the contributions of the thesis committee, Dr. D.L. Anderson, Dr. S. Brzev Dr. S. Cherry and Dr. R.O. Foschi for their many helpful comments. And finally I would like to acknowledge Evelyn Dowdell for her help in the preparation of this document.

Chapter 1: Structural Design and Retrofit – Research Objectives and Methods

1.1 Objectives

This thesis is an examination of the optimal design of structures with passive viscous and friction damper systems in both single degree of freedom (SDOF) and multi-degree of freedom (MDOF) structures. The SDOF structures include semi-active friction dampers. While the aim of designing structures with dampers is to improve their performance in earthquakes and under other possible dynamic loads, a design process is required to ensure that the dampers provide the appropriate level of performance. The objective of this work is to develop methods for designing damper systems for structures through developing an understanding of the fundamental response characteristics of these structures. In considering MDOF structures, active control theory concepts are investigated as a basis for designing passive damper systems. While this work is primarily directed at the design of viscous and friction dampers, hysteretic dampers can be included insofar as they can be represented by friction dampers.

This work draws heavily on the concepts of structural control as the basis for design. As much of control theory relies on information extracted in the frequency domain, this thesis, too, attempts to utilise frequency domain characteristics and frequency domain based analysis procedures as a basis for the design of SDOF structures. By utilising such methods, this thesis provides an improved understanding of the response of a structure with dampers. With this improved understanding, the structural engineer is able to discern situations (load-structure combinations) where viscous or friction dampers would be useful, and conversely, those situations where dampers would be of limited value.

Using a connection established between modern active structural control theory and the design of passive damper systems, a new and potentially useful method is introduced that would enable structural engineers to proportion viscous and friction/hysteretic dampers at preselected locations in a general MDOF structural system. The MDOF work is based on the mathematics of modern, optimal control theory in which the state-space formulation of the system dynamics is utilised. With this alternate formulation, non-classical damping, and combined super-critical and sub-critical damping modes can be more easily incorporated into the solution. It is hoped that by

incorporating such analysis methods, it will help structural engineers to understand and accept structures with significantly higher damping.

The key objective of the MDOF work is to enable the structural engineer to directly determine the optimal damper sizes, given that the damper locations have been preselected. While methods do exist for selecting damper locations, the designer is ultimately responsible for determining the final damper configuration.

The proposed design methods are demonstrated using numerical examples intended to help the reader to fully understand the concepts. Directions for further work are recommended.

1.2 SDOF and MDOF Structures

Figure 1.1 illustrates the various configurations of single degree of freedom (SDOF) structures that are investigated in this thesis. Figure 1.1(a) illustrates a structure containing a passive viscous damper in a lateral bracing element. Figure 1.1(b) shows an extension to the description of the structure by the inclusion of a brace spring constant K . This spring constant may represent a combination of the flexibility of the brace and the flexibility attributed to the damper. Figures 1.1(c) – (e) illustrate variations on friction dampers. Figure 1.1(c) and (d) are passive friction dampers with and without consideration for the brace flexibility while (e) illustrates the semi-active friction damper where the slip load is varied as a function of the motion of the structure, presumably in such a way as to optimize its performance.

Brace elements connected in series with springs are included to represent unwanted flexibility in the brace and/or the damper that is impractical to avoid and detrimental to the ability of the damper to effectively control the structure.

Passive friction dampers are sometimes referred to in this thesis as CSFD – an acronym that stands for “constant slip force friction dampers.” Semi-active friction dampers of the continuously variable type are referred to using the acronym SAFD.

Figure 1.2 illustrates a configuration of a 4DOF friction damped structure corresponding to the control case illustrated in Figure 1.1(d).

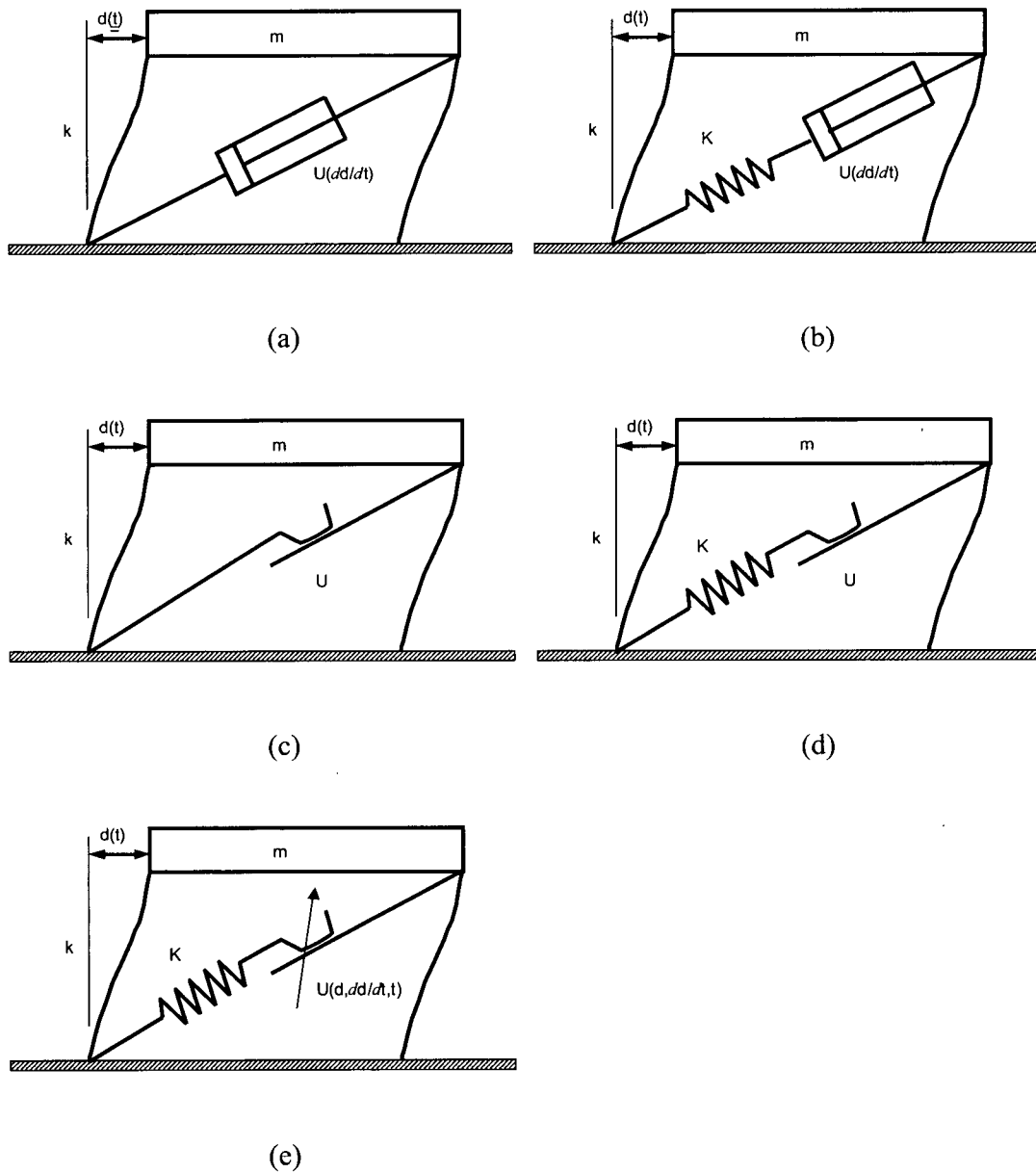


Figure 1.1. Single degree of freedom structures with viscous and friction damping elements. Each structure has mass m , stiffness k , with (a) ideal viscous damper; (b) viscous damper with spring stiffness K representing flexibility of the brace; (c) ideal friction damper; (d) constant slip force friction damper with flexible brace; (e) semi-active friction damper with arrow representing variable slip force.

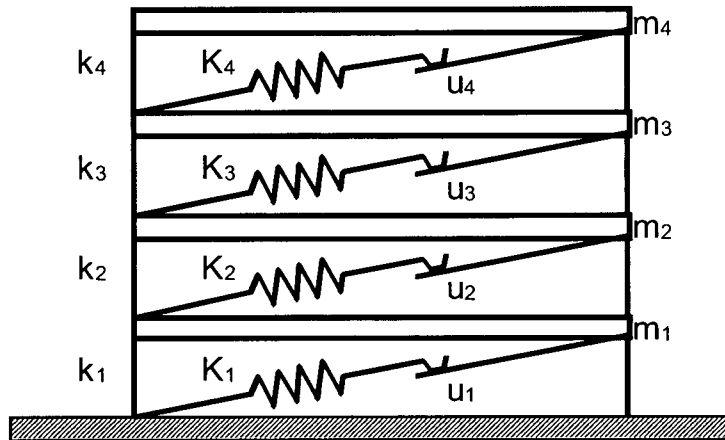


Figure 1.2. Four degree of freedom friction damped structure. Structure has masses designated with masses m_1 to m_4 , stiffness k_1 - k_4 , brace stiffness K_1 - K_4 and friction sliders with slip forces u_1 to u_4 representing the control components.

1.3 Dynamic Loading Characteristics

Although the work contained within this thesis is primarily concerned with seismic loads, other dynamic loads such as wind, traffic, impact, blast or reciprocating equipment can often govern the design of structural members. Developing an understanding of the loading conditions for which a structure is to be designed and also developing an understanding of which loads are critical for each member is a vital prerequisite to carrying out the design of either a new structure or the retrofit of an existing structure.

Dynamic loads provide a particular challenge in design. A load is considered “dynamic” when the response cannot be adequately characterized by a static loading. This is the case when the inertial forces of the structure contribute significantly to the total force experienced by members in the structure. Slowly varying live loads or constant accelerations do not excite vibrations of a structure. Therefore, these would not be considered as dynamic loads.

Dynamic loads can be characterized in part by the following measures:

- Intensity (magnitude of maximum force or displacement)
- Duration (number of cycles)
- Frequency content (narrow-band: harmonic) (wide band: white noise)

Intensity describes the magnitude of the forces applied to the structure; duration, the length of time or number of cycles of the load. Frequency content is an important description of cyclic loading. The presence of a single input frequency (narrow band) or a multitude of frequencies over a wide range (wide band) could be indicated by a power spectral density curve with either a concentration or a wide dispersion of frequencies included as part of the input signal. In Figure 1.3, the above-mentioned loads are compared graphically in terms of duration and frequency content by location on a 2-dimensional plane.

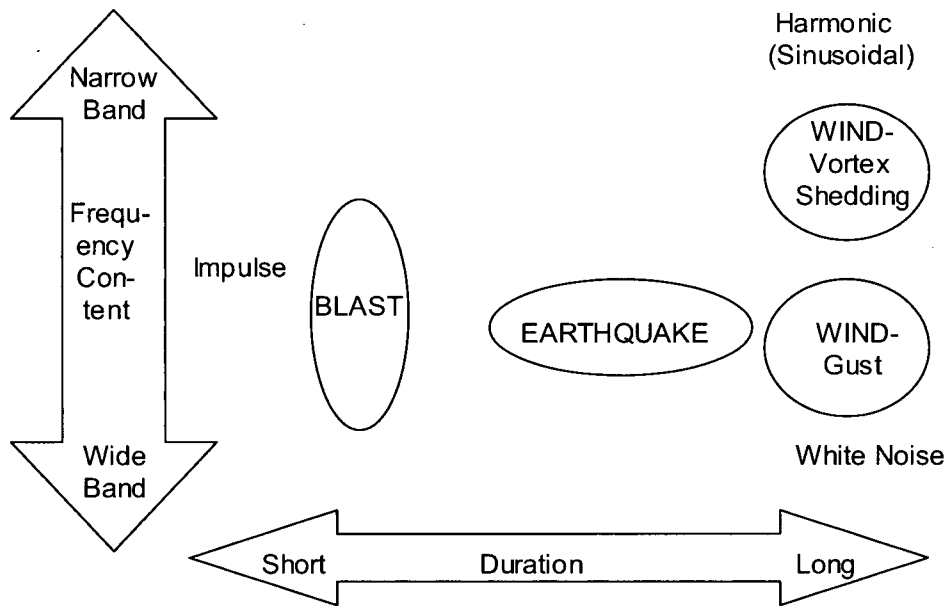


Figure 1.3. Comparison of selected dynamic loadings in terms of duration and frequency content.

Wind loading may produce intense loads on a particular structure, depending on its shape and exposure. Depending on the frequency content of interactions with the structure, the wind may be capable of inducing a large dynamic response. The Tacoma Narrows Bridge is an example of a structure that failed at a wind speed significantly less than the design wind due to the fact that the frequency of vortex shedding corresponded to one of the structures modes (see Scott (1991)). In Figure 1.3, the characteristic wind loading is plotted with narrow band frequency content and long duration. A wind load on a high-rise building structure may last several hours and may produce sinusoidal pressure variations at the characteristic frequency of vortex shedding, proportional to the wind speed, and the dimensions of the structure.

An earthquake on the other hand may last only a few seconds, contain energy over a broad range of frequencies ranging from 0.2-50Hz and contain one or more large pulses. In Figure 1.3, the earthquake character is plotted with a moderate to high frequency, moderate duration and moderate to wide band frequency content.

A blast loading would have a wide band frequency content but a very short duration loading. Reciprocating equipment, on the other hand, may apply a long duration dynamic loading load within an extremely narrow band of input frequencies.

1.4 Seismic Design and Retrofit

In order to design a structure it is necessary to adhere to a performance standard or satisfy other performance requirements. Without such performance requirements, it is not possible to determine if the design is satisfactory or if efforts to improve safety are well placed. Structural performance includes both safety and serviceability criteria, which can be expressed in terms of force and deflection limits. Excellent guidance for the design of building structures can be found in the recommended provisions for FEMA 368 (Building Seismic Safety Council, 2000).

Seismic loads are problematic in design. Often strengthening alone is insufficient to improve the performance of the structure. In typical bridge and building structures, additional stiffness will often attract proportionally higher earthquake loads to critical members, often negating retrofit efforts. Consequently, it is difficult to design a structure, or retrofit an existing structure for earthquake loads, such that it meets both strength and serviceability criteria.

Yielding of the structure itself provides an effective force limiting mechanism, and the inelastic deformation absorbs energy through hysteresis. Such non-linear response is beneficial to the seismic performance. The cost, however, is that portions of the structure may experience damage that leads to the need to repair or even abandon the structure post-earthquake even if the structure performs as required during the earthquake.

Generally, structures that lack inherent damping experience larger demands than would otherwise be the case if a higher level of damping were present. Lightly damped structures are susceptible to resonance, or quazi-resonance, in which deformations continue to grow until the structure reaches its elastic limit and the input energy can be dissipated. These lightly damped structures can benefit from the introduction of elements that provide additional energy dissipation. Viscous dampers, hysteretic and friction damping devices are currently available

that can be used for this purpose. Damping and isolation systems have been used successfully in many structures to modify the dynamic properties of the structure and produce a system that is better able to accommodate earthquake loadings. The displacement reduction provided by the introduction of such devices lessens the demand on the primary structure, reducing or preventing damage that would otherwise occur.

It is important to recognise that the design task may require many iterations before all requirements are met. Because the effect of dynamic loading strongly depends on the dynamic properties of the structure, it is necessary for the engineer to understand these properties. Dynamic properties arise from the interaction of elements within the structural system as a whole. Consequently, computer modelling is used extensively in the analysis and design of more complex structures. The use of commercial software can greatly increase the speed, accuracy and completeness of analysis. However, design capabilities can be limited if the design software does not have sufficient capability to accurately describe the structure and its dynamic characteristics. The concepts presented in this thesis are developed with the intention of being incorporated into computer algorithms.

1.5 Structural Control

Structural control is a field of study that emerged in the 1970's. The concepts upon which structural control is based are taken from electrical and systems engineering. Initially, structural control was the study of structures as systems affixed with devices and instruments that allow the structure to sense its own deformations and/or environmental loads and then invoke a favourable response for improving its performance. Through the 80's and 90's, structural control evolved from theory to the point where practical applications of controlled structures began to appear. Since its inception, however, the concept of structural control has broadened to include a wide variety of systems ranging from active to passive for the improvement of structural performance.

1.5.1 Classical Control Theory and Modern Structural Control Theory

Classical control theory is most commonly associated with mechanical and electrical engineering. With the study of control, the engineer seeks to understand a system's dynamics and stability, and hence be able to design systems that have desirable dynamic characteristics and remain stable. A classical example of this would be the speed governor of a steam engine. A desirable control system would bring the engine to the required speed in a short time period and

hold the engine speed constant against changes in demand. An undesirable control system would be slow to reach speed; overshoot the required speed and allow the speed to fluctuate wildly when demands change.

The classical methods consider only one variable at a time; and with MDOF systems, design becomes more of an art than a science. Modern control theory, however, allows for the design and optimization of multivariable systems.

Structures are systems for which the control concept is applicable. Our basic desire with a structure is that once it is in position, it remain in position despite the variation in demands induced by external excitations such as wind, blast, earthquake or internal occupancy.

Modern structural control theory, sometimes called “optimal” structural control, is so named because it combines design of a control system with an optimization principle. The mathematical framework derived for this purpose is of primary interest in this thesis as it combines the notions of the dynamic properties of the structure with the design of a system for which the response is optimal.

The theory underlying much of the structural control work in this thesis is contained in texts by Soong (1989) and Meirovitch (1990). These books provide a connection between the traditional approach to structural dynamics and modern control theory but concentrate on theoretical, rather than practical aspects. Chapter 2 contains a more detailed description of those structural control concepts relevant to the work contained in this thesis.

1.5.2 Passive Structural Control

Passive control systems continue to be viewed as more practical and reliable than active systems. The reliance of purely active systems on external power, the precise functioning of sophisticated equipment and the fact that for seismic loads much of this equipment would need to stay dormant for many years before being called upon does not seem practical. Passive systems, on the other hand do not require sophisticated sensing equipment, or external power. Some of the systems considered include

- base isolation
- tuned mass dampers
- friction dampers
- viscous dampers

- viscoelastic dampers
- hysteretic dampers

With the exception of base isolation and tuned mass dampers, the objective of these systems is to boost the damping level and thereby suppress the deformations in the primary structure. The objective of a base isolation system is to shift the period of the structure outside of the energetic frequency range of the earthquake thereby limiting the force transmitted to the primary structure; while a tuned mass damper is intended to change the frequency response and introduce damping at the fundamental mode frequency.

1.5.2.1 Tuned Mass Dampers

McNamara (1977) details the design procedure for the design of a tuned mass damper of the Citicorp Centre Building in New York. Utilising 2% of the buildings modal mass, the damping ratio was raised from about 1% of critical to about 4% of critical reducing by half the deflections expected in a windstorm.

Sun, Fujino and Koga (1995), and Modi (1995, 1998) have investigated the use of tuned mass dampers utilising the sloshing of liquid in a tank and capitalizing on the energy dissipation within the fluid.

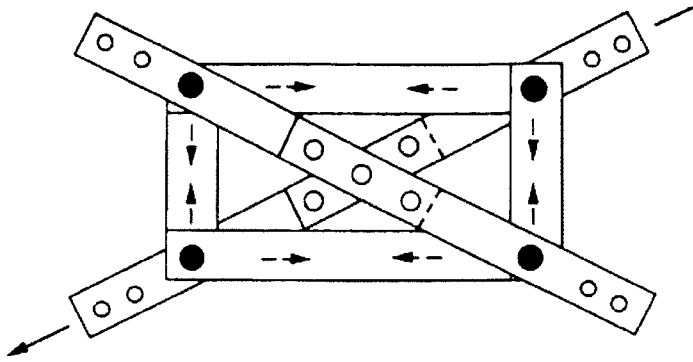
1.5.2.2 Friction Dampers

Friction dampers have been utilised as a practical and cost effective energy dissipation mechanism in many recently constructed structures. Several friction-damping devices are found in the literature. Figure 1.4 illustrates two of them; the Pall device developed by Pall and Marsh (1982) shown in (a), and a device developed by Sumitomo Metal Industries Ltd. of Japan shown in (b). Pall has been successful in implementing bolted devices in frames of buildings to provide energy dissipation capacity, as detailed in Pall (1987) and Pall (1993). Filiatrault and Cherry (1985, 1988) have investigated the performance of the Pall devices in braced frames. The Sumitomo friction damper was investigated by Teramoto (1988). Figure 1.4 shows the hysteresis loops produced by each device under reversed cyclic testing of the device alone. It is observed that the hysteresis loops are not rectangular. This is due to peculiarities in the way the device is constructed. Both devices are able to produce consistent and repeatable hysteresis loops over many dozens of cycles.

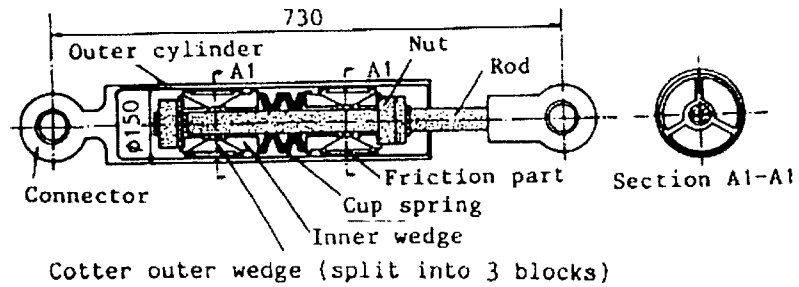
The Pall device was shown to experience a step in the brace force leading up to the full activation of the relatively uniform friction-sliding phase. This step relates to the tolerance in the construction of bearing connections. The Sumitomo device on the other hand experiences slightly higher resistance to sliding at the beginning of a stroke and a sideways hourglass shaped trace of the hysteresis loop. The hourglass shape of the hysteresis loop was found to be more pronounced at deformation rates producing higher temperatures indicating that the shape of the hysteresis loop is the result of a thermal effect in the damper itself. With those minor differences in mind, the resulting hysteresis loops show that both these devices are effective in dissipating energy.

It is well known that materials often have different static and dynamic friction coefficients. Teramoto observed the existence of slight peaks prior to the initiation of sliding. It is seen from the hysteresis loops that the difference between the static and dynamic friction in both the Pall device and the device studied by Teramoto was not significant, and the response of the device could be characterized to a sufficient degree using only the value of dynamic friction.

Friction bolted connections are the simplest and most inexpensive devices to construct, however, under high clamping force it has been found that the generated heat is concentrated in the material adjacent to the bolt hole. This heat build up may lead to stick slip behaviour and damage to the sliding surfaces. See Tremblay (1994).



(a) Pall friction damped X-brace element (from Filiatrault 1988)



(b) Sumitomo friction damper. (from Teramoto, 1991)

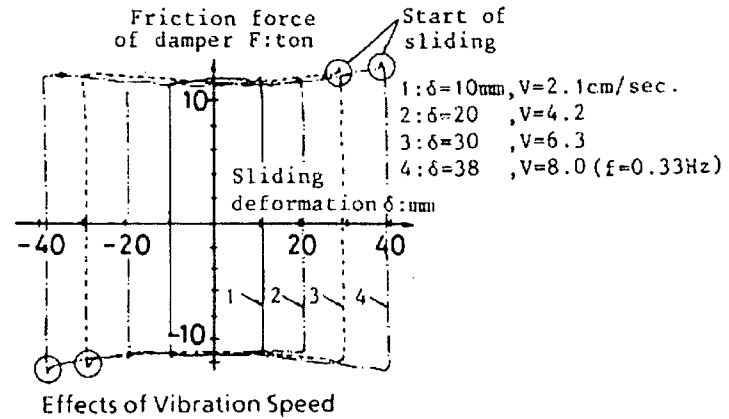
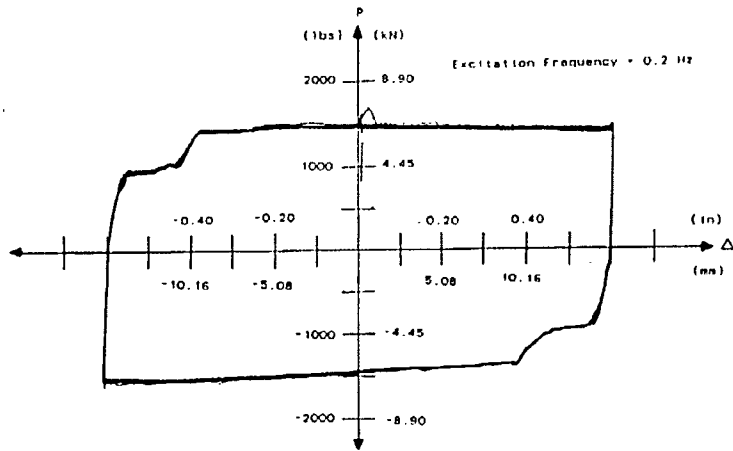


Figure 1.4. Pall friction device and Sumitomo friction device shown with associated hysteresis loops. Note that the direction of trace of the hysteresis loops is clockwise for the pall device, but counter clockwise for the Sumitomo device. Stable and repeatable hysteresis loops were observed with each device.

The friction pendulum connections provide a simple, alternative approach to increasing the seismic energy dissipation capacity of a structure. Zayas and Low (1989) investigated this type of device and found it to be effective. Figure 1.5 illustrates a typical cross-section of a friction pendulum. The normal force transmitted through the sliding surface results from the weight of the structure. Consequently, such devices are able to immediately adjust to changes in the mass of the structure and in the case of a non-symmetrical structure maintain the shear force through the centre of mass of the structure.

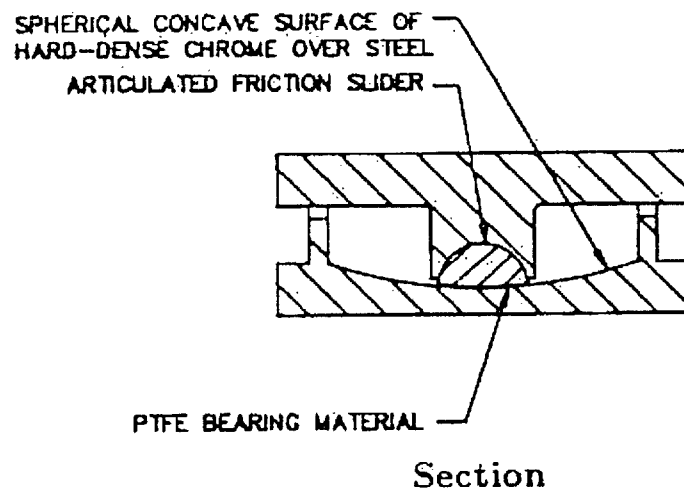


Figure 1.5. Cross-section of a friction pendulum device from Zayas and Low (1989).

While recognising that the incorporation of friction devices was very beneficial to structural performance, Pall (1982) simply suggested that the friction dampers should slip before the capacity of the bracing elements has been reached. This design method, while quite valid in that it optimizes the use of materials, does not provide a basis for which to optimize the performance of the structure. A design method for friction-damped structures based on energy methods was put forth by Filiatrault and Cherry (1988). Following the work by Filiatrault and Cherry, questions about the vertical distribution of slip load remained. The work presented in this thesis is aimed at furthering the understanding of friction dampers and helping to determine the optimal distribution of slip loads in friction damped structures. By incorporating design criteria in the design method, the question of what level of slip load is sufficient to control the structure can be considered.

1.5.2.3 Hysteretic Dampers

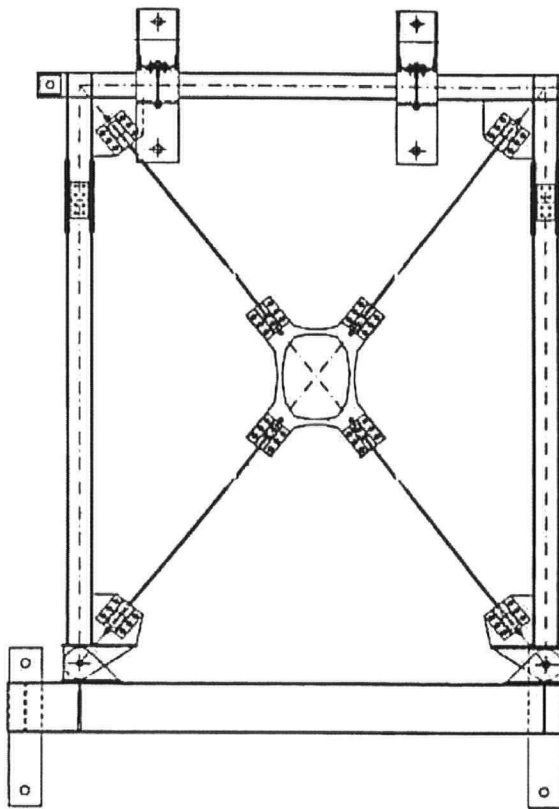
Hysteretic dampers take many forms and provide an economical means of dissipating energy. Some of the many configurations are described by Ciampi (1991) and shown in Figure 1.6. Figure 1.7 shows a typical response for a steel triangular plate damper. Reversed cyclic deformations cause the accumulation of damage within the material that may potentially lead to low cycle fatigue, however, it has been demonstrated that such devices have consistent and repeatable hysteresis loops for a large number of cycles. The key advantage of hysteretic dampers is their robustness.

Unlike the friction dampers, hysteretic dampers utilise the yielding mechanism of the base metal. For a typical steel material the stress-strain curves follow a curvilinear shape shown in Figure 1.7. The theoretical fit of experimental data for a typical friction and hysteretic device is illustrated in Figure 1.8. In order to accurately model the energy dissipation, the post yield stiffness and the yield stress are varied such that the areas under each curve up to a specified strain are equal and the error in estimation is minimised.

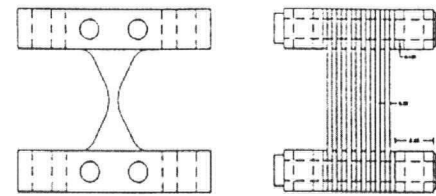
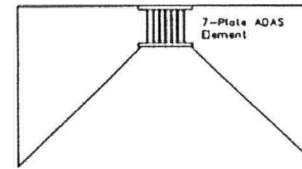
Unlike a friction damper, metals possess a multi-level memory effect that leads to the nesting of hysteresis loops. Fitting a bilinear stress-strain curve over the typical hysteresis curve ignores this multi-level memory effect and subsequently reduces the memory effect to a single level. At present, it is presumed that the single level memory is sufficient to capture the essence of the hysteretic damper. However, this has not been investigated.

1.5.2.4 Viscous and Viscoelastic Dampers

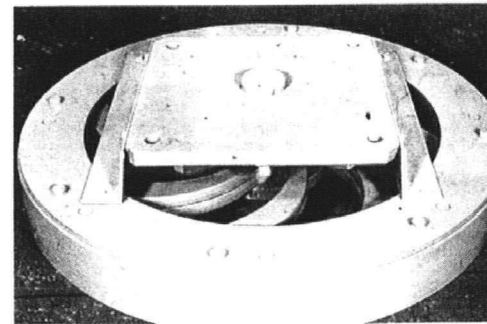
The World Trade Centre was among the first structures to use viscoelastic dampers to improve its dynamic characteristics in wind (See Architectural Record, Sept. 1971 pp155-158). A bracing element containing a viscoelastic material sandwiched between steel plates, as shown in Figure 1.9(a) constitutes a simple viscoelastic device. An alternative device suggested by Scholl (1988) is shown in Figure 1.9(b). The model for such a system is similar to that shown in Figure 1.1(b) with the addition of a spring in parallel with the damper.



(a)



(b)



(c)

Figure 1.6. Examples of hysteretic devices. (a) Dissipative brace by Ciampi, Arcangeli and Ferlito, (1991). (a) Added Damping and Stiffness (ADAS) using triangular steel plates, Grigorian, Yang and Popov (1993). (c) 2-D hysteretic device, Ciampi et al. (1991).

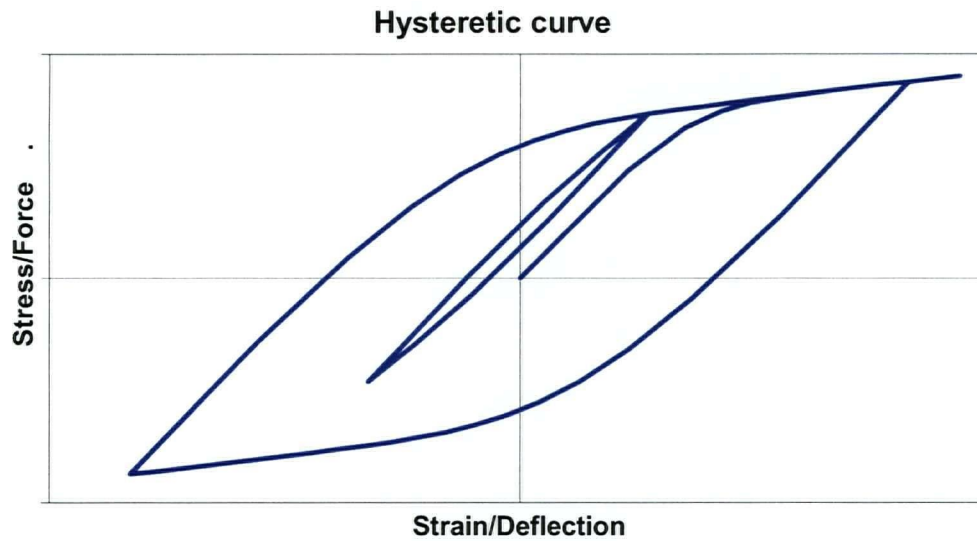


Figure 1.7. Typical hysteretic behaviour of a steel component.

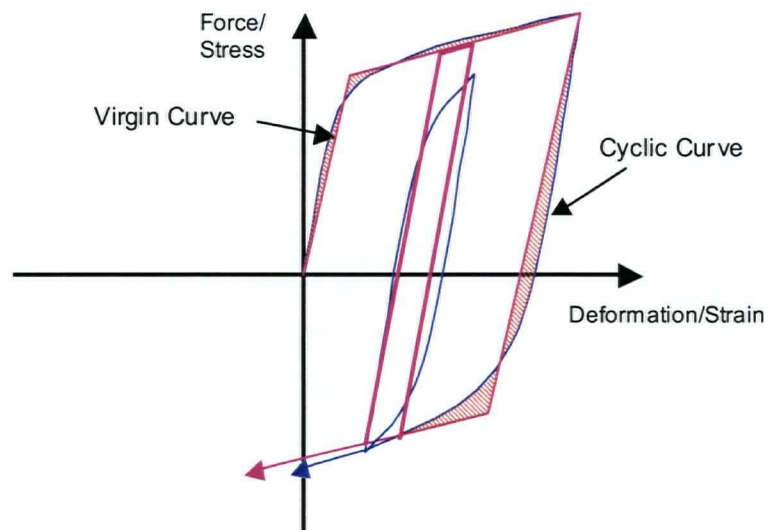


Figure 1.8. Best fit of curvilinear stress-strain function using bilinear hysteresis. The difference is shown hatched. While the large loop is fit with reasonable accuracy, the smaller loop shows a greater deviation.

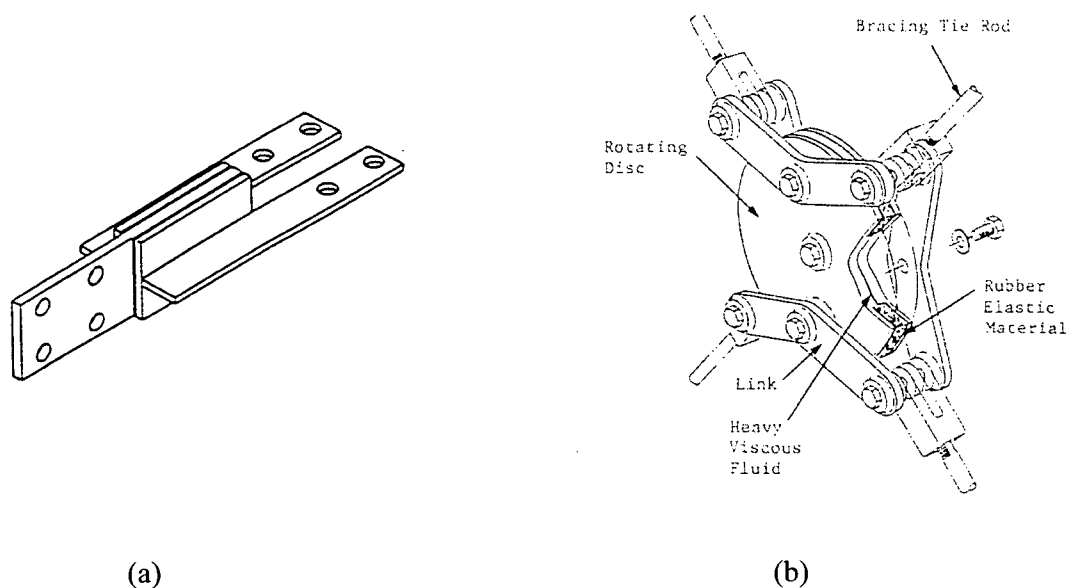


Figure 1.9. Examples of viscoelastic devices. (a) Isometric view of constrained layer viscoelastic damper (From Aiken and Kelly, 1990). (b) Viscoelastic brace damper suggested by Scholl, 1988.

Kelly and Aiken (1991) compared the behaviour of a friction damped and a viscoelastically damped structure subjected to earthquake excitations. They concluded that the friction damped and viscoelastically damped structures appeared to produce similar performances for a wide selection of earthquake inputs in terms of acceleration and displacement responses, while reducing displacements as much as a concentrically braced frame.

Viscous damping devices have gained acceptance for the seismic control of bridge and building structures. This result highlights the effectiveness of pure damping. Niwa *et al.* (1995) considered the feasibility of utilising high damping devices installed in the bracing of a high-rise building yielding damping ratios in the 10% to 20% of critical damping ratio. The results of the study indicate that acceptable performance in even large earthquakes can be achieved.

1.5.3 Semi-Active Control

Semi-active systems are those systems that do not apply control forces directly to a structure, but instead act to improve the performance of the structure by modifying the characteristics of the control elements in time as the structure deforms. The most practical advantage to using such systems over fully active systems is that the semi-active systems have a vastly reduced energy consumption requirement.

Akbay and Aktan (1991), Feng, Shinozuka and Fujii (1993), Dowdell and Cherry (1994a, 1994b) and Patton *et al.* (1994a, 1994b) suggested that the performance of a passive system could be improved substantially by the introduction of an element of control to a passive device. Akbay and Aktan, Dowdell and Cherry, and Feng considered the use of variable slip force friction damping devices while Patton developed a variable viscous damper. Dowdell and Cherry demonstrated that the forcing function near to that of an active system could be generated utilising a variable friction slip device but for SDOF structures suggested a simplified “off-on” control algorithm that acts to maximize the energy dissipation capacity. Feng utilised an instantaneous optimal control algorithm which effectively broadened the effectiveness of the friction controlled system and reduced residual displacements to levels much lower than for structures without controlled friction.

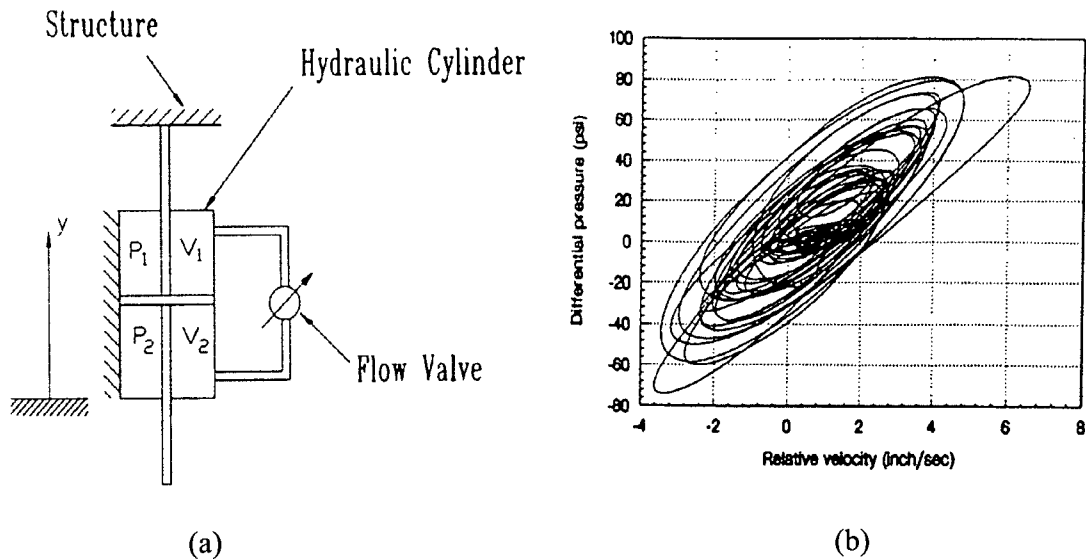


Figure 1.10. Semi-active viscous damper (SAVD) from Patten *et al* (1994a).

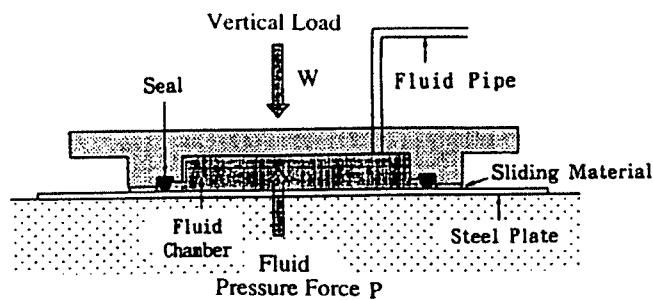


FIG. 2. Idealized View of Friction Controllable Sliding Bearing

Figure 1.11. Variable friction slip force friction damper from Feng (1993).

Later, Chen and Chen (2002) suggested utilising a piezoelectric material to regulate the friction component of a friction-damping device for the control of a tall building.

1.5.4 Hybrid Systems

Hybrid systems combine two or more control strategies such as base isolation and an active mass damper as considered by Reinhorn and Riley (1994), Riley, Reinhorn and Nagarajaiah (1994), and Inaudi and Kelly (1993). Hybrid systems have the potential for superior performance. However, this comes at the cost of the complexity of providing the equipment for more than one means of control such as base isolation and active control.

Yang, Danielians and Liu (1991) proposed two hybrid control systems for seismic protection of structures. The system shown in Figure 1.12 combines an active mass damper with base isolation while the other relies on a passive tuned mass damper in combination with base isolation. The base isolation decouples the structure from the ground while the active or tuned mass damper dissipates the vibration energy. The combination of the two systems produces a very effective deformation control.

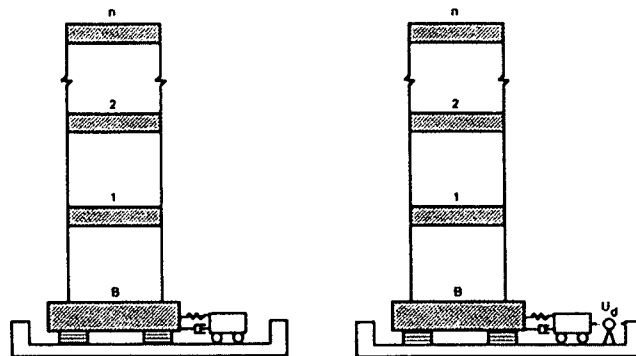


Figure 1.12. Hybrid passive and active systems – example from Yang *et al* (1991). (a) Hybrid base isolation and tuned mass damper; (b) Hybrid base isolation and active mass damper.

1.6 General Discussion and Thesis Organization

It has been well established that increased damping tends to improve the structural performance for a wide variety of dynamic loads. Many devices have been suggested and many have been successfully implemented. Those presented here represent a small portion of those proposed, studied and implemented.

The focus of this thesis is not on the devices themselves, but on the design of structures fitted with energy dissipation devices. Regardless of the devices chosen, the engineer needs to be able to analyse and understand the dynamic characteristics of the structure with the energy dissipation devices and how it will respond to the loading for which it is to be designed. The engineer then has to compare the response with the required performance and make key decisions about the location of the dampers, stiffness and construction of the damper force transfer elements (braces) and the magnitude of the forces carried by the dampers themselves. This thesis is devoted to proposing methods for making these key decisions. In the following chapters, the necessary concepts to undertake the design task are developed.

As structural control plays a key role in this development, Chapter 2 is devoted entirely to introducing and explaining the concepts of classical and modern control theory used in later developments. Its intent is to define the key terminology and set the stage for the analysis to follow.

Chapter 3 is devoted to the design of SDOF structures with passive viscous, friction and semi-active friction dampers. After briefly introducing the concepts of frequency domain analysis, the steady state frequency response of the linear viscous damped structure and the constant slip load viscous damped structure are established analytically and numerically.

Chapter 4 briefly discusses the issues involved in extending the proposed transfer function based SDOF design method to MDOF structures. It is observed that the application of this method is restricted to structures for which the desired distribution of slip loads and the relationship to the optimal SDOF slip load has been established beforehand. Using an optimization procedure called "level set programming" (LSP), the optimal distribution of slip loads in the uniform 4-story structure is established. A comparison of the LSP obtained slip load distribution is made with the results of that predicted using the extended SDOF design method.

In Chapter 5, a more general procedure is developed to determine the magnitude of optimal passive viscous dampers in a general MDOF structure based on modern control theory and the application of response spectral analysis. An extension of the method to include friction-damped structures is also provided. This chapter is focussed on providing the detailed mathematical derivation.

Chapter 6 illustrates the application of the proposed MDOF damper design method derived in Chapter 5 using a set of three example structures with increasing complexity. The first structure

is the same uniform 4-story structure used in Chapter 4. The following examples is a 2-D frame extracted from a typical steel moment frame office building in Los Angeles. The third and final example is an 18 DOF asymmetric structure with simultaneous excitation in two directions.

Chapter 7 provides a summary of the main concepts and findings of the presented material. The final section is devoted to a discussion of the main contributions of this work

Chapter 2: Control Theory Background

In the previous chapter structural control was introduced as an emerging field of study that has the potential to improve the performance of structures under large external loads such as those induced by earthquakes. A distinction is made between the structural control that pertains to single degree of freedom structures and that which is developed for multi degree of freedom structures. Classical control theory for the most part pertains to single degree of freedom systems while modern control theory is developed to deal with multi variable systems.

This chapter introduces the important concepts forming the theoretical basis of classical control theory and modern or optimal control. The concepts introduced here are developed further in later chapters. The ideas that are used to link the concepts of modern active control theory to the design of passive energy dissipation systems are set out.

2.1 Modern vs. Classical Control Theory

Modern control theory differs from classical control in several significant ways. The most important difference is that modern control uses a “systems” approach to the solution of the control problem. In Chapter 1 it was stressed that structural designers should consider the structure as a whole and determine the effect of the proposed control on not only the critical variables or members but also consider the effect on all other members. Classical control deals primarily with SDOF systems and considered extension to MDOF systems an “art”. Modern control on the other hand was developed to deal directly with MDOF systems by utilising a more sophisticated mathematical formulation of the structural dynamics and introducing optimization principles.

Both classical and modern control procedures presented herein use the “state-space” formulation of the equations of motion of the structure as a basis, rather than the second order differential equation used typically in structural dynamics. The state-space formulation converts the second-order differential equations of motion into equivalent first order differential equations with an expanded number of variables. An n -dimensional second order system is transformed into a $2n$ -dimensional first order system. This transformation allows for more generality in the solution at the expense of carrying the expanded number of system variables.

One of the difficulties with the usual second order differential equation of motion is the transition from sub-critically damped to super-critically damped motion. At this juncture, damped sinusoidal impulse response functions become hyperbolic, complicating the solution process. As will be seen in the derivation of the theory, this transition can be handled in a uniform manner.

Modal analysis with the second order differential equation is usually accomplished by neglecting the damping and constructing an orthonormal basis from the undamped modes. These undamped modes have the characteristic that all nodes have zero deflection at the same instant in time during the vibration. For structures that are lightly damped this is true. However, for structures that are highly damped and particularly when the damping is concentrated in discrete units, mode shapes generally do not conform to the undamped mode shapes and are referred to as non-classical modes. Rather than construct an orthonormal basis, with a single set of eigenvectors, the state-space formulation requires the extraction of both right and left eigenvectors that provide a “bi-orthonormal” basis. Although computationally more intense, casting the equations of motion in state-space form enables orderly treatment of non-classical modes.

2.2 Classical Control Algorithms

2.2.1 Minimum Time Problem – Bang-Bang Control

Bang-Bang control is an ideal control algorithm when the objective is to move a single degree of freedom structure from its excited state to an at-rest state in the minimum possible time. As will be seen later this control bears a strong resemblance to the friction damped system.

In order to facilitate an understanding of this control algorithm, consider an undamped single degree of freedom structure subjected to an initial disturbance and plot the motion in the “phase plane”. The phase plane, as referred to herein, is a space with the x-axis proportional to the displacement and the y-axis proportional to the velocity. A single point in the phase plane is sufficient to describe the state vector of the structure. In the absence of external excitation, the trajectory of the function describing the state space response is known to follow an ellipse centred about the origin. The characteristic ratio of major to minor axes is a constant depending on the oscillation frequency of the structure. See Figure 2.1 for an illustration of the phase-plane.

After introducing a constant external force the origin of the ellipse that the trajectory follows is shifted from the origin to a point on the x-axis given by A , a distance of F/K from the origin, as shown in Figure 2.1 (b). If the same magnitude force F acts in the opposite direction, another ellipse centre is found at $-F/K$.

While the applied force remains constant, the phase plane plot of the state vector will orbit the new origin. If we wish to utilise a constant force to bring the state vector to zero, then our phase plane trajectory immediately suggests that control can be affected by switching the control force direction at suitable times so that the ellipse degrades with each half cycle. One method of doing this is to wait until the state vector crosses the x-axis and use the x-axis crossing to trigger the switching of the control force. If this algorithm is followed, one finds that the state space trajectory will move toward, but never reach the zero state. The reason for never reaching the zero state is due to the inability of the switching at the x-axis crossing to improve the trajectory once it crosses between the plus and minus offset origin points.

When the state vector attempts to cross the line between the plus and minus offset origins, the control force will oscillate and the structure will tend to “stick” at the deformation state described by the crossover point. This end result does not accomplish the “minimum time” objective of the control algorithm. The bang-bang algorithm, therefore, includes a slight modification to produce a better performance by slightly offsetting the switching times. Figure 2.2 contains a plot of the phase plane trajectory and the optimal switching times. If the switching is delayed until a crossing of the modified line, then the modified trajectory will pass through the origin.

A friction or hysteretic damper, apart from the inability to bring the state vector exactly to the origin produces a control response very much like the Bang-Bang control.

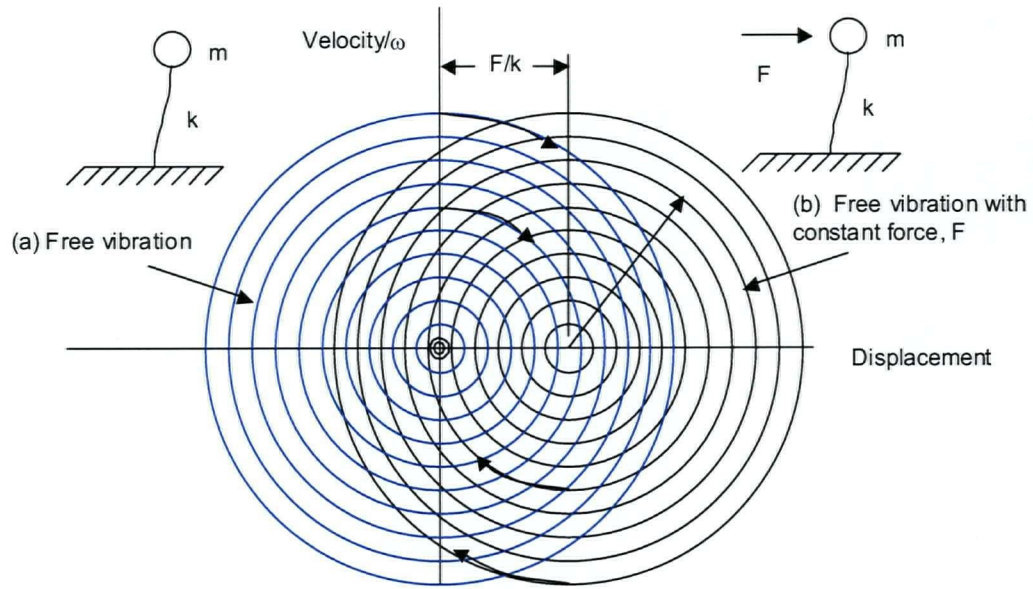


Figure 2.1. Phase plane trajectory of the response of a SDOF structure: (a) undamped free vibration, (b) undamped free vibration with constant force applied.

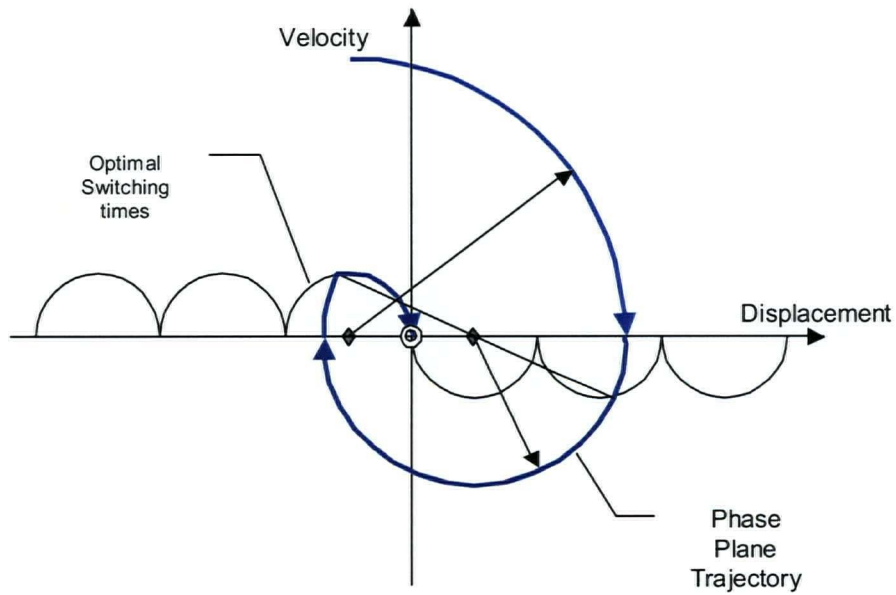


Figure 2.2. Bang-bang control phase plane trajectories.

2.2.2 Minimum Fuel Problems

Another alternative control algorithm of historical significance is the minimum fuel problem. The objective of this control is to bring the state vector of an excited body to the origin using the minimum amount of "fuel". The fuel in this case is the product of the control force by the time duration over which it acts. If the control force is constant such as the thrust from a rocket engine, the minimum fuel problem corresponds directly to the amount of fuel burned. The amount of energy to be dissipated from an excited system in the absence of further excitation is a constant. The objective of a minimum fuel problem is to define the firing periods for which the fuel consumption is a minimum. Conversely, one can view the minimum fuel problem as one of maximizing the efficiency with which the fuel is utilised. It can be shown that the maximum efficiency results when the body to be controlled is at its peak velocity. An impulse at this time acting in the direction opposite to the direction of motion will extract the maximum energy from the moving body. To further elaborate on the algorithm, again we resort to the phase plane, as shown in Figure 2.1. In the absence of control a body will follow an elliptical path. The peak velocity occurs when the body approaches the Y (velocity) axis. It can be shown that the minimum fuel consumption results when the control force is restricted to the region shown in Figure 2.3, a region subtended by an angle α . Since the time spent in each concentric ellipse is the same, the pulse-firing period is identical in each case. The energy extracted in each cycle is reduced as the phase plane trajectory approaches the origin and the displacement associated with each cycle lessens.

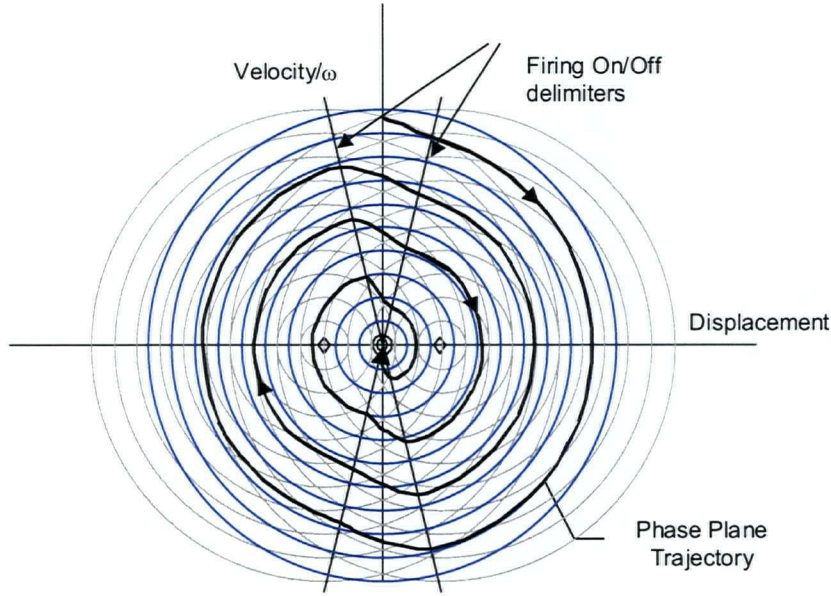


Figure 2.3. Bang-off-bang control example.

2.3 State Space Formulation of the Equations of Motion

Assume a dynamic system in general is described by the 2nd order differential system of equations:

$$M\ddot{\hat{x}}(t) + C\dot{\hat{x}}(t) + K\hat{x}(t) + \tilde{B}u(t) = -M\tilde{L}\ddot{x}_g(t) \quad (2.1)$$

where M is an appropriate mass matrix, C - damping, K -elastic stiffness, \tilde{B} -external force location matrix, u , external force vector, \tilde{L} excitation force location vector and $\ddot{x}_g(t)$ external force time history, and \hat{x} represents the vector of structural displacements.

In general Equation 2.1 can be expressed as a first order differential equation of order $2n$, as follows

$$\begin{bmatrix} \dot{\hat{x}}(t) \\ \dot{\hat{\dot{x}}}(t) \end{bmatrix} = \begin{bmatrix} \dot{\hat{x}}(t) \\ \ddot{\hat{x}}(t) \end{bmatrix} = \begin{bmatrix} 0 & I \\ -M^{-1}K & -M^{-1}C \end{bmatrix} \begin{bmatrix} \hat{x}(t) \\ \dot{\hat{x}}(t) \end{bmatrix} + \begin{bmatrix} 0 \\ -M^{-1}\tilde{B} \end{bmatrix} u(t) + \begin{bmatrix} 0 \\ -\tilde{L} \end{bmatrix} \ddot{x}_g(t) \quad (2.2)$$

where n is the order of the original system. The equation in terms of state vector $x(t)$, where

$$x(t) = \begin{bmatrix} \hat{x}(t) \\ \dot{\hat{x}}(t) \end{bmatrix} \quad (2.3)$$

can be expressed more concisely as

$$\dot{x}(t) = Ax(t) + Bu(t) + L\ddot{x}_g(t) \quad (2.4)$$

where

$$A = \begin{bmatrix} 0 & I \\ -M^{-1}K & -M^{-1}C \end{bmatrix} \quad (2.5)$$

and the definitions of B and L can be determined by comparing Equations 2.2 and 2.4.

Expansion of Equation 2.4 by matrix multiplication will verify the original equation of motion Equation 2.1.

The block diagram describing the above system of equations is shown in Figure 2.4. The matrix A contains the dynamic properties of the structure including boundary conditions; while B and L from Equation 2.4, respectively contain information about the location of applied control forces $u(t)$ and the location of the disturbances $\ddot{x}_g(t)$.

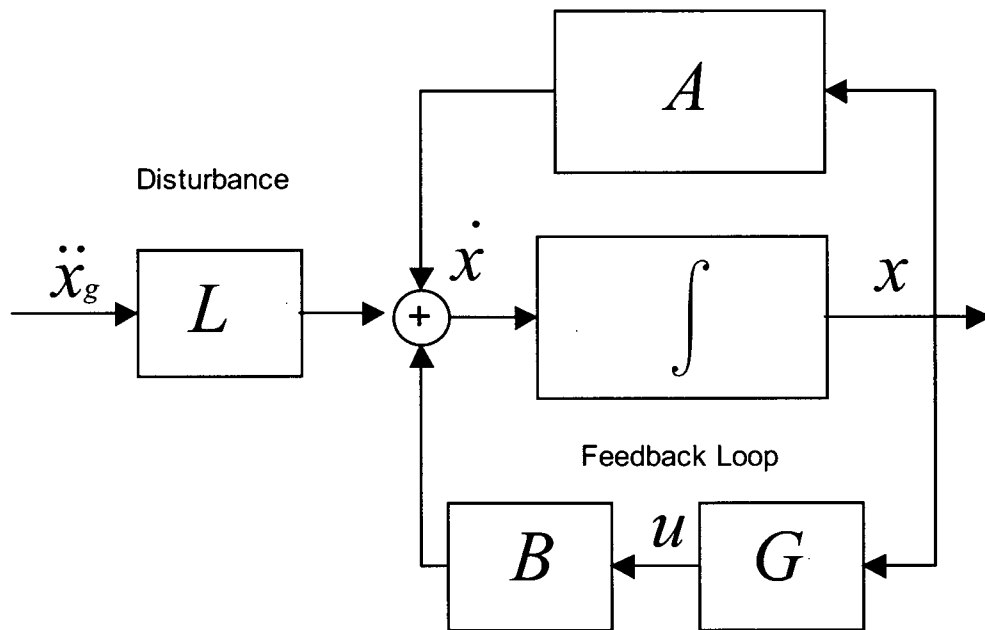


Figure 2.4. Block diagram of state space equation of motion (Equation 2.4)

2.4 Optimal Linear Quadratic (LQ) Regulator: Active Control

The modern approach to structural control combines system theory and optimization to establish the characteristics of the control force defined on interval necessary to provide an optimal response. Books by Meirovitch (1990), Soong (1989) and Sage and White (1977) provide more in-depth discussions than possible here.

Before solving the control problem, one must have an understanding of the properties of the structure and the excitation to which it will be subjected. For a typical earthquake, however, the properties of the external load are not known *a priori*. Fortunately, the optimal regulator problem can be solved without this knowledge under the assumption that the excitation is a white noise. (see Sage and White, 1977) Although white noise is not an ideal model for an earthquake, artificial earthquakes are sometimes modeled as a burst of filtered white noise – (see Gasparini and Vanmarcke, 1976).

The structure and the control system together are referred to as the “plant”. The objective of the control input is to drive the plant from an excited state to a desired final state, in our case the zero state. The optimal control satisfies this while attempting to minimize the control force necessary to do so. The control objective requires the minimization of the quadratic performance index given as

$$J = \frac{1}{2} x^T(t_f) H x(t_f) + \frac{1}{2} \int_{t_0}^{t_f} \{x^T(t) Q x(t) + u^T(t) R u(t)\} dt \quad (2.6)$$

where H and Q are real symmetric positive semi-definite matrices and R is a real, symmetric positive definite matrix.

The quadratic performance index of Equation 2.6 evaluates to a single real value given any set of state variable response time histories and applied control force time histories from an initial time where the structure is assumed to be at rest until a final time after the response to the earthquake or other excitation has occurred. For any given input, the obtained value of J is made lower when the state response variables are reduced in amplitude. Likewise, the value of J is also reduced when the control force requirement is reduced. It is reasonable to expect that an increase in the control effort would produce a lower structural response, thus, minimization of the value of J requires a balance between the control effort and the response.

The weights assigned to the H , Q and R matrices define how much of a penalty to place respectively on the final condition, the structural response and the control force observed on the defined interval (t_0, t_f) . These weighting matrices provide the means by which the designer can influence the sense of the control. Since J is an arbitrary measure of the performance, the absolute value of the quantity is irrelevant. Therefore the absolute values of the weights chosen for H , Q and R are also irrelevant. The relative values remain important to the minimization procedure as they describe the sense of the minimization and subsequently influence the sense of the resulting optimal control.

In the case of a structural control problem where the structure remains elastic and has some inherent damping, the state of the structure will eventually return to the zero state providing the interval (t_0, t_f) is such that t_f concludes well after the end of the excitation. Therefore, the first term of Equation 2.6 is not significant and is therefore dropped from further discussion.

The remaining Q and R terms can be interpreted as “energy” quantities given that appropriate units are selected.

The Q term represents the vibration energy of the structure. As the effectiveness of the control increases, the state vector reduces and this term contributes less to the value of J . But to achieve that result, an increase in the control forces contained in vector u is necessary leading to an increase in the value of the R term and hence the value of J . The objective of the optimal control problem is to find a balance between the structural vibration response output and the control force input. One might view this as finding an appropriate balance between minimum time and minimum fuel requirements.

Given any particular excitation, the control forces leading to the direct minimization of Equation 2.6 can be determined. It is important to recognize, however that since the excitation is not known *a priori*, it therefore becomes necessary to consider the method of generating the control force. The control force can be implemented by introducing the feedback gain vector

$$u(t) = Gx(t) \tag{2.7}$$

where G is an $m \times 2n$ matrix that relates the m forcing functions to the $2n$ state vector response functions. The goal of the following derivation is to determine the coefficients of the gain matrix, G .

The optimization of the performance index of Equation 2.6 can be solved using the method of Lagrange multipliers. Recognising that the structure is constrained to respond according to Equation 2.4, this equation is appended to the performance index (Equation 2.6) by pre-multiplying by a yet unknown vector $\lambda(t)$ to produce a new quantity termed the Lagrangian expressed as

$$\mathcal{L} = \frac{1}{2} \int_{t_0}^{t_f} \{x^T(t)Qx(t) + u^T(t)Ru(t) + \lambda^T(t)[Ax(t) + Bu(t) + L\ddot{x}_g(t) - \dot{x}(t)]\} dt \quad (2.8)$$

Integrating the last term in the integrand by parts yields

$$\begin{aligned} \mathcal{L} = & -\frac{1}{2} \lambda^T(t_f)x(t_f) + \frac{1}{2} \lambda^T(t_0)x(t_0) + \\ & \frac{1}{2} \int_{t_0}^{t_f} \{x^T(t)Qx(t) + u^T(t)Ru(t) + \lambda^T(t)[Ax(t) + Bu(t) + L\ddot{x}_g(t)] + \dot{\lambda}(t)x(t)\} dt \end{aligned} \quad (2.9)$$

The necessary conditions for optimality can be found by taking the first variation of the Lagrangian (Equation 2.9) and setting it equal to zero. The resulting conditions are

$$\delta\mathcal{L} = -\frac{1}{2} \lambda^T(t_f)\delta x(t_f) + \frac{1}{2} \lambda^T(t_0)\delta x(t_0) + \frac{1}{2} \int_{t_0}^{t_f} \left\{ \dot{\lambda}^T(t) + \frac{\partial\mathcal{H}}{\partial x} \right\} \delta x + \frac{\partial\mathcal{H}}{\partial u} \delta u \Big\} dt \quad (2.10)$$

where \mathcal{H} is defined as $\mathcal{H} = x^T Qx + u^T Ru + \lambda^T Ax + \lambda^T Bu + \lambda^T L\ddot{x}_g$. Since under arbitrary excitation $x(t_f)$ is unknown, the boundary condition

$$\lambda^T(t_f) = 0 \quad (2.11)$$

must be satisfied plus the two conditions

$$\frac{\partial\mathcal{H}}{\partial u} = 0 \quad (2.12)$$

and

$$\dot{\lambda}^T(t) + \frac{\partial\mathcal{H}}{\partial x} = 0 \quad (2.13)$$

where Equation 2.13, taken as a zero condition of Equation 2.10, is derived from the integration by parts of the integrand of Equation 2.9. Carrying out the partial differentiation yields

$$\frac{\partial \mathcal{H}}{\partial u} = 0 = 2u^T R + \lambda^T B \quad (2.14)$$

and

$$\dot{\lambda}^T + \frac{\partial \mathcal{H}}{\partial x} = 0 = \dot{\lambda}^T + 2x^T Q + \lambda^T A \quad (2.15)$$

Equation 2.14 simplifies to

$$u = -\frac{1}{2} R^{-1} B^T \lambda \quad (2.16)$$

If one defines the matrix $P(t)$ as

$$\lambda(t) = P(t)x(t) \quad (2.17)$$

then by substituting known expressions into Equation 2.15, one can show that $P(t)$ satisfies

$$\left[\dot{P}(t) + P(t)A - \frac{1}{2} P(t)BR^{-1}B^T P(t) + A^T P(t) + 2Q \right] x(t) + P(t)L\ddot{x}_g(t) = 0 \quad (2.18)$$

When the external excitation $\ddot{x}_g(t)$ is zero, Equation 2.18 implies

$$\dot{P}(t) + P(t)A - \frac{1}{2} P(t)BR^{-1}B^T P(t) + A^T P(t) + 2Q = 0 \quad (2.19)$$

and Equation 2.11 implies

$$P(t_f) = 0 \quad (2.20)$$

Equations 2.19 and 2.20 provide a means of establishing the values contained within the $P(t)$ matrix through backward integration.

The $P(t)$ matrix is known as the Riccati matrix and its solution provides some challenge.

Appendix A is devoted to the solution of the Riccati matrix in its time dependant and time independent forms. It is assumed that the Riccati matrix is symmetrical.

Once established, the Riccati matrix can be used to evaluate the feedback control gains matrix, G , where

$$G(t) = -\frac{1}{2} R^{-1} B^T P(t) \quad (2.21)$$

and the control forces $u(t)$ are given by

$$u(t) = G(t)x(t) \quad (2.22)$$

In our structural problem the top half of the B matrix is zero, indicating that the forces introduced by the control affect only the acceleration components of the state vector in the equation of motion. It is therefore observed that the values of the Ricatti matrix that influence the control force lie only in the lower half of the matrix. In large problems these properties could be used to expedite the computation of the Ricatti matrix.

The controllability depends on the selection of the Q and R matrices. The matrix Q must be positive semi-definite, while R must be positive definite. The Ricatti matrix is not unique, but depends on the choice of matrices, Q and R and on the properties of the structure to be controlled. Therefore, having solved for the Ricatti matrix does not guarantee that the resulting gain matrix G will produce a stable or provide a desirable control. It is therefore necessary to check the stability of the controlled structure. One method of doing this is to examine the poles of the system. If the poles reside in the left hand side of the complex plane (have negative real parts), stability is assured.

The strength of the control is dependent on the relative magnitudes of the values contained in Q and R . To effect a "stronger" control, one would try a control with either an increased Q matrix or a reduced R matrix. With the stronger control, the control forces are expected to increase and the displacements and velocities of the structure are expected to decrease.

It has been demonstrated that the resulting control is optimal under a zero-mean white noise excitation. It is observed, however that seismic loads are not necessarily well represented by white noise excitation. For the purposes of this discussion, the white noise model of earthquake excitation is considered acceptable. Appendix B provides a demonstration of the minimization of the performance index under simulated earthquakes.

2.5 System Response

Important information about the response characteristics of a structural system can be extracted by examining the poles of the state space equation of motion.

Consider Equation 2.4 written in the condensed form

$$\dot{x} = A'x + L\ddot{x}_g \quad (2.23)$$

where $A' = A + BG$ includes the effect of a control system. The time-domain equation can be expressed in the frequency domain by applying the Laplace transform, yielding the expression

$$sIX(s) = A'X(s) + Ls^2X_g(s) \quad (2.24)$$

Equation 2.24 can be solved for $X(s)$, yielding

$$X(s) = (sI - A')^{-1} Ls^2X_g(s) \quad (2.25)$$

The poles are defined as the values of s that cause $(sI - A')$ to become rank deficient. By inspection, the poles are simply the eigenvalues of the matrix A' . If the poles lie in the left hand plane (have negative real parts), then the system is stable. However, if any of the poles lie in the right hand plane and have positive real parts the system will be unstable.

2.6 Observer Design

To this point the full state controller has been developed presuming that the full state vector x for the structure is known at every point in time. For a real structure it may be impractical to track every degree of freedom. The effort would be burdensome in the case of a very intricate structure and perhaps even impossible given a structure such as a shell that behaves essentially as a continuous system. The concept of an "observer" can be used to relate the reduced set of measured variables to the full state vector. A Kalman filter is an operator that relates the state variables to the measurements and provides a method by which the state variables can be approximated based on measured quantities and system parameters. The block diagram in Figure 2.5 illustrates the concept of an observer.

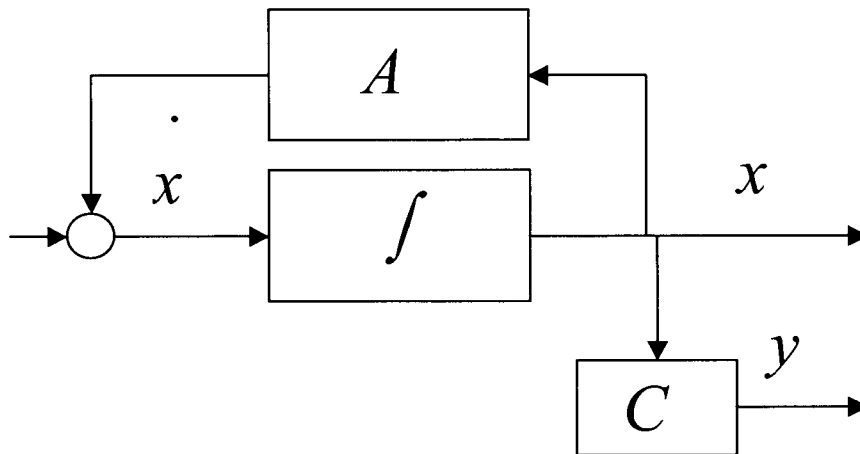


Figure 2.5. Block diagram of an observer of a dynamic system.

Consider a structure having the following state-space equation of motion:

$$\dot{x} = Ax + Bu \quad (2.26)$$

and, in addition, a reduced set of feedback elements related to the state vector given by

$$y = Cx \quad (2.27)$$

where C is a $m \times 2n$ matrix relating the $2n$ elements of the state vector to the m elements measured. The vector y is called the output vector.

The objective of the observer is to include an algorithm as part of the control system to identify the state vector. Once an estimate of the state vector is available, the control algorithm is available to respond accordingly and generate the control action for the entire structure. The portion of the algorithm that is used to estimate the state vector is called the observer. We can write the state-space equation

$$\dot{\tilde{x}} = A\tilde{x} + Bu + K(y - C\tilde{x}) \quad (2.28)$$

for \tilde{x} being the estimated state vector. Comparing this equation with the state-space equation, one can derive an equation for the error $e = \tilde{x} - x$ in the form

$$\dot{e} = [A - KC]e \quad (2.29)$$

The matrix K is known as the observer gain matrix and must be selected such that the poles of the matrix $[A-KC]$ all lie in the left half of the complex plane. Negative real parts of the poles imply asymptotes that approach zero as time increases. It is observed that the observer problem bears a strong resemblance to the control problem. Special techniques, beyond the scope of this thesis, are available to select appropriate optimal values for the observer gain matrix based on the properties of the structure, the measured variables and their susceptibility to external noise. In later chapters the concept of the observer will be re-introduced and direct output feedback control will be developed, eliminating the need for reconstructing the state vector.

2.7 Direct Output Feedback Control

An observer is not necessary if direct feedback is utilised in the control. Direct output feedback control can be applied if the equations of motion of the structure can be reduced to the following form where the vector q contains the same inputs as the reduced order set of measurements

$$M\ddot{q} + C\dot{q} + Kq = Q(t) \quad (2.30)$$

Stability is guaranteed if the control force $Q(t)$ is in the form

$$Q(t) = -G_1q - G_2\dot{q} \quad (2.31)$$

where G_1 and G_2 represent spring and damper combinations. Although one may find a stable set of gains, the optimality of the control is not considered.

In Chapter 5, the derivation of the direct output feedback from the optimal full state control will be considered.

2.8 Sub-Optimal Control

The term “sub-optimal” control refers to the use of a subset of the optimal control. If the subset of the optimal control can represent the action of a set of passive springs and dampers then stability is guaranteed by virtue of the fact that direct output feedback is being utilized. By basing the choice of spring and damping coefficients on the feedback gain values contained in the optimal gain matrix, the chosen set of springs and dampers will contain a measure of the original optimal control. This idea forms the key link between the active control case and the passive control case that will be covered in more detail in the chapters that follow.

The advantage of using the full state LQ feedback gains as a basis is that, mathematically, the problem is tractable, and with the use of Potter's algorithm, the full state feedback gains can be generated rapidly for even a complex system either directly or by backward integration. (For more detailed coverage of the LQ control problem see Meirovitch, (1990), Soong (1989) and Sage and White (1977)) The distribution of actuator force depends on the structural parameters and on the choice of weighting matrices (Q and R) under the assumption that the excitation is either zero or a white noise.

A procedure to be incorporated within finite element software to assist a structural engineer with determining the optimal spring and damper sizes is suggested.

1. Transform the mass stiffness and damping matrices such that the variables of the transformed system correspond to the quantities that are desirable to control, for example story drifts (see Appendix F for transformation of system variables).
2. Choose damper locations, by assigning appropriate values in B , and select weighting matrices Q and R .
3. Formulate the control problem in this transformed space and use Potter's algorithm to produce a set of full state feedback gains.
4. Split G into stiffness and damping components. Ignore all but the positive main diagonal stiffness and damping terms to recommend a set of springs and dampers acting in parallel that will implement the direct passive portion of the control.
5. Analyse the controlled structure to check the performance. Re-select Q and R if necessary and repeat following steps until the performance satisfies the required design criteria.

2.9 Semi-Active Systems

While fully active control systems provide the potential for superior structural performance, the energy input requirements can be large. Alternatively, semi-active control systems are able to provide control performance that is superior to a passive system without the expense of providing for large amounts of externally supplied energy. In a semi-active system, the actuator force only operates to change the system parameters such as slip load or damping coefficient. The energy dissipated is not directly related to the energy supplied. Although large amounts of

energy need not be supplied to the actuators, the implementation of a semi-active control still requires investment in sensors, signal processing and computer equipment sufficient to process the data obtained and to direct the control action.

A semi-active friction damper, for example, activates the control force by regulating the pressure on a sliding surface. Once sliding, the force generated at the sliding surface can be regulated to any chosen value providing it remains less than that which causes the sliding to stop. Semi-active systems, like their active counterparts respond at any one location to deformations sensed from each sensor. However, the resulting semi-active system does not have the same potential effectiveness as the active system. Although the forces generated by a semi-active system appear similar to those in an actively controlled structure, there are times when the force generated may differ, leading to a lesser performance. In the case of a semi-active friction damper the force differs when

- slipping stops
- slipping occurs in the opposite direction to that desired

2.10 Passive Structural Control

Purely passive systems are the least expensive systems due to the fact that there is no requirement for either sensors or actuators. Some types of passive systems have been introduced in Chapter 1. Passive systems differ from active and semi-active systems in that they respond with a local control force responding to local deformations. A passive actuator is incapable of responding to overall deformation characteristics of the structure.

2.11 Conclusion

The most important contribution of the control theory presented in this chapter is its ability to optimize the structures response to dynamic loads. The first order state space formulation that has been traditionally used for control theory provides more information and contains greater flexibility than the traditional second order formulations of the equations of motion used in structural dynamics. In later chapters this theory will be examined in more detail. The link between active and passive control systems will be considered, utilising the concepts of sub-optimal and direct output feedback control.

Important distinctions between active, semi-active and passive systems deal with the sensing and response characteristics. Where active and semi-active control systems sense and respond directly to all (sensed) locations in the structure, semi-active control force is limited due to the fact that there are times when the desired response cannot be achieved. Passive systems sense only the local response where they act, however they are the least expensive and the most reliable.

Chapter 3: Analysis and Design of Dampers in SDOF Structures

Energy dissipation devices are increasingly being used to control the structural response in earthquakes. This chapter discusses the characteristics of SDOF structures fitted with viscous, friction and hysteretic dampers and deals specifically with methods for quantifying their response. In doing so it attempts to give an appreciation of the characteristics of such systems and additionally provides some insights and useful information to assist in the design of such structures.

Although many common structures can be treated as single degree of freedom systems, many cannot. In this case, the study of the SDOF is used as a starting point to discuss issues with MDOF structures.

The configurations of the SDOF structures considered in this chapter are pictured in Figure 3.1. With the exception of Figure 3.1 (a), the brace elements are each comprised of two components, a damping device and a spring connected in series. The role of the spring is to represent the action of unwanted flexibility that prevents the direct transfer of the deformation of the structure to the damping device. In a practical application, this unwanted flexibility arises from

- Flexibility of the bracing element and/or its connections,
- Slope in mechanical devices,
- Compressibility of components internal to the damping device such as hydraulic fluid.

The structures have mass, m , spring constant k , and in the absence of the elements shown on the diagonal would oscillate with frequency f where

$$f = \frac{1}{2\pi} \sqrt{\frac{k}{m}} \quad (3.1)$$

For a structure containing a damper the response frequency becomes

$$f_d = \frac{1}{2\pi} \sqrt{\frac{k}{m} (1 - \xi^2)}. \quad (3.2)$$

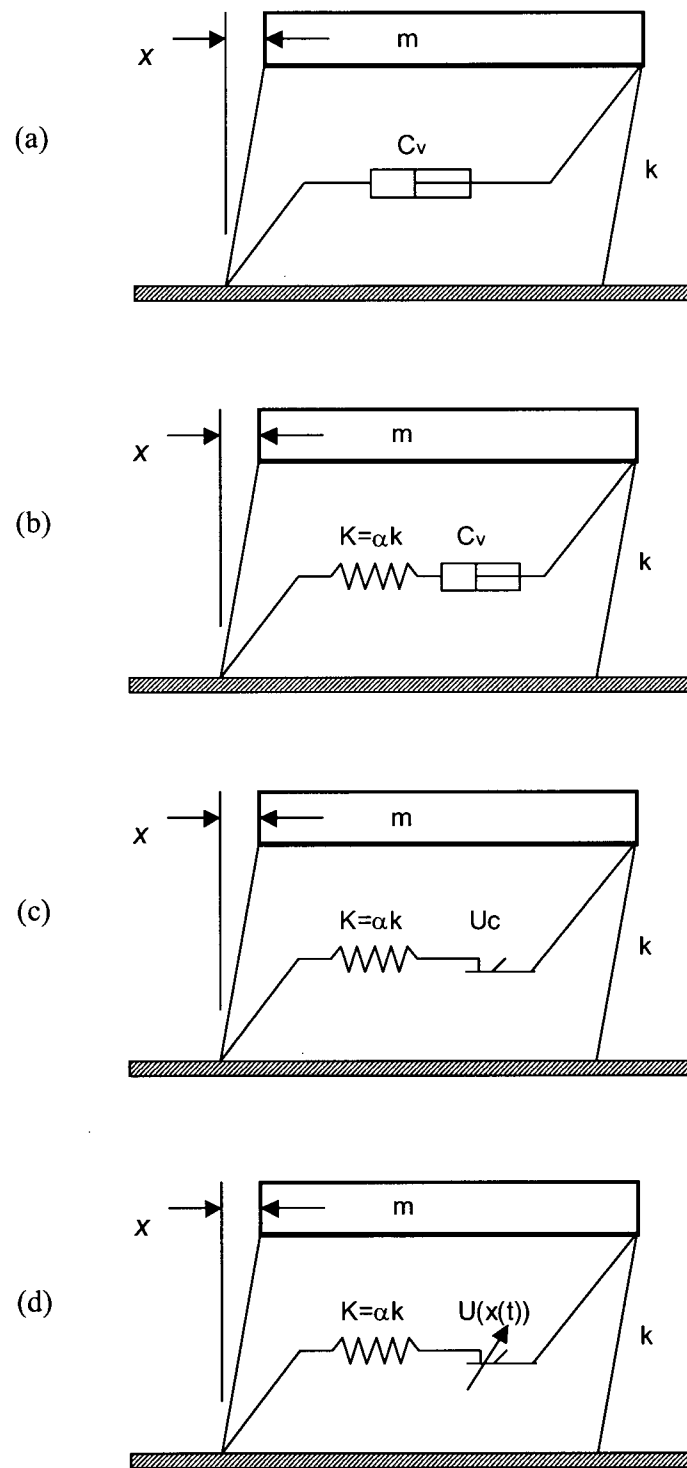


Figure 3.1. Comparison of SDOF structures analysed.

3.1. Linear and Non-Linear Analysis

Linear structural elements are those that generate restoring forces that are directly proportional to imposed deformations (displacements and velocities). These forces remain constant and repeatable for the life of the structure. Non-linear structures, simply stated, are those structures that violate this necessary requirement for linearity. The solution of a non-linear dynamics problem is not straightforward. Solutions, if they exist, may not be unique. And because of the difficulty inherent in finding an analytical solution, iterative solutions are often used.

Analysis of a non-linear structural system is often performed using time history analysis, where the evolution of the non-linear parameters and response variables are tracked as the solution progresses. While a time history analysis can be performed with great accuracy, the results are dependent on the characteristics inherent in the particular input earthquake time history chosen and the initial condition of the structure. Since structural engineers more often have to deal with a range of possible earthquake characteristics (intensity, duration and frequency content) and unknown initial conditions of the structure, a small number of time history analyses often cannot provide a complete picture of the expected response characteristics. This makes it difficult to draw general conclusions from a limited number of time history analyses alone. Performing an extensive number of time history analyses particularly with a large and detailed structural model may be too expensive. Although time history analysis cannot be replaced, other types of analysis are available to fill gaps in understanding and some of these are considered herein.

3.2. Analysis of Linear SDOF Structures

Many of the most useful analytical techniques are only applicable to linear structural systems. In this section two frequency domain analytical techniques are described: response spectrum analysis and Fourier analysis.

3.2.1. Response Spectrum Analysis

For linear structures exposed to earthquakes, convenient methods such as response spectrum analysis (RSA) have been developed. Based on extensive time history analysis of SDOF structures, the response spectrum is a curve or a set of curves that provides the designer information about structure response to site-specific seismic motions. While a response

spectrum can be derived based on a particular earthquake, it is more often used to represent a class of earthquakes or motions rather than any particular event. The most common spectra used are acceleration spectra, which relate the maximum absolute value of acceleration experienced by the structure to the undamped frequency or period of the structure.

It has become common practice to use design spectra in the analysis and design MDOF structures. Application of RSA to MDOF structures is based on the assumption that the structure can be decomposed into a series of modes, where each of the modes responds as an independent SDOF system with its own characteristic frequency and mode shape. The MDOF system response is the superposition of each of the modal components. The modal analysis proceeds assuming that the structure is undamped. The use of RSA presumes that the structure remains linear. Typical design spectra are provided assuming 5% damping; however, other levels of damping can be incorporated through modifying the spectra.

The application of RSA directly provides estimates of the envelope of peak values in the case of a MDOF system. If the spectrum represents peak acceleration due to a particular earthquake, the result of a SDOF RSA analysis will be that peak acceleration. If the spectrum represents an envelope of accelerations resulting from many contributing earthquakes, the results may not be representative of the response experienced by any particular earthquake, as any particular event is not necessarily consistent with the design spectrum.

One advantage in using envelope value estimates from the RSA process is that it gives rise to a consistency in the predicted demands and hence when used in design leads to consistency in design. On the other hand, if one uses an insufficient amount of time history analysis data, loads that may be perceived as small for the chosen events, may be significantly larger when a different event or set of events is chosen. Consistency in predicted demands would ensure that capacities provided would not favour one type of motion over another.

Another advantage arises from the use of the frequency domain used to express the design spectra. In the frequency domain, the designer is provided with a means of conceptualizing the outcome of changes in the design; such as adding stiffness, or mass and can use this information to help get to the final design.

But other types of frequency domain analysis exist, and these too, can be exploited to improve the understanding of structural behaviour.

3.2.2. Frequency Domain Analysis: Fourier Transforms

Classical frequency response curves describe the amplitude of the steady state response to a sinusoidal input excitation. Figure 3.2 shows the characteristic family of curves describing the response of a linear SDOF structure with various levels of viscous damping, given as a proportion of critical damping. The family has a characteristic spike at the resonant frequency, indicating that for zero damping and for input at the natural frequency of vibration, the displacement amplitude will grow without bound.

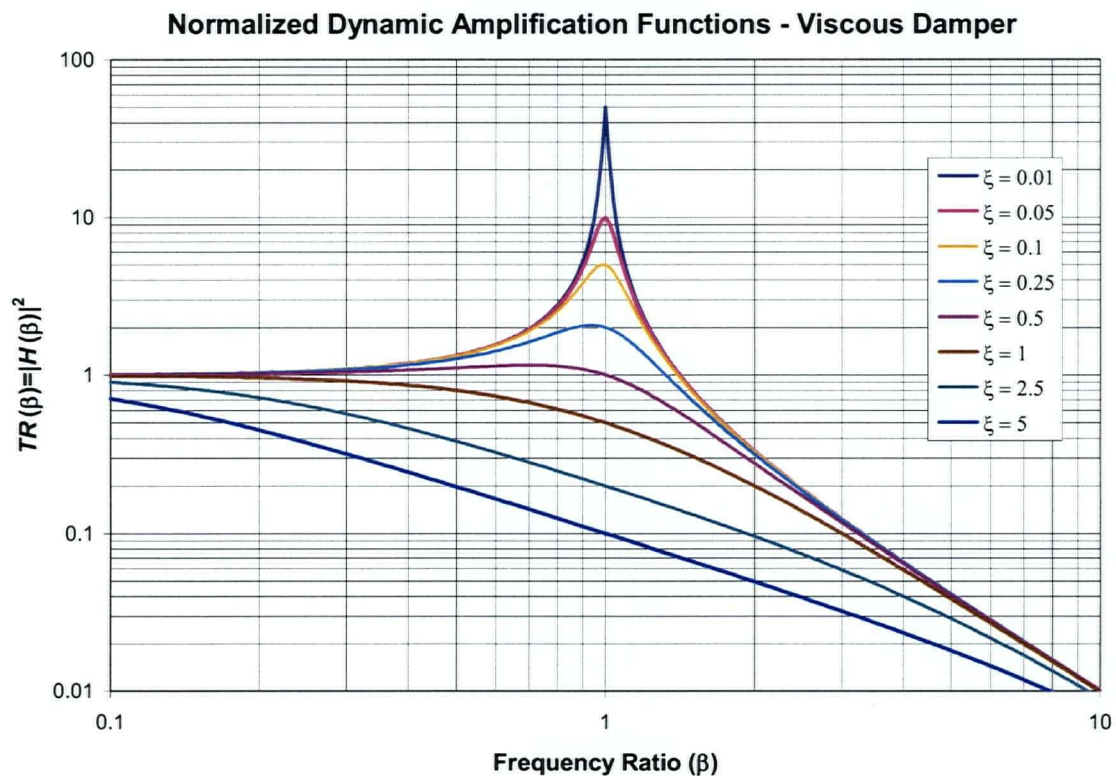


Figure 3.2. Displacement transfer function for structure with ideal viscous damper. The frequency ratio is defined as $\beta = \omega / \omega_0$ where ω is the frequency and ω_0 is the undamped natural frequency.

Any cyclic deterministic time history can be represented in the frequency domain as a sum of sinusoidal wave functions. The Fourier Transform (FT) is one process by which a waveform is broken down into frequency components. H. Joseph Weaver (1983) provides a well laid out development of the theory of Fourier analysis.

In a linear structure, where the principle of superposition holds, the response to an input composed of a series of sinusoidal functions can be considered as the sum of the responses of the structure to the individual components of the excitation. Hence the Fourier transform of the response can be deduced as the product of the Fourier transform of the input and a function sometimes referred to as the complex frequency response function but herein referred to as the transfer function (TF).

3.2.2.1. *Fourier Transform and Random Vibrations*

In connection with random excitation the Fourier transform plays an important role. Although the wave function may be unknown, the frequency content can be described by a function termed the power-spectral density (PSD). Describing the random excitation as the sum of a series

$$\hat{x}(t) = \sum_j a_j e^{i\omega_j t}, \quad -\infty < \omega_j < \infty \quad (3.3)$$

where the real and imaginary components of a_j are random variables interpreted as the complex amplitudes of the different frequency contributions to the total signal chosen in such a way that the sum above is real valued. In a continuous system, the above equation can be re-stated as

$$\hat{x}(t) = \int_{-\infty}^{\infty} A(\omega) e^{i\omega t} d\omega \quad (3.4)$$

where $A(\omega)$ is a continuous complex function. Given that

$$A(\omega) = \int_{-T}^T x(t) e^{-i\omega t} dt \quad (3.5)$$

is the Fourier transform of time history $x(t)$, it can be shown that the power spectrum is defined as

$$S_x(\omega, T) = \frac{1}{4\pi T} |A(\omega)|^2. \quad (3.6)$$

where T is taken as the period of the Excitation from equation 3.5 above.

3.2.2.2. *The Transfer Function and the Dynamic Amplification Function (DAF)*

The transfer function, $H(\omega)$, is a complex function that describes the dynamic characteristics of a particular structure by relating the frequency response of the structure to the frequency response of the input excitation. While often established analytically, it can also be established numerically by taking the ratio of the Fourier transforms of measured input and output signals. In the work presented here, the function $TR(\omega) = |H(\omega)|^2$ is used to represent the transfer function, where $|\cdot|$ indicates the magnitude of the complex function. The phase characteristics of the transfer function are important when dealing with deterministic systems. However, when dealing with random vibrations, only the magnitude of the transfer function is necessary to characterize the response. Therefore $TR(\omega)$ is sufficient to characterize the system dynamics. The dynamic amplification function (DAF) is simply $|H(\omega)|$. The derivation of the transfer function using Laplace transforms is given in Section 3.4.

3.2.2.3. *The Inverse Fourier Transform*

Structural response in the time domain can be obtained by computing the inverse Fourier transform of the product of the complex frequency response function and the Fourier transform of the input, assuming the complex frequency response function to be both linear and time invariant.

3.2.2.4. *RMS Response of a Random Process*

Considering a random process, useful information can be obtained without the need for reverting back to the time domain. In particular, the RMS response can be obtained by evaluating

$$RMS(X(t)) = \sqrt{\int_{-\infty}^{\infty} S_x(\omega) d\omega} = \sqrt{\int_{-\infty}^{\infty} |H(\omega)|^2 S_z(\omega) d\omega} = \sqrt{\int_{-\infty}^{\infty} TR(\omega) S_z(\omega) d\omega} \quad (3.7)$$

corresponding to the area under the PSD curve of the response, $S_x(\omega)$, given excitation PSD $S_z(\omega)$ and system frequency response function $TR(\omega)$.

3.2.2.5. Band Limited Gaussian White Noise

White noise is an ideal random excitation defined as containing equal energy at all frequencies. The PSD of a white noise is a uniform function extending from minus infinity to plus infinity. The energy contained in such a signal is infinite; therefore it is practical to limit the frequency to a prescribed range, thus the term “band-limited.” As shown in Figure 3.3 a cutoff frequency, ω_c , is introduced. The cutoff frequency is referred to as the bandwidth.

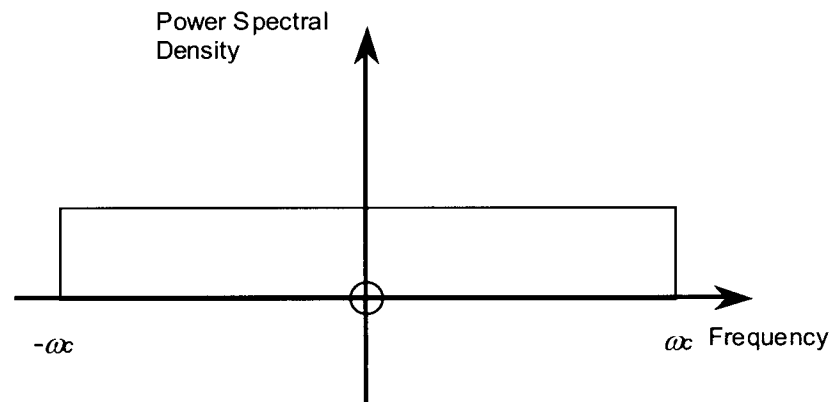


Figure 3.3. PSD function for band limited white noise.

The signal is termed Gaussian if the distribution of the output satisfies the Normal distribution. Practically, a broadband signal can be generated with an approximately Normal distribution by the following steps:

1. Generate two random numbers a and b on the interval $(0,1)$ with uniform distribution
2. Evaluate the formula $x = \cos(\pi a)\sqrt{-2\ln(b)}$

The distribution for the resulting random number, x , is has zero mean, standard deviation 1 and the resulting distribution closely resembles a Normal curve. Appendix E contains a detailed assessment of this procedure.

3.2.2.6. Fourier Transform and Earthquakes

To apply the Fourier transform, the input and output functions are assumed to be steady state, or cyclic. An earthquake is neither cyclic nor steady state. When applying Fourier transform techniques to a data set, it is assumed that this data set cyclically repeats itself. Under cyclically

repeating earthquakes it is easy to visualise that at the end of one earthquake cycle and the beginning of the next, the structure will carry over some vibration from the previous cycle. This carry-over leads to the problem of aliasing, where the residual response at the end of a cycle introduced at the beginning of the next leads to an incorrect assessment of the response. With many analyses, aliasing does not significantly affect the results of interest, however, during the assessment the analyst needs to be aware of the potential so as to avoid conditions where the results of interest are significantly affected.

3.2.2.7. *The Fast Fourier Transform*

The Fast Fourier Transform (FFT) is an implementation of the general Fourier Transform in which a sequence of 2^n data points factorized in a particular way so as to greatly reduce the computational requirements. The FFT is a standard algorithm that is widely available and widely used.

3.2.2.8. *RMS Estimate from FFT*

The RMS of a signal can be obtained from the complete set of FFT data by computing

$$RMS(X(t)) = \frac{1}{N} \sqrt{\sum FFT(X(t))^2} \quad (3.8)$$

3.2.2.9. *RMS of a White Noise*

The RMS of a white noise random sequence with uniform PSD $S_X(\omega) = S_0$ can be obtained by applying the formula

$$RMS(\hat{X}(t)) = \sqrt{\int_{-\infty}^{\infty} S_X(\omega) d\omega} = \sqrt{2\omega_c S_0} . \quad (3.9)$$

3.2.2.10. *Energy Concepts*

There are five types of energy identified that can be tracked in a vibrating structure

- 1) Elastic potential energy, E_E
- 2) Kinetic energy, E_K
- 3) Viscous damped energy, E_V

4) Hysteretic damped energy, E_H

5) Energy imparted to the structure by the ground motion, E_G

The energy balance at any given time is

$$E_E + E_K + E_V + E_H = E_G \quad (3.10)$$

This energy imparted to the structure must be equal to the sum of the energy in the structure plus the energy dissipated. The energy terms are calculated as follows:

$$E_E(t) = \frac{1}{2}kd(t)^2 + \frac{1}{2}Ke(t)^2 \quad (3.11)$$

$$E_K(t) = \frac{1}{2}m\dot{d}(t)^2 \quad (3.12)$$

$$E_V = \int_{t_0}^{t_f} c\dot{d}(t)^2 dt \quad (3.13)$$

$$E_H = \int_{t_0}^{t_f} u(t)\dot{d}(t)dt \quad (3.14)$$

where d and \dot{d} are components of the state vector, e is the elastic deformation of a flexible brace member, and $u(t)$ is an applied control force representing that carried by a control device.

3.3. Nonlinear SDOF System Analysis

3.3.1. Modelling Friction/Hysteretic Damped Structures

As introduced in the previous chapter, the friction damper is a simple device composed of a sliding surface and a clamping force. The sliding surface transmits force across the device to the structural elements connecting it to points within the structure. The sliding surface permits the interfaces to displace relative to one another while a clamping force is provided such that the lateral shear carried across the sliding surface cannot exceed a pre-determined value. The force required to initiate and to maintain motion on the sliding surface is called the slip force. When

the slip force remains constant, the system is referred to as a constant slip force friction damper (CSFD).

Hysteretic systems utilise the long yield plateau of a deforming metal to limit the force in a particular element and as such have response characteristics that are similar to the friction damper. Primarily, materials such as steel, aluminium and lead are used as the yielding medium.

Unlike a viscous damper, to model a friction or hysteretic damper it is essential to include an additional variable to represent the “memory” of the device. A friction slider system requires a single additional variable to characterize the memory. A hysteretic system on the other hand has a multi-level memory effect [see Dowdell, Leipholz and Topper (1987a and b)] and therefore requires many additional variables to characterize the state of the damper. Extension to multi-level memory, however, is beyond the scope of this thesis and hysteretic systems are only considered here insofar as they can be modeled using a single memory friction slider.

The additional variable can be chosen to represent either the elastic deformation of the brace, or the slip deformation experienced by the slider. By including an additional variable that tracks slip deformation, the force in the damper is related to the elastic deformation of the brace, determined as the difference between the total deformation and the slip deformation.

3.3.2. Bilinear Hysteresis

The behaviour of a friction/hysteretic damper within a structural frame can be modelled as a bilinear elastic-plastic system. The theoretical bilinear model includes not only the effect of the damper but also the effect of a brace in series with the damper and the effect of stiffness of the structure itself.

If the brace stiffness is K and structure stiffness is k , then two characteristic stiffnesses of the combined frame can be defined as follows

$$K_0 = k + K \quad (3.15)$$

and

$$K_y = k \quad (3.16)$$

where K_0 and K_y represent the pre and post-yield stiffnesses exhibited by the structure. The hysteretic behaviour of this structure is illustrated in Figure 3.4. In this figure the x -axis is a measure of the deformation or strain while the y -axis represents the force or stress carried in the damper. The yield force characteristic of the brace is found on the diagram where the projection of the post-yield line intersects the force axis (at zero displacement).

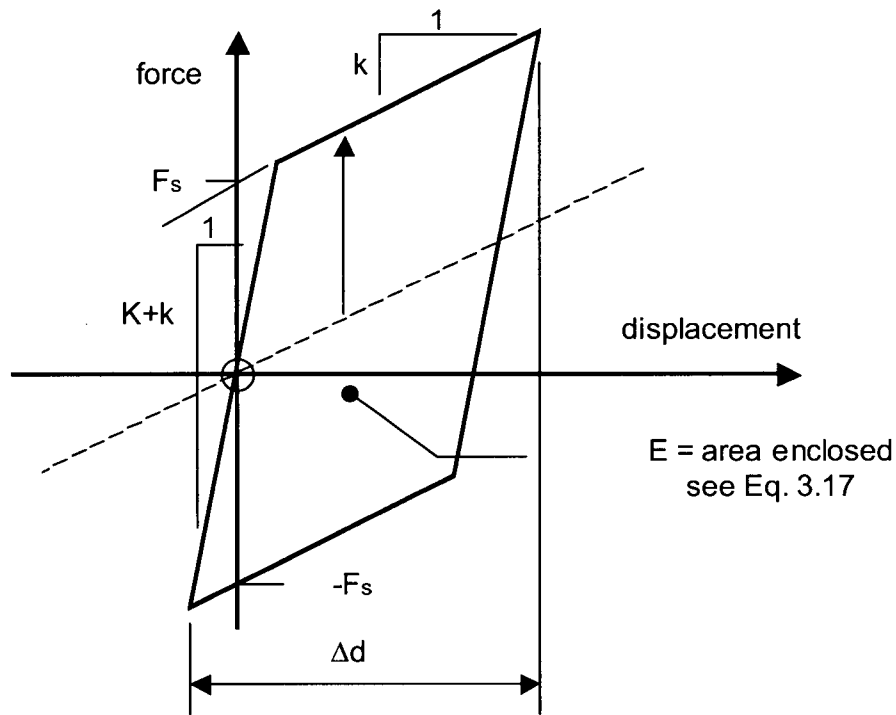


Figure 3.4. Bilinear hysteresis.

Upon initial loading, the force rises linearly with displacement at a slope of K_0 until the slip force of the damper is reached. After this, the device begins to slip, and while slipping the brace carries a constant force. The post yield line rises with slope K_y .

At the end of the stroke, the direction of deformation changes. At this point slipping/yielding stops and the force begins to unload along a line with the same slope as the initial loading, K_0 . When the force falls to the level of the dashed line, the force in the brace and damper is zero, but a restoring force is still present due to the force of the structural frame. As the deformation continues in the opposite direction the damper and brace element continue to pick up force until

the slip load in the opposite direction is reached. The total deformation experienced by the brace following the reversal in direction is twice the yield deformation.

The area enclosed by the hysteresis loop traced after deforming one full cycle indicates the amount of energy dissipated. Based on a total deformation cycle Δd , the amount of energy dissipated can be calculated by the formula

$$E = 2F_s \left(\Delta d - \frac{2F_s}{K} \right), \quad \Delta d > \frac{2F_s}{K} \quad (3.17)$$

If the amplitude of the deformation $\Delta d < 2F_s/K$, then the area enclosed by the hysteresis loop is zero and no energy is dissipated. One can see that the brace flexibility is detrimental to the ability of the system to dissipate energy when the deformations are small. It is possible that if the brace is too flexible with respect to the expected deformations, the damper may not slip. In this case, the system would be unable to dissipate energy.

3.3.3. Modelling One-Step Memory in State-Space

Modelling a structure with a bilinear hysteretic damper requires one additional variable (per damper) to be included in the state vector to track the elastic and plastic deformation in the damper. The chosen variable can be either the elastic (brace) or the plastic (damper) deformation. In this derivation, the elastic deformation, e , is used. The state variables are $[d \quad \dot{d} \quad e]^T$. Based on these variables it is possible to uniquely determine the damper force. The diagram in Figure 3.5 illustrates the algorithm for determining the state of the damper and then evaluating the force. Assume that the slip or yield load is indicated by the variable u_c and the brace stiffness K .

Given that the previous state was known and a new estimate of the state has been generated. The first step is to check the quantity e . If

$$-\frac{u_c}{K} < e < \frac{u_c}{K} \quad (3.18)$$

then the damper is not slipping and the damper force in the current state is given by

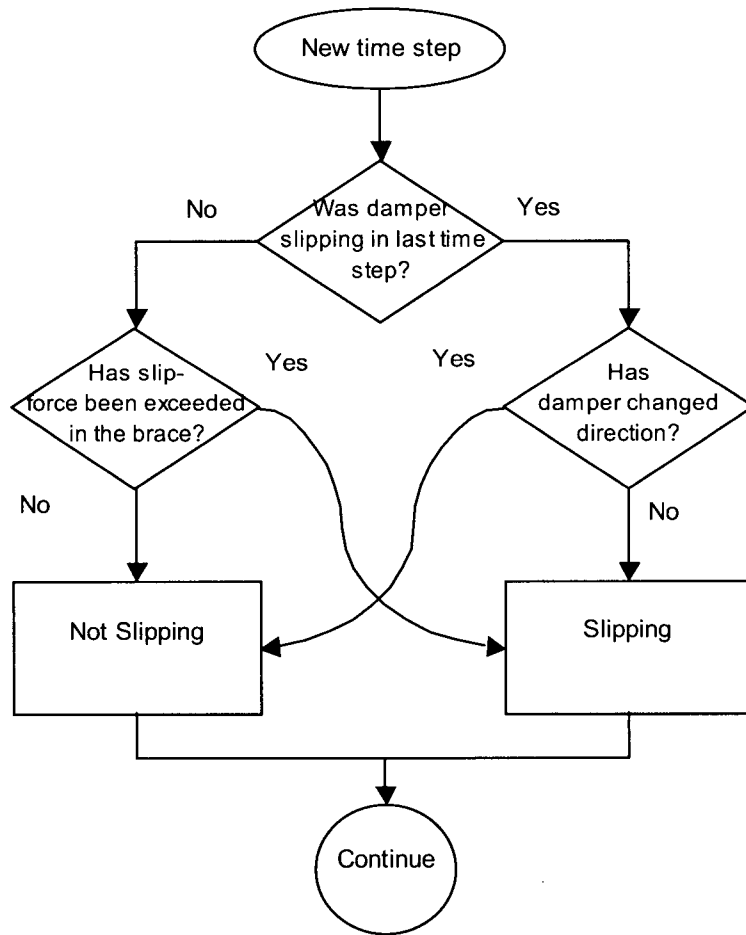


Figure 3.5. Decision tree for analysing bilinear hysteretic system in state-space.

$$u = Ke \tag{3.19}$$

in this state the differential of the state vector satisfies

$$\dot{e} = \dot{d} \tag{3.20}$$

However, if Equation 3.13 is not satisfied and $e > u_c/K$, then

$$u = u_c \text{ and } \dot{e} = 0 \tag{3.21}$$

and if $e < -u_c/K$, then

$$u = -u_c \text{ and } \dot{e} = 0 \tag{3.22}$$

Practically in analysis the checks above produce accurate results only if extremely small time steps are chosen. Inaccuracies result from the effect of overshooting of the specified slip load. These effects can be corrected for, but the correction algorithms are beyond the scope of this treatment of the subject.

3.3.4. Variable Slip Force Semi-Active Friction Damper

If the slip load arises from a variable slip force friction damper, the system is referred to as a semi-active friction damper (SAFD). With a variable slip force, the evaluation of the state of the damper becomes more complicated. The decision process is described in Figure 3.6. Two parameters are required, $u_s(t)$ and $\dot{u}_s(t)$ representing the time varying slip force which may, at times, differ from the damper force $u(t)$. The check depends on these variables and the state of the previous step. As with the bilinear constant slip force friction or hysteretic damper, one additional variable, in this case chosen as the elastic brace deformation, needs to be carried to identify the state of the system.

The first check performed establishes whether the damper is sliding or not and in which direction. If the damper was previously sliding, this check establishes if the sliding continues or is stopped. If the damper continues to slide, the brace force will be equal to the slip load (or minus the slip load) at the current time step. Sliding will stop if the rate of increase of the slip force exceeds the rate of deformation

$$\frac{\dot{u}_s}{K} > \dot{d} \quad \text{or} \quad -\frac{\dot{u}_s}{K} < \dot{d} \quad (3.23)$$

for forward or reverse slippage, respectively. Otherwise, sliding continues. When sliding continues $\dot{e} = \frac{\dot{u}_s}{K}$ and $u = \pm u_s(t)$ where the sign is taken consistent with the sliding direction and u represents the effective force of the damper and brace.

If the damper is not sliding,

$$u = Ke \quad \text{and} \quad \dot{e} = \dot{d} \quad (3.24)$$

Sliding will commence if

$$u > u_s \quad \text{or} \quad u < -u_s \quad (3.25)$$

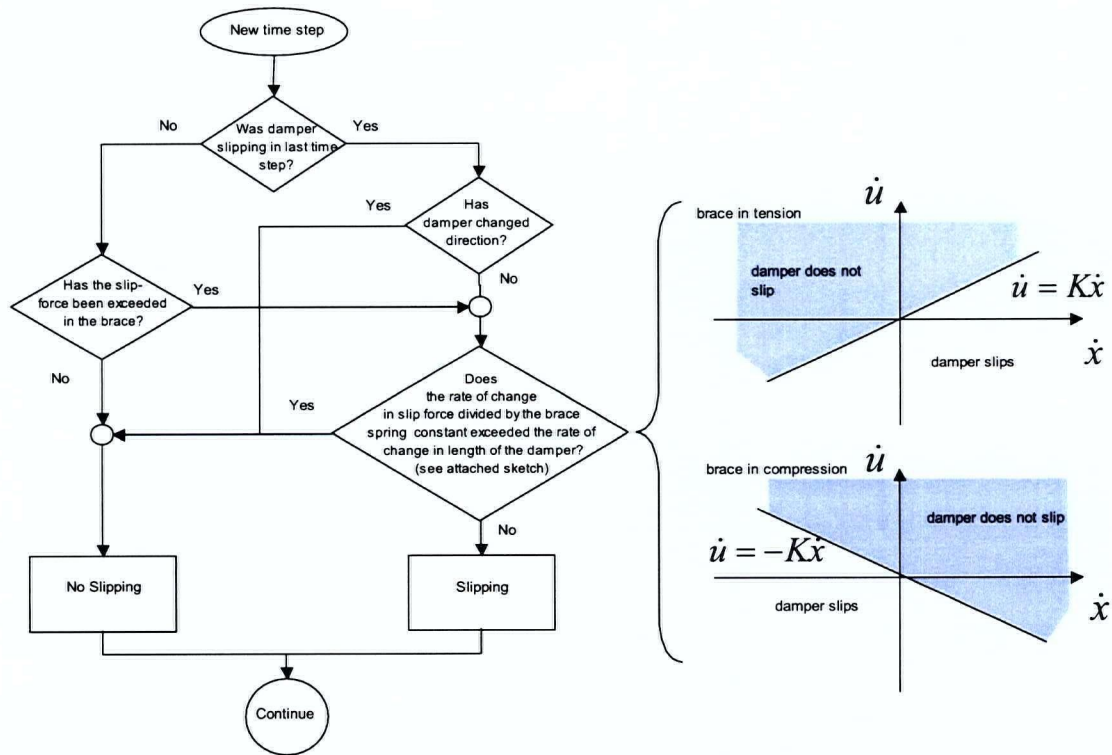


Figure 3.6. Decision tree for evaluating slip load in a variable slip force friction damper.

in the forward and reverse directions respectively, providing conditions that stop sliding are not met simultaneously.

3.3.5. Off-On Friction Damper

The off-on semi-active friction damper is similar to the CSFD except that at the point of direction reversal, the elastic force in the brace is set to zero, which implies a rapid drop in slip load at this point in time.

Implementing the algorithm can be accomplished by providing a variable slip load limited to the minimum of either the absolute value of a velocity feedback with a sufficiently high gain, or a preset constant slip load. When the structure reverses deformation direction, the velocity will change sign by passing through zero. At this instant, the clamping force on the slip surface will be zero and any elastic force in the brace will be released. The objective of this process is to fatten as far as possible the hysteresis loops thereby maximizing the amount of energy that can be dissipated by the system.

Figure 3.7 is an interesting comparison of hysteresis loops extracted from simulation data. In these plots both time history data and corresponding hysteresis loops are compared. Figure 3.7(a) shows the CSFD. Note that $K_y=0$ because the plots are of the damper in isolation, rather than the damper plus structure as shown in Figure 3.4. The imperfect precision of the calculation has led to some overshooting of the slip load. The off-on time history plot in (b) shows the form of the time history plot in more detail. The thin solid line represents the programmed slip load and its negative trace dropping to zero at critical times during the response. The line with markers represents the brace/damper force time history obtained. After dropping the slip load to zero, it seems to take considerable time before the brace load builds up. The result on the hysteresis loop is dramatic, substantially increasing the amount of energy dissipated per cycle. Figure 3.7(c) illustrates a continuously variable SAFD with three traces. The medium weight solid line represents the force that would be imparted to the structure if an active control was being implemented while the thin line represents its negative. The brace force time history shows some of the same characteristic of the off-on brace time history in which the brace takes some time to build up brace load after a reversal in sign of the slip load, but otherwise always seems to be trying to mimic the active control force.

3.3.6. Phase Plane Analysis of Off-On and CSFD Damped Structures

Phase plane analysis is a useful tool for visualising the behaviour of a SDOF structure. It is essentially a plot of the trajectory of the state vector of the structure as it moves and deforms with the x -axis representing its displacement and the y -axis representing its velocity. The target of the control is to bring the structure to rest at the origin where it has both zero deflection and zero displacement.

Figure 3.4 shows the hysteresis loop of a single degree of freedom structure containing a bilinear hysteretic damper. Phase plane analysis is complicated by the fact that two stiffnesses need to be incorporated into the analysis; one representing the elastic or non-slipping state, and one representing the sliding or yielding phase of the response. The steep slope of the hysteresis loop represents the interval where the dampers are not sliding. In this interval the stiffness of the structure is the sum of the stiffness of the brace supporting the damper and the stiffness of the structure's frame. The lesser slope corresponds to the intervals where the damper is sliding. In this interval the damper force does not vary due to the sliding/yielding mechanism. The essential models for the not-sliding (stick) and sliding (slip) phases are illustrated in Figure 3.8.

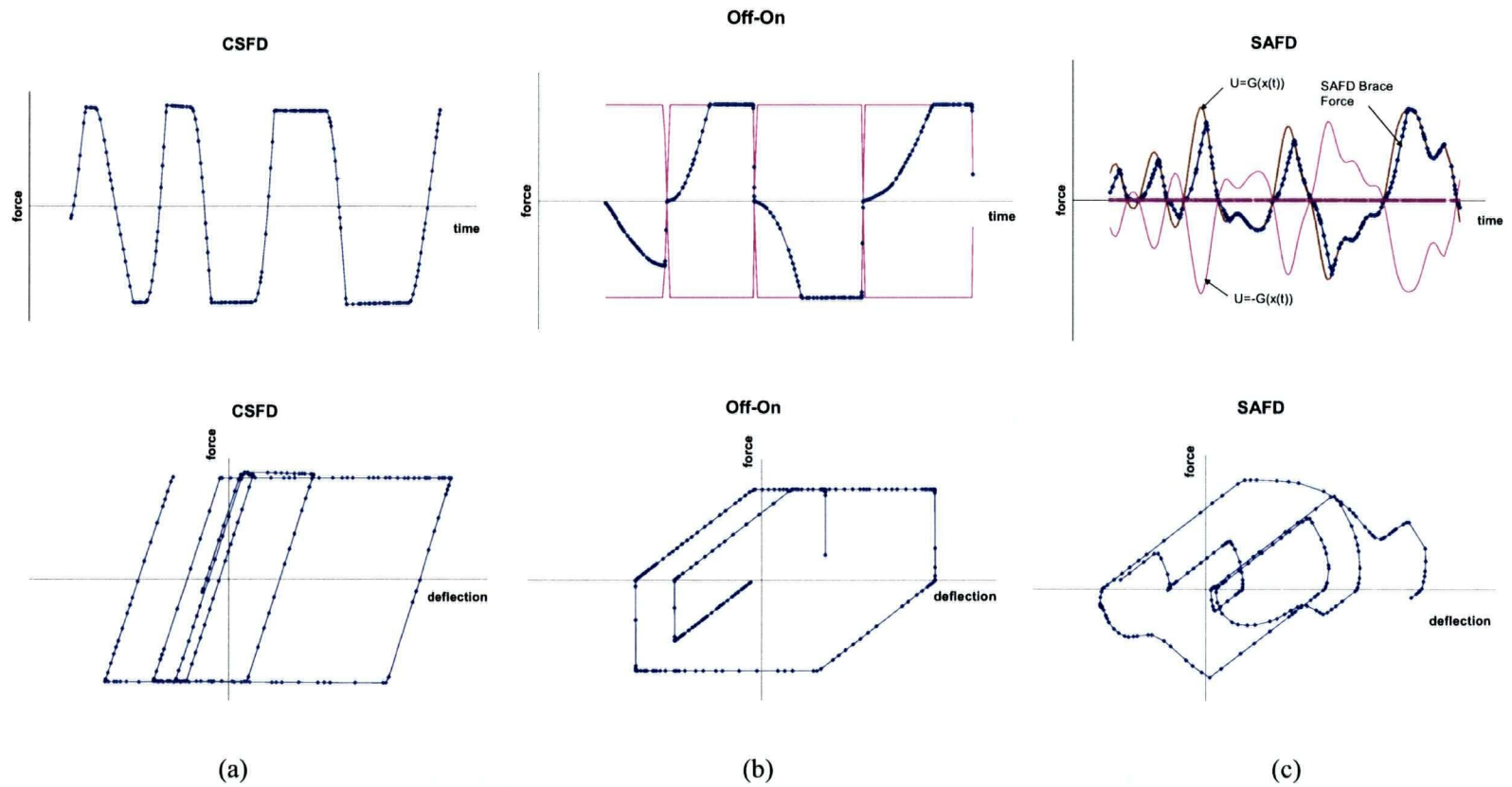


Figure 3.7. Comparison of time history traces and hysteresis loops produced by (a) a friction damper; (b) an Off-on semi-active friction damper and (c) a Semi-active variable slip force friction damper (SAFD).

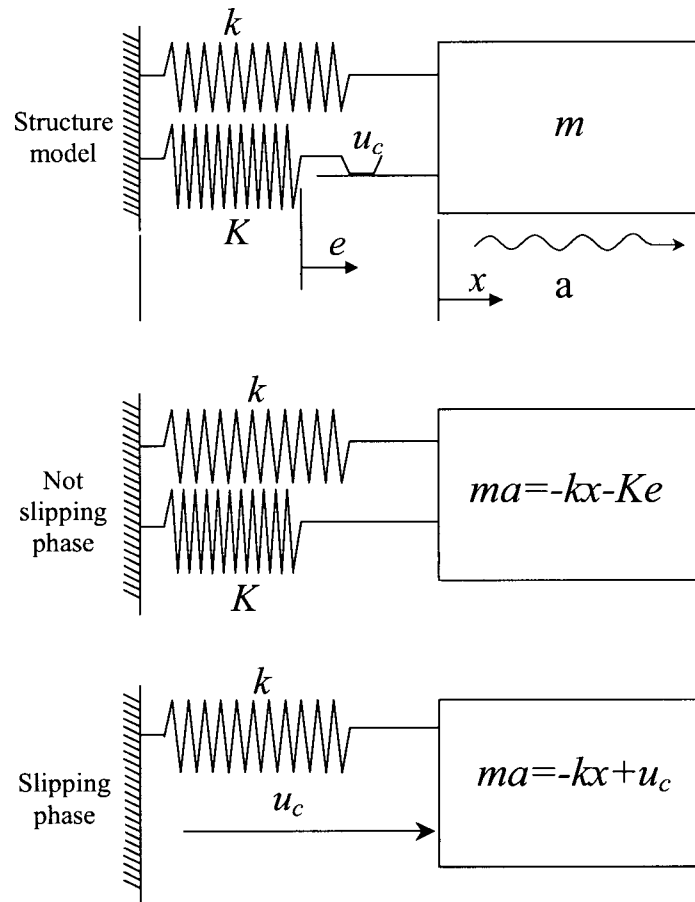


Figure 3.8. Models for the sliding and non-sliding phases of response of a bilinear hysteretic damper.

As the structure oscillates, the effective stiffness oscillates from that for the not-sliding (stick) state to that for the sliding (slip). Therefore, in the phase plane, two characteristic curves need to be used to describe the behaviour of the structure.

The curve associated with the undamped oscillation of a mass and spring forms an ellipse centred on the origin. The aspect ratio of the ellipse is such that the kinetic energy at zero displacement $\frac{1}{2}mv^2$ is equal to the potential energy contained in the spring at maximum displacement (zero velocity). The curve associated with a spring and mass plus a sustained force, u , is an ellipse with the centre shifted along the displacement axis in the direction of the force by

a displacement equal to u_c/k_{eff} . For a structure with a bilinear hysteretic damper, three possible families of ellipses can be chosen

- 1) centre: $d_c = \frac{Kd_0 - u_c}{k + K}$, effective stiffness: $k_{eff} = K + k$
- 2) centre: $-u_c/k_{eff}$, effective stiffness: $k_{eff} = k$ (forward movement)
- 3) centre: $+u_c/k_{eff}$, effective stiffness: $k_{eff} = k$ (reverse movement)

In order to construct a plot it is necessary to determine the locations at which the response switches between each of the above response curves. Curves 2 and 3 represent the slip state in either of the forward or reverse directions of movement. The transition from slip to stick states always occurs when the velocity of the mass passes through the displacement axis (zero velocity). Assuming that the zero crossing occurs at d_0 the updated centre of the ellipse is d_c computed as shown above where K is the stiffness of the brace, k is the stiffness of the structure and u_c is the slip load. Therefore the trace will always depart from the displacement axis on curve (1). The transition from the stick to the slip state, curve (1) to either (2) or (3) will occur when the brace force has exceeded the differential displacement $\Delta = u_c/K$ necessary to initiate slip in the ideal friction slider. Figure 3.9 shows a typical trace for a structure with zero displacement and initial velocity at time zero.

One of the problems with the constant slip force friction damper is the final state. The desirable final state for the structure is with the trajectory to end at the origin of the phase plane. This point is the zero energy state with no residual deformation. The friction damper in general will not reach the zero energy state. Instead the structure will end with an oscillating trajectory about some point within the bounds of $\pm u_c/2K$, illustrated in Figure 3.10.

A bilinear hysteretic damped single degree of freedom (SDOF) structure has an idealized response that is similar in character to the bang-bang control. It is particularly so when the brace stiffness of the hysteretic damper is high enough to neglect the initial elastic deformations (Curve 1 in Figure 3.9). For the most part, the dampers act with a constant restoring force to oppose the velocity of motion of an excited structure with switching times at zero velocity times.

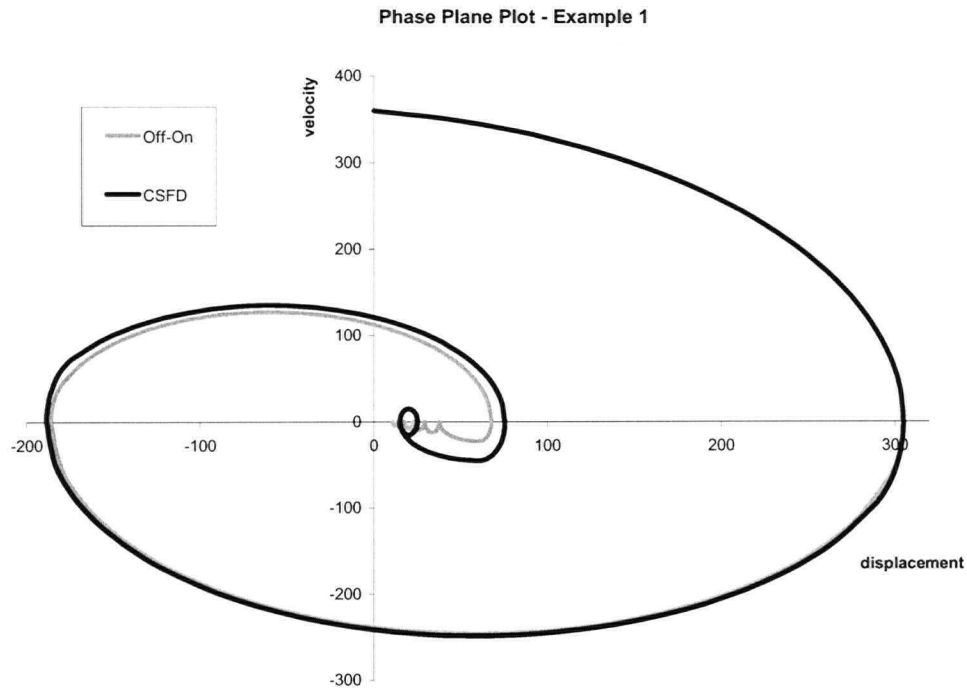


Figure 3.9. Phase plane plot of a structure excited by an impulse with a weak control.

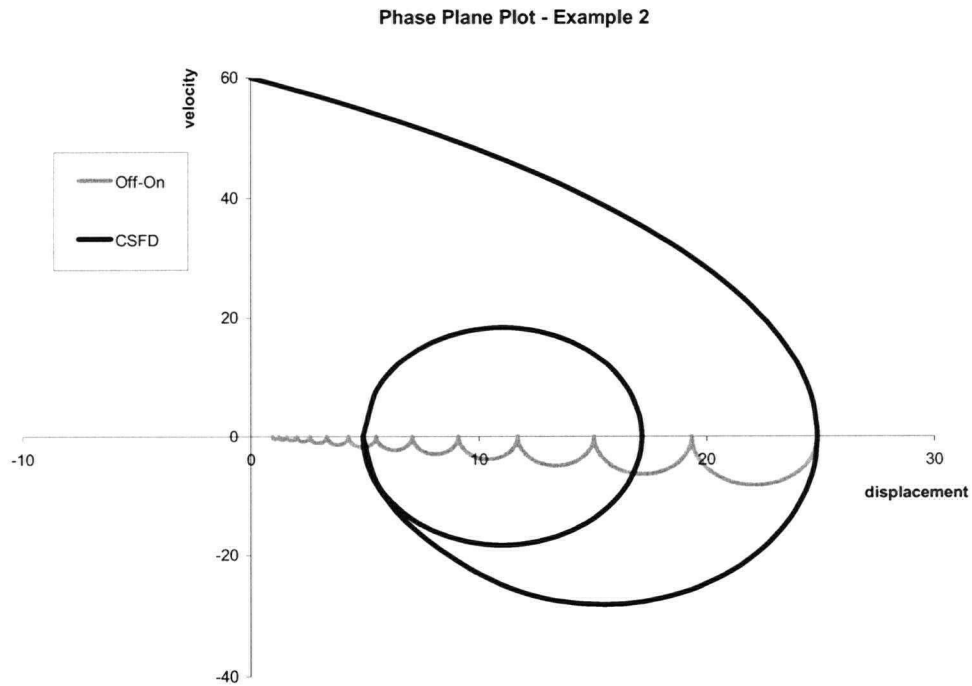


Figure 3.10. Phase plane plot of a structure excited by an impulse with a strong control. The CSFD case ends in a cyclic oscillation while the off-on control gradually moves towards the zero state.

3.4. Design of SDOF Viscous Damped Structures

3.4.1. The Ideal Viscous Damped Structure

In order to illustrate some important characteristics of a linear damped system, the case of an ideal viscous damped structure is first considered. If the underlying structure is linear, the viscous damped structure is linear providing that the damper forces are directly proportional to the velocities. Figure 3.1 (a) and (b) illustrate the single degree of freedom viscous damped structures upon which the analysis is based. In Figure 3.1(a) the structure has an ideal viscous damper rigidly connected in the frame, while in (b) the damper is held by a flexible brace. The presence of flexibility in the brace in Figure 3.1(b) degrades the performance of the structure but it is assumed that it cannot be avoided.

The DAF of the SDOF structure in Figure 3.1(a) has a well-known classical solution that is easily derived. Figure 3.2 illustrates the family of transfer functions, the shape of which is easily derived using Laplace transforms. Writing the equation of motion for a single degree of freedom structure

$$m\ddot{x}(t) + c\dot{x}(t) + kx(t) = -m\ddot{x}_g(t) \quad (3.26)$$

Taking the Laplace transform yields the following expression

$$ms^2 X(s) + csX(s) + kX(s) = -mX_g(s) \quad (3.27)$$

that can be solved for $X(s)$ yielding

$$X(s) = \frac{-mX_g(s)}{ms^2 + cs + k} = \frac{-X_g(s)}{s^2 + 2\omega_0\xi s + \omega_0^2} \quad (3.28)$$

where $\omega_0 = \sqrt{k/m}$ is the undamped natural frequency of the structure and $c/m = 2\omega_0\xi$. The parameter ξ indicates the structure's inherent damping as a fraction of critical damping. The structures inherent damping has not been shown in Figure 3.1 but a nominal damping ratio has been included in the assessment of the transfer functions. Substituting $s = i\omega$ and evaluating the magnitude of $TR(\omega) = |H(\omega)|^2 = |X(i\omega)/X_g(i\omega)|^2$ yields for the transfer function

$$TR(\omega) = |H(\omega)|^2 = \left| \frac{X(i\omega)}{X_g(i\omega)} \right|^2 = \left| \frac{1}{(\omega_0^2 - \omega^2) + 2i\omega_0\xi\omega} \right|^2 = \frac{1}{(\omega_0^2 - \omega^2)^2 + (2\omega_0\xi\omega)^2} \quad (3.29)$$

For the structure shown in Figure 3.1(b), the same steps can be used to evaluate the transfer function for the case where an additional brace and spring are present. Given that the spring and damper are in series it can be observed that the spring and damper experience deformations that must sum to equal the deformation of the structure. This is expressed as follows.

$$x = x_s + x_d \quad (3.30)$$

where given x_s is the deformation of the spring and x_d the deformation of the damper. In addition it can be observed that the force in the brace is equal to the force in each of the components

$$f_{brace} = Kx_s = C\dot{x}_d \quad (3.31)$$

where K and C respectively represent the spring constant and the damping coefficient of the brace element. Defining $r = C/K$ Equation 3.31 can be expressed in terms of the damper deformation alone

$$x = x_d + r\dot{x}_d. \quad (3.32)$$

The quantity r carries the units of time and expresses the decay rate associated with deformation of the brace alone. The equation of motion can be expressed as

$$\ddot{x}(t) + 2\xi\omega_0\dot{x}(t) + \omega_0^2 x(t) + \frac{C}{m}\dot{x}_d(t) = -\ddot{x}_g(t) \quad (3.33)$$

including the additional brace force as a function of the damper velocity. The parameters ω_0 and ξ are as defined in Equation 3.29. Taking the Laplace transform of Equation 3.33 yields the expression

$$X(s) \left[s^2 + 2\xi\omega_0 s + \omega_0^2 + \frac{Cs}{m(1+rs)} \right] = -X_g(s) \quad (3.34)$$

and, similarly, evaluating the transfer function yields

$$TR(\omega) = \left| \frac{1}{(\omega_0^2 - \omega^2) + i2\xi\omega\omega_0 + \frac{iC\omega}{m(1 + ir\omega)}} \right|^2 \quad (3.35)$$

The family of transfer functions for the structure in Figure 3.1(b) shown in Figure 3.10 differs from the shape of the curves shown in Figure 3.2 by the inclusion of a second peak in the frequency domain. When the damping value C becomes large, the damper will provide a high resistance to any imposed deformation. The response will therefore be dominated by the elastic response of the brace. The frequency of the second peak is determined by the frequency of the structure with the added stiffness of the brace.

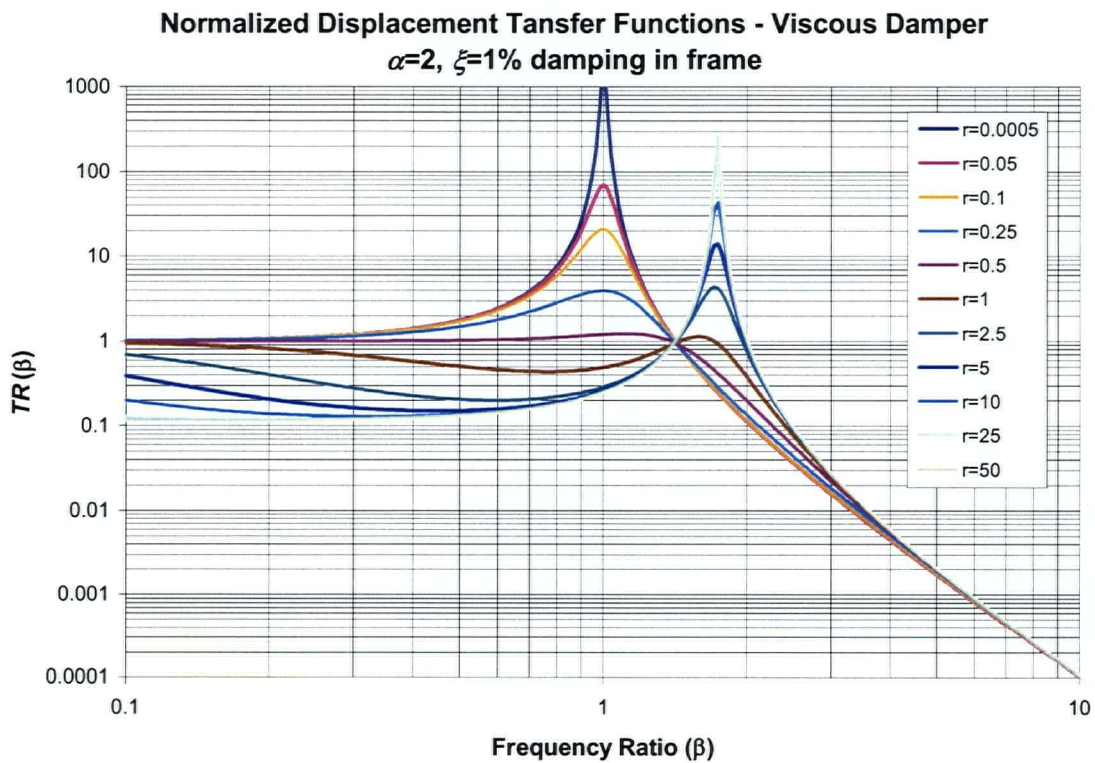


Figure 3.11. Family of transfer functions for viscous damped structure with flexible brace.

3.4.1.1. Evaluation of RMS Response

When subjected to an ideal white noise of unit intensity, the RMS response can be derived as the area under the transfer function curve. Evaluating this integral, one can plot the maximum inter-story drift vs. the damping coefficient. Figure 3.12 shows the family of curves for the transfer functions shown and for the case where the brace stiffness ratio with the structure varies. It is notable that the minimum value of the RMS drift always occurs for a damping ratio with parameter $r = 1/\omega_0$.

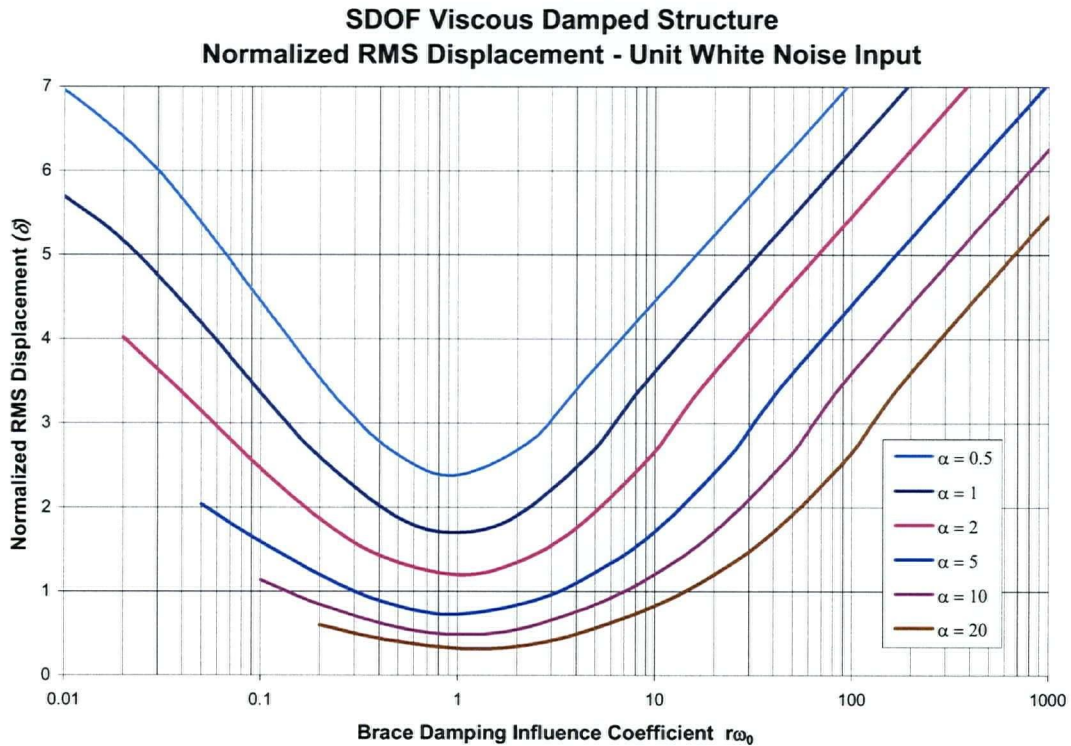


Figure 3.12. Normalized RMS displacement for viscous damped structure with flexible brace.

The important points illustrated by the discussion above include the following:

- 1) There is an optimum damping value for the given input when the brace stiffness is taken into account
- 2) The ideal performance is independent of the magnitude of the load (property of a linear system)

Extending the concept of optimal performance of viscous dampers in general to multi degree of freedom structures would be a very interesting course of study. This study, however, is beyond the scope of this thesis.

3.5. Design of SDOF Friction Damped Structures

To this point the discussion has been directed towards modelling of the SDOF structure with a friction damper for analysis in the time domain. Because of the non-linear character an analytical solution for the frequency response function is not accessible as it was shown for the structure containing a viscous damper. Characterizing the frequency response, however, is desirable in order to provide information to assist in designing of structures with friction dampers. The frequency response of a SDOF structure was evaluated three different ways:

1. Time history analysis using sinusoidal input
2. Analysis using an energy balance approach
3. Fourier spectrum analysis of input and response time history functions.

The following sections are devoted to describing the methods used in each of the above analyses and discussing the results obtained.

In an effort to make the work more general, the response is cast in a non-dimensional form using the following variables

$$\alpha = \frac{K}{k} = \text{brace stiffness ratio} \quad (3.36)$$

$$\beta = \frac{\omega}{\omega_0} = \text{frequency ratio} \quad (3.37)$$

$$\gamma = \frac{u_c}{ma_{rms}} = \text{slip force ratio} \quad (3.38)$$

$$\delta = d \frac{\omega_0^2}{a_0} = \text{drift ratio} \quad (3.39)$$

$$\tau = \omega_0 t = \text{time ratio} \quad (3.40)$$

where $\omega_0 = \sqrt{k/m}$ is the undamped natural frequency of the unbraced frame. The quantity a_0 can be taken as the RMS lateral base acceleration of the input disturbance a_{rms} or the amplitude of a harmonic excitation a_{max} depending on the purposes of the investigation. The variable d may represent the time history of the story drift response or the amplitude of a steady state sinusoidal response. The variables ω and t are frequency and time variables respectively.

3.5.1. Sinusoidal Input

It is recognised that a structure can be subjected to loadings having both narrow band and wide band frequency content. Initial studies of the characteristic response of bilinear hysteretic structures to sinusoidal input were carried out using a combination of analytical and time history analysis. The initial objective was to provide a basic understanding of the character of structural response to harmonic loads. It is important to provide a distinction between transient and steady state loads. Transient loads occur early in the application of the load and cover the period until the response of the structure settles down to a response that is repeats each cycle. Although transient loads were observed, they were not explicitly studied. As transients dominate the response to earthquakes, there appears to be significant room to expand the understanding in this area. This problem was previously investigated by Caughey and Stumpf (1961) and many other researchers.

The main analytical effort was to determine the steady state frequency response of the generalized structure. The procedure used was based on matching of energy dissipated per cycle and displacements.

3.5.2. Frequency Response with Equivalent Viscous Damping

An iterative solution for determining the frequency response of a structure fitted with friction dampers was attempted. The work is discussed in Dowdell and Cherry (1994) using the non-dimensional form as described above. Once established, the theoretical associated transfer function was subsequently used to predict the optimal slip load of a structure subjected to a white noise time history, and this was compared to numerical results obtained from time history analysis.

3.5.2.1. Theoretical Derivation

Since the friction damper restoring force is non-linear, an exact analytical solution of the transfer function of a structure containing this element was not attempted. Instead, the friction damper was modelled using an equivalent viscous damper and an iterative solution was used to find the most likely form of the function.

Given a friction damper is to be modelled by a viscous damper, with this approach, two conditions are assumed to establish equivalence

- i. The energy dissipated in one cycle be equal
- ii. The displacement of each cycle be equal

The energy dissipated per cycle in friction damping is given by the expression

$$E_f = 4u_c \left(d - \frac{u_c}{K} \right) = 4\gamma \left(\delta - \frac{\gamma}{\alpha_f} \right) \frac{m^2 a_0^2}{k} \quad (3.41)$$

where δ and $a_0 = a_{\max}$ represent the drift ratio and the base acceleration amplitude, respectively.

The non-dimensional variable $\alpha_f = K/k$ represents the ratio of the brace stiffness to the structure stiffness. The cyclic energy dissipated in viscous damping is given by the expression

$$E_v = \pi \omega d_v^2 C = \pi \frac{\delta^2 \alpha_v \beta r}{r^2 + \beta^2} \frac{m^2 a_0^2}{k} \quad (3.42)$$

Setting the areas equal yields the energy balance equation

$$4\gamma \left(\delta - \frac{\gamma}{\alpha_f} \right) - \pi \frac{\delta^2 \alpha_v \beta r}{r^2 + \beta^2} = 0 \quad (3.43)$$

The displacement of the friction damper, δ_f , expressed in non-dimensional variables is

$$\delta_f = \delta - \frac{\gamma}{\alpha_f} \quad (3.44)$$

while the corresponding viscous damper displacement, δ_v , is

$$\delta_v = \delta \frac{r}{\sqrt{r^2 + \beta^2}} \quad (3.45)$$

leading to the displacement condition

$$\delta - \frac{\gamma}{\alpha_f} - \frac{\delta r}{\sqrt{r^2 + \beta^2}} = 0 \quad (3.46)$$

Solving for γ and substituting the result into the energy balance equation establishes a relationship between the stiffness of the equivalent viscous damper brace and the friction damper brace stiffness expressed as the ratio α_v as follows

$$\alpha_v = \frac{\alpha_f^4}{\pi\beta} \left(\sqrt{r^2 + \beta^2} - r \right) \quad (3.47)$$

The equivalent viscous damped transfer functions $T(\beta) = \delta^2(\beta)$ are evaluated for each chosen γ and β pair by finding the value of r that satisfies both the energy and displacement conditions in the following manner: (i) assume a trial value of r and evaluate α_v from Equation 3.47, then (ii) determine the drift ratio from the transfer function of the damped system by substituting the values of r , β and α_v in

$$\delta(\beta) = \frac{1}{\omega_0^2} \sqrt{z(\beta)z^*(\beta)} \quad (3.48)$$

where $z^*(\beta)$ is the complex conjugate of $z(\beta)$ and

$$z(\beta) = \frac{1}{1 + \alpha_v - \beta^2 + 2\xi\beta i - \frac{\alpha_v r}{i\beta + r}} \quad (3.49)$$

Next, (iii) use Equation 3.46 evaluate a new estimate for r . Steps (ii) and (iii) are repeated until the new estimate for r is equal to the estimated value. When the values of r agree, the equivalent viscous damped system is found and the calculated non-dimensionalized drift $\delta(\beta)$ is then the amplitude of the response at the chosen frequency, and for the chosen slip load.

3.5.2.2. Results

The preceding procedure was carried out for 5 brace stiffness ratios, $\alpha = \alpha_f = 0.5, 1, 2, 3$ and 5 . Frequency ratios were chosen over a range so as to capture the characteristic of the frequency response. Slip force ratios (γ) were also chosen to cover a practical range from 0.1 to 5.0 . Figures 3.13 to 3.17 show the resulting curves for each of the brace stiffness ratios. In general, the curves follow the expected trend: As the slip load increases, the shape transitions from the shape of the unbraced response to that of the fully braced response. Theoretical envelope curves for the case of the fully braced and unbraced structure are superimposed over the data. For intermediate and high slip loads, $\gamma=0.8$ and greater, at $\alpha=2$, the family of curves exhibits a discontinuity where the frequency response curve deviates from a curve approximating the fully braced case and rises to a value at or slightly above the unbraced case. This is not surprising as it represents the shift from the state where the forces are insufficient to allow slip to a state where the response is dominated by slipping of the friction damper. At frequencies above this shift in state, the response attenuates rapidly before rejoining the downward slope of the amplitude curve approximating that of the fully braced structure.

The obtained curves were also compared to data obtained by sinusoidal excitation of the non-linear system. Figures 3.18 and 3.19 show the comparison for the obtained steady state values of displacement and brace force for $\alpha=2.0$. Overall the agreement was found to be acceptable, indicating that the analytical procedure used to establish the base curves appears to be acceptable. One interesting observation is that for frequencies greater than the braced frequency, the friction-damped amplitudes exceed the envelope somewhat. This perhaps results from the fact that the brace stiffness of the equivalent viscous damped structure is not necessarily equal to the brace stiffness of the friction damped structure upon which the analysis is based. The data obtained from numerical simulation, however appears to confirm that this apparent stiffness increase, although slight may be valid.

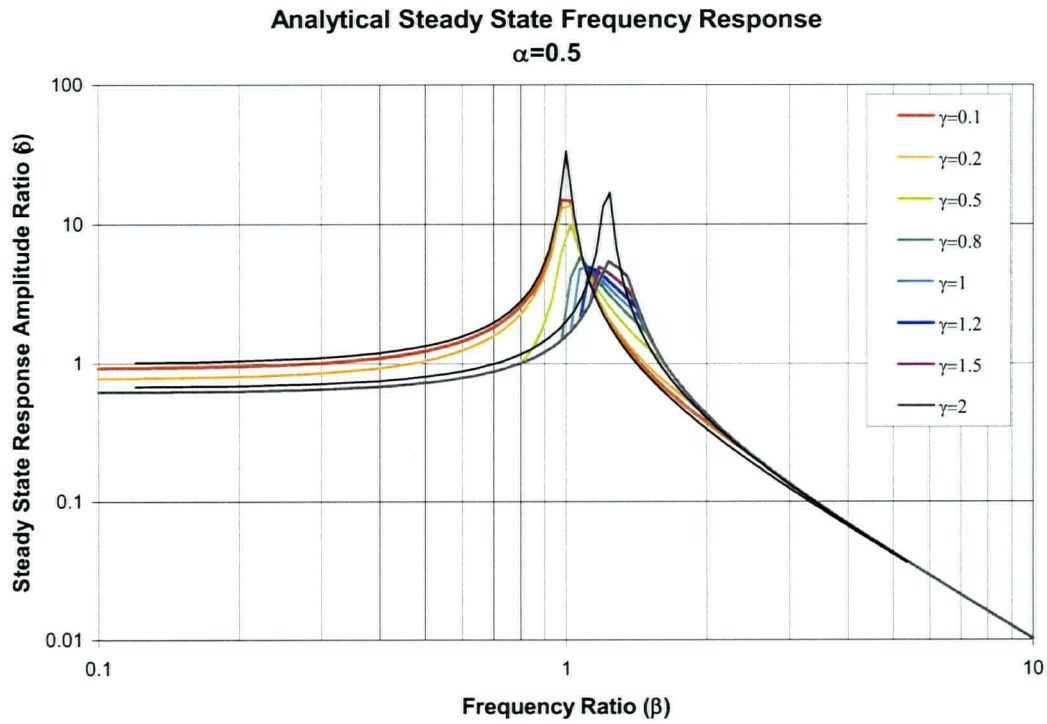


Figure 3.13. Steady state frequency response function friction damped structure $\alpha=0.5$.

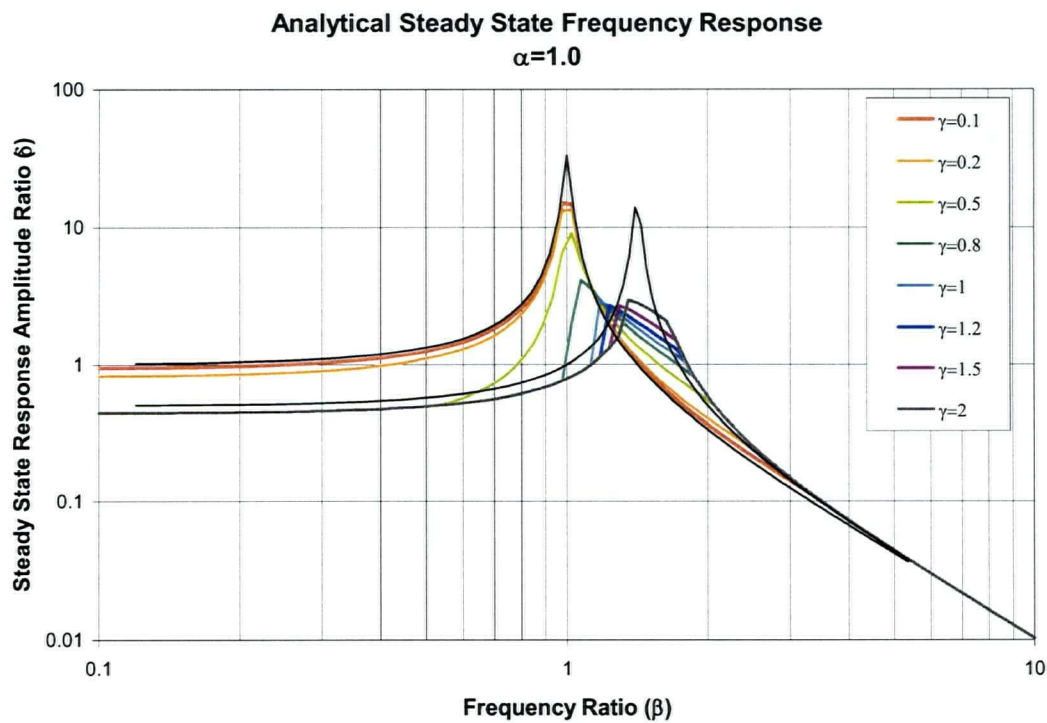


Figure 3.14. Steady state frequency response function friction damped structure $\alpha=1.0$.

Analytical Steady State Frequency Response $\alpha=2.0$

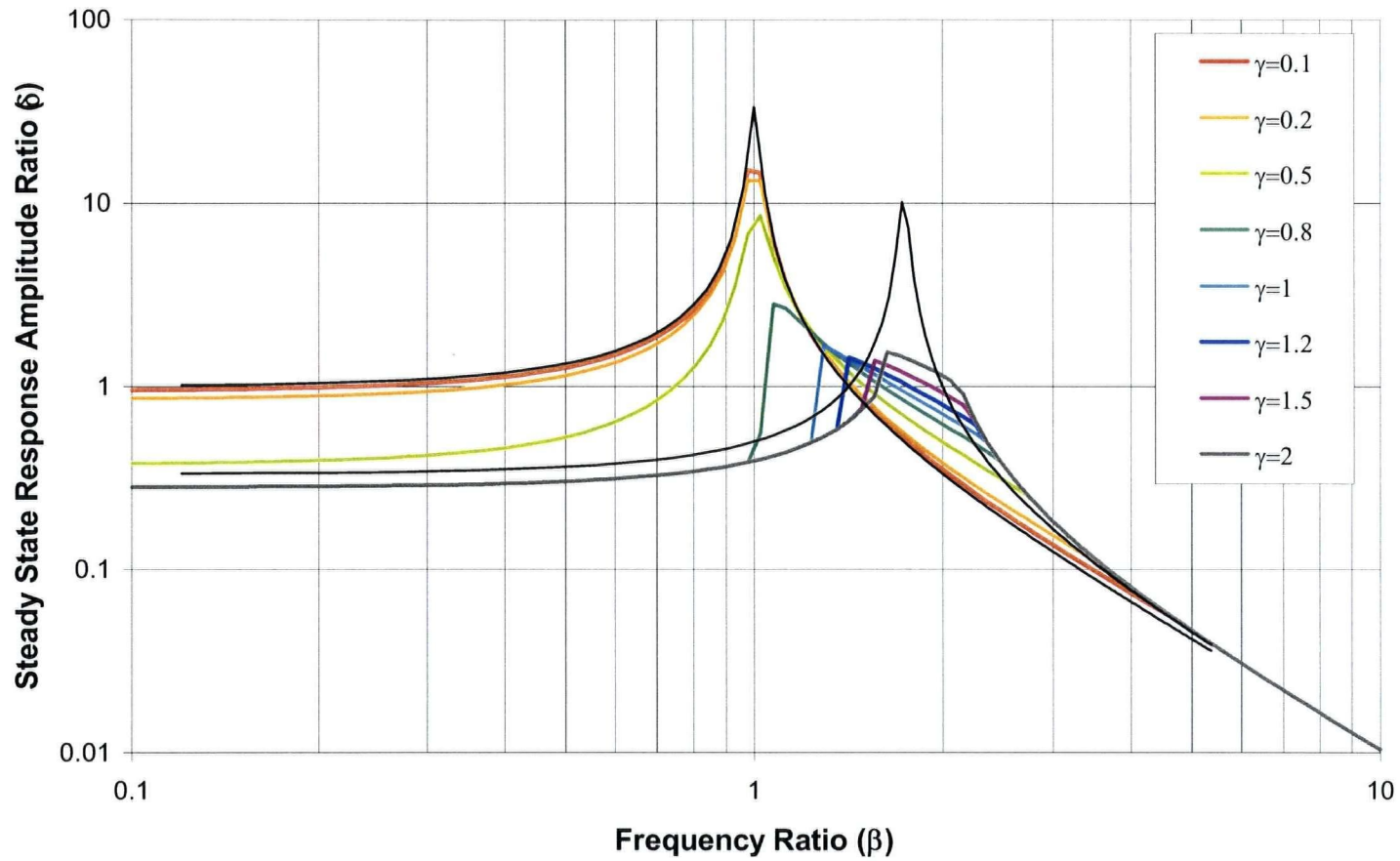


Figure 3.15. Steady state frequency response function friction damped structure $\alpha=2.0$.

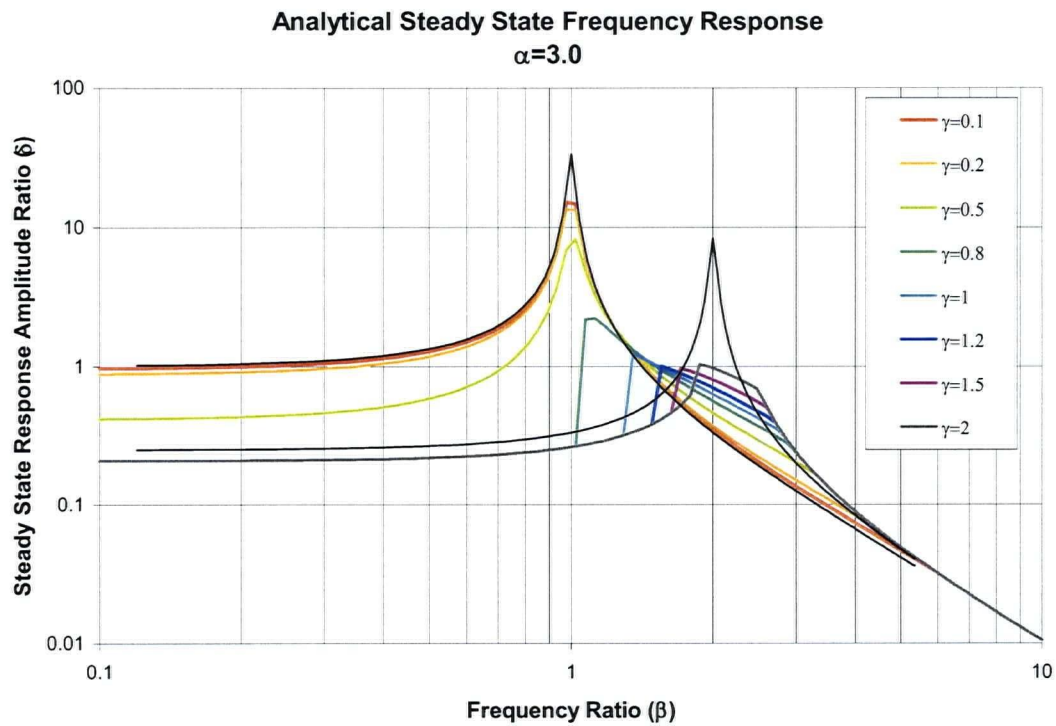


Figure 3.16. Steady state frequency response function friction damped structure $\alpha=3.0$.

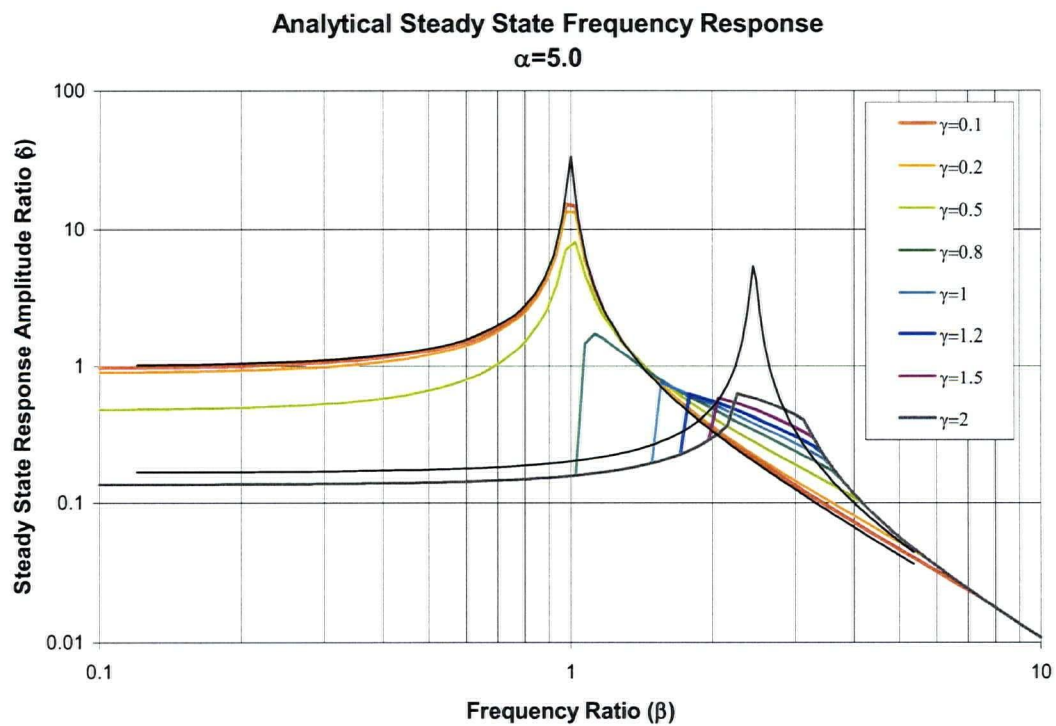


Figure 3.17. Steady state frequency response function friction damped structure $\alpha=5.0$.

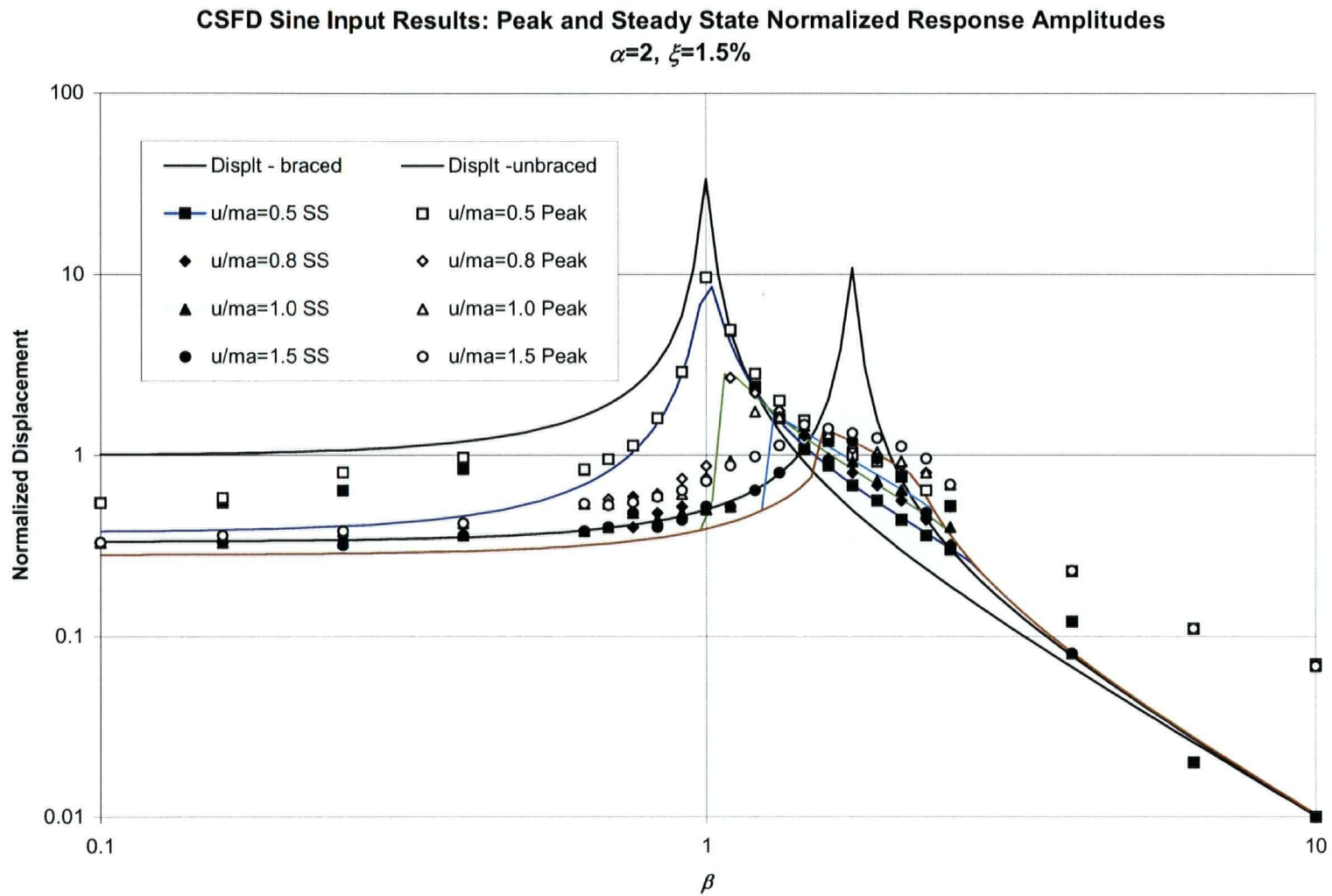


Figure 3.18. Comparison of steady state displacements amplitudes of a friction damped structure obtained from simulation data – sinusoidal input.

CSFD Sine Input Results: Peak and Steady State Base Shear Force
 $\alpha=2, \xi=1.5\%$

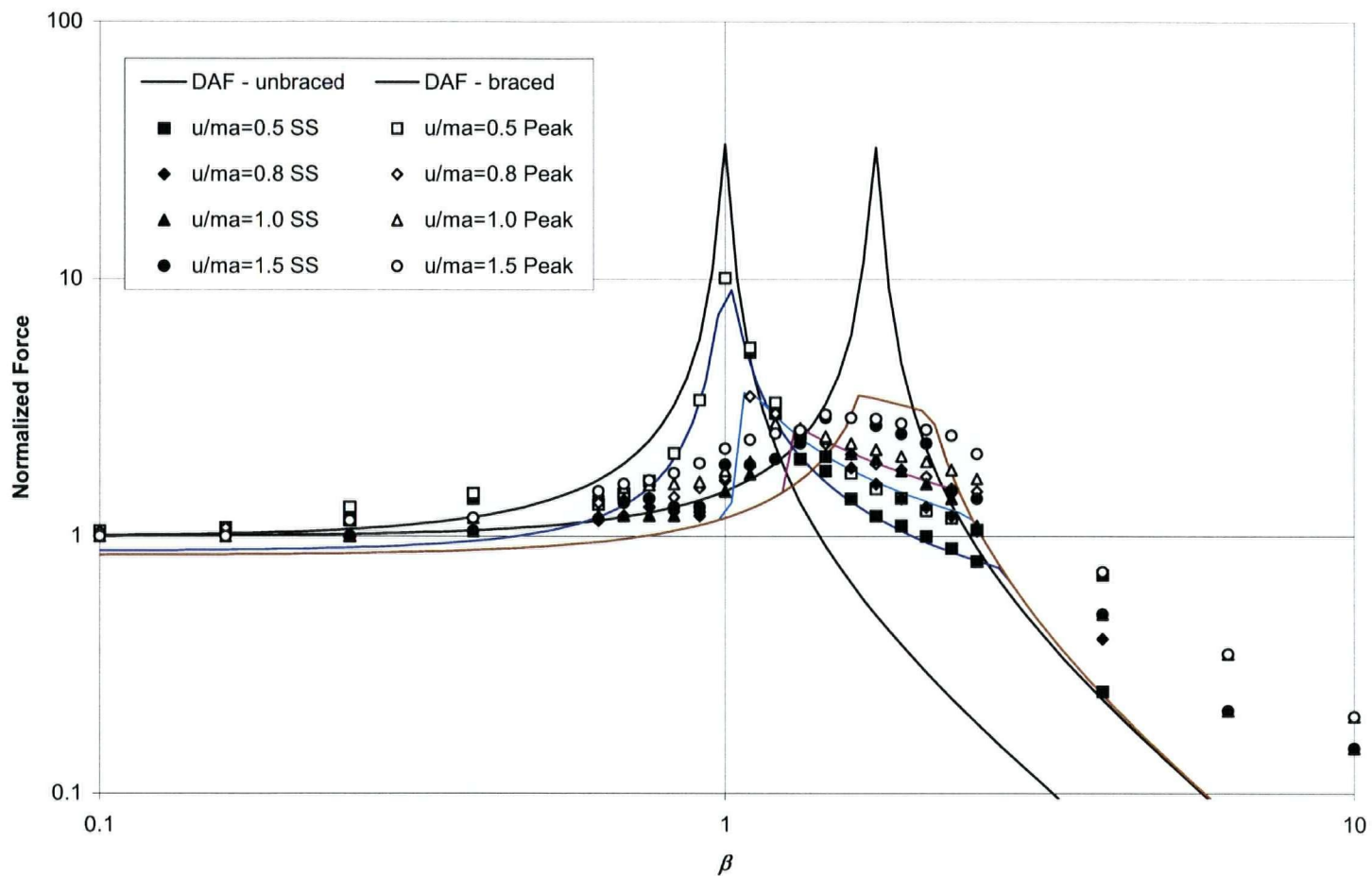


Figure 3.19. Steady state base shear data obtained from numerical simulation sinusoidal input.

3.5.2.3. Optimal Slip Load Prediction

An attempt was made to utilise the obtained set of transfer functions to predict the response amplitude when subjected to a random white noise excitation. The power spectral density of a white noise with a frequency cut-off ω_c is defined as

$$S_0 = \frac{a_{rms}^2}{2\omega_c} \quad (3.50)$$

The mean square drift ratio of a structure excited by this white noise is given by

$$\delta_{rms} = \sqrt{\frac{\omega_0}{\omega_c} \int_0^{\frac{\omega_c}{\omega_0}} T(\beta) d\beta} \quad (3.51)$$

This integration was carried out for a set of theoretical transfer functions corresponding to various slip load ratios. The curve for $\alpha = 2$ is shown in Figure 3.20. The predicted optimal slip load ratio was determined to be about 1.3. These results were compared to simulation data for a friction-damped structure having the same brace stiffness ratio. This data showed that the optimal slip ratio to be at about 0.8, significantly less than the value obtained using the theoretically derived curves. Interestingly, the minimum drift ratio obtained from the simulation data was about 0.5, a little larger than that predicted using the theoretical curves, but similar. It is also noted that the minimum drift is relatively flat between a slip load ratio of about 0.5 and 1.25, indicating that a high degree of accuracy is not generally necessary in predicting optimal slip loads. Slip loads taken in the range of plus or minus 40% about the optimal slip load were observed to produce similar RMS drifts.

The lack of fit between the theoretically predicted slip load and the RMS drift indicates that the theoretical procedure is unable to capture the essence of the response. One very important consideration not mentioned thus far is that the transfer function based analysis is inherently a linear analysis, and using curves established from a non-linear process is a violation of this basic assumption. It is also observed that the time history response to a harmonic input has a response that contains both a steady state and a time varying components. Some simulations with high frequency input indicated that the time varying component of the response can exceed and

Comparison Optimal Slip Load Prediction
Band Limited White Noise Input, $\alpha=2$

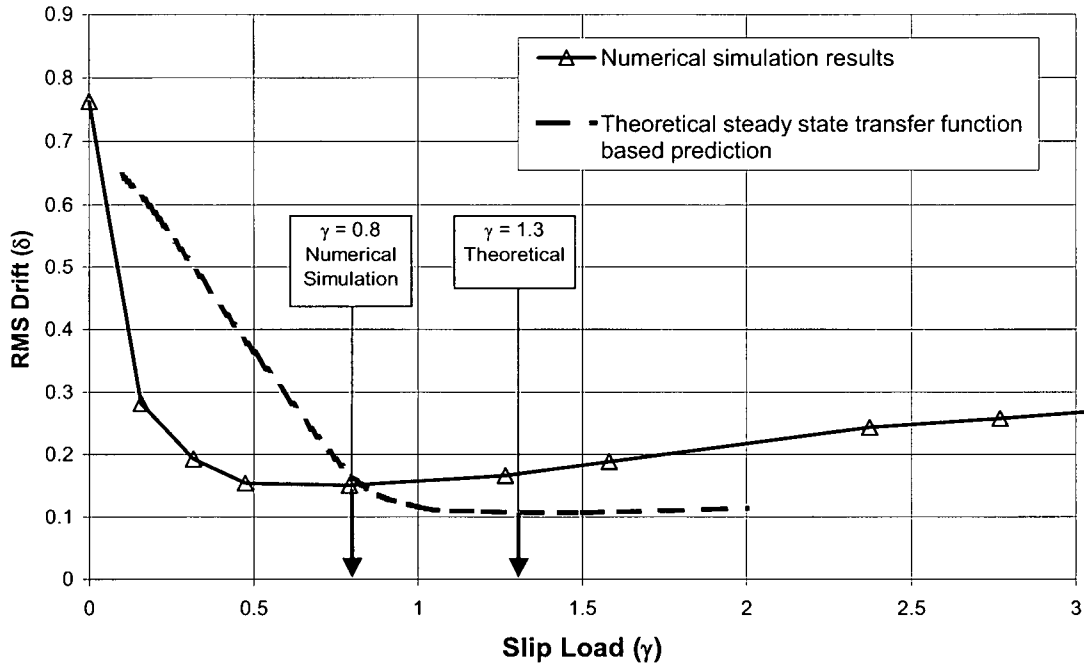


Figure 3.20. Prediction of optimal slip load based on steady-state transfer function.

dominate the response. For these two reasons, it is not surprising that such a significant mismatch exists in the slip load prediction.

3.5.3. Fourier Transform of Time Histories

Understanding that the concept of using theoretically established transfer functions as a basis for implementing an optimization procedure contains inherent flaws, an alternative set of transfer functions was sought. Keeping with the concept of using a transfer function based technique to predict the response to the PSD of an imposed load, an alternate set of transfer functions was established directly based on a comparison of the FFT of input and output signals of a friction damped structure. The work done to establish these curves and their ability to be used to predict the slip load for a structure subjected to an earthquake loading is covered in this section.

Strictly speaking, the transfer function technique is not applicable to a non-linear friction damped structure. However, the justification for using the transfer function technique is that it will provide a set of curves that will be useful in an approximate design procedure.

Many non-linear analyses are necessary to produce a statistically significant set of results, and to reduce the scatter. The purpose of this investigation is not to establish the design curves, but to establish whether such a set of curves can be used as a practical design tool.

3.5.3.1. Frequency Domain Analysis Procedure

The SDOF structure used in this assessment has unit mass and stiffness. Subsequently, the fundamental period in the unbraced state is 6.3 seconds. Simulations were conducted using white noise input over a total simulation time of 204.8 seconds with a time step of 0.2 seconds. The number of time steps per cycle was approximately 31 at the fundamental period and 12 per cycle with the maximum brace stiffness ratio. The number of fundamental period cycles over the simulation time was approximately 32, which was felt to be sufficient for the structure to reach steady state. This would be typical of a 2.5Hz structure in an earthquake with 12 seconds of strong motion. A small inherent damping of $\xi = 1.5\%$ was used. For each choice of brace stiffness and slip load 10 simulations were run and the input and output signals processed using the 1024 pt FFT algorithm.

The white noise input was established as the sum of a set of equal amplitude sine waves having random phase. It was opted to use this procedure so that the shape of the input PSD could be strictly controlled, rather than relying on the procedure described in Section 3.2.2.5 with a randomly variable input PSD. Signals were generated using 599 sine waves ranging from 0.01 Hz to 3.0 Hz at 0.005 Hz intervals.

For each of the established inputs, output was obtained by performing non-linear time-history analyses of the friction damped structure with varying slip load ratios.

Complex valued transfer functions were computed as the ratio of the input and output FFT's and averaged across each of the 12 simulations. Raw output from the simulation results is given in Figures 3.21 to 3.25. Applying a moving average further smoothed the transfer functions. This process produced a much smoother set of curves, used here to illustrate the trend in the data more clearly, as shown in Figures 3.26 to 3.30. Although much smoother, the variability of the signal is still apparent. The moving average technique also shifts the frequency content; therefore, subsequent calculations to determine the RMS response to a random input used the raw data, rather than the smoothed.

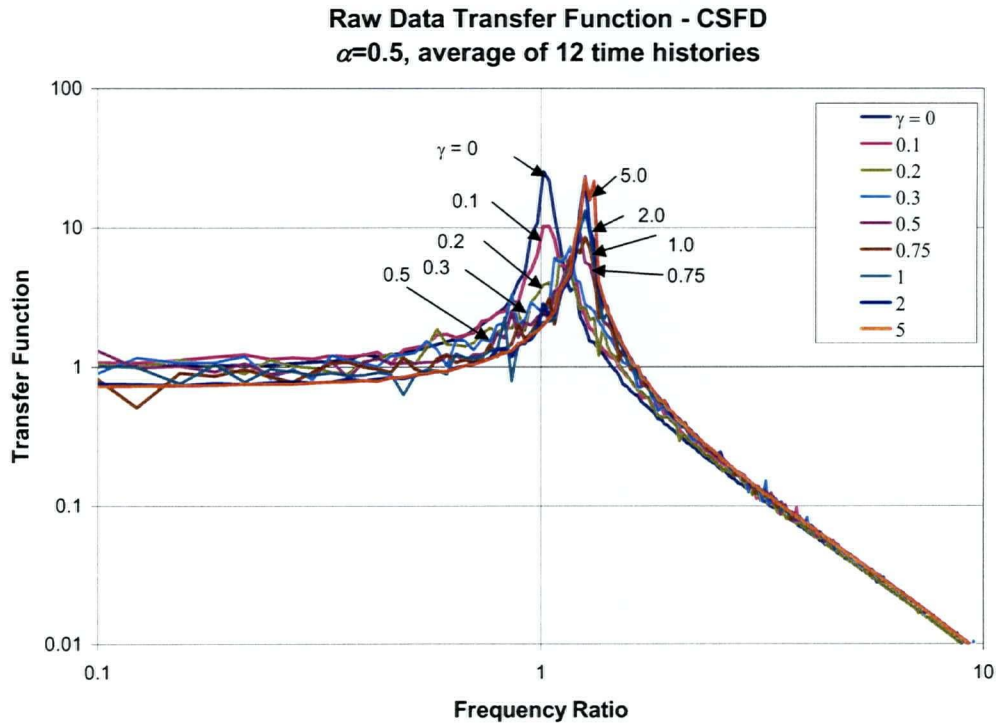


Figure 3.21. Transfer function derived from friction damped structure response to white-noise, $\alpha=0.5$.

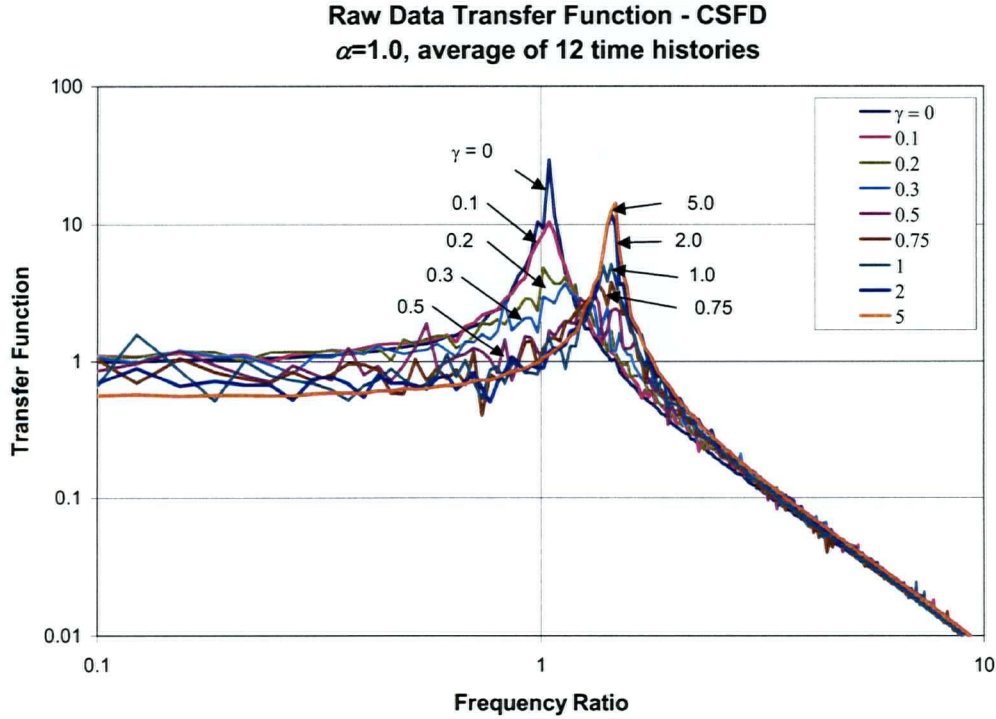


Figure 3.22. Transfer function derived from friction damped structure response to white-noise, $\alpha=1.0$.

Raw Data Transfer Function - CSFD
 $\alpha=2.0$, average of 12 time histories

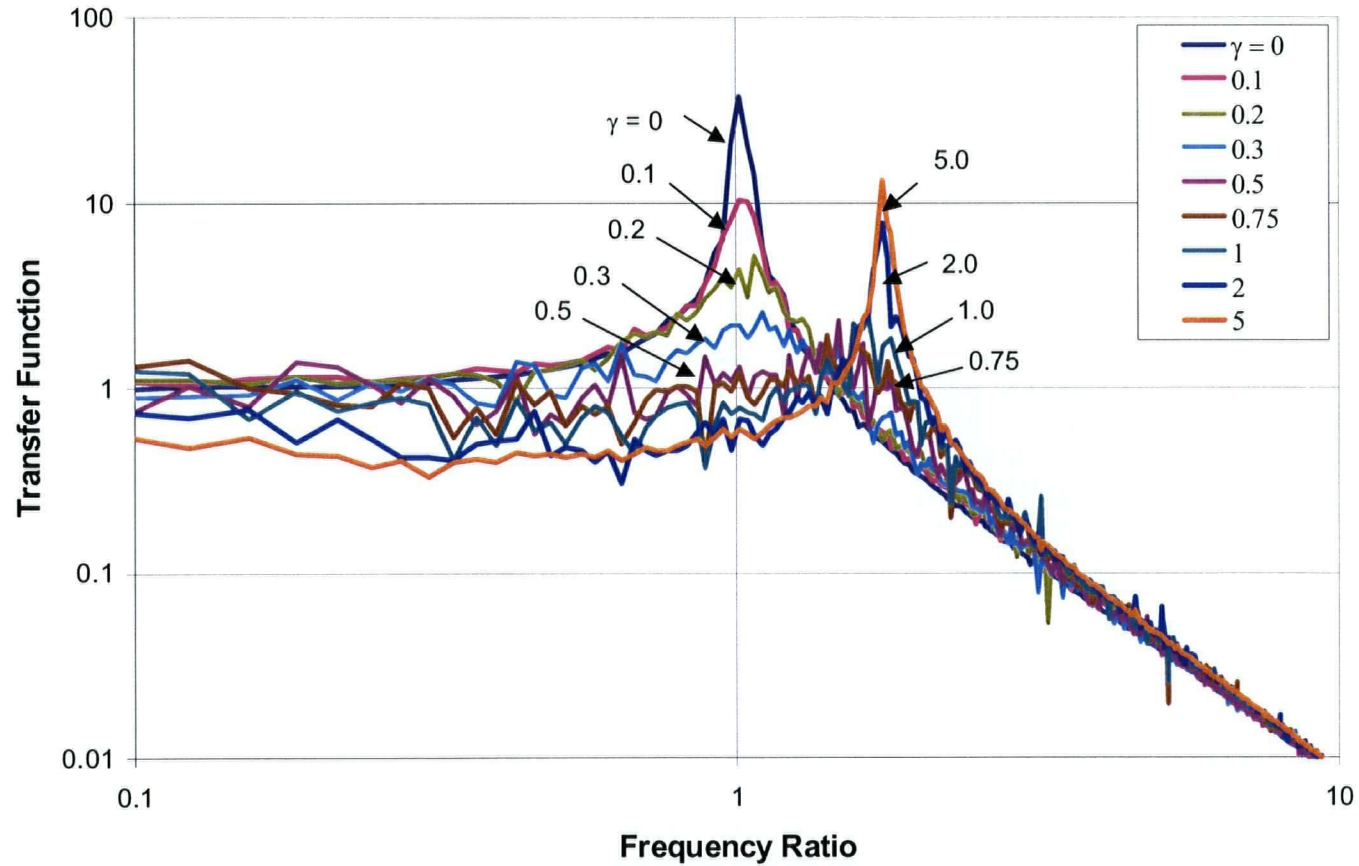


Figure 3.23. Transfer function derived from friction damped structure response to white noise, $\alpha=2.0$.

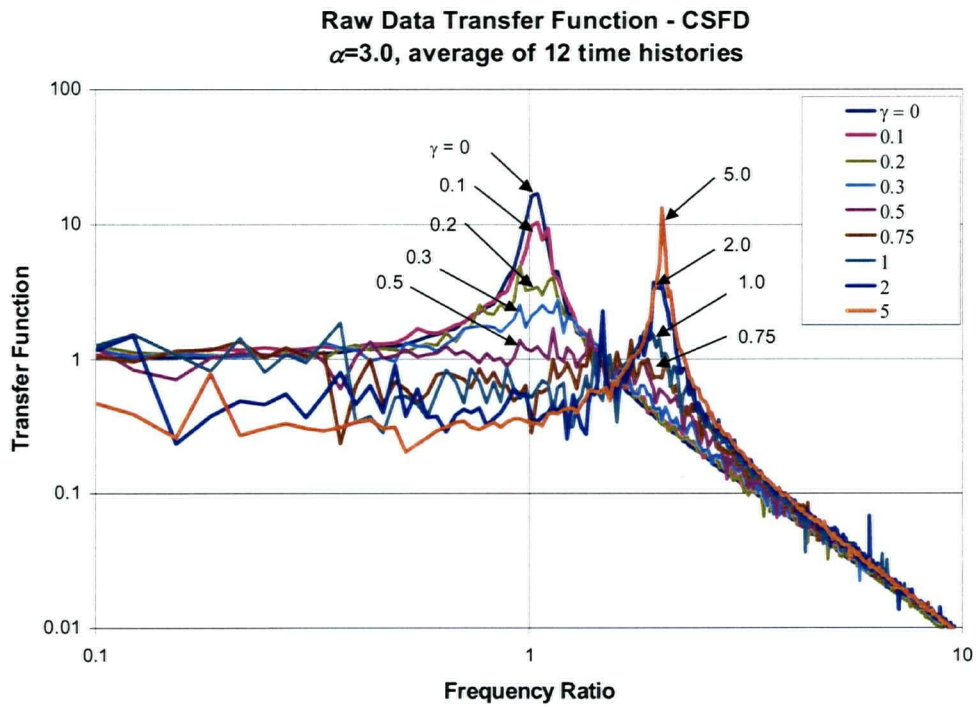


Figure 3.24. Transfer function derived from friction damped structure response to white-noise, $\alpha=3.0$.

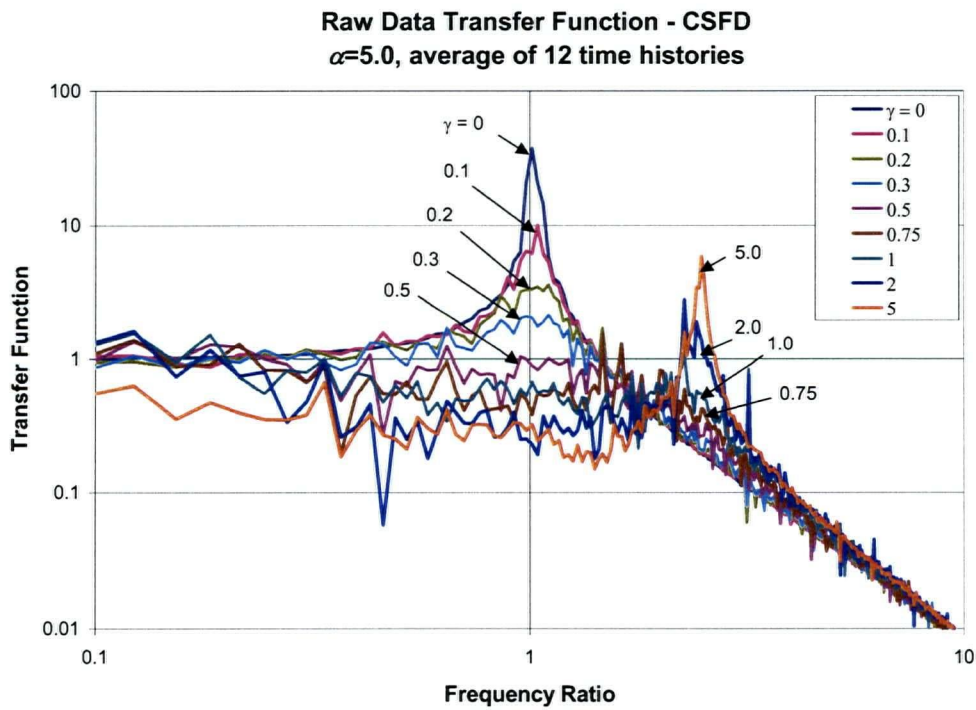


Figure 3.25. Transfer function derived from friction damped structure response to white-noise, $\alpha=5.0$.

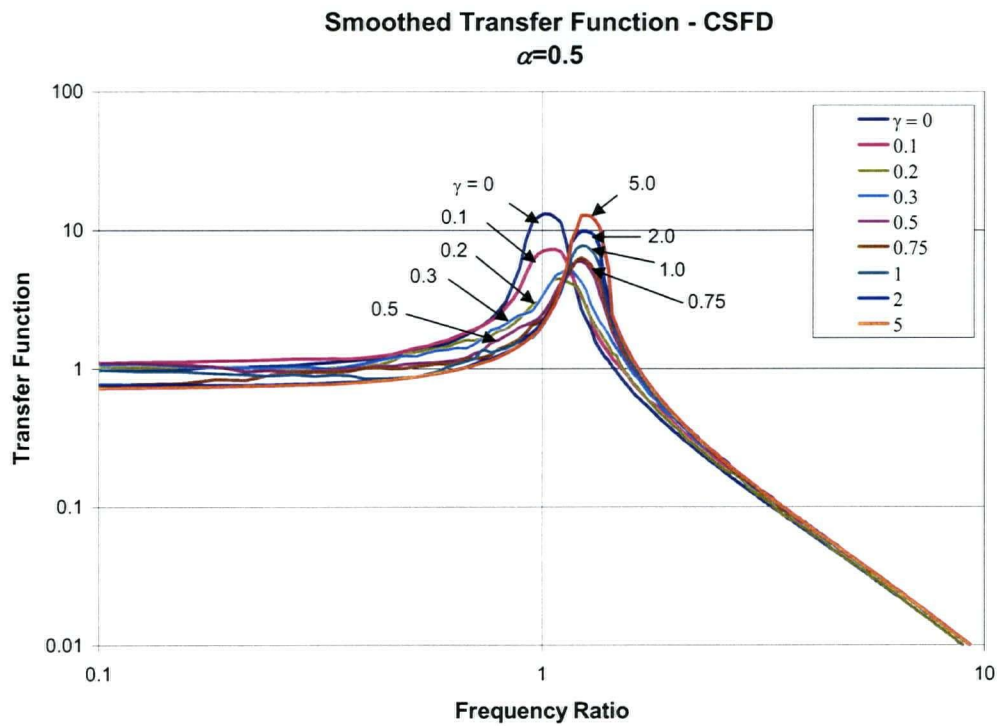


Figure 3.26. Smoothed white-noise response transfer function, $\alpha=0.5$.

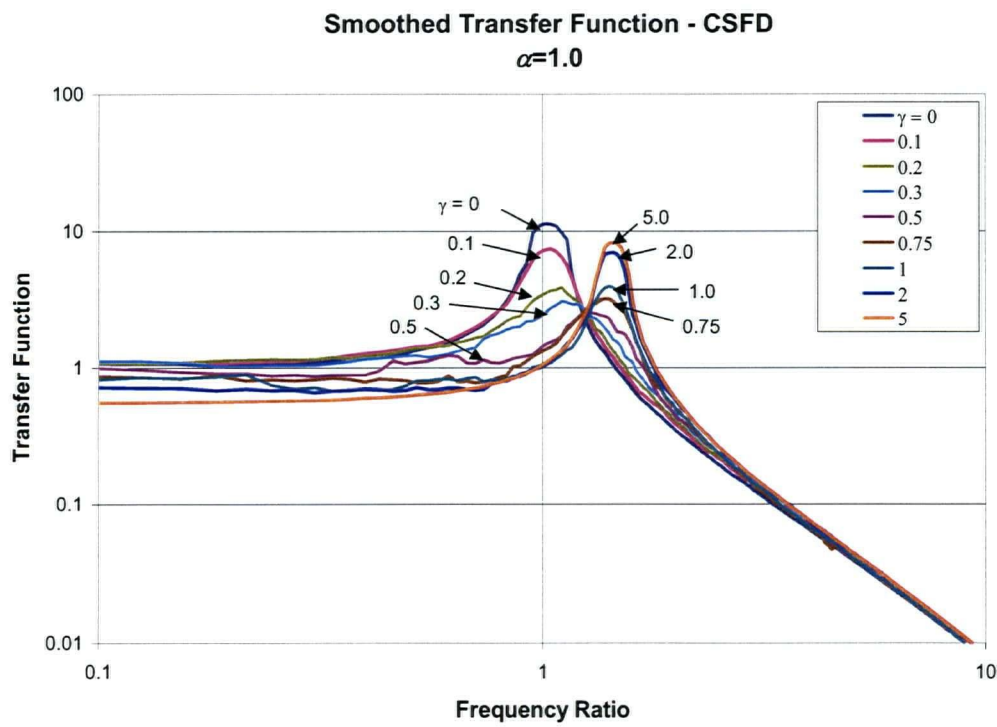


Figure 3.27. Smoothed white-noise response transfer function, $\alpha=1.0$.

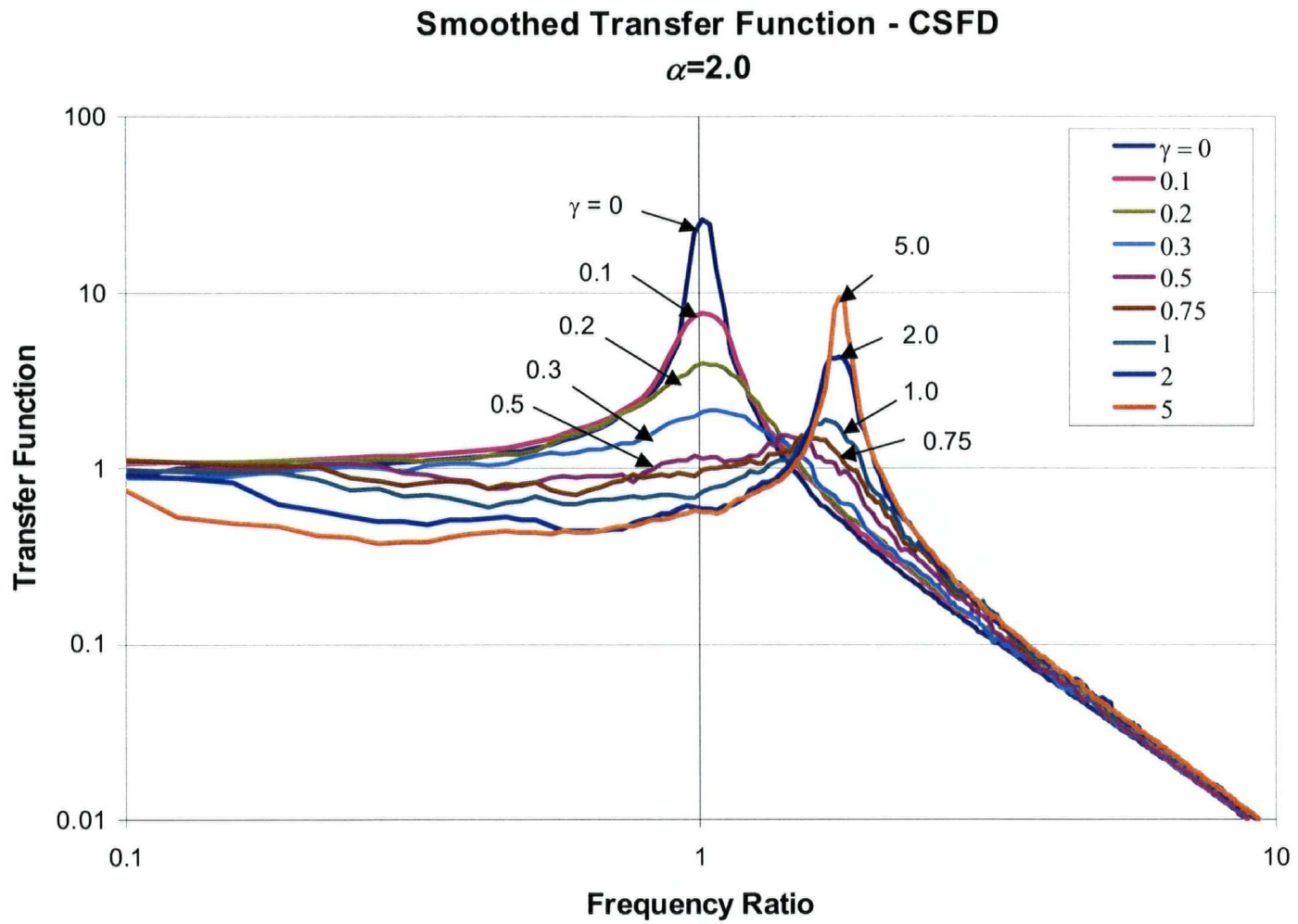


Figure 3.28. Smoothed white-noise response transfer function, $\alpha=2.0$.

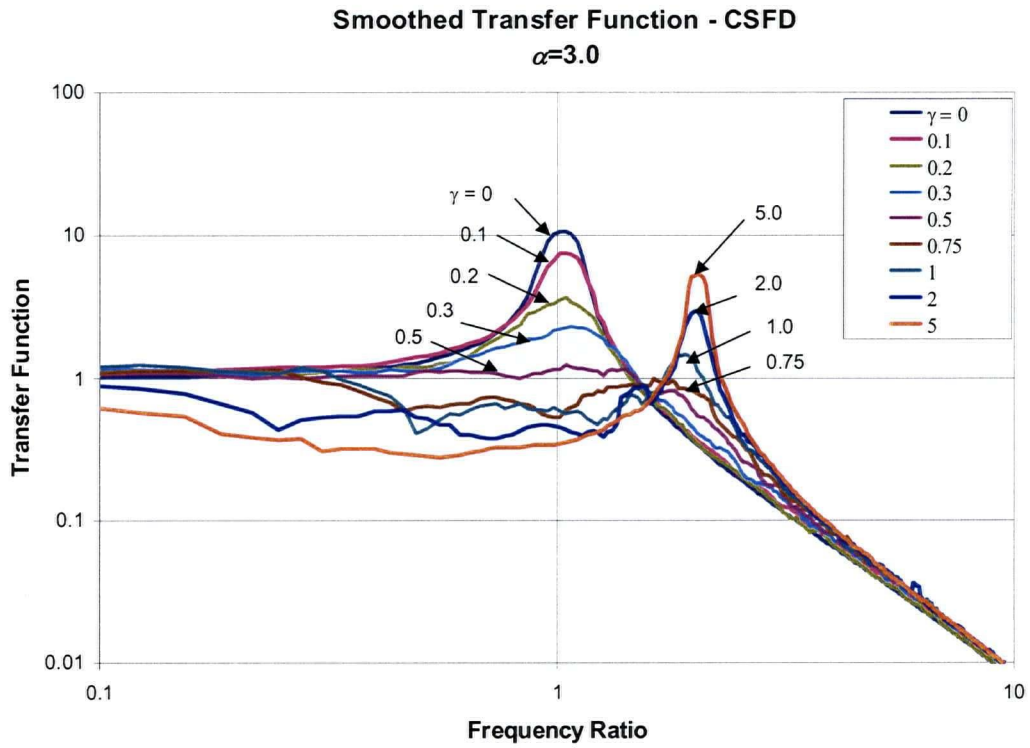


Figure 3.29. Smoothed white-noise response transfer function, $\alpha=3.0$.

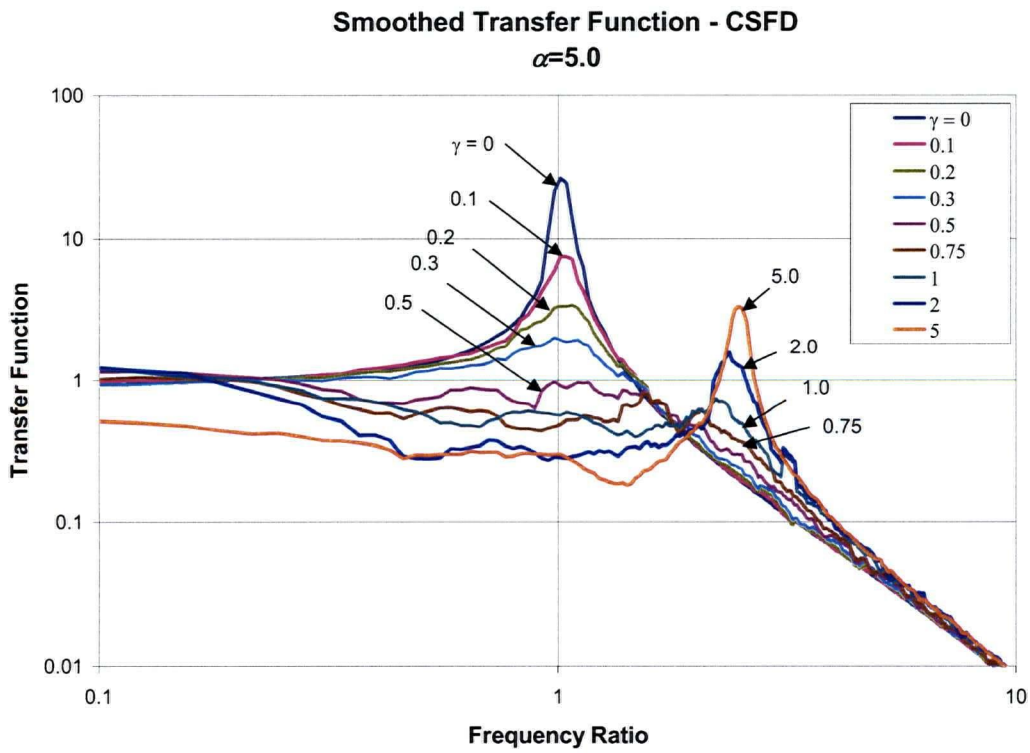


Figure 3.30. Smoothed white-noise response transfer function, $\alpha=5.0$.

3.5.3.2. White Noise Input Slip Load Optimization

The response to various slip loads using the transfer function calculation was carried out and compared to the slip loads established by comparing RMS drifts obtained from time-history data. The comparison is illustrated in Figure 3.31. As expected, the two curves were found to be very similar. The optimal slip load predicted by the FT technique was about 0.8, identical to that obtained by numerical simulation.

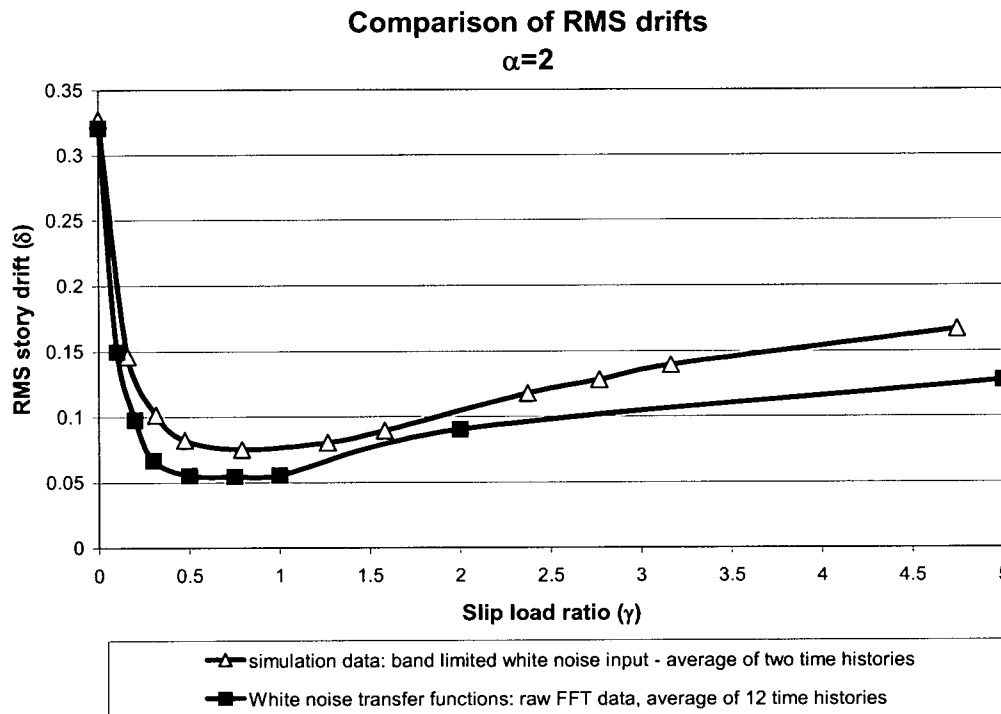


Figure 3.31. Prediction of optimal slip load – white noise input, $\alpha=2$.

3.6. Semi-Active Off-On Friction Damped Structures

The frequency response of the off-on semi-active friction damped structure was not investigated using the analytical procedure applied to the bilinear hysteretic structure. However, the transfer functions were derived from a comparison of input and output response time histories as described for the analysis of the constant slip force friction damper in the previous section.

Figure 3.32 illustrates the averaged raw data and Figure 3.33 illustrates the smoothed transfer

functions obtained for the brace stiffness ratio $\alpha = 2$. It is significant to note that the high frequency spike characteristic of the frequency of the braced structure does not appear. Prediction of optimal slip load using these curves would not lead to a minimum displacement response as the second spike does not exist, even for very high slip loads. This characteristic of the off-on friction damped response transfer functions indicates that the concept of optimal performance does not apply to the off-on controlled structures. The slip load in an off-on structure needs only be sufficiently high to eliminate the peak at the structures resonant frequency. If the slip force were to be set higher, no further improvement or deterioration in the performance would be expected.

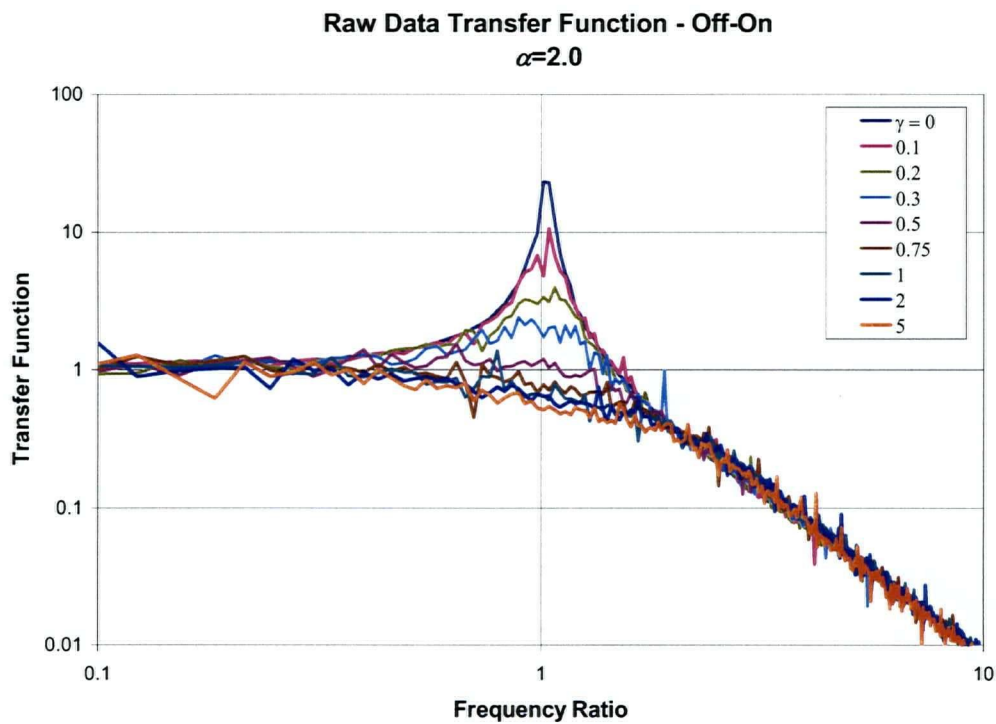


Figure 3.32. Raw data transfer function – off-on semi-active friction damped structure, $\alpha=2.0$.

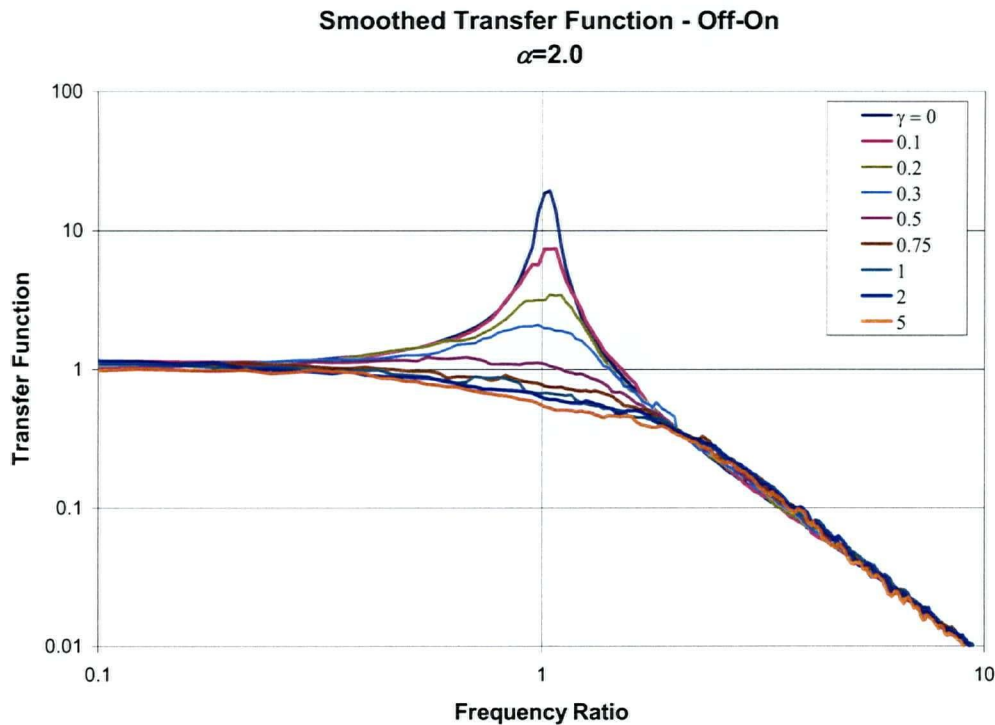


Figure 3.33. Smoothed transfer function – off-on semi-active friction damped structure, $\alpha=2.0$.

3.7. General Discussion

This chapter considered the response characteristics of a single degree of freedom structure with a control element consisting of a passive viscous, friction or hysteretic damper, and touched on the response of an off-on semi-actively friction damped structure. By modelling the constant and variable slip load friction dampers in the time domain the behaviour of structures with each damping device was established. In order to model the structures, an extended set of state variables was used to account for the memory effect of the dampers. Frequency domain analysis was introduced for the purpose of providing a better understanding of the response characteristics of such controlled structures and to provide a basis for predicting the response. The RMS response is determined as a combination of the PSD of the input and the frequency response function of the structure. An effort was made to cast the problem in non-dimensional form to aid in the application of the obtained curves to structures with a wide range of properties. The frequency response functions for viscous dampers in series with a flexible brace could be established analytically. When subjected to white noise input, the viscous damping coefficient leading to minimum story drift depends on the frequency of the structure and the stiffness of the

brace, and not the magnitude of the excitation. This is expected for the linear viscous damped structure. While it is expected that the damping coefficient leading to minimum response for a non-white noise excitation would not be the same as that for the white noise input, the magnitude independence is still expected to hold.

The friction damped structure, however, is non-linear, and as such provides a greater challenge due to the dependence of the optimal slip load on both the magnitude and character of the excitation.

Through estimating the response amplitude, the optimal slip load is determined as the slip load that leads to the minimum demands on the structure, in this case taken simply as story drift. It is recognised that in practical design situations other response quantities may also be important. In order to apply this technique it is presumed that the slip load level that leads to a minimization of the RMS drift leads to the minimization of the peak story drift. While there may be some difference between the slip load that leads to minimum RMS response and that leading to the minimum peak drift, it is observed that the minimum of the RMS response curve is relatively broad and therefore the response is not sensitive to the particular value of slip load. Therefore, the difference is not expected to be significant.

Figure 3.34 shows a comparison of the peak and RMS drifts obtained for a series of time history analyses in which a friction damped structure was subjected to a burst of white noise. The curves shown are an average of two simulations each conducted with the same two input time histories. One can see that the minimum slip load ratio for the RMS response is a reasonable indicator of a slip load that would lead to an optimum performance in peak response. The RMS data appears to contain fewer irregularities that are the result of peculiarities in the input data and may therefore better identify the optimum slip load given that the actual loading is not known. It is noted that the white noise input used in this case is very well behaved compared to earthquake loading. With earthquake loading neither the magnitude nor the frequency content can be described with any accuracy.

Although frequency response techniques are strictly valid only for linear systems, by computing the ratio of the FFT's of the input and output, the resulting set of PSD functions include the non-linear properties. For sinusoidal input, the analytically established frequency response functions were able to predict the steady state response amplitudes of structures with friction dampers.

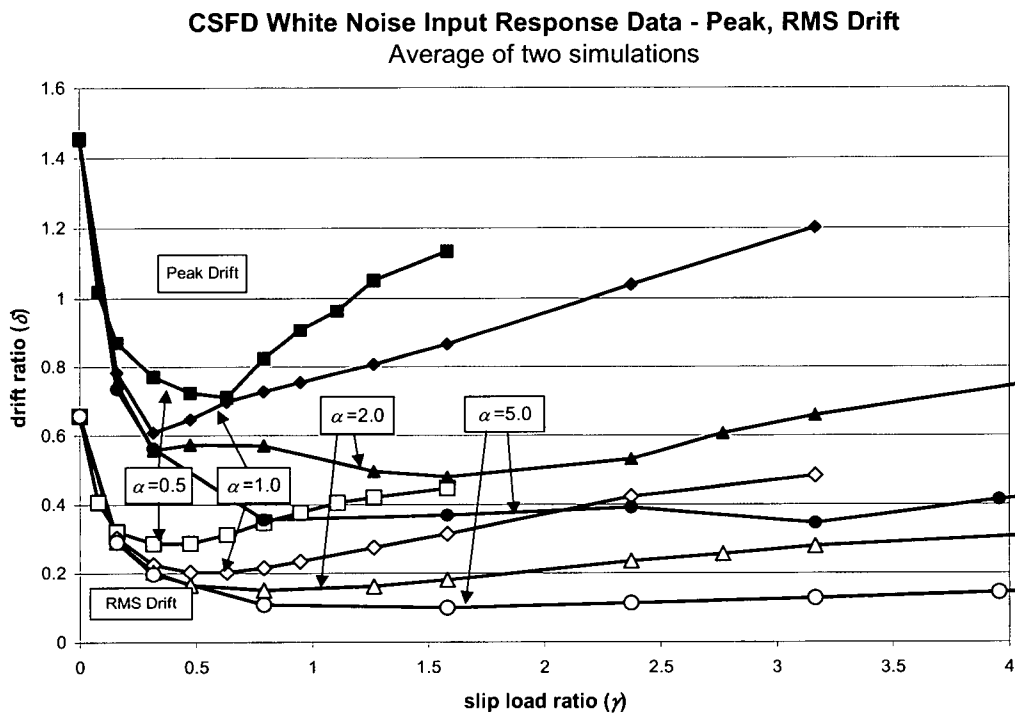


Figure 3.34. Comparison of peak, RMS drift vs. slip load.

However, this was not the case for the structures subjected to white noise input. While the shape of the curve of response amplitudes vs. slip load established using the analytically established curves turned out to be unlike that observed by examining time history data, the shape of the curve determined using the PSD functions as a basis reflected that observed in the non-linear response time history data.

This observation highlights the fact that in dealing with the non-linear response of friction dampers, the response characteristics depend on the character of the input excitation. Accuracy of the predicted response amplitude depends on the suitability of the frequency response functions used to describe the non-linear response. While white noise cannot be considered as a substitute for an earthquake, it is presumed here that it provides a basis that is not biased in any one frequency. The lack of a frequency bias is important to allow the curves to be scaled to represent as wide a variety of structures as possible.

Presuming that the deflection of the structure governs the demands, the results obtained show that the frequency content of the excitation and its relationship to the braced and unbraced

frequencies of the structure can in some cases be used to indicate whether or not an optimal slip load exists. If the input has frequency content concentrated at or below the unbraced frequency, the optimal response will be produced for a high slip load, a slip load that will not lead to any slip. Conversely, if the input is composed of frequencies above the braced natural frequency, the optimal performance will be produced for zero slip load: i.e. the brace completely disconnected from the structure. All other input containing frequencies between the braced and unbraced frequency will be sensitive to the slip load. Only in these remaining cases will optimization be necessary. Further, structures for which very stiff braces can be provided, a high slip load would lead to minimum demands on the primary structure.

Many of the loads for which structures are designed, including earthquakes, winds and blasts are wide band in nature, and as such fall into the category where an optimal slip leading to minimum deflection load exists. Stiff braces, while highly desirable, are not easy to provide. While stiff braces may lead to minimum deflections of the primary structure, the demands (forces) imposed on the structure by the bracing system or the accelerations experienced within the structure may not be substantially reduced and may even be increased. Considerations such as this could only be evaluated once faced with a specific structure and its specific design requirements.

Portions of structures that experience loads filtered through other structures, or a structure subject to a sinusoidal loading from reciprocating machinery may fall into one of the former two categories and as such may best be handled either through bracing or not bracing.

Figure 3.35 shows a comparison of the RMS drift vs. slip load and the total energy dissipated for the structure subjected to bursts of white noise excitation. It is noted that for high brace stiffness ratios $\alpha = 2$ and $\alpha = 5$, the energy function becomes very flat. This is an indication that there is a finite amount of energy available for the dampers to dissipate, and the more stiffly braced structures have the capability to dissipate all of it providing the slip load is set to an appropriate level. Comparison of the responses for $\alpha = 5$ shows that the lowest slip load corresponding to maximum energy dissipation does not necessarily lead to minimum drift.

The frequency response functions established for the semi-active off-on friction dampers differed from the character of the passive dampers (viscous and friction) by the absence of the peak associated with oscillation at the braced natural frequency. While the passive systems have a minimum response associated with a particular slip load (or range of slip loads), the semi-active off-on damped structure does not. For any given excitation, the slip load should be made as high

as possible. This property of the semi-active system is desirable because it can be depended on to act optimally regardless of the magnitude of the excitation, as does a viscous damper. Further, the optimality of the semi-active off-on system is independent of the frequency content of the excitation. The only limiting factor is the brace stiffness and the maximum force in the brace. The brace stiffness and the maximum force it can carry is limited by other factors not necessarily at the control of the engineer.

While the performance of the semi-active system is superior to that of the passive systems, it is not necessarily the ideal solution. The complexity and expense of the structure is greatly increased by the inclusion of the control sensing and actuation, even if an external energy source is not required. The superior performance of the off-on system as seen in the ideal SDOF structure does not extend to MDOF structures, as observed by Dowdell and Cherry, (1994a). Therefore the semi-active systems have not been extended to MDOF structures.

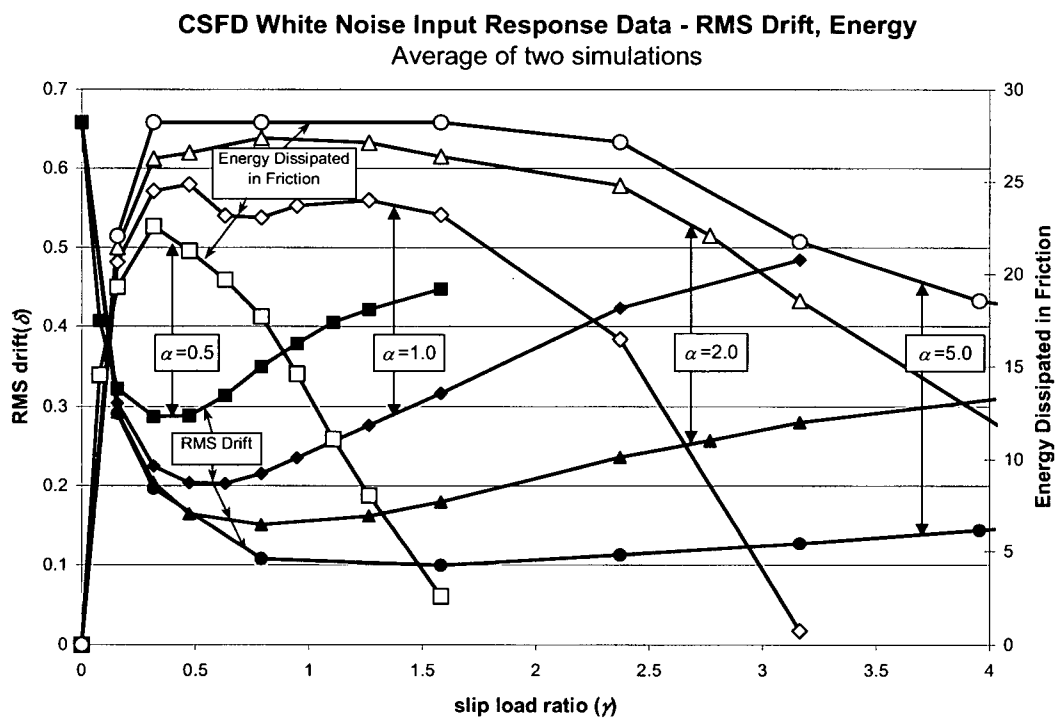


Figure 3.35. Comparison of RMS drift and dissipated energy vs. slip load.

Chapter 4: Extension of SDOF Damper Design Procedures to MDOF Structures

In this chapter, the extension of the single degree of freedom method of sizing friction slip loads in a MDOF structure is considered. Semi-active systems are not included in the discussion since initial trials with a 6-story structure, reported by Dowdell and Cherry (1994a), indicated that the semi-active off-on control was unable to produce a better response than that of the passive CSFD. While the optimization of viscous dampers in a general MDOF system presents an interesting problem, it is beyond the scope of this investigation.

Although passive friction dampers are more economical to implement than active or semi-active systems, the corresponding design procedure is more complex. Previous studies relating to the implementation of such devices include work by Filiatrault and Cherry (1988, 1990) and Hanson and Soong (2001). Design of such damped structures is also covered in the Building Seismic Safety Council (2000) design standard.

Filiatrault and Cherry (1990) proposed a simple and practical design method for optimizing the slip force in friction damped braced frame structures. In this study it was observed that the performances of the structures considered were relatively insensitive to the distribution of slip force and suggested that a uniform slip load distribution be used. Early investigations in the course of this study indicated that the system performance is indeed affected by the distribution of slip loads and the uniform distribution was not necessarily the optimal distribution.

In order to extend the SDOF procedure to an MDOF structure using the frequency response curves established in Chapter 3, the following conditions need to be met:

- The structure responds primarily in a single identifiable mode with little influence of other (higher) modes;
- The form of the structure (mass and stiffness distribution) does not deviate significantly from that of a structure studied in detail for which the slip load distribution is available.

Within these limitations a general procedure is sought that will provide reliable estimates of slip loads, taking into account the influence of the excitation. Not all structures have a response for any particular excitation that can be adequately characterized by the response of a single mode.

Only when one mode is sufficient to characterize the structural response can the extension of the SDOF procedure be considered. It is necessary to limit the variation in the structural form such as mass and stiffness distribution. If the mass and stiffness distribution differ substantially from that used as a basis, the slip load distribution and any calibration factors derived for one structural form may not be applicable. The procedure suggested here for designing the dampers in a particular structure is as follows:

1. Model the structure as a single degree of freedom system
2. Determine the first story slip load using the SDOF frequency domain based method described in Chapter 3
3. Based on the structural form and previous experience, proportion the slip loads in the remaining dampers

In order to compute the slip loads in an MDOF structure based on a SDOF model, it is important to predetermine the slip load distribution as well as any factors (calibration coefficients) necessary to relate the SDOF optimal slip load to the MDOF optimal slip loads. With this information, the results obtained in Steps 1 and 2 can be extended to the MDOF structure in Step 3. In the following section, the uniform 4-story structure shown in Figure 4.1 will be used to illustrate the procedure.

4.1 Dynamic Properties of MDOF Structures

Consider that the 4DOF structure depicted in Figure 4.1 is subjected to an earthquake excitation. Its natural frequencies and mode shapes influence the response to the earthquake. The transfer functions that relate the story drifts to the earthquake excitation are plotted for each story in Figure 4.2(a). These illustrate the complexity of the interactions in the MDOF structure. Appendix D contains the MathCad worksheet used to evaluate the dynamic properties of the given structure.

The system can be reduced to the response of a single degree of freedom structure having transfer functions as shown in Figure 4.2(b). A comparison of the two figures illustrates that in the neighbourhood of the first mode frequency, about 2 Hz, the first mode transfer functions fit reasonably well. However, it is observed that at higher frequencies, the peaks associated with higher modes, some more prominent than others, are truncated. Whether or not the truncated

peaks are significant depends on the frequency content of the excitation, particularly if it coincides with a higher mode frequency.

In order to test the ability of the method proposed herein to provide slip loads near to that of the true optimal slip loads, work was first done to establish the optimal slip loads and to understand the characteristics of the optimal distribution. Level Set Programming, a computationally intensive but useful method for optimizing multivariable systems, was used extensively for this purpose. The LSP results were used to study the distribution of friction damper slip loads that lead to the optimal performance of the uniform 4-story moment frame shown in Figure 4.1.

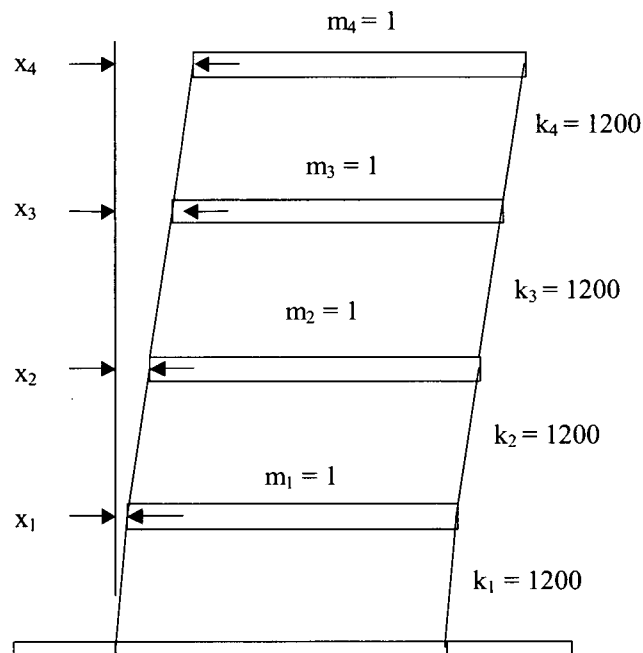


Figure 4.1. 4-Story regular moment frame structure.

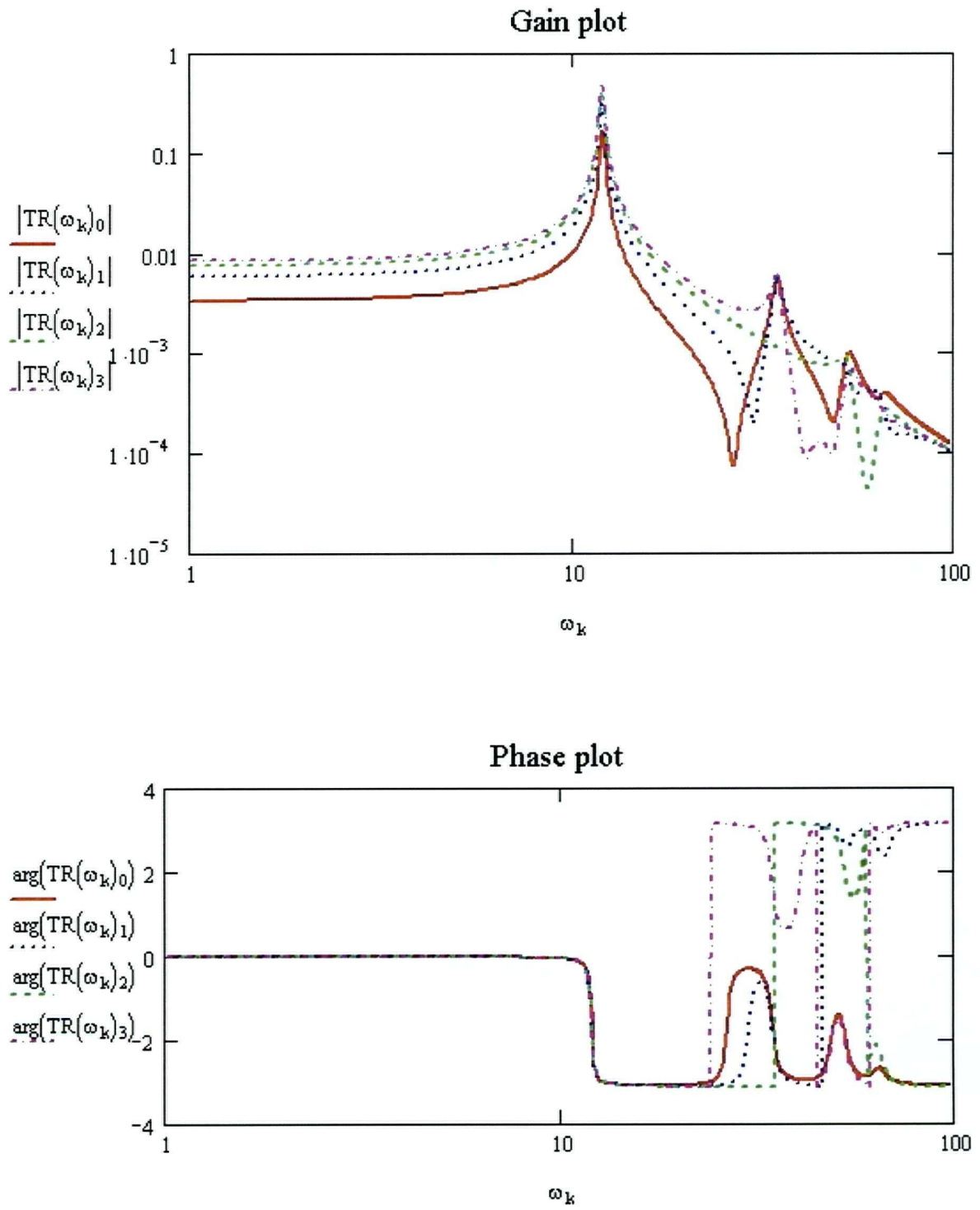
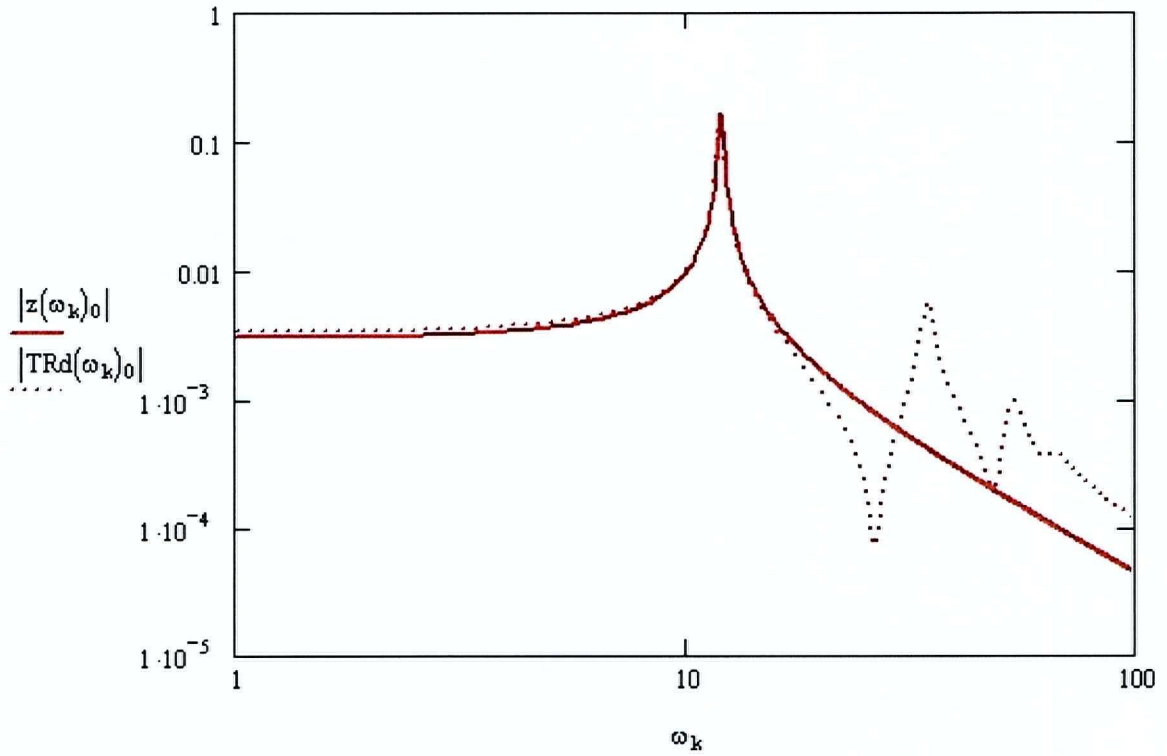


Figure 4.2(a). Gain and phase of transfer function of displacement response of 4-story structure.

SDOF and MDOF TF's - First Story Shear



SDOF and MDOF TF's - First Story Shear

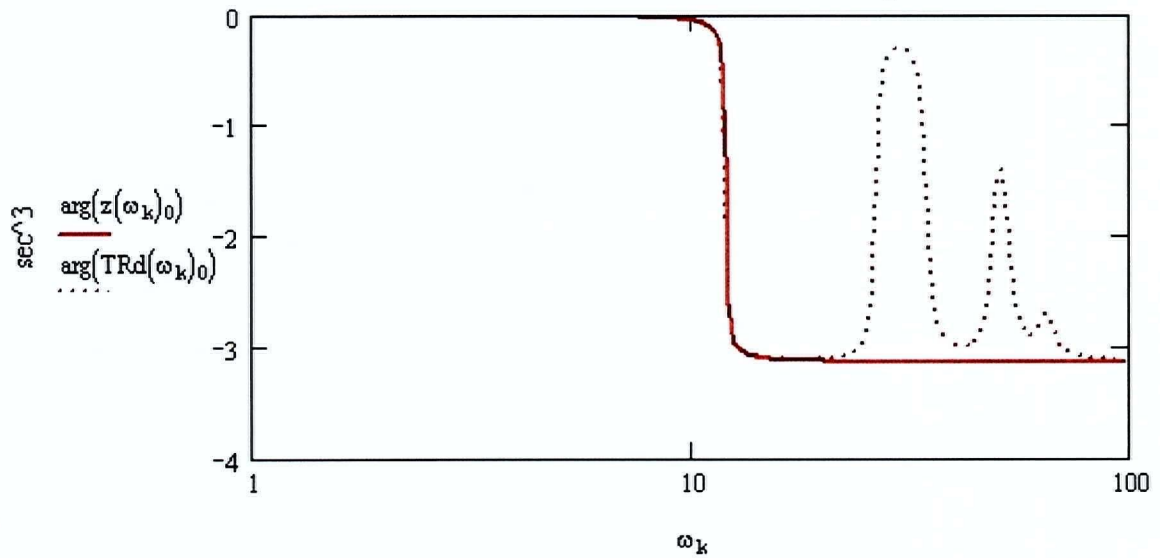


Figure 4.2(b). Gain and phase of transfer function of displacement response of SDOF system representing 4-story structure.

4.2 Level Set Programming

Level Set Programming (LSP) is an optimization procedure, developed by Yassien (1994), that is capable of handling problems where the function or its derivatives are discontinuous, have steep or infinite gradients or possess “fuzzy” objective functions. The LSP investigation is detailed in Appendix F using the uniform 4-story structure of Figure 4.1. With the results of this investigation it was attempted to find a general rule by which the slip loads can be proportioned. The results obtained using LSP are also used in this thesis as a point of comparison to evaluate the validity of the proposed design methods. Only the given 4-story structure with uniform mass and stiffness distribution was considered. Appendix F also includes the LSP investigation of the semi-active off-on control, the results of which will only briefly be covered here.

4.2.1 General Description

The optimization procedure is a search for a set of parameters, in this case representing slip loads of the dampers in the chosen 4-story structure, that lead to the minimum response as measured by an “objective function.” Objective functions are chosen functions that evaluate to a single real valued number, which represents the magnitude of the response experienced by the structure. In the control theory presented in Chapter 2, the response was measured using a “performance index”. The two terms, for the purposes of this investigation are synonymous.

The level set programming method provides an alternative to gradient methods commonly used to establish minimum values of performance functions. As indicated gradient methods break down if the function to be determined or its differentials are discontinuous, steep or “fuzzy” in the region of interest. The method is based on the concept of a “level set” based on a sampling of the performance function with randomly chosen input variables $x_1, x_2 \dots x_n$. For a selected level L , the level set is the set of randomly selected input variables that lead to an objective function $f(x_1, x_2 \dots x_n)$ that satisfies the relation

$$f(x_1, x_2 \dots x_n) \leq L \quad (4.1)$$

For a function $f(x_1, x_2 \dots x_n)$ that has a single global minimum

$$f_{\min} = f(x_1^*, x_2^* \dots x_n^*). \quad (4.2)$$

It can be said that as L approaches the value of f_{min} , the dispersion of each of the input variables satisfying the level-set will approach zero. The search for f_{min} continues until the range of each of the input variables within the level set is acceptably small.

The search space is the n -dimensional hypercube with each dimension corresponding to initial search space of each input variable. In this case $n=4$ and the hypercube is a 4-dimensional cube. A level set is typically comprised of 60 sets of input variables, each representing a point in the hypercube, for which the objective function satisfies Equation 4.1. For each point evaluated (whether or not it is found to be a member of the level set) it is required to perform a time history simulation and subsequently evaluate the objective function based on the time-history output. This is a time consuming process.

Within the search space, input variables are chosen having a uniform distribution. However, because the level set is restricted to functions that are less than L , as L becomes more restrictive, the points in the hypercube will begin to form a cluster. The scatter-plot in the hypercube can be viewed to get some understanding of the behaviour of the system by the shape and location of the level set point cluster.

Because random sampling of the input variables is being utilised, random sampling over the entire search space is not practical when the level set is restricted to a small cluster. It is therefore required that as the search progresses, the search ranges be reduced to avoid unnecessary function evaluations. This process is built into the LSP search algorithm.

The chief drawback of LSP is that it often requires a large number of evaluations of the objective function to find the optimum.

4.2.2 Chosen Objective Functions

Two objective functions were chosen

- maximum RMS drift
- total strain energy area

The former was chosen as a direct representation of the demands placed on the structure, while the latter was included because it is similar to the performance index used in the linear quadratic control, and also that used by Filiatrault and Cherry (1990).

4.2.3 General Results

Appendix F contains the details of the LSP assessment. Only the key results are reproduced here. Figures 4.3 to 4.6 illustrate the optimal slip loads obtained with earthquake input. The minimum total energy objective function results are illustrated with solid lines while the obtained min RMS drift objective function results are plotted with dashed lines. El Centro results are plotted with solid diamond markers while results obtained with San Fernando record input are plotted with hollow triangular markers. The optimal slip loads are expressed in terms of kN/tonne of story mass. The total weight of the structure is about 39kN therefore the maximum slip load observed was just over 20% of this total weight.

For all trials it was observed that the optimal slip loads for the El Centro input record are significantly higher than the corresponding slip loads for the San Fernando input, and the slip loads corresponding to the min RMS drift objective function are significantly higher than for the corresponding minimum total energy. For $\alpha=1$, San Fernando earthquake and minimum RMS drift, a wide variation in slip load distributions was observed that was not observed with the other trials. With the San Fernando earthquake and minimum RMS drift, in each case, the slip load obtained at the fourth story turned out to be greater than the slip load at the third.

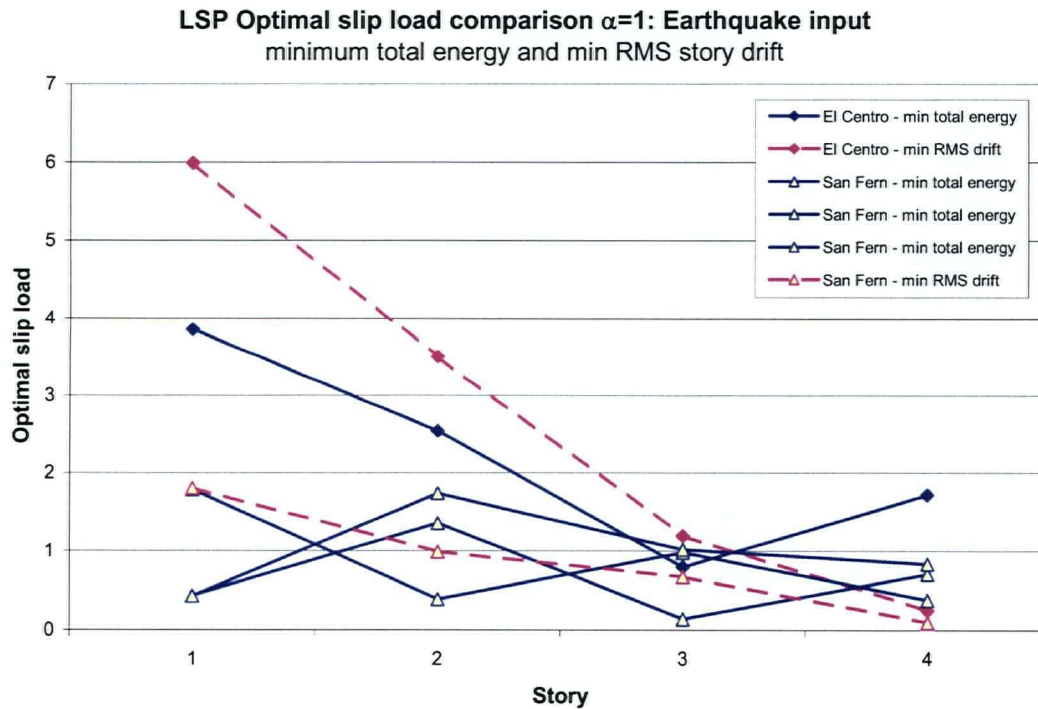


Figure 4.3. LSP optimal slip load comparison – earthquake input – min energy, min drift, $\alpha=1$.

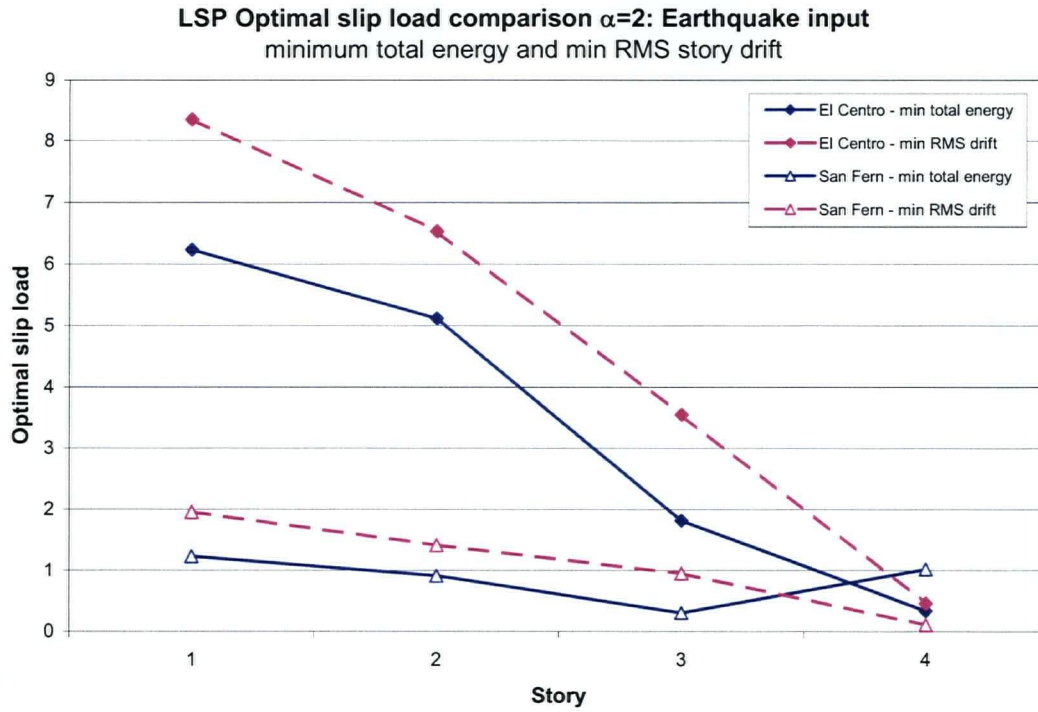


Figure 4.4. LSP optimal slip load comparison – earthquake input – min energy, min drift, $\alpha=2$.

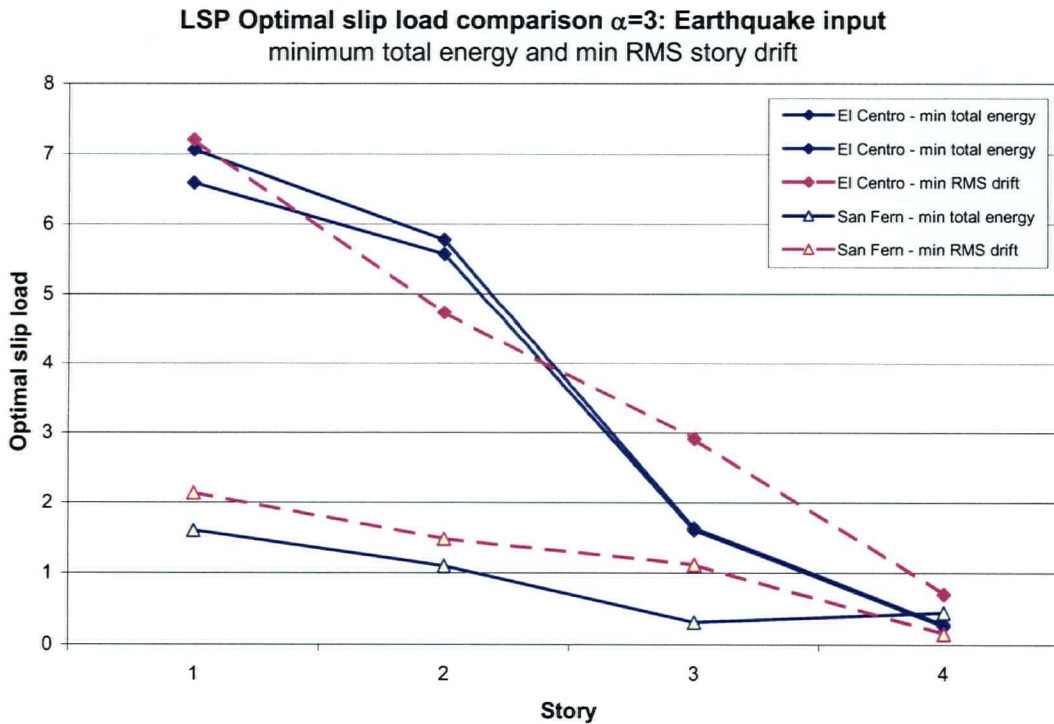


Figure 4.5. LSP optimal slip load comparison – earthquake input – min energy, min drift, $\alpha=3$

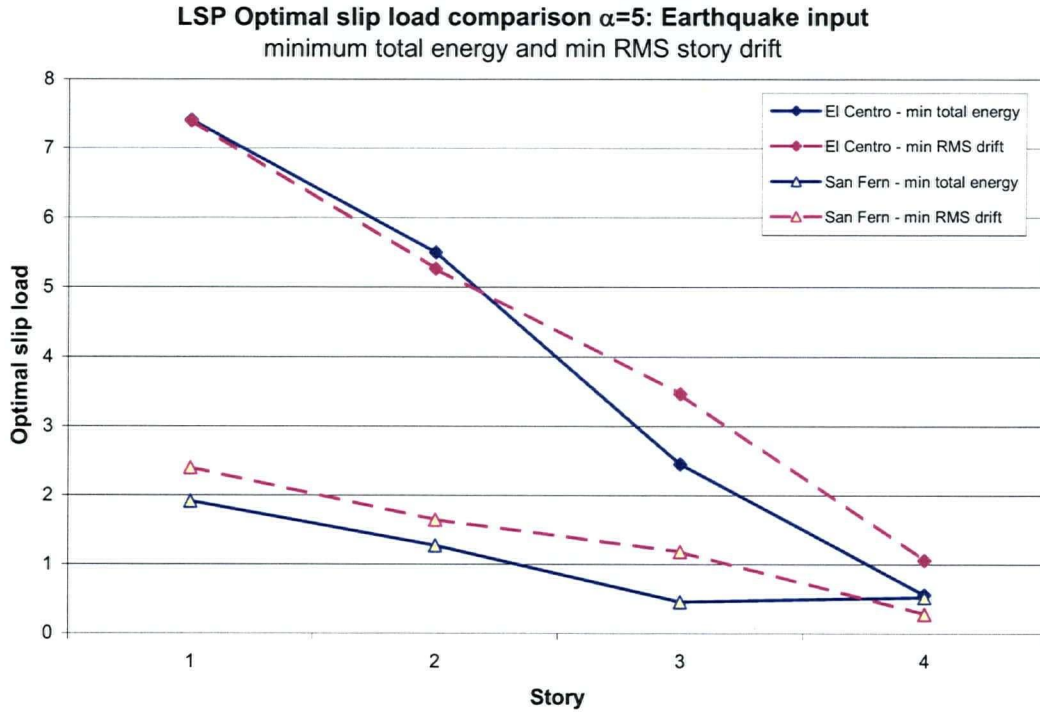


Figure 4.6. LSP optimal slip load comparison – earthquake input – min energy, min drift, $\alpha=5$.

4.3 Suggested Distribution of CSFD Slip Loads

Recognising that the optimal slip load distribution involves maximizing energy dissipation, and assuming that the fundamental contributor to the response of the first mode with mode-shape ϕ_0 , in terms of the inter-story drift, the kinetic energy associated with oscillation is proportional to the product of the mass and the square of the mode shape.

$$E \propto \phi_0^T M^* \phi_0 \quad (4.3)$$

Energy absorption on the other hand is proportional to the product of the slip loads and the story drifts.

$$E \propto \phi_0^T S \quad (4.4)$$

If the energy is equated, it follows then that the slip load is likely to be proportional to the mass and the first mode shape.

$$S \propto M^* \phi_0 \quad (4.5)$$

where M^* is taken as a matrix containing the masses M_i^* on the main diagonal which indicate the amount of mass carried above level i .

It is recognised that in the story drift-shear form, the mass in Equations 4.3 and 4.5 at any one story is equal to the sum of the mass above that story level. Dowdell and Cherry (1996) suggested using the product of the mode shape and the sum of the masses above any given story as a basis for the distribution. This shape was found to be in general agreement with observed slip load distributions for the uniform 4-story structure, but has not been investigated with non-uniform mass and stiffness distributions.

4.4 Prediction of MDOF Slip Loads Using the Transfer Function Method

Having pre-determined the slip load distribution, the MDOF design problem is reduced to a single DOF design problem. Once one slip load is set, the others can be directly computed. In a multi-story building structure, the slip load at the base is the obvious choice for the slip load on which to base the design.

The steps involved in the proposed transfer function based method are as follows

1. Determine the undamped structural properties
2. Determine the non-dimensional input PSD function
3. Apply the non-dimensional transfer functions for the various slip force ratios and compute the RMS drift associated with each
4. Select the base slip force ratio that yields a minimum response
5. Determine the base slip force from the slip ratio obtained in Step 4
6. Compute the remaining brace forces

The preceding procedure was applied to the 4-story structure used in the LSP optimization. This allowed for a direct comparison of the results obtained by LSP and the proposed transfer function procedure. The normalized drift vs. slip load functions for the two input earthquakes were computed and are plotted in Figure 4.7. The slip load ratios leading to minimum drift were found to be $\gamma = 1.0$ for El Centro input and $\gamma = 0.3$ for San Fernando input. Slip loads were computed at the base using the RMS acceleration from each earthquake and the total structure

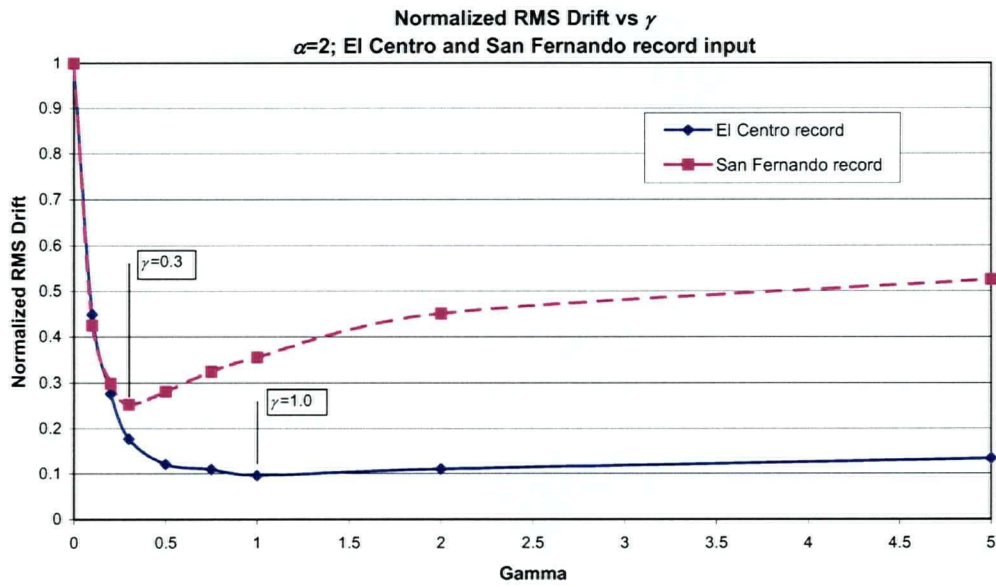


Figure 4.7. Normalized RMS drift vs. slip load ratio, γ , El Centro and San Fernando.

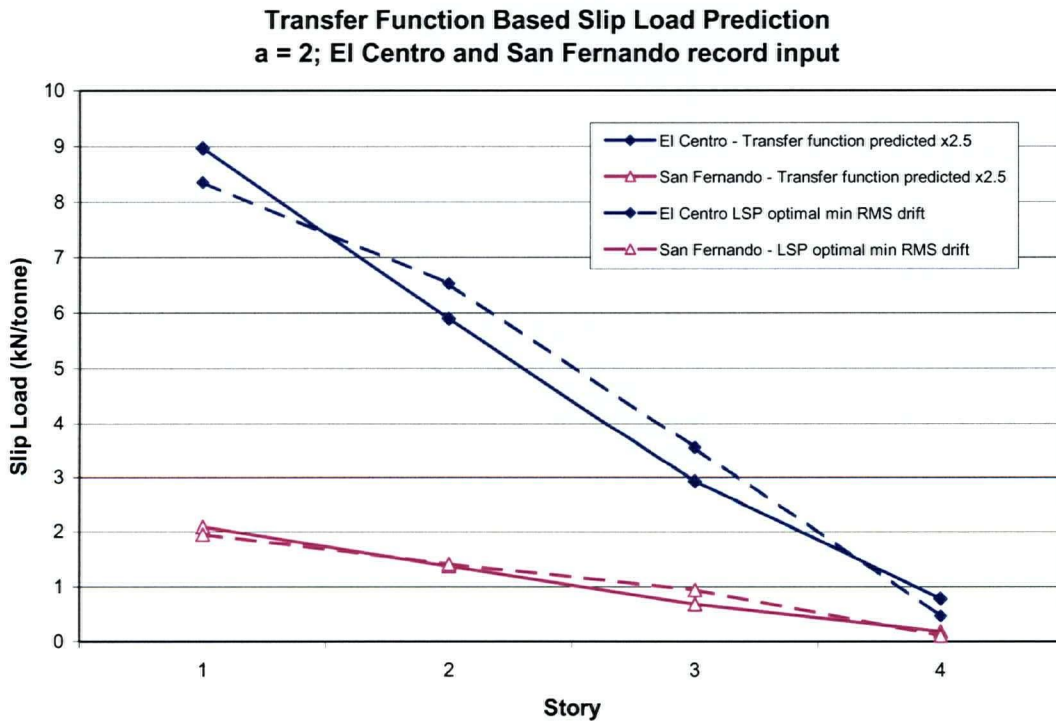


Figure 4.8. Transfer function based predicted slip loads for El Centro and San Fernando earthquake record input. A calibration factor of 2.5 was used to match the data to the LSP results.

mass. Finally, the slip loads at the remaining stories were computed according to the chosen distribution. To fit the optimal slip loads obtained by LSP, it was necessary to apply a calibration factor of 2.5. With the inclusion of this factor, the slip loads, as shown in Figure 4.8 match well with those determined using LSP.

4.5 Need for a General Procedure for MDOF Structures

It is observed that, although the input RMS excitation of each of the chosen earthquake records was nearly identical, the frequency response is quite dissimilar in the 1.9Hz to 3.4Hz range corresponding to the fundamental mode of the unbraced and braced structure, as illustrated in Figure 4.9. As might be expected, the San Fernando record produced a significantly lower response than did El Centro and required a proportionally lower optimal slip load. For this reason the choice of input records did provide good test of the procedure. The resulting estimated slip loads turned out to fit the slip loads obtained directly by the LSP procedure reasonably well for both the San Fernando and the El Centro record input case once a calibration factor was applied. It should not be surprising that the distribution matched reasonably well since the distribution function was determined after having access to the LSP data.

The minimum RMS drift objective function used in the LSP procedure corresponds directly to the objective of minimizing the PSD of the response computed using the PSD of the input and the frequency response function of the damped system. Using the minimum energy objective function was found to result in lower slip loads than using the minimum RMS drift.

The calibration factor used relates the SDOF structure to the 4-story MDOF structure. Although a great deal of variability was observed in the LSP results, the need to provide a calibration factor to fit the LSP obtained data highlights the fact that it is necessary to include a large component of experience in order to proceed with such a method. Only an elementary example was attempted within the scope of this work, and it should be emphasized that the results obtained using this technique is limited to 4-story structures that have uniform mass and stiffness distribution. The lack of a generality indicates that the transfer function based procedure is not suitable for use beyond the single degree of freedom structures.

Alternatively, a more general procedure is required. Chapter 5 is devoted to using control theory as a basis for development of a new procedure for analysis and retrofit design of general structural systems.

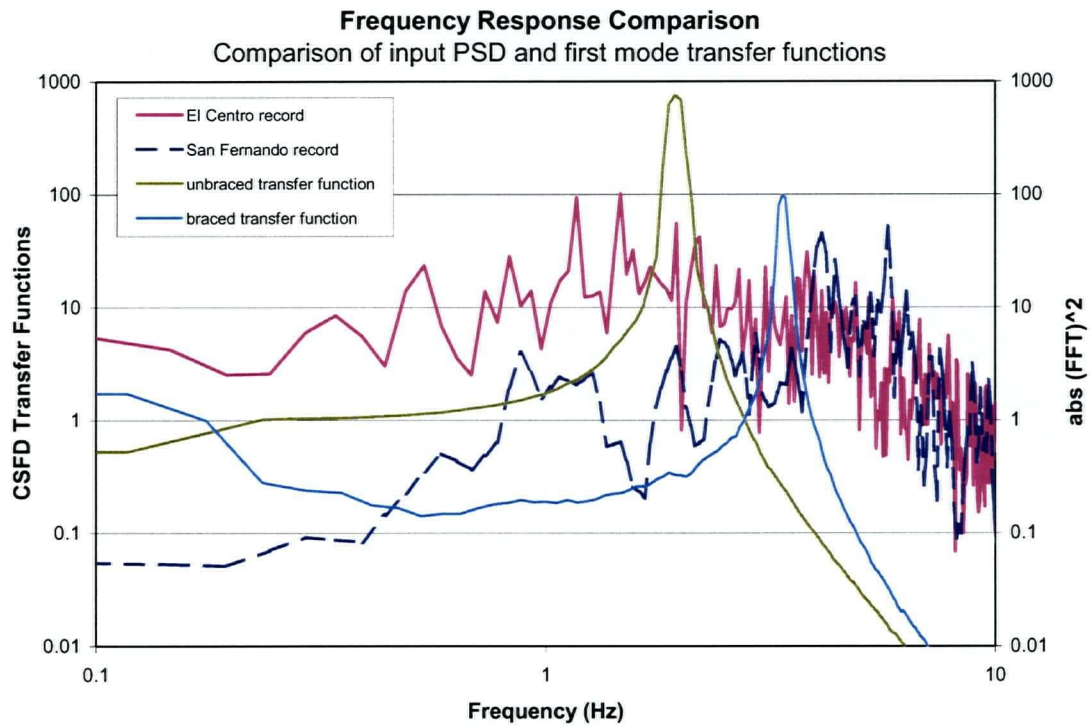


Figure 4.9. Comparison of Power Spectral Density functions for the two input time histories. “El Centro” and “San Fernando”. Transfer functions corresponding to low and high slip load are superimposed.

Chapter 5: A General Procedure for the Design of Dampers in MDOF Structures Based on Structural Control Concepts

In the previous chapter the extension of the SDOF procedure to a uniform MDOF structure was investigated. It was shown to be of value providing the distribution of slip loads for the particular structural form has been pre-established and calibrated. Without knowledge of the slip load distribution, the extension of the SDOF procedure could not be considered. Having this limitation prevents application of this method to structures that are either complex or unique. Therefore it is desirable to have a method that deals with general structural systems.

In this chapter a new method of designing passively damped structures with viscous and friction dampers is developed based directly on the Linear Quadratic regulator LQ control algorithm. The concept of an observer is used in the formulation to describe within the structural system where the dampers are located and how they act.

While the viscous damper design is influenced by the frequency content of the excitation, the friction damper design is influenced by both the magnitude and the frequency content of the excitation. The proposed method uses response spectral analysis (RSA) as a basis for determining the influence of the excitation. RSA is based on estimates of response amplitudes rather than explicitly determined response amplitudes. While not as accurate as a time history analysis for any particular input, RSA has several advantages. It directly incorporates design spectra and avoids the need to undertake a series of long and expensive time history analyses. Utilising RSA gives a consistency in the retrofit by preserving symmetry and avoids unnecessarily low or high input at any given frequency due to peculiarities inherent in chosen time histories. The resulting damper designs, therefore, are consistent with the design requirements.

The general method given in this chapter is formulated with the intention of utilising large and detailed finite element models as a basis and incorporating a relatively small number of dampers. Application of the proposed method requires that the designer select locations in the structure where dampers are to be placed. While methods exist for the optimal placement of a limited number of dampers, often the designer has to deal with restrictions on damper location that would be difficult if not impossible to incorporate into a modelling process. The designer must

ultimately determine the location of dampers, therefore the methods presented here are best utilised after the designer has narrowed down the design to a number of possible configurations.

5.1 Theoretical Derivation Including Observer

Assume as before that a general dynamic system is described by the state space equation

$$\dot{x} = Ax + Bu + Lg(t) \quad (5.1)$$

where x is the entire state variable of the structure. Practically, the entire state of the structure can only be known through the measurement of a smaller set of variables y , where

$$y = Cx \quad (5.2)$$

Since we are seeking to design dampers, the variable y is composed entirely of combinations of velocity measurements and therefore the left half of C is filled with zeros.

With passive viscous dampers, the control forces are proportional to the individual velocity measurements expressed as

$$u = Dy \quad (5.3)$$

Necessarily the matrix D must be square and diagonal and all of the elements must be nonnegative. The coincidence of the measured velocities and the acting control force locations allows us to make the following observations about the matrices B and C :

Since C is restricted to be composed of only velocity measurements

$$C = \begin{bmatrix} 0 & \bar{C} \end{bmatrix} \quad (5.4)$$

and

$$B = \begin{bmatrix} 0 \\ \bar{B} \end{bmatrix} = \begin{bmatrix} 0 \\ -M^{-1}\bar{C}^T \end{bmatrix} \quad (5.5)$$

We wish to optimize the sizes of the dampers in the chosen locations by minimising the usual quadratic performance index

$$J = \int_{t_0}^{t_f} (x^T Qx + u^T Ru) dt \quad (5.6)$$

Following the steps presented in Chapter 2 we append the constraints of Equations 5.1, 5.2 and 5.3 to Equation 5.6 and obtain the Lagrangian

$$\mathcal{L} = \int_{t_0}^{t_f} \left[(x^T Q x + u^T R u) + \lambda_1^T (-\dot{x} + Ax + Bu) + \lambda_2^T (Cx - y) + \lambda_3^T (\hat{D}y - u) \right] dt \quad (5.7)$$

The observer feedback gain matrix \hat{D} has been substituted for the passive damping matrix D . Methods of extracting the passive damping components of this active gain matrix will be subsequently examined. Integrating the term containing \dot{x} by parts one obtains

$$\begin{aligned} \mathcal{L} = & \lambda_1^T(t_f)x(t_f) - \lambda_1^T(t_0)x(t_0) + \\ & \int_{t_0}^{t_f} \left[(x^T Q x + u^T R u) + \lambda_1^T (Ax + Bu) + \lambda_2^T (Cx - y) + \lambda_3^T (\hat{D}y - u) + \dot{\lambda}_1^T(t)x(t) \right] dt \end{aligned} \quad (5.8)$$

Taking the variation of the Lagrangian and setting it equal to zero yields the conditions necessary for an extremum.

$$\begin{aligned} \delta \mathcal{L} = & \lambda_1^T(t_f)\delta x(t_f) - \lambda_1^T(t_0)\delta x(t_0) + \\ & \int_{t_0}^{t_f} \left[(x^T Q x + u^T R u) + \lambda_1^T (A\delta x + B\delta u) + \lambda_2^T (C\delta x - \delta y) + \lambda_3^T (\hat{D}\delta y - \delta u) + \dot{\lambda}_1^T \delta x \right] \end{aligned} \quad (5.9)$$

Note that the variations of the Lagrange multipliers were not included since they lead directly to the constraint Equations 5.1, 5.2 and 5.3. Since $x(t_f)$ is unknown, $\lambda_1(t_f) = 0$ is a final condition. Setting the terms associated with δx , δy and δu equal to zero yields the following equations

$$\dot{\lambda}_1 + 2Qx + A^T \lambda_1 + C^T \lambda_2 = 0 \quad (5.10)$$

$$2Ru + B^T \lambda_1 - \lambda_3 = 0 \quad (5.11)$$

and

$$-\lambda_2 + \hat{D}^T \lambda_3 = 0 \quad (5.12)$$

Substituting Equation 5.12 in Equation 5.10 yields the expression

$$\dot{\lambda}_1 = -2Qx - A^T \lambda_1 + C^T \hat{D}^T \lambda_3 \quad (5.13)$$

From Equation 5.11 we get an expression for the control force

$$u = -\frac{1}{2}R^{-1}(B^T \lambda_1 - \lambda_3) \quad (5.14)$$

Defining co-state variables λ_1 and λ_3 as follows

$$\lambda_1 = Px \quad (5.15)$$

$$\lambda_3 = -Z^T Px \quad (5.16)$$

where P and Z are yet unknown matrices, and observing that

$$\dot{\lambda}_1 = \dot{Px} + P\dot{x} = \dot{Px} + P(Ax + Bu) \quad (5.17)$$

substituting Equations 5.15, 5.16 and 5.17 in Equations 5.13 and 5.14 yields the expressions

$$u = -\frac{1}{2}R^{-1}(B + Z)^T Px \quad (5.18)$$

and

$$\dot{Px} = -2Qx - PAx - A^T Px + \frac{1}{2}PBR^{-1}(B + Z)^T Px - C^T \hat{D}^T Z^T Px. \quad (5.19)$$

Observing that

$$u = \hat{D}Cx = -\frac{1}{2}R^{-1}(B + Z)^T Px = Gx \quad (5.20)$$

yields

$$C^T \hat{D}^T = -\frac{1}{2}P(B + Z)R^{-1} = G^T \quad (5.21)$$

Substituting this expression into Equation 5.19 and eliminating the x term yields a modified version of the Riccati matrix

$$\dot{P} = -2Q - PA - A^T P + \frac{1}{2}PBR^{-1}(B + Z)^T P + \frac{1}{2}P(B + Z)R^{-1}Z^T P \quad (5.22)$$

subject to the condition that

$$P(t_f) = 0 \quad (5.23)$$

The solution of the steady state values of the modified Riccati matrix

$$0 = -2Q - PA - A^T P + \frac{1}{2} PBR^{-1}(B+Z)^T P + \frac{1}{2} P(B+Z)R^{-1}Z^T P \quad (5.24)$$

can proceed by either backward integration of Equations 5.22 or by applying a modified Potter's algorithm for any given choice of Q , R and Z . Once the Ricatti matrix is obtained Equation 5.21 can be used to get the gain matrix G .

5.1.1 Modified Potter's Algorithm

Potter's Algorithm can be applied to solve for the stationary values in the Ricatti matrix. The derivation is repeated here in its modified form. The stationary form of the modified Ricatti matrix is given as

$$-2Q - PA - A^T P + \frac{1}{2} PBR^{-1}(B+Z)^T P + \frac{1}{2} P(B+Z)R^{-1}Z^T P = 0 \quad (5.25)$$

Considering the matrix

$$W = \frac{1}{2} BR^{-1}(B+Z)^T P + \frac{1}{2} (B+Z)R^{-1}Z^T P - A \quad (5.26)$$

we attempt to write the eigenvalue problem in the form

$$WF = FJ \quad (5.27)$$

where F is the matrix of eigenvectors and J is the matrix of eigenvalues.

Combining Equations 5.25 and 5.26 and post-multiplying by F then comparing to Equation 5.27, one can write the equation for PWF

$$PWF = 2QF + A^T PF = PFJ \quad (5.28)$$

One can also write the equation for WF directly from Equation 5.26

$$WF = \frac{1}{2} BR^{-1}(B+Z)^T PF + \frac{1}{2} (B+Z)R^{-1}Z^T PF - AF = FJ \quad (5.29)$$

Substituting $PF=E$ into the Equation 5.28 above yields

$$A^T E + 2QF = EJ \quad (5.30)$$

and Equations 5.29 and 5.30 can be combined in the following equation

$$\begin{bmatrix} A^T & 2Q \\ \frac{1}{2}BR^{-1}(B+Z)^T + \frac{1}{2}(B+Z)R^{-1}Z^T & -A \end{bmatrix} \begin{bmatrix} E \\ F \end{bmatrix} = \begin{bmatrix} E \\ F \end{bmatrix} [J] \quad (5.31)$$

Retaining only the positive eigenvalues and corresponding eigenvectors, the Ricatti matrix is then determined by evaluating

$$P = EF^{-1} \quad (5.32)$$

5.1.2 The Gain Matrix

Once the Ricatti matrix has been established, the full-state gain matrix G can be determined as

$$G = -\frac{1}{2}R^{-1}(B+Z)^T P = \hat{D}C \quad (5.33)$$

The matrix \hat{D} is a square matrix representing the direct feedback associated with the observed variables. In general \hat{D} is a fully populated matrix with order usually less than that of the full state, however as will be seen later on, not necessarily. Since the C matrix is not square, the solution for \hat{D} is not unique but can only be determined in the least squares sense given that it is of reduced order, and as such, the ability of the quantity $\hat{D}C$ to represent G is limited by the contents of C . For example G contains feedback relating to displacement and velocity components of the state vector, G_1 and G_2 , respectively. Since we have already identified in Equation 5.4 that the observer matrix C is composed strictly of velocities, the quantities in the left hand side of $\hat{D}C$ will be zero contradicting those of G . Likewise, if \bar{C} is itself deficient in its description of the state of the structure, the velocity component $\hat{D}\bar{C}$ will also be deficient in its description of G_2 .

Obtaining a solution to Equation 5.32 can proceed as follows: For C and X being any non-square $n \times m$ matrices such that the product CX^T is invertible, one can state that

$$CX^T(CX^T)^{-1} = I \quad (5.34)$$

A logical choice for X is to take $X = C$. In taking $X = C$ it can be demonstrated that non-contributing degrees of freedom will be ignored and the solution will conform to the least-squares solution of the problem. Combining Equations 5.32 and 5.33 it is concluded that

$$\hat{D} = GC^T(CC^T)^{-1} = -\frac{1}{2}R^{-1}(B+Z)^T PC^T(CC^T)^{-1} \quad (5.35)$$

The matrix Z is curious. Z is an unknown similar to the Riccati matrix but it can be observed that if Z is zero or equal to B , familiar forms of the Riccati matrix and the gain matrix emerge. In this study Z will be chosen to be

$$Z = B \quad (5.36)$$

The Riccati matrix simplifies to the form

$$\dot{P} = -2Q - PA - A^T P + 2PBR^{-1}B^T P \quad (5.37)$$

and

$$\hat{D} = -R^{-1}B^T PC^T (CC^T)^{-1} \quad (5.38)$$

5.1.3 Deriving Passive Damping Coefficients from the Gain Matrix

In order to represent the equivalent passive system, we wish to extract the passive component of \hat{D} . A passive feedback system would not permit application of control force at one location due to response of a variable at a different location. The passive component of the control is represented by diagonal matrix D , as indicated in Equation 5.3. In general \hat{D} is not diagonal. To obtain the diagonal matrix, the following two methods are suggested

1. Truncation of \hat{D}
2. Matching through response spectral analysis.

5.1.3.1 Truncation

One possibility is simply to truncate all off-diagonal terms such that

$$D = \text{diag}(\hat{D}) \quad (5.39)$$

The problem with this approach is that the strength of the control is greatly limited. As a structure responds dynamically to input from an external source, nearby variables (measured or not) move in sympathy. If several are measured, the output of each will contribute to the response of the others. The truncation procedure ignores these contributions and as a result produces a weak control.

5.1.3.2 Response Spectrum Analysis

Reinhorn *et al* (1988) suggested using a least-squares fitting method or a first undamped mode for establishing a diagonal D matrix. This procedure specifically includes excitation in the form

of time histories. The main drawback with this process is that the computation is based on specific earthquakes, which may not directly reflect the design criteria. As an alternative procedure it is suggested here to use a response spectral analysis procedure in place of the time history analysis procedure proposed by Reinhorn *et al.*

The objective of the proposed RSA analysis procedure is to establish the diagonal matrix

$$D = \begin{bmatrix} D_1 & 0 & \cdots & 0 \\ 0 & D_2 & & 0 \\ \vdots & & \ddots & \vdots \\ 0 & 0 & \cdots & D_n \end{bmatrix} \quad (5.40)$$

using the formulae

$$D_i = \frac{u_{\max}^i}{\dot{y}_{\max}^i} \quad (5.41)$$

where the repeated index does not imply summation. The quantities u_{\max}^i and \dot{y}_{\max}^i are the maximum force and velocity components that would be predicted for the i^{th} damper in its selected location established based on the RSA results.

5.2 Response Spectrum Analysis Procedure

Response spectral analysis procedures are commonly used in the seismic analysis of structural systems and provide some distinct advantages over alternative pseudo-static and time history analysis procedures. RSA provides an approximate method aimed at directly establishing envelope quantities using a superposition of modal contributions. There are many modal combination procedures available for combining contributions from individual modes, including the Complete Quadratic Combination (CQC), but one of the simplest and often used procedure is the Square Root of the Sum of the Squares (SRSS). Further discussion of modal combination procedures is beyond the scope of this investigation, although it is recognised that the type of modal combination performed can significantly affect the results and is therefore an important consideration for further research.

Given that the individual modal contributions to the response of the structure

$$x(t) = \begin{bmatrix} x_1(t) \\ x_2(t) \\ \vdots \\ x_n(t) \\ \dot{x}_1(t) \\ \dot{x}_2(t) \\ \vdots \\ \dot{x}_n(t) \end{bmatrix} = \sum_{j=1}^m x_j(t) = \begin{bmatrix} \sum x_1^j(t) \\ \sum x_2^j(t) \\ \vdots \\ \sum x_n^j(t) \\ \sum \dot{x}_1^j(t) \\ \sum \dot{x}_2^j(t) \\ \vdots \\ \sum \dot{x}_n^j(t) \end{bmatrix} = \sum_{j=1}^m \alpha_j(t) \phi_j \quad (5.42)$$

where $x(t)$ is the state vector response, n represents the number of degrees of freedom of the structure and m represents the number of modes used for the response spectral analysis of the structure. The vector $x_j(t)$ represents the time history response of mode j , which in turn can be expressed as the product of a scalar amplitude function of time and a time invariant mode shape associated with mode j .

The envelope values of $x(t)$ can be estimated by evaluating the SRSS of each of the modal contributions

$$x_{\max} = \begin{bmatrix} \max(x_1) \\ \max(x_2) \\ \vdots \\ \max(x_n) \\ \max(\dot{x}_1) \\ \max(\dot{x}_2) \\ \vdots \\ \max(\dot{x}_n) \end{bmatrix} \cong \sqrt{\sum_{j=1}^m \max(x_j(t))^2} = \sqrt{\sum_{j=1}^m \max(\alpha_j(t))^2 \phi_j^2} \quad (5.43)$$

The vector of control forces can be established by evaluating

$$u_{\max} = \begin{bmatrix} \max(u_1(t)) \\ \max(u_2(t)) \\ \vdots \\ \max(u_k(t)) \end{bmatrix} \cong \sqrt{\sum_{j=1}^k \max(Gx_j(t))^2} \cong \sqrt{\sum_{j=1}^k \max(\alpha_j(t))^2 (\hat{D}C\phi_j)^2} \quad (5.44)$$

Similarly the vector of envelope observed velocities can be determined using

$$y_{\max} = \begin{bmatrix} \max(y_1(t)) \\ \max(y_2(t)) \\ \vdots \\ \max(y_k(t)) \end{bmatrix} \cong \sqrt{\sum_{j=1}^k \max(Cx_j(t))^2} = \sqrt{\sum_{j=1}^k \max(\alpha_j(t))^2 (C\phi_j)^2} \quad (5.45)$$

Once determined, the values established in Equation 5.44 can be divided by the corresponding value in Equation 5.45 to yield the diagonal matrix D of Equation 5.40.

5.2.1 Modal Superposition

Before it is possible to deal with envelope values from a RSA, it is necessary to consider the modal superposition in the state-space form. Meirovitch (1990) states that the modal superposition state vector $x(t)$ can be shown to be

$$x(t) = \int_{\tau=0}^t U e^{\Lambda(t-\tau)} V^T X(\tau) d\tau \quad (5.46)$$

where homogeneous initial conditions are assumed. The matrices U and V represent the set $2n$ right and left complex eigenvectors corresponding to diagonal matrix Λ containing the associated complex eigenvalues or “poles”. Note that for a large model the number of mode shape vectors necessary for sufficiently accurate computation of $x(t)$ may be a fraction of the total number of modes. It is therefore understood that the matrices U , V and Λ may be truncated.

Assuming $2k$ modes are being carried, the dimensions of the matrices in Equation 5.46 are as follows: U and $V - 2n \times 2k$; $\Lambda - 2k \times 2k$; $X - 2n \times 1$. The vector $X(t)$ represents the set of applied accelerations derived from either of the following expressions, depending on the type of input

$$X(t) = \begin{bmatrix} 0 \\ -M^{-1}F(t) \end{bmatrix} \quad (5.47)$$

or

$$X(t) = L\ddot{x}_g(t) \quad (5.48)$$

In Equation 5.47, $F(t)$ represents a vector of input forces, and in Equation 5.48 $\ddot{x}_g(t)$ represents a vector of input accelerations and associated matrix L describes the relationship between the acceleration function and the response of the state variables.

Re-arranging Equation 5.46, and recognising that the shorthand expression $e^{\Lambda t}$ evaluates to a sum, the following expression is obtained

$$x(t) = \sum_{j=1}^k \left[\int_0^t \left(U_j e^{\Lambda_j(t-\tau)} V_j^T L + \bar{U}_j e^{\bar{\Lambda}_j(t-\tau)} \bar{V}_j^T L \right) \ddot{x}_g(\tau) d\tau \right] \quad (5.49)$$

where j in this case represents the number of pairs of eigenvectors being carried in the solution. The overbar ($\bar{\cdot}$) in the above equation represents the complex conjugate.

Explicitly defining the real and imaginary components of the above vectors and their complex conjugates as

$$\begin{aligned} U_j &= U_j^{\text{Re}} + iU_j^{\text{Im}}; & \bar{U}_j &= U_j^{\text{Re}} - iU_j^{\text{Im}}; \\ V_j &= V_j^{\text{Re}} + iV_j^{\text{Im}}; & \bar{V}_j &= V_j^{\text{Re}} - iV_j^{\text{Im}}; \\ \Lambda_j &= \zeta_j^{\text{Re}} + i\omega_j^{\text{Im}}; & \bar{\Lambda}_j &= \zeta_j^{\text{Re}} - i\omega_j^{\text{Im}}. \end{aligned} \quad (5.50)$$

then, evaluating the product, the following real valued expression is obtained

$$\begin{aligned} x(t) &= 2 \sum_{j=1}^k \int_0^t e^{\zeta_j(t-\tau)} \left[\cos(\omega_j(t-\tau)) \left(U_j^{\text{Re}} V_j^{\text{Re}T} L - U_j^{\text{Im}} V_j^{\text{Im}T} L \right) \right. \\ &\quad \left. + \sin(\omega_j(t-\tau)) \left(U_j^{\text{Im}} V_j^{\text{Re}T} L + U_j^{\text{Re}} V_j^{\text{Im}T} L \right) \right] \ddot{x}_g(t-\tau) d\tau \end{aligned} \quad (5.51)$$

which can be re-arranged to

$$\begin{aligned} x(t) &= 2 \sum_{j=1}^k \left[\left(U_j^{\text{Re}} V_j^{\text{Re}T} L - U_j^{\text{Im}} V_j^{\text{Im}T} L \right) \int_0^t e^{\zeta_j(t-\tau)} \cos(\omega_j(t-\tau)) \ddot{x}_g(\tau) d\tau \right. \\ &\quad \left. + \left(U_j^{\text{Im}} V_j^{\text{Re}T} L + U_j^{\text{Re}} V_j^{\text{Im}T} L \right) \int_0^t e^{\zeta_j(t-\tau)} \sin(\omega_j(t-\tau)) \ddot{x}_g(\tau) d\tau \right] \end{aligned} \quad (5.52)$$

Identifying that the integrals in Equation 5.52 as spectral values that depend on the period, damping and on the particular characteristics of the input time history. The vector combinations $V_j^{\text{Re}T} L$ and $V_j^{\text{Im}T} L$ represent participation factors and are scalar if $\ddot{x}_g(t)$ contains only one time history. Replacing these quantities with P_j^{Re} and P_j^{Im} respectively and identifying the integrals in Equation 5.51 as

$$\begin{aligned} S_j^C(t) &= \int_0^t e^{\zeta_j(t-\tau)} \cos(\omega_j(t-\tau)) \ddot{x}_g(\tau) d\tau \\ S_j^S(t) &= \int_0^t e^{\zeta_j(t-\tau)} \sin(\omega_j(t-\tau)) \ddot{x}_g(\tau) d\tau \end{aligned} \quad (5.53)$$

Equation 5.52 can be simplified to

$$x(t) = 2 \sum_{j=1}^k \left[(U_j^{\text{Re}} P_j^{\text{Re}} - U_j^{\text{Im}} P_j^{\text{Im}}) S_j^C(t) + (U_j^{\text{Im}} P_j^{\text{Re}} + U_j^{\text{Re}} P_j^{\text{Im}}) S_j^S(t) \right] \quad (5.54)$$

and further to

$$x(t) = 2 \sum_{j=1}^k [x_j^C S_j^C(t) + x_j^S S_j^S(t)] \quad (5.55)$$

where

$$x_j^C = U_j^{\text{Re}} P_j^{\text{Re}} - U_j^{\text{Im}} P_j^{\text{Im}} \quad (5.56)$$

and

$$x_j^S = U_j^{\text{Im}} P_j^{\text{Re}} + U_j^{\text{Re}} P_j^{\text{Im}} \quad (5.57)$$

are the two characteristic real valued modes and can be seen to correspond each to one time-history component in Equation 5.43.

5.2.2 SRSS Modal Combination

The integrals of Equation 5.53 represent the time history response corresponding to component $\alpha(t)$. In order to perform the response spectral analysis the following quantities need to be either evaluated or provided ahead of any subsequent modal combination procedure. Defining

$$\max(S_j^C) = \max \left(\left| \int_0^t e^{\zeta_j(t-\tau)} \cos(\omega_j(t-\tau)) \ddot{x}_g(\tau) d\tau \right| \right) \quad (5.58)$$

and

$$\max(S_j^S) = \max \left(\left| \int_0^t e^{\zeta_j(t-\tau)} \sin(\omega_j(t-\tau)) \ddot{x}_g(\tau) d\tau \right| \right) \quad (5.59)$$

as members of a function called the response spectrum, these quantities represent envelope values of the response of a single degree of freedom structure with a given frequency and exponential decay function (related to damping). These quantities can be used together with the vectors extracted from the mode shapes and participation factors from Equations 5.56 and 5.57. Using the SRSS procedure established in Equations 5.43, 5.44 and 5.45, the following expressions are obtained

$$x_{\max} \cong 2 \sqrt{\sum_{j=1}^m (\max(S_j^C) x_j^C)^2 + (\max(S_j^S) x_j^S)^2} \quad (5.60)$$

$$y_{\max} \cong 2 \sqrt{\sum_{j=1}^m (\max(S_j^C) C x_j^C)^2 + (\max(S_j^S) C x_j^S)^2} \quad (5.61)$$

$$u_{\max} \cong 2 \sqrt{\sum_{j=1}^m (\max(S_j^C) G x_j^C)^2 + (\max(S_j^S) G x_j^S)^2} \quad (5.62)$$

or, alternatively

$$u_{\max} \cong 2 \sqrt{\sum_{j=1}^m (\max(S_j^C) \hat{D} C x_j^C)^2 + (\max(S_j^S) \hat{D} C x_j^S)^2} \quad (5.63)$$

Note that where the square or square root function is applied to a vector quantity, $(\dots)^2$ or $\sqrt{(\dots)}$, the operation is applied individually to each element of the vector.

The above derived response spectra are investigated in detail in Appendix C.

5.3 Worked Example: Uniform 4-Story Structure

The following is intended to demonstrate with a numerical example how the derived equations are to be applied to carry out the design of a set of passive viscous and passive friction dampers for a simple structure. The structure chosen is the 4-story structure with uniform mass and stiffness used in Chapter 4 and shown in Figure 4.1. This structure was assigned a Rayleigh damping of approximately 2.5% in the first two modes. Appendix D contains a more detailed account of the dynamic properties of this structure.

The state-space equation of motion of the structure, Equation 5.1, is given as

$$\begin{bmatrix} \dot{x}_1 \\ \dot{x}_2 \\ \dot{x}_3 \\ \dot{x}_4 \\ \ddot{x}_1 \\ \ddot{x}_2 \\ \ddot{x}_3 \\ \ddot{x}_4 \end{bmatrix} = \begin{bmatrix} 0 & 0 & 0 & 0 & 1 & 0 & 0 & 0 \\ 0 & 0 & 0 & 0 & 0 & 1 & 0 & 0 \\ 0 & 0 & 0 & 0 & 0 & 0 & 1 & 0 \\ 0 & 0 & 0 & 0 & 0 & 0 & 0 & 1 \\ -2400 & 1200 & 0 & 0 & -3.1 & 1.3 & 0 & 0 \\ 1200 & -2400 & 1200 & 0 & 1.3 & -3.1 & 1.3 & 0 \\ 0 & 1200 & -2400 & 1200 & 0 & 1.3 & -3.1 & 1.3 \\ 0 & 0 & 1200 & -1200 & 0 & 0 & 1.3 & -1.8 \end{bmatrix} \begin{bmatrix} x_1 \\ x_2 \\ x_3 \\ x_4 \\ \dot{x}_1 \\ \dot{x}_2 \\ \dot{x}_3 \\ \dot{x}_4 \end{bmatrix} + \begin{bmatrix} 0 & 0 & 0 & 0 \\ 0 & 0 & 0 & 0 \\ 0 & 0 & 0 & 0 \\ 0 & 0 & 0 & 0 \\ -1 & 1 & 0 & 0 \\ 0 & -1 & 1 & 0 \\ 0 & 0 & -1 & 1 \\ 0 & 0 & 0 & -1 \end{bmatrix} \begin{bmatrix} u_1 \\ u_2 \\ u_3 \\ u_4 \end{bmatrix} + \begin{bmatrix} 0 \\ 0 \\ 0 \\ 0 \\ 1 \\ 1 \\ 1 \\ 1 \end{bmatrix} \ddot{x}_g(t) \quad (5.64)$$

with the observer matrix (Equation 5.2) defined as

$$y = \begin{bmatrix} 0 & 0 & 0 & 0 & 1 & 0 & 0 & 0 \\ 0 & 0 & 0 & 0 & -1 & 1 & 0 & 0 \\ 0 & 0 & 0 & 0 & 0 & -1 & 1 & 0 \\ 0 & 0 & 0 & 0 & 0 & 0 & -1 & 1 \end{bmatrix} \begin{bmatrix} x_1 \\ x_2 \\ x_3 \\ x_4 \\ \dot{x}_1 \\ \dot{x}_2 \\ \dot{x}_3 \\ \dot{x}_4 \end{bmatrix} \quad (5.65)$$

and the definition of matrices A , B , L and C , and vectors x , \dot{x} , y and L are obvious by comparison with the above mentioned equations. Given the weighting matrices

$$Q = \begin{bmatrix} k & 0 \\ 0 & m \end{bmatrix} = \begin{bmatrix} 2400 & -1200 & 0 & 0 & 0 & 0 & 0 & 0 \\ -1200 & 2400 & -1200 & 0 & 0 & 0 & 0 & 0 \\ 0 & -1200 & 2400 & -1200 & 0 & 0 & 0 & 0 \\ 0 & 0 & -1200 & 1200 & 0 & 0 & 0 & 0 \\ 0 & 0 & 0 & 0 & 1 & 0 & 0 & 0 \\ 0 & 0 & 0 & 0 & 0 & 1 & 0 & 0 \\ 0 & 0 & 0 & 0 & 0 & 0 & 1 & 0 \\ 0 & 0 & 0 & 0 & 0 & 0 & 0 & 1 \end{bmatrix} \quad (5.66)$$

and

$$R = \begin{bmatrix} 0.06 & 0 & 0 & 0 \\ 0 & 0.06 & 0 & 0 \\ 0 & 0 & 0.06 & 0 \\ 0 & 0 & 0 & 0.06 \end{bmatrix} \quad (5.67)$$

the damping coefficients will be determined by

- i. truncation of the optimal gains, and
- ii. modal combination based on response spectrum values provided.

5.3.1 Solution

Solution of the optimal control problem proceeds first with establishing the Ricatti matrix. This has been covered in Chapter 2 and the corresponding example appears in Appendix A. The Ricatti matrix is

$$P = \begin{bmatrix} 478.0 & -125.1 & -29.1 & -14.3 & 0.987 & 0 & 0 & 0 \\ -125.1 & 448.9 & -139.5 & -43.4 & 0 & 0.987 & 0 & 0 \\ -29.1 & -139.5 & 434.6 & -186.6 & 0 & 0 & 0.987 & 0 \\ -14.3 & -43.4 & -186.6 & 309.5 & 0 & 0 & 0 & 0.987 \\ 0.987 & 0 & 0 & 0 & 0.250 & 0.114 & 0.079 & 0.067 \\ 0 & 0.987 & 0 & 0 & 0.114 & 0.328 & 0.181 & 0.146 \\ 0 & 0 & 0.987 & 0 & 0.079 & 0.181 & 0.395 & 0.260 \\ 0 & 0 & 0 & 0.987 & 0.067 & 0.146 & 0.260 & 0.509 \end{bmatrix} \quad (5.68)$$

The full-state gain matrix is then evaluated as (note that $Z = 0$)

$$G = -\frac{1}{2}R^{-1}B^T P = \begin{bmatrix} 16.4 & 0 & 0 & 0 & 4.16 & 1.90 & 1.31 & 1.12 \\ -16.4 & 16.4 & 0 & 0 & -2.26 & 3.57 & 1.71 & 1.31 \\ 0 & -16.4 & 16.4 & 0 & -0.59 & -2.46 & 3.57 & 1.90 \\ 0 & 0 & -16.4 & 16.4 & -0.19 & -0.59 & -2.26 & 4.16 \end{bmatrix} \quad (5.69)$$

Next, solve for the direct observer feedback matrix. Finding the least-squares invert of the C matrix

$$C^T(CC^T)^{-1} = \begin{bmatrix} 0 & 0 & 0 & 0 \\ 0 & 0 & 0 & 0 \\ 0 & 0 & 0 & 0 \\ 0 & 0 & 0 & 0 \\ 1 & -1 & 0 & 0 \\ 0 & 1 & -1 & 0 \\ 0 & 0 & 1 & -1 \\ 0 & 0 & 0 & 1 \end{bmatrix} \begin{bmatrix} 1 & -1 & 0 & 0 \\ -1 & 2 & -1 & 0 \\ 0 & -1 & 2 & -1 \\ 0 & 0 & -1 & 2 \end{bmatrix} = \begin{bmatrix} 0 & 0 & 0 & 0 \\ 0 & 0 & 0 & 0 \\ 0 & 0 & 0 & 0 \\ 0 & 0 & 0 & 0 \\ 1 & 0 & 0 & 0 \\ 1 & 1 & 0 & 0 \\ 1 & 1 & 1 & 0 \\ 1 & 1 & 1 & 1 \end{bmatrix} = (C^{-1}) \quad (5.70)$$

and evaluating the product

$$\hat{D} = G(C^{-1}) = \begin{bmatrix} 8.49 & 4.33 & 2.43 & 1.12 \\ 4.33 & 6.59 & 3.02 & 1.31 \\ 2.43 & 3.02 & 5.47 & 1.90 \\ 1.12 & 1.31 & 1.90 & 4.16 \end{bmatrix} \quad (5.71)$$

Note that this matrix is not strongly diagonal.

Applying the truncation method one obtains the estimate for D

$$D = \begin{bmatrix} 8.49 & 0 & 0 & 0 \\ 0 & 6.59 & 0 & 0 \\ 0 & 0 & 5.47 & 0 \\ 0 & 0 & 0 & 4.16 \end{bmatrix} \quad (5.72)$$

Next apply response spectral analysis. The first step is to perform a modal analysis and extract the eigenvalues and corresponding right and left eigenvectors

The eigenvalues are found to be

$$\Lambda = \text{diag} \begin{bmatrix} -1.16 - 12.06i \\ -1.16 + 12.06i \\ -3.35 - 34.72i \\ -3.35 + 34.72i \\ -5.38 - 53.16i \\ -5.38 + 53.16i \\ -6.83 - 65.19i \\ -6.83 + 65.19i \end{bmatrix} \quad (5.73)$$

while the right eigenvectors are found to be

$$U = \begin{bmatrix} 0.00151 - 0.011i & 0.00151 + 0.011i & -0.095 + 0.0136i & -0.095 - 0.0136i \\ 0.0284 - 0.021i & 0.0284 + 0.021i & -0.095 + 0.0136i & -0.095 - 0.0136i \\ 0.0383 - 0.028i & 0.0383 + 0.028i & 0 & 0 \\ 0.0435 - 0.032i & 0.0435 + 0.032i & 0.095 - 0.0136i & 0.095 + 0.0136i \\ -0.152 - 0.169i & -0.152 + 0.169i & 0.5024 + 0.284i & 0.5024 - 0.284i \\ -0.285 - 0.318i & -0.285 + 0.318i & 0.5024 + 0.284i & 0.5024 - 0.284i \\ -0.384 - 0.429i & -0.384 + 0.429i & 0 & 0 \\ -0.437 - 0.487i & -0.437 + 0.487i & -0.5024 - 0.284i & -0.5024 + 0.284i \\ -0.0077 + 0.0096i & -0.0077 - 0.0096i & 0.012 - 0.0064i & 0.012 + 0.0064i \\ 0.0027 - 0.0033i & 0.0027 + 0.0033i & -0.018 + 0.0099i & -0.018 - 0.0099i \\ 0.0067 - 0.0084i & 0.0067 + 0.0084i & 0.016 - 0.0087i & 0.016 + 0.0087i \\ -0.0050 + 0.0063i & -0.0050 - 0.0063i & -0.006 + 0.0034i & -0.006 - 0.0034i \\ 0.551 + 0.356i & 0.551 - 0.356i & -0.427 - 0.0313i & -0.369 + 0.0313i \\ -0.191 - 0.124i & -0.191 + 0.124i & 0.655 + 0.0479i & 0.566 - 0.0479i \\ -0.485 - 0.313i & -0.485 + 0.313i & -0.576 - 0.0421i & -0.497 + 0.0421i \\ 0.359 + 0.232i & 0.359 - 0.232i & 0.227 + 0.0166i & 0.196 - 0.0166i \end{bmatrix} \quad (5.74)$$

and the left eigenvectors are

$$V = \begin{bmatrix} 1.037 + 0.929i & 1.949 + 1.746i & 2.625 + 2.352i & 2.986 + 2.674i \\ 1.037 - 0.929i & 1.949 - 1.746i & 2.625 - 2.352i & 2.986 - 2.674i \\ -4.979 - 8.810i & -4.979 - 8.810i & 0 & 4.979 + 8.810i \\ -4.979 + 8.810i & -4.979 + 8.810i & 0 & 4.979 - 8.810i \\ -9.574 - 14.81i & 3.325 + 5.143i & 8.419 + 13.02i & -6.249 - 9.666i \\ -9.574 + 14.81i & 3.325 - 5.143i & 8.419 - 13.02i & -6.249 + 9.666i \\ 1.031 + 14.09i & -1.580 - 21.58i & 1.389 + 18.98i & -0.549 - 7.495i \\ 1.031 - 14.09i & -1.580 + 21.58i & 1.389 - 18.98i & -0.549 + 7.495i \\ -0.068 + 0.093i & -0.068 + 0.213i & -0.173 + 0.234i & -0.196 + 0.267i \\ -0.068 - 0.093i & -0.068 - 0.213i & -0.173 - 0.234i & -0.196 - 0.267i \\ 0.238 - 0.166i & 0.281 - 0.076i & 0 & -0.238 + 0.166i \\ 0.238 + 0.166i & 0.281 + 0.076i & 0 & -0.238 - 0.166i \\ 0.258 - 0.206i & -0.103 + 0.050i & -0.227 + 0.181i & 0.168 - 0.134i \\ 0.258 + 0.206i & -0.103 - 0.050i & -0.227 - 0.181i & 0.168 + 0.134i \\ -0.212 + 0.038i & 0.269 - 0.191i & -0.286 + 0.051i & 0.113 - 0.020i \\ -0.212 - 0.038i & 0.269 + 0.191i & -0.286 - 0.051i & 0.113 + 0.020i \end{bmatrix}$$

(5.75)

Note that the eigenvectors satisfy the bi-orthogonality relations

$$VU = I \quad (5.76)$$

and

$$V(A + BG)U = \Lambda \quad (5.77)$$

Based on the real and imaginary components of the matrix of left eigenvectors, modal participation factors are computed

$$P^{\text{Re}} = \text{Re}(V^*)L = \text{diag}[-0.565 \quad 0.238 \quad 0.110 \quad 0.060] \quad (5.78)$$

and

$$P^{\text{Im}} = \text{Im}(V^*) = \text{diag}[-0.767 \quad 0.166 \quad 0.088 \quad -0.011] \quad (5.79)$$

Where V^* indicates that only vectors associated with poles in the upper left quadrant are retained for brevity. Combining the real and imaginary parts such that the cosine and sine related mode shapes can be isolated yields

$$M^C = \text{Re}(U)P^{\text{Re}} - \text{Im}(U)P^{\text{Im}} = \begin{bmatrix} 0 & 0 & 0 & 0 \\ 0 & 0 & 0 & 0 \\ 0 & 0 & 0 & 0 \\ 0 & 0 & 0 & 0 \\ 0.2155 & 0.1667 & 0.0918 & 0.0260 \\ 0.4050 & 0.1667 & -0.0319 & -0.0398 \\ 0.5457 & 0 & -0.0807 & 0.0350 \\ 0.6206 & -0.1667 & 0.0599 & -0.0138 \end{bmatrix} \quad (5.80)$$

and

$$M^S = \text{Im}(U)P^{\text{Re}} + \text{Re}(U)P^{\text{Im}} = \begin{bmatrix} -0.0179 & -0.0048 & -0.0017 & -0.004 \\ -0.0336 & -0.0048 & 0.0006 & 0.006 \\ -0.0453 & 0 & 0.0015 & -0.005 \\ -0.0515 & 0.0048 & -0.0011 & 0.002 \\ 0.0207 & 0.0161 & 0.0093 & 0.0027 \\ 0.0390 & 0.0161 & -0.0032 & -0.0042 \\ 0.0525 & 0 & -0.0082 & 0.0037 \\ 0.0597 & -0.0161 & 0.0061 & -0.0014 \end{bmatrix} \quad (5.81)$$

note that the first column contains values that are larger than those in the remaining columns indicating that if the input were equal for every mode, the first mode would provide the largest contribution to the response.

To carry out the response spectral analysis one must have prepared sin and cosine spectra to describe the input. Evaluating the integrals in Equations 5.58 and 5.59 with El Centro earthquake input in units of acceleration yields the quantities

$$S^C = [0.6064 \quad 0.1466 \quad 0.0710 \quad 0.0527] \quad (5.82)$$

and

$$S^S = [0.5937 \quad 0.1693 \quad 0.0967 \quad 0.0728] \quad (5.83)$$

which carry the units of velocity following integration with respect to time.

Carrying out the modal combination using the SRSS modal combination procedure the system response envelope is estimated as

$$x_{\max} \cong \sqrt{\sum_{i=1}^k \left[(2M_i^c S_i^c)^2 + (2M_i^s S_i^s)^2 \right]} = \begin{bmatrix} 0.0213 \\ 0.0399 \\ 0.0537 \\ 0.0611 \\ 0.2675 \\ 0.4959 \\ 0.6649 \\ 0.7576 \end{bmatrix} \quad (5.84)$$

similarly the envelope damper peak velocities can be established as

$$y_{\max} \cong \sqrt{\sum_{i=1}^k \left[(2CM_i^c S_i^c)^2 + (2CM_i^s S_i^s)^2 \right]} = \begin{bmatrix} 0.2675 \\ 0.2317 \\ 0.1786 \\ 0.1057 \end{bmatrix} \quad (5.85)$$

the corresponding peak control force is established as

$$u_{\max} \cong \sqrt{\sum_{i=1}^k \left[(2GM_i^c S_i^c)^2 + (2GM_i^s S_i^s)^2 \right]} = \begin{bmatrix} 3.738 \\ 3.280 \\ 2.446 \\ 1.319 \end{bmatrix} \quad (5.86)$$

Using the above values, the viscous damping coefficients corresponding to the passive control can be evaluated

$$D = \text{diag} \left(\frac{u_{\max}}{y_{\max}} \right) = \begin{bmatrix} 14.0 & 0 & 0 & 0 \\ 0 & 14.2 & 0 & 0 \\ 0 & 0 & 13.7 & 0 \\ 0 & 0 & 0 & 12.5 \end{bmatrix} \quad (5.87)$$

As expected the dampers evaluated based on the peak values are larger than those computed using the truncation method. The ratio

$$\frac{D_{\text{peak}}}{D_{\text{truncated}}} = D_{\text{truncated}}^{-1} D_{\text{peak}} = \begin{bmatrix} 1.65 & - & - & - \\ - & 2.15 & - & - \\ - & - & 2.50 & - \\ - & - & - & 3.00 \end{bmatrix} \quad (5.88)$$

which can be seen to have a more pronounced difference in the upper portions of the structure. If friction dampers are to be used, and the braces can be considered to be rigid, the slip loads can be established by multiplying u_{\max} by $\pi/4$ such that

$$s = \frac{\pi}{4} u_{\max} = \begin{bmatrix} 2.94 \\ 2.58 \\ 1.92 \\ 1.04 \end{bmatrix} \quad (5.89)$$

However, if the braces are flexible, a more detailed procedure needs to be followed taking into account of the expected peak deflection experienced by the friction devices. In this case slip loads are determined such that the dampers will have the capability of dissipating similar peak cycle energy as the proposed viscous damper system.

In situations where the flexibility cannot be ignored, it is necessary to supply (tangent) stiffness values K_i to adequately account for brace flexibility and information about the deformations that the braces will be subjected to also needs to be gathered from the response spectral analysis of the model.

Extracting estimates of envelope values of deformations is accomplished using a procedure similar to that used for extracting estimates of envelope velocities and control forces. A modified observer is defined as

$$d = C_d x \quad (5.90)$$

where d refers to the displacements of the dampers. Presuming small deflections, the matrix C_d takes the form

$$C_d = \begin{bmatrix} \bar{C} \\ 0 \end{bmatrix} \quad (5.91)$$

where \bar{C} is the same as that used in Equation 5.4. The displacement envelope estimate therefore takes the form

$$d_{\max} \cong \sqrt{\sum_{i=1}^k \left[(2C_d M_i^C S_i^C)^2 + (2C_d M_i^S S_i^S)^2 \right]} \quad (5.92)$$

5.4 Extension to Friction Dampers

Establishing the diagonal constants of Equation 5.88 establishes a set of linear viscous damping coefficients that imitate the effect of the active control necessary to provide an optimal response of the structure – a trade-off between the control effort and the control effect in the sense of the LQR performance index. Extension of the performance to friction dampers can also be considered.

In the first stage, the extension to friction dampers was made under the assumption that the brace supporting the friction dampers is essentially rigid. Next, the case where the rigid brace assumption no longer holds will be considered. In Chapter 3 and 4, the flexibility of the system supporting the dampers was taken into account using a brace stiffness ratio, α . In this section, following on the same lines as the previous development, the brace stiffnesses must be explicitly supplied before being able to proceed.

In the case of either the rigid or the flexible brace, the proportioning of friction dampers assumes that in the peak cycle the energy dissipated by the viscous damper and the friction damper are equal.

The energy dissipated by the viscous dampers is equal to the area enclosed by the elliptical hysteresis loop and is determined by the following expression

$$E_v = \pi u_{\max} d_{\max} \quad (5.93)$$

5.4.1 Rigid Brace

The energy dissipated in a friction damper with a perfectly rigid brace is given as

$$E_f = 4s d_{\max} \quad (5.94)$$

where s represents the slip force characteristic of the friction damper. Equating Equations 5.93 and 5.94 above and solving for the slip load s gives the result

$$s = \frac{\pi}{4} u_{\max} \quad (5.95)$$

which is independent of the peak displacement d_{\max} .

5.4.2 Flexible Brace

In the case of a flexible brace, the hysteresis loop characteristic of the brace and damper together has the form as shown in Figure 5.1(c). The energy enclosed by this hysteresis loop is given as

$$E_f = 4s \left(d_{\max} - \frac{s}{k} \right) \quad (5.96)$$

and equating the energy to Equation 5.96 yields the result

$$s = k \left(\frac{d_{\max}}{2} \pm \sqrt{\left(\frac{d_{\max}}{2} \right)^2 - \frac{\pi u_{\max} d_{\max}}{4k}} \right) \quad (5.97)$$

which has a solution only if

$$d_{\max} > \frac{\pi u_{\max}}{k} \quad (5.98)$$

or otherwise stated, the brace stiffness must satisfy the following in order to be effective

$$k > \frac{\pi u_{\max}}{d_{\max}} \quad (5.99)$$

where it is emphasized that the quantity k expresses unwanted stiffness in the bracing system connecting the friction damper to the rest of the structure, and is not necessarily under the control of the designer.

Equation 5.98 provides an option to choose which slip load should satisfy the energy equilibrium by either adding or subtracting the quantity of the radical. In the case of a control design it is advisable to use the lower valued slip force

$$s = k \left(\frac{d_{\max}}{2} - \sqrt{\left(\frac{d_{\max}}{2} \right)^2 - \frac{\pi u_{\max} d_{\max}}{4k}} \right) \quad (5.100)$$

both for economy and to permit the devices to act during events that are smaller than the design event.

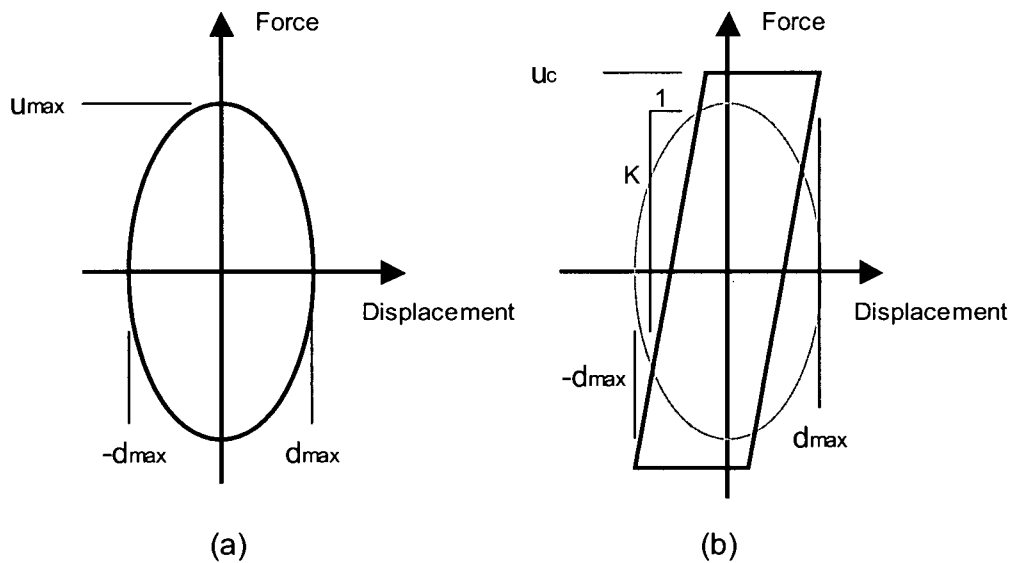


Figure 5.1. Assumed peak cycle hysteresis loops for (a) an ideal viscous damper and (b) a friction damper with a flexible brace having brace stiffness K .

5.5 Summary of the Proposed RSA Procedure

Proposed method for selecting viscous dampers using the above described response spectral analysis procedure is summarised in the following steps:

1. Define the structural system to be controlled using m , k and c matrices. With these matrices, formulate the system dynamics in the state space form by defining the A , B and C matrices.
2. Select desirable and practical damper locations and construct location matrices C , C_d and control force influence matrix B to describe the locations and effects of the damper forces on the state variables of the structure.
3. Choose the form of weighting matrices Q and R to regulate the control strength leaving one or more variables to regulate the strength of the control (see Equations 5.66 and 5.67 and Appendix A).
4. Solve the control problem to determine full state feedback matrix G so as to establish the target (active) control. This involves by solving the time independent Ricatti matrix,

Equation 5.24 and then Equation 5.33 to establish the full state gains, and, if desired, the observer feedback Equation 5.38.

5. Obtain response spectra that represent the appropriate design criteria with an acceptable level of risk for the structure. Using these spectral values, estimate using RSA the peak cycle displacements, velocities and control forces for the given excitation using the controlled system $(A+BG)$ or $(A+BDC)$ as a target. With the target system, the RSA procedure involves the following sub-steps
 - 5.1 establish eigenvalues λ , and the right and left eigenvectors U and V and scaled mode shapes from Equations 5.56 and 5.57
 - 5.2 compute SRSS modal combinations to establish envelope damper velocities, y_{max} , and full state control forces, u_{max} , using Equations 5.44 and 5.45 and the established mode shapes
6. Evaluate the viscous damping coefficients necessary to satisfy the target control level using Equation 5.41.
7. If necessary, estimate a more appropriate value for R and repeat Steps 2-6 as necessary until an acceptable configuration of dampers is found that satisfy all design criteria.

Following these steps, a recommended set of viscous damping coefficients at the selected locations that satisfy the performance requirements will be obtained. If the intent is to design a set of friction dampers, additional steps are required.

8. compute peak displacements using a modified Equation 5.61, as described in Equations 5.91 and 5.92
9. for each individual damper compute the slip load using Equation 5.100, if a real value exists

If a real value for the slip load does not exist, then with the given level of deformation and brace stiffness a friction damper will not be capable of dissipating the amount of energy necessary to achieve the target level of control. If this is the case then the target level of control must be set lower by accepting higher displacements and velocities, find ways of reducing the unwanted brace flexibility, or abandon the use of friction dampers.

5.6 Discussion

The preceding derived methodology overcomes some of the deficiencies of the method put forth by Reinhorn *et al.* (1988) when considering application to a design problem. Both methods make use of the gain matrix obtained for the linear quadratic regulator (LQ) control. As in Chapters 3 and 4 Reinhorn *et al.* have chosen to transform the structural system into a system utilising story drifts and shears and in doing so have limited the applicability to high-rise building type structural arrangements with the number of dampers equal to the number of stories. The preceding development endeavours to provide a higher degree of generality to the procedure. Reinhorn *et al.* utilised a least squares fit of time history data as a basis and subsequently suggested three additional methods (approaches), a "peak fit", a "single mode estimator" and a "truncation" method. The "peak fit" results were not presented. The remaining two methods the single mode and the truncation approaches were carried out and the single mode estimator produced a control consistent with and nearly equivalent to optimal design for the example earthquakes. The formula derived herein best represents the "peak fit" method suggested by Reinhorn *et al.*, however the formulation presented here differs in two ways –

1. The formulation in this thesis uses an SRSS combination of control forces obtained from operating on individual modes with the gain matrix.
2. The SRSS modal combination is carried out in state space form for the damped structural system

These improvements make the proposed procedure more general. In the following Chapter 6, design examples are provided to demonstrate the proposed method.

The work by Reinhorn *et al.* utilises the LQ control algorithm. The time independent component of the formulation of the LQ algorithm is the simplest starting point for incorporating control theory into the design procedure and was chosen for the work in this thesis. Since a passive system is by definition time and excitation independent, one would not expect that an excitation dependent component would translate into improved performance of the passive system. Time and excitation independent forms of other control algorithms may be considered in future studies, especially if the measures are more consistent with the true underlying design objectives, where these include the very complex notions of efficient material utilisation and reduced costs. Other available algorithms include Instantaneous Optimal Control (see Yang, Akbarpour and Ghaemmaghami, (1987)) and, more recently, the H_∞ control.

The instantaneous optimal control algorithm minimises at every instant in time the kernel of the quadratic performance index used in LQ control and produces a control capability comparable to the LQ control, but with a simplified formulation that does not require the computation of the Ricatti matrix. This algorithm would be important particularly when dealing with non-linear structures or control devices.

H_∞ control is mathematically very complex but is used to deal with practical issues in active control such as time delay in finding a robust control. It remains to be seen if the H_∞ control algorithm could contribute significantly to the computation of a passive control.

Chapter 6: Example Application of the Passive Control Design Procedure

In Chapter 5, a control theory based method was advanced as a method of determining optimal viscous damper sizes at pre-selected locations in a general structural system corresponding to a chosen target feedback control level in combination with a specified response spectrum representing the excitation. Subsequently, based on the rule of equal energy dissipation per cycle, friction damper slip loads could be estimated.

In contrast to the SDOF procedure in which the absolute minimum structural response is sought directly, the detailed control theory based technique proposed in Chapter 5 seeks to find a set of dampers that target a chosen control strength whether or not it leads to the absolute minimum response. This technique fits naturally within an iterative design procedure. Initially, the desired level of control that leads to an acceptable performance is not known, but after some trials during the course of the analysis this value can eventually be determined. The Response Spectral Analysis (RSA), derived for application to non-classically damped structures, provides a means of rapidly assessing the key response quantities necessary to evaluate conformance with the performance objectives. Therefore, the task of determining the optimal control level is not expected to be an onerous task.

The RSA technique is naturally suited to using a reduced number of modes enabling a reduction in computation effort. Reducing the computation effort is seen as a positive feature that extends the application of the method to large finite element structural models.

The procedure, summarized below basically follows that presented at the end of the last chapter.

1. Define the structural system to be controlled using m , k and c matrices.
2. Select desirable and practical damper locations and construct location matrices C , C_d and control force influence matrix B to describe the locations and effects of the damper forces on the state variables of the structure.
3. Choose the form of weighting matrices Q and R to regulate the control strength leaving one or more variables to regulate the strength of the control (see Equations 5.66 and 5.67 and Appendix A).

4. Solve the control problem to determine full state feedback matrix G .
5. Obtain response spectra that represent the appropriate design criteria with an acceptable level of risk for the structure. Using these spectral values, estimate using RSA the peak cycle displacements, velocities and control forces for the given excitation.
6. Evaluate the viscous damping coefficients necessary to satisfy the target control level.
7. Based on the energy dissipated at the peak cycle and the brace stiffness, evaluate the slip/yield load necessary to dissipate that energy, if possible.
8. Repeat Steps 2-7 as necessary until an acceptable configuration of dampers is found that satisfy all design criteria.

With this procedure the designer seeks to find both an optimal arrangement and sizes of dampers. As will be seen in the examples, important information necessary to check for feasibility of using friction/hysteretic dampers is available to assist the designer to find a workable and optimal solution. Once a design is settled on, it is important to recognise that the design arrived at during the above process is based on estimates of response quantities made using some simplifying assumptions such as the assumption that the underlying structure remains elastic. Following the above procedure does not eliminate the requirement to prove the design with a detailed non-linear analysis.

This chapter contains three design examples of increasing complexity. The first example is a continuation of the analysis of the 4-story shear structure used as an illustrative example in Chapter 5. The design of dampers is carried out using the method described above to satisfy the desired performance criteria. This control objective is compared with the minimization of story drift used in previous chapters.

The second example is taken from a typical low-rise office building located in Burbank, California (Los Angeles area). This example is chosen as being representative of the type of structure for which the added damping is thought to be a very effective means of improving the structural performance. Built of a flexible moment frame, the deformations induced by an earthquake would be sufficient to activate friction and viscous dampers.

The third and final example is an 18DOF eccentric building based on the geometry of a reinforced concrete hospital structure located in Palo Alto, California (San Francisco area). While the original structure was found to be too stiff relative to its foundation, the structural

arrangement, having an open garage area leading to eccentric mass and stiffness was felt to be sufficient to begin to explore the capabilities of the proposed methodology for dealing with more complex structures.

6.1 Example 1: 4-Story Frame Structure

In this section, the same four-story structure that was used as an example in demonstrating the proposed transfer function technique in Chapter 4 and also used to illustrate the numerical analysis procedures in Chapter 5 is again used as a basis to illustrate the application of the new proposed methodology in design. A diagram of the structure is given in Figure 4.1. Input accelerograms representing possible “design” events are plotted in Figure 4.4 consisting of the El Centro and the San Fernando records.

One cycle of the calculation is presented in detail to enable the reader to replicate the steps. Then using subsequent iterations, the necessary steps in the design cycle are illustrated. The results are then compared to the LSP results reported in Chapter 5.

6.1.1 Control Objective

With the transfer function technique and later with level set programming the underlying control objective was to reduce the response displacements, drifts and velocities to as low a level as possible. With the proposed control based method, the control objective is to balance control force with the response of the structure. Depending on the selection of the weighting matrices in the performance index, the strength of the target control can be regulated to any desired level. The designer then needs to decide what strength is sufficient to provide adequate structural performance. This control objective is different from and more practical than the absolute minimization of the response quantities (drifts, energy) considered in the earlier work. A system based on the minimization of the response may not be advantageous in that material and money may be wasted in accommodating control forces that may overshoot the required performance by a considerable margin. It is reasonable to expect that, in many cases, regulation of the control strength will lead to systems that are more cost effective. With the method described herein, the strength of control sufficient to satisfy the design objectives becomes the target.

The objective of the structural design and the design of the control elements is to limit or prevent damage or failure to structural and non-structural elements, equipment etc. as per the

performance requirements of the structure. The selection of a suitable control strength should consider all aspects of the performance of the structure such as:

- Beam and column strength and ductility demands must be kept within the member capacities taking into account the construction type, details and standards in force the time of design/construction;
- Deflections, velocities and acceleration limits should be set considering such things as pounding with neighbouring structures, vibration demands on critical equipment, occupant comfort and safety, etc.

Each structure differs in its requirements but it is assumed that the information necessary to determine adequate performance can be obtained from the modal combination results for the model used in the assessment.

To demonstrate the use of the proposed damper design method a simple drift displacement criterion was used in this example.

The BSSC NEHRP Recommended Provisions for Seismic Regulations for New Buildings (2000) in Section 5.2.8 require that the drift of any story including torsion effects shall be less than $0.01h$ ($h/100$) if the structure is designated as an essential facility with a post-earthquake function. The National Building Code of Canada (1995 NBCC) contains an equivalent requirement for critical structures, reportedly soon to be replaced with more stringent requirements in 2005. The deflection requirements are meant to ensure structural safety. However, recognising that a more strict requirement would be consistent with an attempt to not only ensure structural safety, but to limit damage, it was opted to use in this example an inter-story drift displacement limit of half of the current NBCC and BSSC recommended values. Therefore, with this 4-story structure example the maximum story drift ratio was chosen not to exceed $h/200$.

It is recognised that the story drift control objective above is highly simplified and is presented for the purpose of this example. A practical structure is almost certain to have many more and complex performance indicators.

6.1.2 Step 1: Structure definition

The model structure is a 4-story shear frame having mass and stiffness matrices repeated below for completeness

$$m = \begin{bmatrix} 1 & 0 & 0 & 0 \\ 0 & 1 & 0 & 0 \\ 0 & 0 & 1 & 0 \\ 0 & 0 & 0 & 1 \end{bmatrix} \frac{kNs^2}{m} \quad (6.1)$$

$$k = \begin{bmatrix} 2400 & -1200 & 0 & 0 \\ -1200 & 2400 & -1200 & 0 \\ 0 & -1200 & 2400 & -1200 \\ 0 & 0 & -1200 & 1200 \end{bmatrix} \frac{kN}{m} \quad (6.2)$$

The inherent damping in the structure, in this case taken at 2.5 % critical damping, is provided by mass and stiffness proportional Rayleigh damping matrix. The constants α and β are set to 0.44 and 0.0011 respectively yield the following damping matrix

$$c = \alpha m + \beta k = \begin{bmatrix} 3.08 & -1.32 & 0 & 0 \\ -1.32 & 3.08 & -1.32 & 0 \\ 0 & -1.32 & 3.08 & -1.32 \\ 0 & 0 & -1.32 & 1.76 \end{bmatrix} \frac{kNs}{m} \quad (6.3)$$

With these mass, stiffness and damping matrices, the damping evaluated for each modal frequency is specified in Table 6.1 below illustrating that the damping is equal to the specified 2.5% in the first two modes, and slightly higher for the remaining two modes.

Table 6.1. Uniform 4-story structure undamped response frequencies

Mode	Circular Frequency (rad/sec)	Frequency (Hz)	Period (sec)	Damping (%)
1	12.03	1.915	0.5523	2.5%
2	34.64	5.513	0.1814	2.5%
3	53.07	8.447	0.1184	3.3%
4	65.10	10.362	0.0965	3.9%

In state-space form, the equation of motion is given by

$$\dot{x} = Ax + Bu + L\ddot{x}_g = \begin{bmatrix} 0 & I \\ -m^{-1}k & -m^{-1}c \end{bmatrix} \begin{bmatrix} \hat{x} \\ \dot{\hat{x}} \end{bmatrix} + \begin{bmatrix} 0 \\ -m^{-1}C_R^T \end{bmatrix} u + \begin{bmatrix} 0 \\ m^{-1}1 \end{bmatrix} \ddot{x}_g \quad (6.4)$$

where

$$A = \begin{bmatrix} 0 & 0 & 0 & 0 & 1 & 0 & 0 & 0 \\ 0 & 0 & 0 & 0 & 0 & 1 & 0 & 0 \\ 0 & 0 & 0 & 0 & 0 & 0 & 1 & 0 \\ 0 & 0 & 0 & 0 & 0 & 0 & 0 & 1 \\ -2400 & 1200 & 0 & 0 & -3.08 & 1.32 & 0 & 0 \\ 1200 & -2400 & 1200 & 0 & 1.32 & -3.08 & 1.32 & 0 \\ 0 & 1200 & -2400 & 1200 & 0 & 1.32 & -3.08 & 1.32 \\ 0 & 0 & 1200 & -1200 & 0 & 0 & 1.32 & -1.76 \end{bmatrix} \quad (6.5)$$

and

$$L = \begin{bmatrix} 0 \\ 0 \\ 0 \\ 0 \\ 1 \\ 1 \\ 1 \\ 1 \end{bmatrix} \quad (6.6)$$

remain constant. The earthquake excitation in this case is given by the May 8, 1940 Imperial Valley Earthquake El Centro Record N00E and the Feb 9, 1971 San Fernando Earthquake, Lake Hughes Array Station 12 record N21E as shown in Figure 4.4. These earthquakes were used so that a direct comparison could be made with previous results. Further, design spectra in the form required by this method of analysis are not available at present. It was found expedient to generate spectral values based on the earthquake time history records rather than to derive a general function.

6.1.3 Step 2: Select damper locations

Added damping is presumed to be provided by dampers situated between each adjacent story. The damper location matrix, C , is given by

$$C = [0 \quad C_R] = \begin{bmatrix} 0 & 0 & 0 & 0 & 1 & 0 & 0 & 0 \\ 0 & 0 & 0 & 0 & -1 & 1 & 0 & 0 \\ 0 & 0 & 0 & 0 & 0 & -1 & 1 & 0 \\ 0 & 0 & 0 & 0 & 0 & 0 & -1 & 1 \end{bmatrix} \quad (6.7)$$

and

$$B = \begin{bmatrix} 0 & 0 & 0 & 0 \\ 0 & 0 & 0 & 0 \\ 0 & 0 & 0 & 0 \\ 0 & 0 & 0 & 0 \\ -1 & 1 & 0 & 0 \\ 0 & -1 & 1 & 0 \\ 0 & 0 & -1 & 1 \\ 0 & 0 & 0 & -1 \end{bmatrix} \quad (6.8)$$

6.1.4 Step 3: Choose weighting matrices; control strength

In order to formulate the control problem, the matrices Q and R need to be established. As selected previously, the Q matrix was chosen as

$$Q = \begin{bmatrix} k & 0 \\ 0 & m \end{bmatrix} = \begin{bmatrix} 2400 & -1200 & 0 & 0 & 0 & 0 & 0 & 0 \\ -1200 & 2400 & -1200 & 0 & 0 & 0 & 0 & 0 \\ 0 & -1200 & 2400 & -1200 & 0 & 0 & 0 & 0 \\ 0 & 0 & -1200 & 1200 & 0 & 0 & 0 & 0 \\ 0 & 0 & 0 & 0 & 1 & 0 & 0 & 0 \\ 0 & 0 & 0 & 0 & 0 & 1 & 0 & 0 \\ 0 & 0 & 0 & 0 & 0 & 0 & 1 & 0 \\ 0 & 0 & 0 & 0 & 0 & 0 & 0 & 1 \end{bmatrix} \quad (6.9)$$

such that the first term in the quadratic performance index function, Equation 5.6, is comprised of potential and kinetic energy terms. The R matrix was selected to be

$$R = R_{factor} I = \begin{bmatrix} 0.06 & 0 & 0 & 0 \\ 0 & 0.06 & 0 & 0 \\ 0 & 0 & 0.06 & 0 \\ 0 & 0 & 0 & 0.06 \end{bmatrix} \quad (6.10)$$

where I represents the identity matrix with dimension equal to the number of dampers modelled in the structure and $R_{factor} = 0.06$ is chosen initially.

6.1.5 Step 4: Solve the control problem

Given the above matrices, enough information is available to solve for the Riccati matrix

$$P = \begin{bmatrix} 478.0 & -125.1 & -29.1 & -14.3 & 0.99 & 0 & 0 & 0 \\ -125.1 & 448.9 & -139.5 & -43.4 & 0 & 0.99 & 0 & 0 \\ -29.1 & -139.5 & 434.6 & -168.6 & 0 & 0 & 0.99 & 0 \\ -14.3 & -43.4 & -168.6 & 309.5 & 0 & 0 & 0 & 0.99 \\ 0.99 & 0 & 0 & 0 & 0.25 & 0.11 & 0.08 & 0.07 \\ 0 & 0.99 & 0 & 0 & 0.11 & 0.33 & 0.18 & 0.15 \\ 0 & 0 & 0.99 & 0 & 0.08 & 0.18 & 0.40 & 0.26 \\ 0 & 0 & 0 & 0.99 & 0.07 & 0.15 & 0.26 & 0.51 \end{bmatrix} \quad (6.11)$$

And subsequently solve for the full state feedback gain matrix using Equation 2.21.

$$G = \begin{bmatrix} 16.44 & 0 & 0 & 0 & 4.16 & 1.89 & 1.31 & 1.12 \\ -16.44 & 16.44 & 0 & 0 & -2.26 & 3.57 & 1.71 & 1.31 \\ 0 & -16.44 & 16.44 & 0 & -0.59 & -2.46 & 3.57 & 1.90 \\ 0 & 0 & -16.44 & 16.44 & -0.19 & -0.59 & -2.26 & 4.16 \end{bmatrix} \quad (6.12)$$

Next investigate the feedback gains corresponding to co-located sensors and actuators by estimating the inverse of C . Observe that the matrix

$$C^T(CC^T)^{-1} = \begin{bmatrix} 0 & 0 & 0 & 0 \\ 0 & 0 & 0 & 0 \\ 0 & 0 & 0 & 0 \\ 0 & 0 & 0 & 0 \\ 1 & -1 & 0 & 0 \\ 0 & 1 & -1 & 0 \\ 0 & 0 & 1 & -1 \\ 0 & 0 & 0 & 1 \end{bmatrix} \left(\begin{bmatrix} 1 & -1 & 0 & 0 \\ -1 & 2 & -1 & 0 \\ 0 & -1 & 2 & -1 \\ 0 & 0 & -1 & 2 \end{bmatrix} \right)^{-1} = \begin{bmatrix} 0 & 0 & 0 & 0 \\ 0 & 0 & 0 & 0 \\ 0 & 0 & 0 & 0 \\ 0 & 0 & 0 & 0 \\ 1 & 0 & 0 & 0 \\ 1 & 1 & 0 & 0 \\ 1 & 1 & 1 & 0 \\ 1 & 1 & 1 & 1 \end{bmatrix} \quad (6.13)$$

$= (C^{-1})$

and subsequently the square observer feedback matrix becomes (Equation 5.38)

$$G_s = G(C^{-1}) = \begin{bmatrix} 8.49 & 4.33 & 2.43 & 1.12 \\ 4.33 & 6.59 & 3.02 & 1.31 \\ 2.43 & 3.02 & 5.47 & 1.90 \\ 1.12 & 1.31 & 1.90 & 4.16 \end{bmatrix} \quad (6.14)$$

By truncation of the matrix above a set of passive viscous dampers is estimated

$$G_D = \begin{bmatrix} 8.49 & 0 & 0 & 0 \\ 0 & 6.59 & 0 & 0 \\ 0 & 0 & 5.47 & 0 \\ 0 & 0 & 0 & 4.16 \end{bmatrix} \quad (6.15)$$

The matrix G_D provides a set of dampers that represent the direct passive component of the specified control, however the strength of the control, defined as the ability of the control system to reduce the deformations and velocities of the structure, is observed to be far less than that of the full state or the observed state feedback controlled structures.

Figure 6.1 (a) shows the comparison for the example case (weak control) with $R_{factor} = 0.06$ and (b) for the case of a strong control having $R_{factor} = 0.0001$. The plots show that the truncated feedback is only able to attain between 57% and 70% of the control capability obtained with the full state feedback. The observer feedback and the matched passive system in this case show good agreement with the target full state active control system.

6.1.6 Step 5: Estimate peak cycle RSA quantities

The identified velocities are established from the equation

$$y = Cx = \begin{bmatrix} 0 & 0 & 0 & 0 & 1 & 0 & 0 & 0 \\ 0 & 0 & 0 & 0 & -1 & 1 & 0 & 0 \\ 0 & 0 & 0 & 0 & 0 & -1 & 1 & 0 \\ 0 & 0 & 0 & 0 & 0 & 0 & -1 & 1 \end{bmatrix} \begin{bmatrix} x_1 \\ x_2 \\ x_3 \\ x_4 \\ \dot{x}_1 \\ \dot{x}_2 \\ \dot{x}_3 \\ \dot{x}_4 \end{bmatrix} \quad (6.16)$$

Introducing a new matrix, C_d , allows for the determination of displacements, d , which will be used subsequently in the friction damper selection process.

$$d = C_d x = [C_R \quad 0] x = \begin{bmatrix} 1 & 0 & 0 & 0 & 0 & 0 & 0 & 0 \\ \tau^{-1} & 1 & 0 & 0 & 0 & 0 & 0 & 0 \\ 0 & -1 & 1 & 0 & 0 & 0 & 0 & 0 \\ 0 & 0 & -1 & 1 & 0 & 0 & 0 & 0 \end{bmatrix} \begin{bmatrix} x_1 \\ x_2 \\ x_3 \\ x_4 \\ \dot{x}_1 \\ \dot{x}_2 \\ \dot{x}_3 \\ \dot{x}_4 \end{bmatrix} \quad (6.17)$$

The control force, u , is established using the following equation

$$u = Gx \quad (6.18)$$

or alternatively,

$$u_s = G_s y = G_s Cx \quad (6.19)$$

if observer feedback is used.

6.1.7 Step 6. Estimate peak cycle displacements, velocities and control forces using RSA

The RSA modal analysis technique is quite involved. The numerical steps are included here to clearly illustrate the process, presuming that all of the poles are complex, representing sub-critically damped modes.

The eigenvalues of the structure controlled with the specified active control are found to be

$$\Lambda = eig(A + BG) = \begin{bmatrix} -1.16 - 12.1i \\ -1.16 + 12.1i \\ -3.74 - 34.7i \\ -3.74 + 34.7i \\ -5.38 - 53.2i \\ -5.38 + 53.2i \\ -6.83 - 65.2i \\ -6.83 + 56.2i \end{bmatrix} \quad (6.20)$$

The right and left eigenvectors are found to be

$$U = \begin{bmatrix} 0.0151 - 0.0111i & 0.0151 + 0.0111i & -0.0095 + 0.0136i & -0.0095 - 0.0136i \\ 0.0284 - 0.0209i & 0.0284 + 0.0209i & -0.0095 + 0.0136i & -0.0095 - 0.0136i \\ 0.0383 - 0.0282i & 0.0383 + 0.0282i & 0 & 0 \\ 0.0435 - 0.032i & 0.0435 + 0.032i & 0.095 - 0.0136i & 0.095 + 0.0136i \\ -0.1516 - 0.1963i & -0.1516 + 0.1963i & 0.5024 + 0.2839i & 0.5024 - 0.2839i \\ -0.2850 - 0.3181i & -0.2850 + 0.3181i & 0.5024 + 0.2839i & 0.5024 - 0.2839i \\ -0.3839 - 0.4286i & -0.3839 + 0.4286i & 0 & 0 \\ -0.4366 - 0.4874i & -0.4366 + 0.4874i & -0.5024 - 0.2839i & -0.5024 + 0.2839i \\ -0.0077 + 0.0096i & -0.0077 - 0.0096i & 0.0012 - 0.0064i & 0.0012 + 0.0064i \\ -0.0027 - 0.0033i & -0.0027 + 0.0033i & -0.0018 + 0.0099i & -0.0018 - 0.0099i \\ -0.0067 - 0.0084i & -0.0067 + 0.0084i & 0.0016 - 0.0087i & 0.0016 + 0.0087i \\ -0.0050 + 0.0063i & -0.0050 - 0.0063i & -0.0006 + 0.0006i & -0.0006 - 0.0006i \\ 0.5512 + 0.3564i & 0.5512 - 0.3564i & -0.4273 - 0.0313i & -0.4273 + 0.0313i \\ -0.1914 - 0.1238i & -0.1914 + 0.1238i & 0.6547 + 0.0479i & 0.6547 - 0.0479i \\ -0.4848 - 0.3134i & -0.4848 + 0.3134i & -0.5757 - 0.0421i & -0.5757 + 0.0421i \\ 0.3598 + 0.2326i & 0.3598 - 0.2326i & 0.2274 + 0.0166i & 0.2274 - 0.0166i \end{bmatrix} \quad (6.21)$$

and the left eigenvectors are

$$V = \begin{bmatrix} 1.0369 + 0.9288i & 1.9487 + 1.7456i & 2.625 + 2.352i & 2.986 + 2.674i \\ 1.0369 + 0.9288i & 1.9487 + 1.7456i & 2.625 - 2.352i & 2.986 - 2.674i \\ -4.9787 - 0.8097i & -4.9787 - 8.8097i & 0 & 4.979 + 8.810i \\ -4.9787 + 0.8097i & -4.9787 + 0.8097i & 0 & 4.979 - 8.810i \\ -9.5741 - 14.809i & 3.3251 + 5.1429i & 8.419 + 13.02i & -6.429 - 9.666i \\ -9.5741 + 14.809i & 3.3251 - 5.1429i & 8.419 - 13.02i & -6.429 + 9.666i \\ 1.031 + 14.085i & -1.580 - 21.58i & 1.389 + 18.98i & -0.5486 - 7.495i \\ 1.031 - 14.085i & -1.580 + 21.58i & 1.389 - 18.98i & -0.5486 + 7.495i \\ -0.0681 + 0.0926i & -0.1280 + 0.1739i & -0.1725 + 0.2343i & -0.1962 + 0.2665i \\ -0.0681 - 0.0926i & -0.1280 - 0.1739i & -0.1725 - 0.2343i & -0.1962 - 0.2665i \\ 0.2377 - 0.1664i & 0.2377 - 0.1664i & 0 & -0.2377 + 0.1664i \\ 0.2377 + 0.1664i & 0.2377 + 0.1664i & 0 & -0.2377 - 0.1664i \\ 0.2577 - 0.2062i & -0.0895 + 0.0716i & -0.2266 + 0.1813i & 0.1682 - 0.1346i \\ 0.2577 + 0.2062i & -0.0895 - 0.0716i & -0.2266 - 0.1813i & 0.1682 + 0.1346i \\ -0.2121 + 0.0380i & 0.3249 - 0.0583i & -0.2857 + 0.0512i & 0.1128 - 0.0202i \\ -0.2121 - 0.0380i & 0.3249 + 0.0583i & -0.2857 - 0.0512i & 0.1128 + 0.0202i \end{bmatrix} \quad (6.22)$$

Note that the eigenvectors satisfy the bi-orthogonality relations

$$VU = I \quad (6.23)$$

and

$$V(A + BG)U = \Lambda \quad (6.24)$$

Based on the real and imaginary parts of the left eigenvectors, the modal participation factors are computed as follows

$$P^R = \text{Re}(V)L = \begin{bmatrix} -0.5648 \\ 0.2377 \\ 0.1098 \\ 0.0600 \end{bmatrix} \quad (6.25)$$

and

$$P^C = \text{Im}(V)L = \begin{bmatrix} -0.7673 \\ 0.1664 \\ 0.0878 \\ -0.0108 \end{bmatrix} \quad (6.26)$$

Combining the real and imaginary mode shapes yields the real mode shapes to be carried into the modal combination

$$M^C = \text{Re}(U)\text{diag}(P^R) - \text{Im}(U)\text{diag}(P^C) = \begin{bmatrix} 0 & 0 & 0 & 0 \\ 0 & 0 & 0 & 0 \\ 0 & 0 & 0 & 0 \\ 0 & 0 & 0 & 0 \\ 0.2155 & 0.1667 & 0.0918 & 0.0260 \\ 0.4050 & 0.1667 & -0.0319 & -0.0398 \\ 0.5457 & 0 & -0.0807 & 0.0350 \\ 0.6202 & -0.1667 & 0.0599 & -0.0138 \end{bmatrix} \quad (6.27)$$

and

$$M^S = \text{Im}(U)\text{diag}(P^R) + \text{Re}(U)\text{diag}(P^C) = \begin{bmatrix} -0.0179 & -0.0048 & -0.0017 & -0.0004 \\ -0.0336 & -0.0048 & 0.0006 & 0.0006 \\ -0.0453 & 0 & 0.0015 & 0.0005 \\ -0.0515 & 0.0048 & -0.0011 & 0.0002 \\ 0.0207 & 0.0161 & 0.0093 & 0.0027 \\ 0.0390 & 0.0161 & -0.0032 & -0.0042 \\ 0.0525 & 0 & -0.0082 & 0.0037 \\ 0.0597 & -0.0161 & 0.0061 & -0.0014 \end{bmatrix} \quad (6.28)$$

note that the first column generally contains the largest contribution to the modal response.

To carry out the response spectral analysis using the square root of the sum of the squares method one should have prepared design spectra. Here the spectral values have been extracted by performing a spectral analysis of the El Centro earthquake record directly

$$S^C = [0.6064 \quad 0.1466 \quad 0.0710 \quad 0.0527] \quad (6.29)$$

and

$$S^S = [0.5937 \quad 0.1693 \quad 0.0976 \quad 0.0728] \quad (6.30)$$

Carrying the SRSS modal response with all terms for the state vector envelope response yields, noting that it applies when all modes are complex valued

$$x_{SRSS} = 2 \sqrt{\sum_i \left((M_i^C S_i^C)^2 + (M_i^S S_i^S)^2 \right)} = \begin{bmatrix} 0.0213 \\ 0.0399 \\ 0.0537 \\ 0.0611 \\ 0.2675 \\ 0.4959 \\ 0.6649 \\ 0.7576 \end{bmatrix} \quad (6.31)$$

Similarly, carrying out spectral analysis for the observed velocities, observed displacements and the control force yields

$$y_{SRSS} = 2 \sqrt{\sum_i \left((C M_i^C S_i^C)^2 + (C M_i^S S_i^S)^2 \right)} = \begin{bmatrix} 0.2675 \\ 0.2317 \\ 0.1786 \\ 0.1057 \end{bmatrix} \quad (6.32)$$

and

$$d_{SRSS} = 2 \sqrt{\sum_i \left((C_d M_i^C S_i^C)^2 + (C_d M_i^S S_i^S)^2 \right)} = \begin{bmatrix} 0.0213 \\ 0.0187 \\ 0.0140 \\ 0.0076 \end{bmatrix} \quad (6.33)$$

$$u_{SRSS} = 2 \sqrt{\sum_i \left((GM_i^c S_i^c)^2 + (GM_i^s S_i^s)^2 \right)} = \begin{bmatrix} 3.738 \\ 3.280 \\ 2.447 \\ 1.319 \end{bmatrix} \quad (6.34)$$

again assuming only complex modes.

If real poles are encountered, the modal combination procedure needs to be modified slightly. At this time only complex valued modes are considered. The extension to real valued modes is straightforward but requires treating the real valued modes individually rather than in conjugate pairs.

6.1.8 Step 7: Estimate SRSS damping coefficients

The estimated damping coefficients based on these obtained results is

$$\bar{D}_{SRSS} = \frac{u_{SRSS}}{y_{SRSS}} = \begin{bmatrix} 13.976 \\ 14.16 \\ 13.699 \\ 12.483 \end{bmatrix} \quad (6.35)$$

Comparing \bar{D}_{SRSS} to $\bar{D}_{truncated}$ yields

$$Ratio = \frac{\bar{D}_{SRSS}}{\bar{D}_{truncated}} = \begin{bmatrix} 1.64 \\ 2.15 \\ 2.50 \\ 3.00 \end{bmatrix} \quad (6.36)$$

indicating that the SRSS extracted (matched) damping coefficients are substantially greater than those determined using the truncation method. It is also observed that the ratio is not uniform indicating that basing the distribution on the truncated D matrix does not provide a good estimate of the optimal distribution.

Figure 6.1 also compares the control results for the matched passive viscous dampers. The peak displacements were found to be very similar to the full state feedback case with displacement and velocities observed to range from 89% to 98% of those observed for the case of full state feedback.

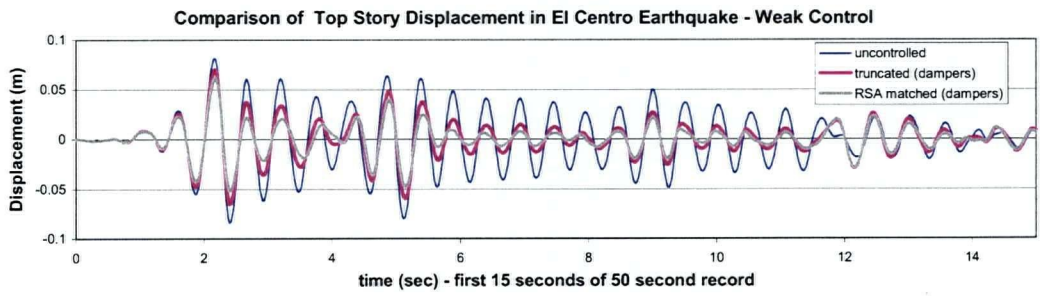
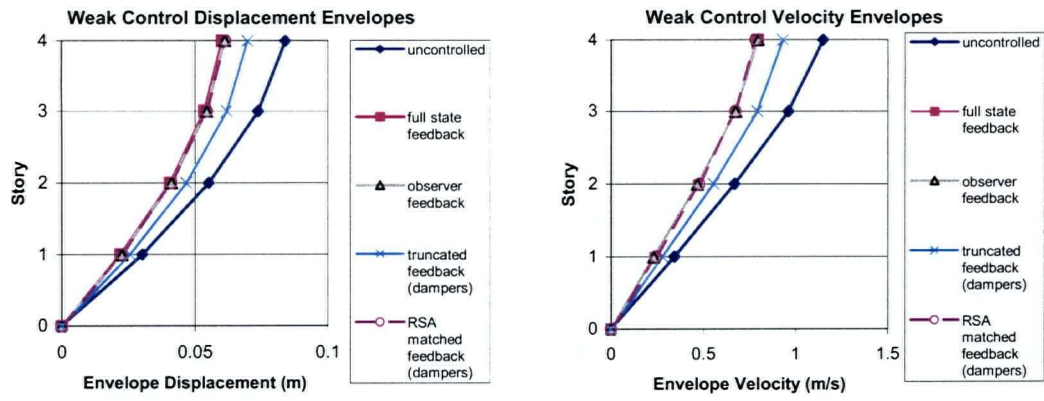
6.1.9 Step 8: Evaluate slip load

The slip load can be evaluated based on the assumption that the energy dissipated in the peak cycle matches that of the viscous damper.

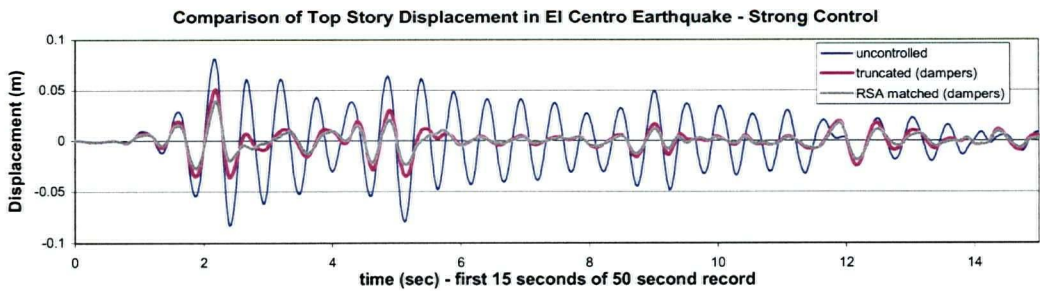
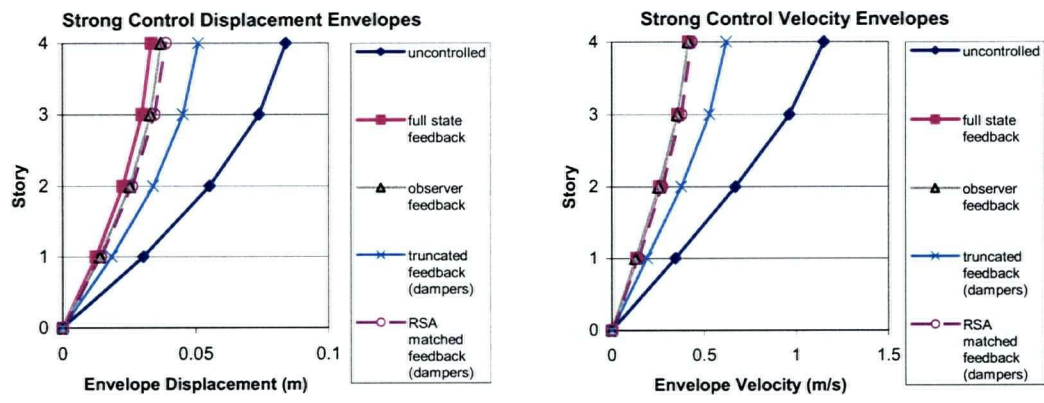
By varying the level of the control with R_{factor} and examining the resulting RSA predicted displacements, the appropriate level of control could be established for a given excitation. Based on R_{factor} ranging from 0.06 down to approximately 0.0016, damping coefficients were established and appear in Columns 8 to 11 of Table 6.2(a). Corresponding drifts estimated by the modal analysis procedure are included in columns 4 to 7 where the drifts correspond to the lateral component of damper displacement.

The slip load corresponding to an ideal (infinitely stiff) brace, assumed to be at the peak cycle is determined from Equation 5.89 appears in Columns 12-15 of Table 6.2(a). This ideal slip load corresponds to the case that the brace is infinitely stiff, which practically cannot be achieved. Presuming that the horizontal component of the brace stiffness is twice the horizontal stiffness of the structure, the desired slip load can be determined assuming that the damper will be capable of dissipating under the peak cycle the same amount of energy as the viscous damper by applying Equation 5.97.

The slip loads corresponding to the flexible brace are shown in Columns 16-19 of Table 6.2(b). As can be seen not all control strengths have a slip load for the flexible brace. The solution of Equation 5.100 does not always produce a real result. Practically, this is interpreted as a failure of the brace to provide sufficient stiffness to activate the friction damper at the expected level of excitation. The ideal case implies infinitely stiff braces, and it should be understood that it is often not possible to provide structures with braces that are stiff enough to be represented by the ideal case. The brace stiffness must necessarily include all deformations necessary to reach the control force including the deformation of connections plus any mechanical slop present in connections. Although these deformations cannot be avoided altogether, use of the expression above can provide feedback as to what level of brace stiffness is or isn't acceptable.



(a)



(b)

Figure 6.1. Comparison of displacements and velocities for an active, and passively damped 4DOF structure (a) a “weak” control and (b) a “strong” control.

Table 6.2 Comparison of response of 4DOF structure to varying levels of control strength.

(a) columns 1-15 (columns 16-23 following page)

Earthquake	Run	Rfactor	Controlled Displacements (m)				Damping Coefficient (kN.s/m)				Ideal Slip Load (kN)			
			1	2	3	4	1	2	3	4	1	2	3	4
El Centro	1	0.060	0.0222	0.0185	0.0130	0.0067	15.8	14.2	12.3	11.1	2.79	2.58	2.09	1.19
	2	0.040	0.0208	0.0173	0.0121	0.0062	19.9	17.8	15.5	14.0	3.23	2.99	2.41	1.37
	3	0.027	0.0192	0.0159	0.0112	0.0058	24.8	22.4	19.4	17.6	3.68	3.40	2.73	1.55
	4	0.0178	0.0176	0.0145	0.0102	0.0053	29.3	28.0	24.3	22.0	4.11	3.80	3.03	1.72
	5	0.0119	0.0159	0.0131	0.0092	0.0048	33.7	34.5	30.2	27.5	4.52	4.17	3.30	1.87
	6	0.0079	0.0143	0.0117	0.0082	0.0042	38.1	42.5	37.5	34.4	4.91	4.51	3.53	1.99
	7	0.0053	0.0127	0.0103	0.0072	0.0037	42.1	52.1	46.4	42.9	5.25	4.81	3.72	2.08
	8	0.00351	0.0111	0.0090	0.0063	0.0032	45.2	63.6	57.5	53.5	5.56	5.06	3.90	2.13
	9	0.00234	0.0097	0.0077	0.0054	0.0028	48.7	71.8	71.5	66.6	5.83	5.27	4.04	2.18
	10	0.00156	0.0084	0.0066	0.0046	0.0024	57.4	77.7	88.4	83.1	6.17	5.43	4.14	2.23
	Run	Rfactor	Controlled Displacements(m)				Damping Coefficient (kN.s/m)				Ideal Slip Load (kN)			
			1	2	3	4	1	2	3	4	1	2	3	4
San Fernando	1	0.060	0.0058	0.0037	0.0047	0.0036	9.4	11.9	7.3	6.5	0.83	0.75	0.77	0.56
	2	0.040	0.0054	0.0036	0.0045	0.0034	13.3	15.1	9.4	8.4	1.04	0.95	0.92	0.66
	3	0.027	0.0050	0.0036	0.0043	0.0031	18.6	19.1	12.1	10.7	1.31	1.19	1.08	0.76
	4	0.0178	0.0045	0.0036	0.0041	0.0028	23.8	24.0	15.6	13.8	1.63	1.49	1.27	0.87
	5	0.0119	0.0040	0.0036	0.0038	0.0025	30.4	30.1	20.5	17.7	2.02	1.83	1.50	0.97
	6	0.0079	0.0036	0.0035	0.0035	0.0023	38.8	37.8	27.3	22.7	2.48	2.24	1.76	1.08
	7	0.0053	0.0035	0.0034	0.0032	0.0020	49.2	47.4	35.2	29.2	3.02	2.70	2.05	1.19
	8	0.00351	0.0035	0.0033	0.0029	0.0018	61.9	59.4	44.1	38.6	3.63	3.22	2.34	1.32
	9	0.00234	0.0034	0.0031	0.0026	0.0015	76.7	74.4	56.3	51.1	4.31	3.79	2.70	1.47
	10	0.00156	0.0033	0.0029	0.0023	0.0013	94.5	89.3	73.4	63.5	5.08	4.38	3.13	1.61

* structure's inherent damping 2.5%

(b) Table 6.2, continued (columns 1-3 repeated and columns 16-23)

Earthquake	Run	Rfactor	Slip Load: K=2400 ($\alpha=2$)				Drift Ratio Demands(3m storey height)			
			1	2	3	4	1	2	3	4
El Centro	1	0.060	2.96	2.75	2.25	1.30	0.0074	0.0062	0.0043	0.0022
	2	0.040	3.47	3.24	2.65	1.53	0.0069	0.0058	0.0040	0.0021
	3	0.027	4.02	3.77	3.08	1.78	0.0064	0.0053	0.0037	0.0019
	4	0.0178	4.61	4.33	3.54	2.05	0.0059	0.0048	0.0034	0.0018
	5	0.0119	5.23	4.93	4.04	2.35	0.0053	0.0044	0.0031	0.0016
	6	0.0079	5.91	5.62	4.61	2.71	0.0048	0.0039	0.0027	0.0014
	7	0.0053	6.71	6.48	5.38	3.30	0.0042	0.0034	0.0024	0.0012
	8	0.00351	7.83	7.97			0.0037	0.0030	0.0021	0.0011
	9	0.00234					0.0032	0.0026	0.0018	0.0009
	10	0.00156					0.0028	0.0022	0.0015	0.0008
	Run	Rfactor	Slip Load: K=2400 ($\alpha=2$)				Drift Ratio Demands(3m storey height)			
San Fernando	1	0.060	0.88	0.83	0.83	0.60	0.0019	0.0012	0.0016	0.0012
	2	0.040	1.14	1.09	1.01	0.72	0.0018	0.0012	0.0015	0.0011
	3	0.027	1.49	1.43	1.23	0.86	0.0017	0.0012	0.0014	0.0010
	4	0.0178	2.00	1.90	1.49	1.02	0.0015	0.0012	0.0014	0.0009
	5	0.0119	2.86	2.64	1.88	1.22	0.0013	0.0012	0.0013	0.0008
	6	0.0079			2.51	1.48	0.0012	0.0012	0.0012	0.0008
	7	0.0053				2.03	0.0012	0.0011	0.0011	0.0007
	8	0.00351					0.0012	0.0011	0.0010	0.0006
	9	0.00234					0.0011	0.0010	0.0009	0.0005
	10	0.00156					0.0011	0.0010	0.0008	0.0004

drift/H; H=3 - <1/200 acceptable >1/200 unacceptable

In a practical application, the acceptable/unacceptable displacement levels may be influenced by many factors such as member size and shape and construction details. However, since this is a hypothetical problem, we shall assign an arbitrary story height of $H=3\text{m}$ and limit the inter-story displacement to less than $(1/200)H$ or $0.005H$. Therefore the maximum acceptable inter-story displacement is limited to 15mm .

To be practical, it must be recognised that the viscous damped structure will not be capable of fully replicating the strength of the target active control system, therefore it is necessary to exceed the control objectives by a margin sufficient to cover the difference.

6.1.10 Viscous and Friction/Hysteretic Dampers for $R_{factor} = 0.06$

Table 6.2(a) and (b) contain the results of computed response of the structure to both El Centro and San Fernando earthquake records.

Of the displacements calculated for $R_{factor} = 0.06$ with the El Centro record input, the largest story drift ratio is at the bottom story equal to 0.0074 (approx $1/135$). It can be surmised that the control is not strong enough at this level to satisfy the displacement criteria. However, for the San Fernando record, the resulting controlled displacements at this level are less than $1/500$ and already satisfy this design requirement. The uncontrolled drift ratios for the bottom story in each earthquake are respectively, 0.010 ($1/99$) and 0.0027 ($1/370$) for the El Centro record and for the San Fernando record, indicating that the uncontrolled structure would satisfy the drift requirements if subjected to the San-Fernando input record.

If the El Centro record is indicative of the design event, it is necessary to find an increased level of control for which the required drift ratio is satisfied. By reducing the value of R_{factor} , the weighting on the control force relative to the total vibration energy is reduced, permitting the control force to increase and subsequently, the response to decrease. By trial and error, an acceptable R_{factor} can be found. In this case, a series of 10 different control levels were carried through the analysis such that the variations of the deformations and the damper forces could be studied. Table 6.2 (a) summarises the displacements, damping coefficients and ideal friction damper slip loads corresponding to the varying control levels for both the El Centro input record. The results show that as the target control strength increases, the displacements decrease, and in general the magnitude of the damping coefficients and the slip loads increase. The damping

coefficients appear to be relatively uniformly distributed from the base to the top over most of the range investigated, except for the San Fernando record, the second and third stories pick up a higher damping coefficient. This could indicate that at higher levels of control, this particular earthquake is exciting the higher modes to a greater extent than the El Centro record. The frequency analysis of these two records has indicated that the San Fernando record is more likely to excite higher modes than is the El Centro record.

The corresponding ideal slip loads, however, turn out to be distributed more heavily towards the base, as previously observed with the LSP optimization results.

Observing that the displacements at the upper limit of the control cases are quite small, the next step was to determine using the controlled displacements as a basis, what actual slip load would be required for the case of a flexible brace.

The drift ratio of 0.0048 (1/210) results from using a value of $R_{factor} = 0.0079$, producing a control strength that is just sufficient to satisfy the design requirement for the El Centro record input. For the San Fernando record input, however the uncontrolled drift ratio is 0.0027 (1.370) which is already acceptable according to the selected performance criterion. If the San Fernando record used were indicative of the design event, providing strength and ductility criteria were met for all members in the structure, additional dampers would not be necessary.

6.1.11 Friction Damper Analysis Results

Using the equal energy criteria for each of the dampers included in the structure at every level of control the corresponding set of friction dampers was computed. The brace stiffness was set at 2400 kN/m corresponding to a brace stiffness ratio of $\alpha=2$, equivalent to that used in the LSP study presented in Chapter 4. It can be seen in Table 6.2(b) that for both El Centro and For San Fernando input records, not all friction damper slip load values are present. Values that are absent could not be computed due to the displacements being insufficient to activate the necessary slip load in the brace. The control that is just able to meet the energy criteria has special significance in that this level of control corresponds to the minimum drifts possible for the given brace. The slip load values can be related to the absolute optimal slip loads reported in Chapter 4 determined using level set programming. It is not clear whether these slip loads correspond to the LSP results for the minimum total energy objective function, or the minimum

RMS drift. It is observed that the LQ control problem on which the control distribution is based on the performance index function that includes minimum energy. The search procedure for the strength of the control, however, has led to a condition whereby the minimum drift is obtained. It is therefore concluded that the optimum slip force determined in this way contains elements of both minimum energy and minimum drift and therefore cannot be compared directly to either.

Consequently, Figures 6.2 and 6.3 compare the slip load distributions obtained for both El Centro and San Fernando input using the control theory based method taken to its minimum with the LSP minimum energy and minimum RMS drift distributions, as well as the slip load distributions obtained using the SDOF transfer function based method. The fit for the El Centro record seems reasonable with the control theory method based slip loads in the first story, lying between the LSP optimal slip loads obtained using the minimum drift and the minimum energy objective functions. In the upper stories, however, the slip loads do not appear to be as well represented, with the control theory based method obtained slip loads being larger than those obtained using the LSP procedure.

The results obtained for the San Fernando record in Figure 6.3 seem to show the opposite. While the distribution of slip loads seem to be well represented, the magnitudes of the slip loads obtained using the control theory based method were approximately 50% greater than the LSP obtained slip loads in the first story and proportionally higher in the upper stories.

The results obtained using each of the proposed approach has produced a different character of response than that determined using LSP. The differences observed have favoured higher slip loads than that determined by LSP, which due to the shape of the typical drift vs. slip load plot would produce acceptable response. The intent of the control theory based method is not to identify the absolute minimum, as the transfer function based method was set up to do, but rather to find a level of control sufficient to satisfy the design requirements.

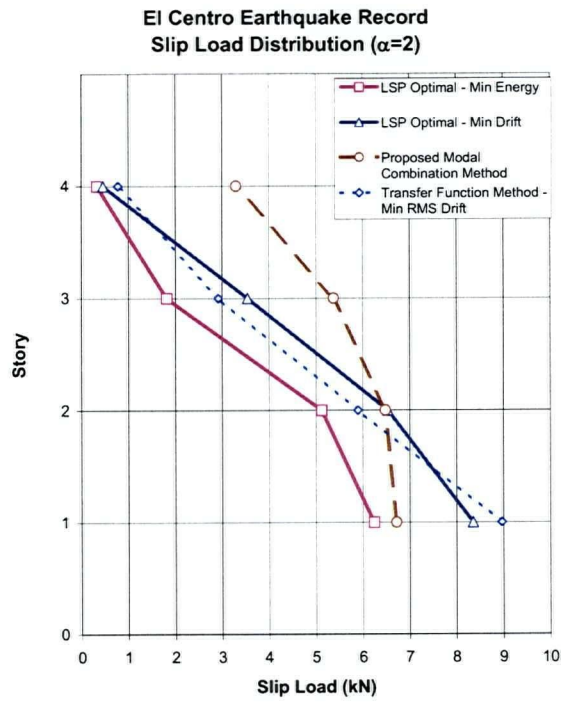


Figure 6.2. Comparison of slip load distributions obtained using LSP and the proposed control method with El Centro record input.

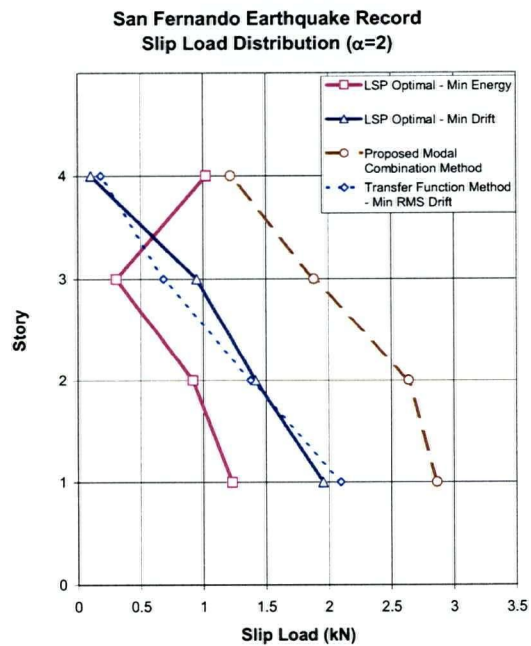


Figure 6.3. Comparison of slip load distributions obtained using LSP and the proposed control procedure with San Fernando record input.

6.2 Example 2: Burbank 6-Story Office Building

The Burbank Office building is a typical 6-story steel moment frame structure located in the Los Angeles area. It is a structure for which the strong motion response during the Northridge earthquake (January 17, 1994) and the Whittier Earthquake (1987) has been recorded and consequently the structural response is quite well understood (see Bakhtavar, Ventura and Prion, 2000). Therefore, this structure was chosen as a candidate for the demonstration of the control methodology.

Constructed in 1976-77, the structure is square in plan with N-S and E-W plan dimensions of 36.6m (120ft). The floors structure consists of a 3-1/4" (80mm) concrete slab over a metal deck. Vertical loads from the floor slabs are carried by a steel beam and column moment frame, while the lateral force resistance is provided by perimeter moment resisting steel frames depicted in Figure 6.4.

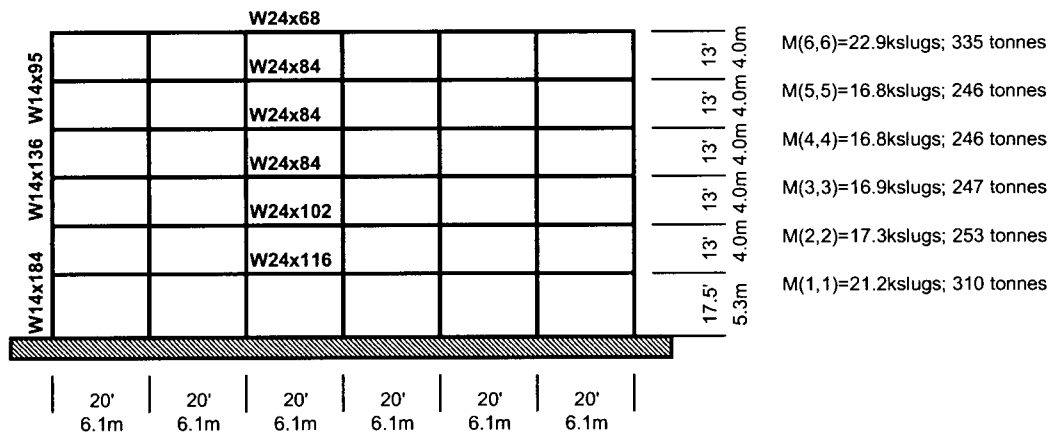


Figure 6.4. Uncontrolled Burbank 6-story office building perimeter frame (imperial and metric units).

The objective of this example is to demonstrate the application of the control theory based viscous and friction damper design method and to compare the characteristics of the seismic response resulting from the implementation of each. Up to this point only the horizontal component the resistance provided by added braces have been considered. With this example it is necessary to deal with the implementation of horizontal resistance using diagonal braces.

6.2.1 Consideration for Control Loss

With the control theory based design method, the objective is to determine the set of viscous dampers that best replicates the response produced by the active control system. During this

process it is expected that the strength of the control will diminish due to the inability of the passive system to fully replicate the effect of the active control. In a subsequent step, based on the energy dissipated by the viscous dampers, and the displacements experienced by the controlled structure, friction dampers are selected to provide as nearly as possible the equivalent control effect to the viscous dampers. During this second step it is expected that some further loss in control effectiveness will result due to the different response characteristics of a friction damped structure as compared to a viscous damped structure. It is the objective of this investigation to illustrate the performance levels of the three control systems. Understanding the difference in the performance level and the characteristics of the controlled system will enable the designer to provide an appropriate margin in the performance requirement in the first step, active control design, in order to meet performance requirements with the subsequently determined passive viscous or friction damped passive structures. This example emphasizes that the control theory based methodology proposed provides a starting point, but is not in itself a sufficient basis on which to advance the design of a control system particularly in the case of a friction damped structure. Time history analysis is still a necessary to provide an understanding the expected performance.

6.2.2 Structural Modeling

A model of a single North-South frame was constructed in ADINA (2002) based on the information provided by Bakhtavar (2000). Figure 6.4 shows an elevation of the frame and gives the imperial designation of the members. The current CISC handbook is based on metric designations and does not include the members sizes specified. Similar weight and depth metric members were substituted for the specified imperial members to provide estimates of their geometric properties. A simple 2-D plane frame was constructed with a single beam column element representing each beam or column. The model was constrained against translations and rotations at the base. The tributary mass for the frame was applied as distributed mass on the floor beams.

The ADINA model contained 126 degrees of freedom. The MATLAB (MathWorks 1999) model of the structure, however, was reduced to 6 lateral degrees of freedom by introducing unit displacements at each of the floors in the horizontal direction in turn and then extracting the total shear force carried across all of the columns in each story. Introducing unit displacements in this way enabled the rapid evaluation of the reduced order stiffness matrix from the complex model.

The mass matrix was found to be in imperial units

$$m = \begin{bmatrix} 21.2 & 0 & 0 & 0 & 0 & 0 \\ 0 & 17.3 & 0 & 0 & 0 & 0 \\ 0 & 0 & 16.9 & 0 & 0 & 0 \\ 0 & 0 & 0 & 16.8 & 0 & 0 \\ 0 & 0 & 0 & 0 & 16.8 & 0 \\ 0 & 0 & 0 & 0 & 0 & 22.9 \end{bmatrix} [kslugs] \quad (6.37)$$

and the stiffness matrix was determined to be in the units of kips/ft

$$k = \begin{bmatrix} 63.09 & -47.09 & 14.98 & -3.12 & 0.57 & -0.09 \\ -47.09 & 66.32 & -42.18 & 13.26 & -2.43 & 0.37 \\ 14.99 & -42.19 & 55.44 & -34.75 & 10.26 & -1.54 \\ -3.13 & 13.27 & -34.75 & 44.94 & -26.94 & 6.14 \\ 0.57 & -2.43 & 10.26 & -26.94 & 31.78 & -13.17 \\ -0.09 & 0.37 & -1.54 & 6.14 & -13.16 & 8.27 \end{bmatrix} * 10^3 \quad (6.38)$$

6.2.2.1 Frequency Comparison

A modal analysis of the ADINA model, extracted MATLAB model was performed and the results obtained compared to that obtained by Bakhtavar (1991) in Table 6.3.

Table 6.3. Burbank 6-Story Office Building. Comparison of ADINA and MATLAB model obtained frequencies with those obtained by Bakhtavar (2000)

Mode	ADINA model (Hz)	MATLAB model (extracted from ADINA model - Hz)	X-DIR Frame 'A' (Bakhtavar, 2000 - Hz)
1	0.662	0.662	0.723
2	2.06	2.06	2.04
3	4.05	4.05	3.68
4	6.86	6.86	5.63
5	10.3	10.3	8.11
6	14.3	14.3	11.0

The MATLAB model was extracted directly from the ADINA model, therefore it is expected that the frequency response would be identical. In comparison to the results obtained by Bakhtavar (2000), however, in which a more sophisticated 3-D model was used, the results

obtained using the above-described model had a lower first mode frequency, but higher frequencies in all modes above the second mode. It was concluded, however, that the frequency match was sufficient for the purposes of this example.

6.2.2.2 Structural Damping

Damping inherent in the structure was modeled using Rayleigh damping, set at 2% of critical in the fundamental mode. It was found that by setting the second mode to 2% damping, damping values obtained for the highest mode was about 10%. This was felt to be too high for the purposes of this example. Damping in the higher modes was reduced by setting mass and stiffness proportionality constants respectively at $\alpha = 0.15$ and $\beta = 0.001$ thereby shifting the frequency of 2% damping to a frequency between the 3rd and 4th mode. Figure 6.5 illustrates the relationship between the Rayleigh damping and the target 2% damping for each mode. Markers on the damping lines indicate the modal frequencies identified above.

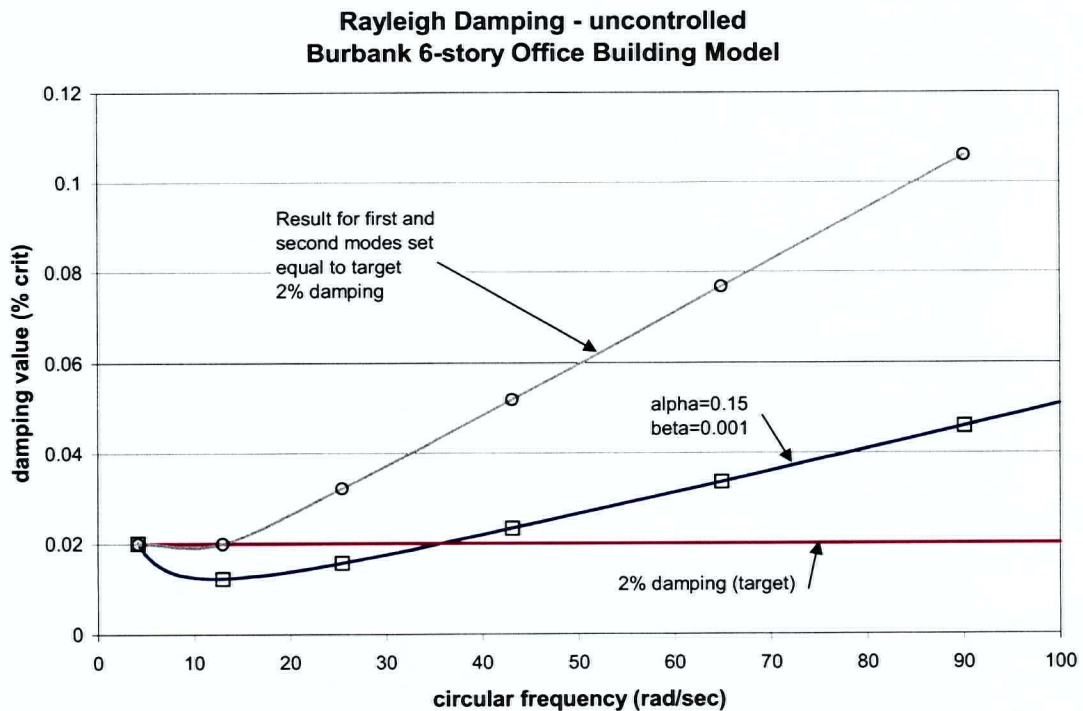


Figure 6.5. Rayleigh damping assumed for Burbank 6-story office building.

6.2.3 LQ Gains, System Poles and Characteristic Damping

Results were obtained for two control strengths; a “weak” control strength determined by setting $R_{factor} = 0.0006$ and a “strong” control by setting $R_{factor} = 0.0002$. The designation “strong” and “weak” are meant to imply the relative strengths rather than to indicate the overall performance. This is emphasized by the use of quotations surrounding “strong” and “weak”. As will be seen later on, the so-called “weak” control is actually quite capable of producing a desirable structural response to the given earthquake. The “strong” control on the other hand carries the control just beyond the limit where a brace stiffness ratio of $\alpha=2$ can be considered.

The Q matrix was used composed of the mass and stiffness matrix as in the previous example. Subsequently, the gain matrices were computed using the standard LQR algorithm as described in Chapter 2 and detailed in the first example. The resulting full state feedback gain matrix G given for the for the “strong” control only, was found to be (rounded to the nearest unit)

$$G = \begin{bmatrix} 3705 & 47 & -71 & 29 & 37 & 42 & 352 & 123 & 76 & 61 & 52 & 66 \\ -4768 & 3940 & 14 & -36 & 43 & 46 & -200 & 280 & 116 & 75 & 63 & 78 \\ 650 & -4798 & 4016 & -111 & -18 & 52 & -55 & -207 & 268 & 112 & 78 & 94 \\ 70 & 493 & -4542 & 3956 & -163 & 20 & -19 & -57 & -211 & 265 & 111 & 112 \\ 25 & 21 & 485 & -4334 & 3879 & -200 & -11 & -21 & -55 & -209 & 270 & 158 \\ 2 & 10 & 21 & 530 & -4078 & 3441 & -5 & -10 & -19 & -48 & -202 & 361 \end{bmatrix} \quad (6.39)$$

The observer feedback gain matrix associate with this gain matrix was computed to be (rounded to the nearest unit)

$$G_1 = \begin{bmatrix} 730 & 378 & 255 & 179 & 118 & 66 \\ 411 & 612 & 332 & 216 & 141 & 78 \\ 289 & 345 & 551 & 284 & 172 & 94 \\ 202 & 221 & 278 & 488 & 223 & 112 \\ 133 & 144 & 165 & 220 & 428 & 158 \\ 76 & 82 & 92 & 111 & 159 & 361 \end{bmatrix} \quad (6.40)$$

It is noted that this matrix is not strongly diagonal, therefore it is expected that the truncated form of this feedback gain matrix (that represents the portion that is directly possible to implement with passive viscous dampers) would provide significantly lower damping than its fully populated, active counterpart. The truncated gain matrix is given by

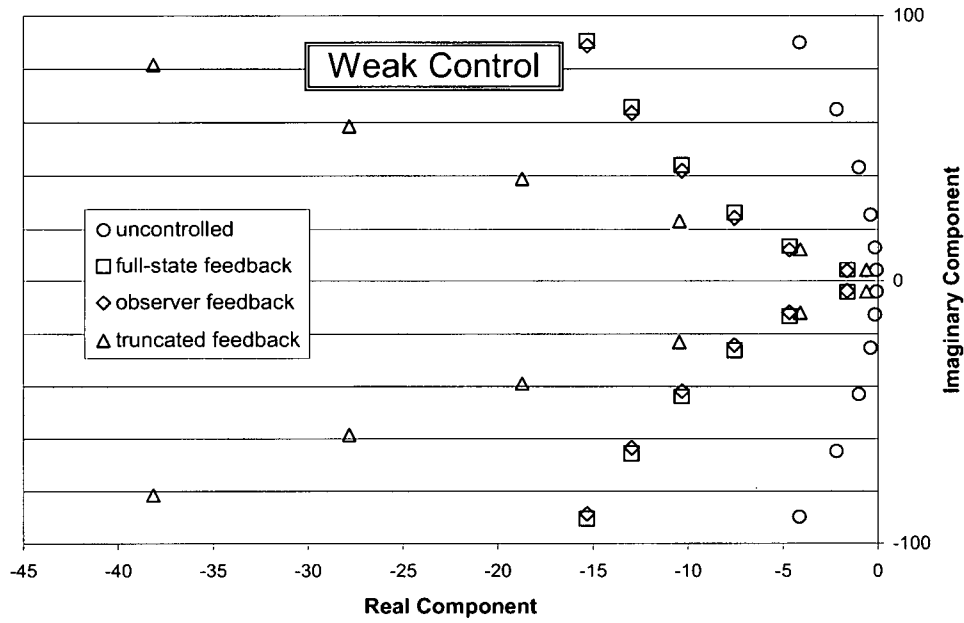
$$G_2 = \begin{bmatrix} 730 & 0 & 0 & 0 & 0 & 0 \\ 0 & 612 & 0 & 0 & 0 & 0 \\ 0 & 0 & 551 & 0 & 0 & 0 \\ 0 & 0 & 0 & 488 & 0 & 0 \\ 0 & 0 & 0 & 0 & 428 & 0 \\ 0 & 0 & 0 & 0 & 0 & 361 \end{bmatrix} \quad (6.41)$$

The poles locations associated with the uncontrolled and the controlled structure for both “weak” and “strong” feedback is given in Figure 6.6 and also summarized in Table 6.4 (a) and (b) together with the computed damping in each mode. The pole plot is useful in that it provides an indication of the control strength associated with the full state feedback; observer feedback and truncated observer gain matrix. It is interesting to note that the observer gain matrix has damping values slightly higher than those associated with the full state feedback in all but the first two modes of the “strong” control. In this case the damping associated with these modes is substantially more. While the full state feedback tends to increase the frequencies in each mode (imaginary component), the observer feedback tends to lower the frequency substantially. These have a balancing effect, and although not identical, the net result is a control performance that is essentially equivalent.

6.2.4 Computation of Passive Viscous Damping Coefficients

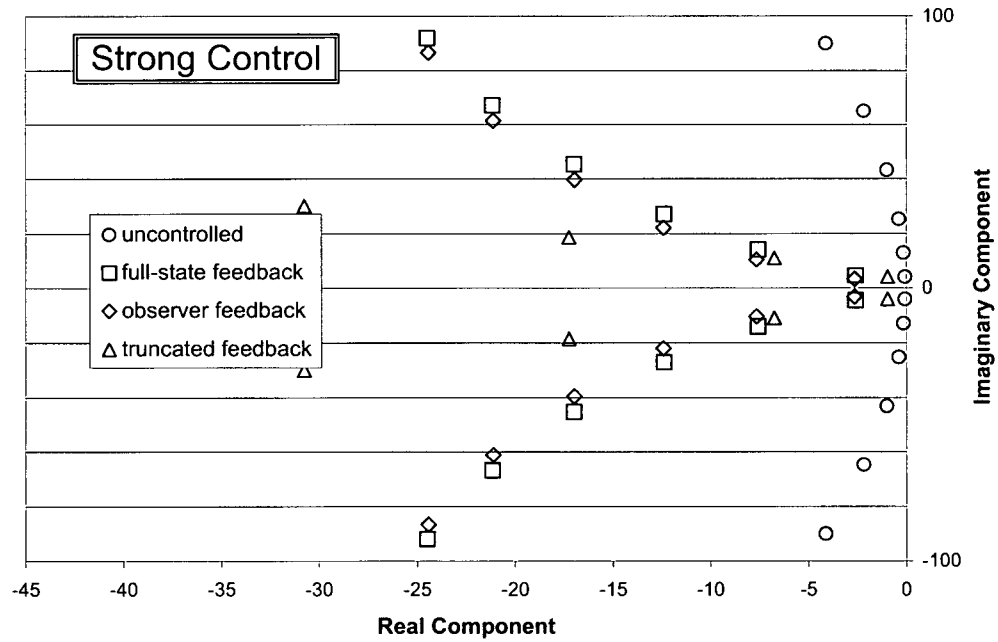
Modal superposition and response spectra analysis using the exact spectral values computed for the El Centro N00E record as input were carried out for each of the “strong” and “weak” levels of control. Two diagonal braces are intended to support the dampers, as shown in Figure 6.7. From the RSA output, peak values of control force and story drift velocities were extracted. These were then used to establish the viscous damping coefficients using Equation 6.86. The calculation is detailed in Tables 6.5 (a) and (b) for dampers oriented horizontally and then transformed to correspond to the dampers oriented in the direction of the braces. The distribution of the damping resulting from this computation is illustrated graphically in Figures 6.8 and 6.9.

Pole Locations - Burbank 6-story Office Building
 uncontrolled, full-state, observer and truncated feedback cases



(a) Weak control pole locations

Pole Locations - Burbank 6-story Office Building
 uncontrolled, full-state, observer and truncated feedback cases



(b) Strong control pole locations

Figure 6.6. Pole locations, weak and strong control. Transformation of the horizontal stiffness follows the simple formula

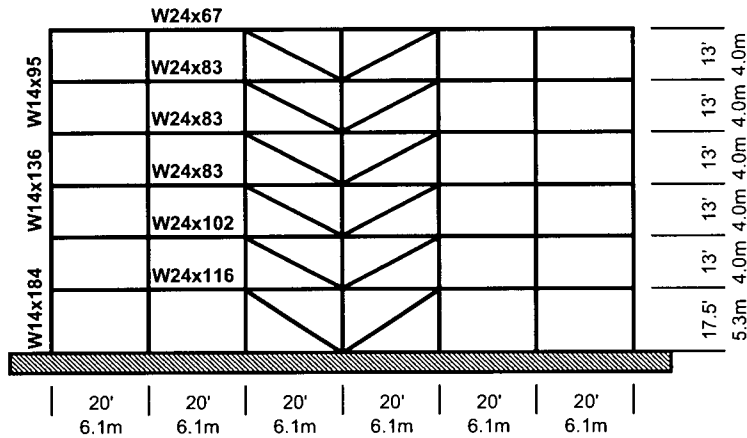


Figure 6.7. Implementation of control using diagonal braces in the perimeter frame

$$K_{horizontal} = k_{diagonal} \cos^2 \theta \quad (6.42)$$

where θ represents the angle of the brace measured from horizontal and p represents the brace property. This relationship also holds true for damping coefficient.

The trend in the viscous damping coefficients observed with the 6-story structure was similar to that obtained for the 4-story example in the previous section with the highest viscous damping coefficient at the base and progressively lower towards the top story. Considering the implementation of the viscous dampers on two diagonal braces as shown in Figure 6.7, the damping coefficients on the diagonal are computed in Table 6.4.

Table 6.4. Comparison of system poles and associated modal damping with “weak” and “strong” control.

(a) “Weak” Control Poles $R_{factor}=0.0006$

Uncontrolled: eig(A)			Full State Feedback: eig(A+BG)			Observer Feedback: eig(A+BG ₁ C)			Truncated Observer Feedback: eig(A+BG ₂ C)		
real	imag	damp	real	imag	damp	real	imag	damp	real	imag	damp
-0.084	-4.16	2.0%	-1.61	4.36	34.7%	-1.64	-3.84	39.2%	-0.62	-4.11	14.8%
-0.084	4.16		-1.61	-4.36		-1.64	3.84		-0.62	4.11	
-0.159	-13.0	1.2%	-4.65	13.6	32.4%	-4.67	-12.08	36.0%	-4.09	-12.3	31.6%
-0.159	13.0		-4.65	-13.6		-4.67	12.08		-4.09	12.3	
-0.398	-25.4	1.6%	-7.55	26.3	27.6%	-7.55	-24.25	29.7%	-10.5	-23.2	41.1%
-0.398	25.4		-7.55	-26.3		-7.55	24.25		-10.5	23.2	
-1.00	-43.1	2.3%	-10.3	44.0	22.9%	-10.3	-41.83	24.0%	-18.7	-38.8	43.4%
-1.00	43.1		-10.3	-44.0		-10.3	41.83		-18.7	38.8	
-2.18	-64.8	3.4%	-13.0	65.7	19.4%	-13.0	-63.52	20.0%	-27.8	-58.6	42.9%
-2.18	64.8		-13.0	-65.7		-13.0	63.52		-27.8	58.6	
-4.13	-90.0	4.6%	-15.3	90.6	16.7%	-15.3	-88.75	17.0%	-38.2	-81.6	42.4%
-4.13	90.0		-15.3	-90.6		-15.3	88.75		-38.2	81.6	

(b) "Strong" Control Poles $R_{factor}=0.0002$

Uncontrolled: eig(A)			Full State Feedback: eig(A+BG)			Observer Feedback: eig(A+BG ₁ C)			Truncated Observer Feedback: eig(A+BG ₂ C)		
real	imag	damp	real	imag	damp	real	imag	damp	real	imag	damp
-0.084	-4.16	2.0%	-2.61	-4.55	49.7%	-2.67	-3.23	63.7%	-0.98	-4.04	23.6%
-0.084	4.16		-2.61	4.55		-2.67	3.23		-0.98	4.04	
-0.159	-13.0	1.2%	-7.59	-14.2	47.3%	-7.66	-10.44	59.2%	-6.76	-11.1	52.1%
-0.159	13.0		-7.59	14.2		-7.66	10.44		-6.76	11.1	
-0.398	-25.4	1.6%	-12.40	-27.2	41.4%	-12.40	-22.11	48.9%	-17.2	-18.7	67.9%
-0.398	25.4		-12.40	27.2		-12.40	22.11		-17.2	18.7	
-1.00	-43.1	2.3%	-17.0	-45.3	35.1%	-17.0	-39.57	39.4%	-30.8	-30.2	71.3%
-1.00	43.1		-17.0	45.3		-17.0	39.57		-30.8	30.2	
-2.18	-64.8	3.4%	-21.2	-67.1	30.1%	-21.1	-61.26	32.6%	-45.3	-46.4	69.9%
-2.18	64.8		-21.2	67.1		-21.1	61.26		-45.3	46.4	
-4.13	-90.0	4.6%	-24.5	-91.9	25.7%	-24.4	-86.64	27.1%	-61.5	-65.7	68.4%
-4.13	90.0		-24.5	91.9		-24.4	86.64		-61.5	65.7	

Note: System poles are given as the eigenvalues of the matrix (A+BG) where G is a gain matrix. G represents the full state feedback coefficient matrix; G₁ represents the direct observer feedback matrix; G₂ is equal to G₁ truncated to its diagonal terms.

Although not shown in this set of results, the response of the structure to the El Centro N00E input record with dampers implemented on the diagonal braces of the full frame model were computed using ADINA and it was verified that the modal superposition computation of the time-history response in the simplified model implemented in MATLAB were identical. This step was necessary to gain confidence with the model prior to the implementation of the friction dampers, as ADINA is the only structural analysis program used to obtain the friction damped time history response.

Equation 5.86 was used to equate the peak cycle energy dissipated in friction to that dissipated by the target viscous damper resulting in a modification of the slip load from the peak slip force. The computation of the friction slip force for both control strengths is detailed in Table 6.6 (a) and (b).

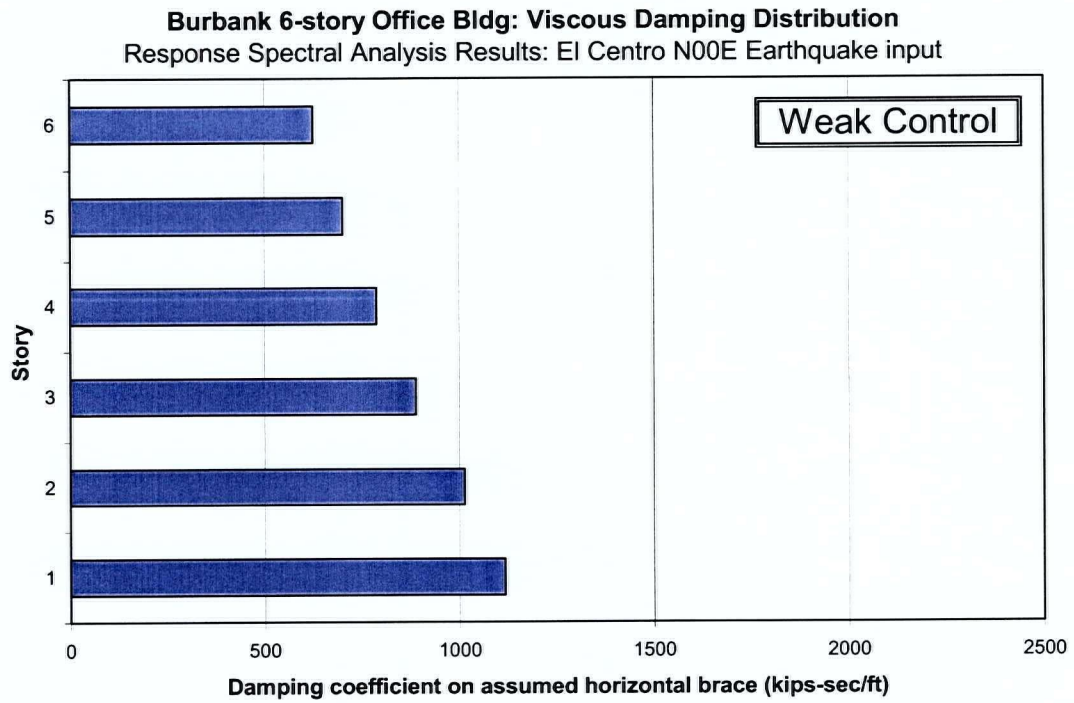


Figure 6.8. Distribution of viscous dampers – weak control.

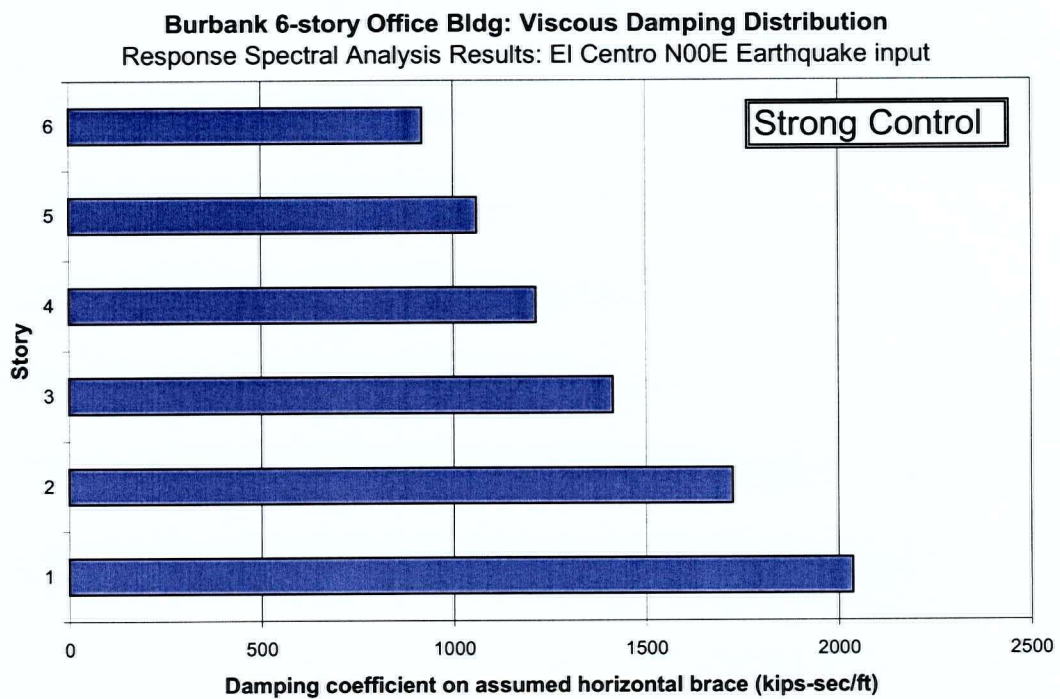


Figure 6.9. Distribution of viscous dampers – strong control.

Table 6.5. Detailed evaluation of damping coefficients based on peak cycle energy. Damping is given on horizontal plane and also computed for each of two diagonal braces.

(a) "Weak" control. Evaluation of viscous damping coefficients.

Story	Bay Width	Height	Angle	Slip Frc	Vel	Damp	on diag	on each of 2
	(ft)	(ft)	(rad)	(kips)	(ft/sec)	(kip-s/ft)	(kip-s/ft)	diagonals (kip-s/ft)
1	20	17.5	0.719	315	0.282	1117	1484	742
2	20	13	0.576	353	0.348	1014	1209	605
3	20	13	0.576	369	0.415	889	1060	530
4	20	13	0.576	333	0.423	788	939	470
5	20	13	0.576	267	0.380	702	837	418
6	20	13	0.576	175	0.280	626	746	373

(b) "Strong" control. Evaluation of viscous damping coefficients.

Story	Bay Width	Height	Angle	Slip Frc	Vel	Damp	on diag	on diag of 2
	(ft)	(ft)	(rad)	(kips)	(ft/sec)	(kip-s/ft)	(kip-s/ft)	diagonals (kip-s/ft)
1	20	17.5	0.719	517	0.25	2036	2705	1353
2	20	13	0.576	548	0.32	1724	2056	1028
3	20	13	0.576	543	0.38	1414	1687	843
4	20	13	0.576	476	0.39	1215	1449	724
5	20	13	0.576	373	0.35	1061	1266	633
6	20	13	0.576	238	0.26	920	1097	548

Table 6.6. Detailed evaluation of friction damper slip loads based on peak cycle energy. Friction slip loads are evaluated on a horizontal plane then converted to that for a single and each of two diagonal braces. For comparison purposes, the slip load is expressed in terms of the ratio to the story weight.

(a) "Weak" control. Evaluation of friction damper slip loads.

Story	Peak Control Force	Diag Peak Control Force	Peak Displ. (horizontal)	Slip Load (horizontal)	Diagonal Slip Force	Slip Load per Brace (assume 2)	Storey mass (kslugs)	Storey Weight (kips)	Slip Load per Story Weight Ratio (%)
	(kips)	(kips)	(ft)	(kips)	(kips)	(ft ²)			
1	315	418	0.0525	272	361	181	21.2	683	40%
2	353	420	0.0641	296	353	177	17.3	558	53%
3	369	440	0.0759	312	372	186	16.9	544	57%
4	333	397	0.0769	283	338	169	16.8	541	52%
5	267	318	0.0690	230	274	137	16.8	541	43%
6	175	209	0.0508	158	188	94	22.9	739	21%

(b) "Strong" control. Evaluation of friction damper slip loads.

Story	Peak Control Force	Diag Peak Control Force	Peak Displ. (horizontal)	Slip Load (horizontal)	Diagonal Slip Force	Slip Load per Brace (assume 2)	Storey mass (kslugs)	Storey Weight (kips)	Slip Load per Story Weight Ratio (%)
	(kips)	(kips)	(ft)	(kips)	(kips)	(ft ²)			
1	517	687	0.0376	545	725	362	21.2	683	80%
2	548	654	0.0457	512	610	305	17.3	558	92%
3	543	648	0.0540	508	606	303	16.9	544	93%
4	476	567	0.0544	451	538	269	16.8	541	83%
5	373	445	0.0486	368	439	219	16.8	541	68%
6	238	284	0.0357	271	324	162	22.9	739	37%

6.2.5 Comparison of Performance: Active vs Passive Viscous and Friction Dampers

Using the viscous dampers and the friction dampers obtained, time history results were obtained for the Elcentro N00E record input. These were obtained using the modal superposition procedure implemented in MATLAB (1999) for the uncontrolled, target full state feedback controlled, passive viscous damped structures. The passive friction damped structure response was evaluated using ADINA (2002) to expedite the analysis of the non-linear structure. Figures 6.10 and 6.11 contain time history data for the “weak” control level displacement and velocity results while Figures 6.12 and 6.13 contain the corresponding time history results for the “strong” control. Tables 6.7 and 6.8 summarize the peak absolute values obtained in each case.

6.2.5.1 Observations

The time history plots shown illustrate of the type of behaviour that can be expected of the three control systems. With the “weak” control it is observed that the response of the target actively controlled structure was significantly less than the uncontrolled structure. The active control is shown to reduce the velocities over the uncontrolled structure but the margin of reduction appears to be much less than that achieved for displacements. The lower stories appear to contain more higher frequency content while the upper stories respond primarily at the fundamental frequency of the structure. The active control does not appear to alter the frequency content of the response significantly.

The viscous damped structure was designed to replicate the response of the actively controlled structure (target). The time history plots indicate that the passively controlled viscous damped structure does to a significant degree replicate the response of the actively controlled structure. The viscous damped structure tends to experience larger peaks than its actively controlled counterpart.

The response of the friction-damped structure on the other hand produces a response that does not follow the trace of the active and viscous damped structures. Instead it responds with a higher frequency, corresponding to the frequency characteristic of the braced structure. This is particularly evidenced by the high frequency oscillation near the end of the segment of the time history shown.

With the “strong” control case the actively controlled structure performed significantly better than its counterpart with the “weak” control. The viscous damped structure was not able to replicate the actively controlled structure response as well as with the “weak” control. The trace of the friction damped structure response appeared similar to that of the “weak” control case, with the exception that the oscillation appears to be offset from the origin.

6.2.5.2 *Comparison of the Performance*

Table 6.7 details the peak responses obtained for the “weak” control and Table 6.8 provides the corresponding envelope values obtained using the “strong” control. The response for the target active control is computed both by modal superposition (exact) and estimated by RSA using the SRSS modal combination. Columns 3 and 4 compare the envelope values obtained by each method. It is observed that for the “weak” control case, the displacements computed agree very well and the velocities, although not as accurately predicted, still appear to be within an acceptable level of error (max 10% error). With the “strong” control case the agreement in displacement was not as good as that for the “weak” control with maximum error of 14% in the bottom story, however, the velocities were predicted to the same level of precision with a maximum error of 13% on the top story.

The target active controlled structure displacements were found to range from 37-41% of the corresponding uncontrolled values, while the viscous damped structure experienced displacements ranging from 43-48% of the uncontrolled displacements. The friction damped structure, curiously, experienced displacements ranging from 34-59% of those experienced by the uncontrolled structure with rooftop displacements being less than that observed in the case where active control is implemented. With the friction damped system, the poorest performance was experienced by the lowest stories, with displacements up to 47% higher than the target actively controlled structure.

The active controlled structure experienced velocities ranging from 36% to 59% of those experienced by the uncontrolled structure. The viscous damped counterpart achieved velocities ranging from 33-52% of the uncontrolled structure. The friction damped structure experienced velocities ranging from 63-88% of the uncontrolled velocities. While the friction damped structure experienced velocities much higher than the target actively controlled structure, the velocities at every story were the same or better than those corresponding to the target control.

The trends shown with the “weak” control were largely replicated by the “strong” control but to a greater degree. While the “strong” active control target displacements were exceeded by up to 30% by the viscous damped structure, this was greater than the 18% increase in observed displacements with the “weak” control. With the “strong” friction damped structure, the resulting displacements exceeded the target displacements by 94%, as compared to the maximum 47% with the “weak” control. The reduction in the peak velocities with the passive viscous damped structure ranged from 3-23% under those experienced by the actively controlled target structure, while the friction damped structure experienced velocities exceeding the target controlled structure by up to 122%.

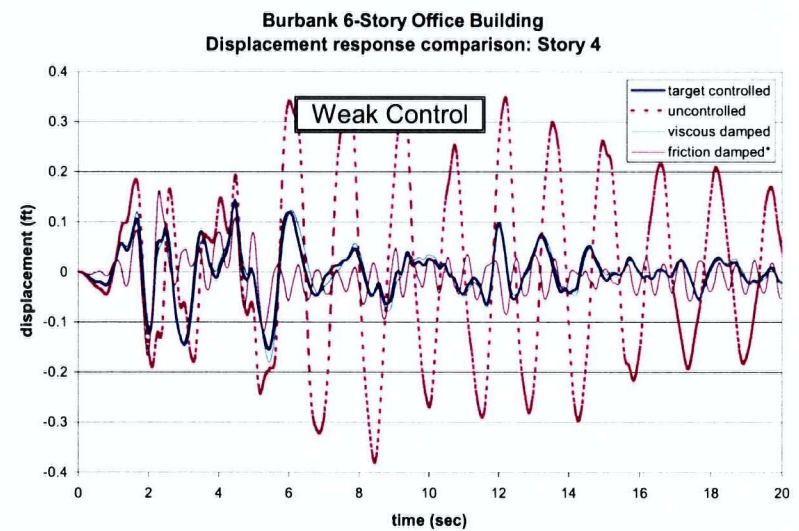
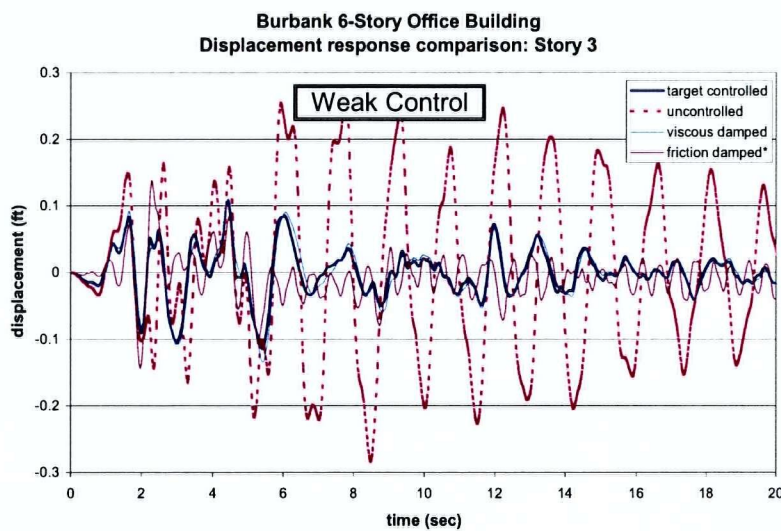
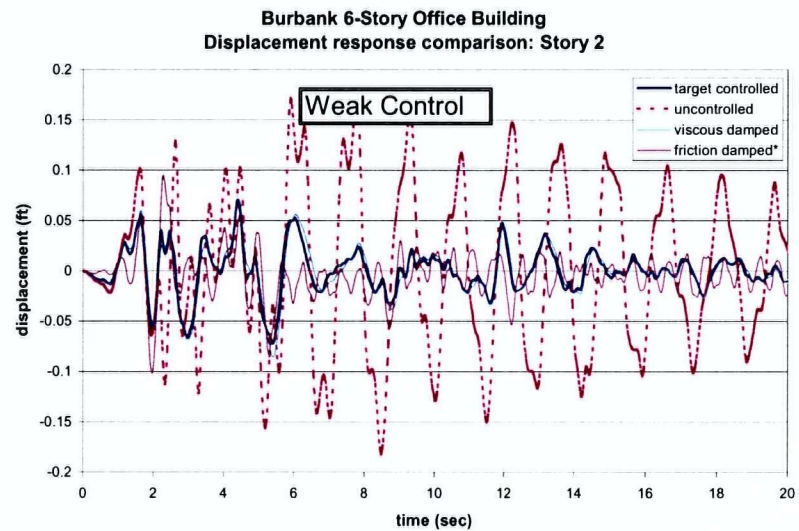
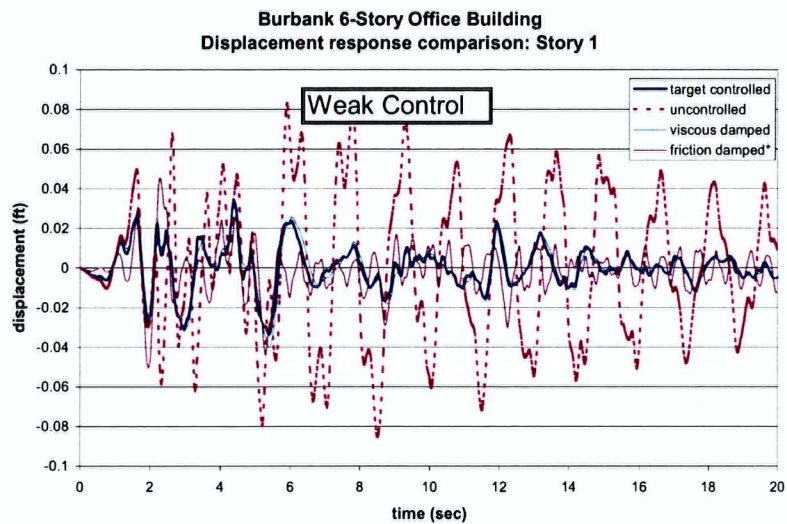


Figure 6.10. Undamped and controlled displacement response data obtained for the Burbank 6-story office building. (continued next page)

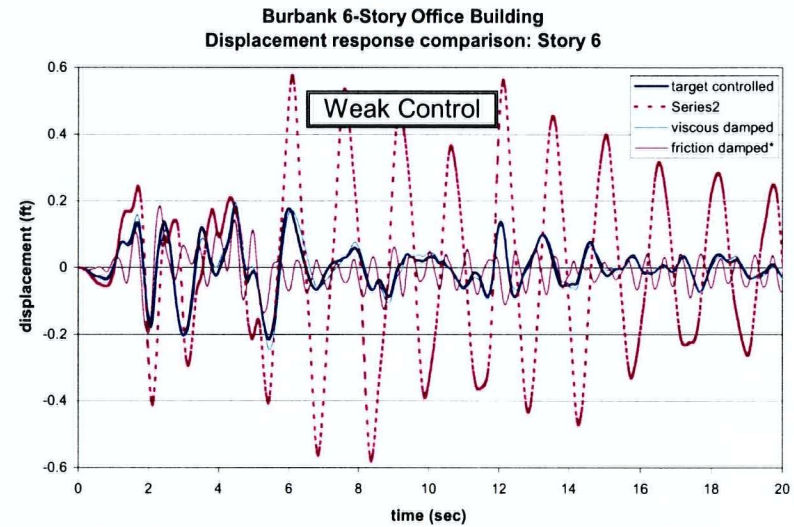
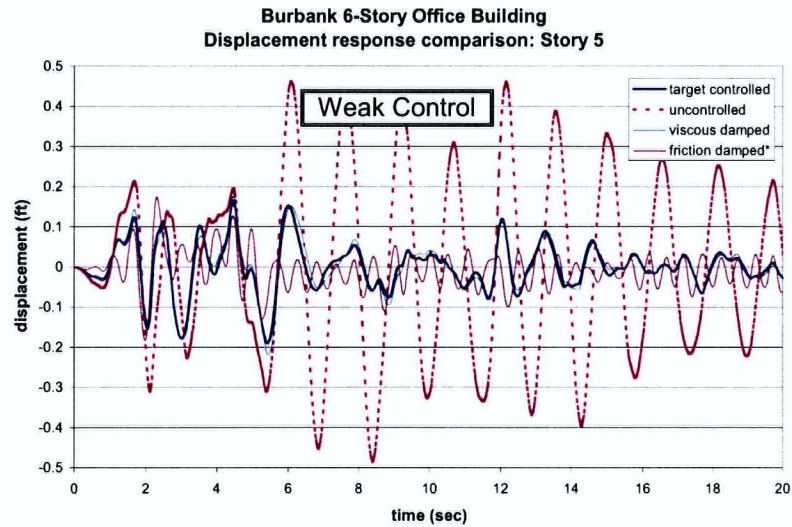


Figure 6.10. Undamped and controlled displacement response data obtained for the Burbank 6-story office building for the “weak” control having $R_{factor}=0.006$. Uncontrolled, Target controlled and Viscous Damped time histories were obtained using modal superposition procedure implemented in MATLAB, while the Friction Damped response was obtained using a non-linear time history analysis in ADINA. Only the first 20 seconds of response are shown to provide sufficient scale to distinguish the different waveforms.

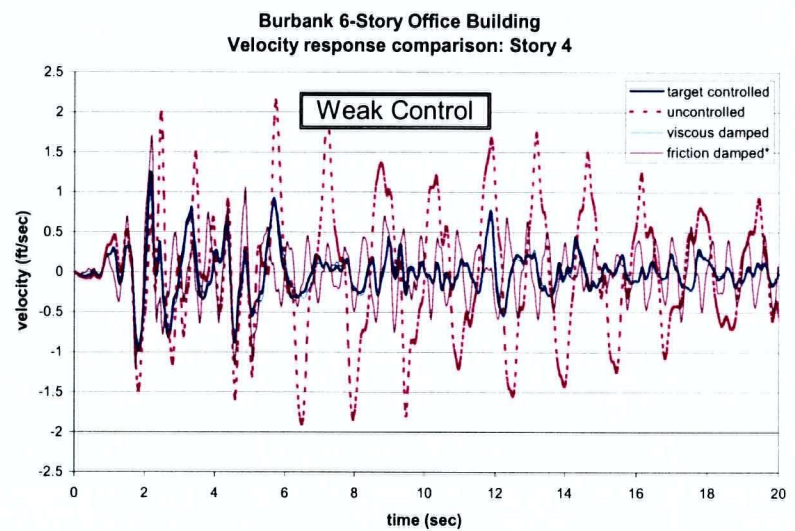
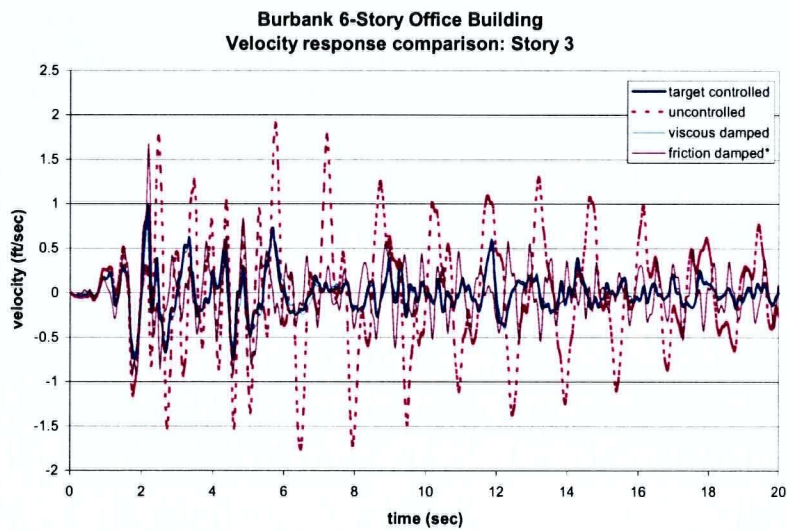
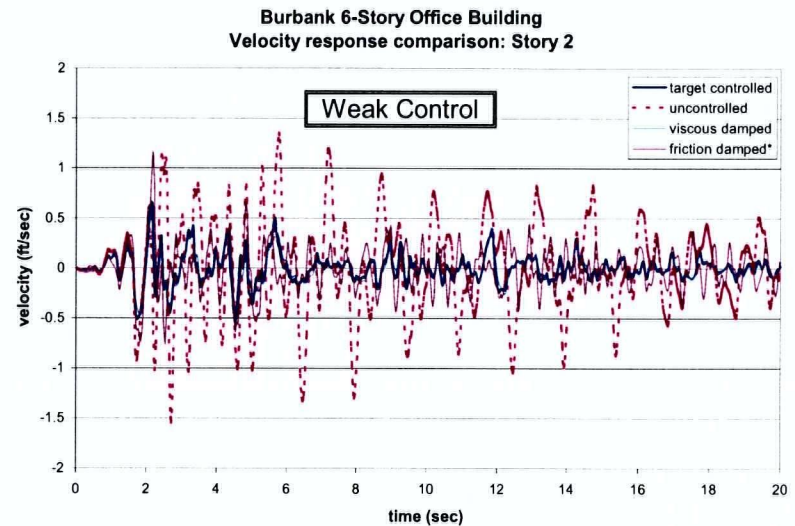
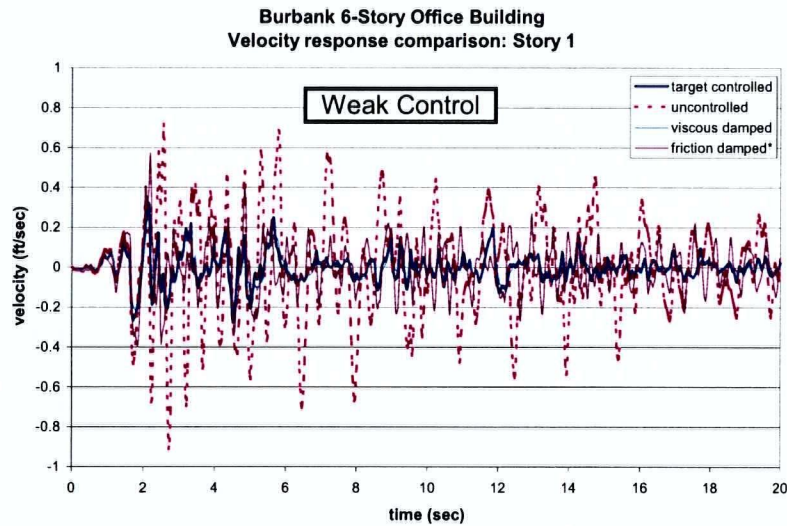


Figure 6.11. Undamped and controlled response data obtained for the Burbank 6-story office building. (Continued on next page)

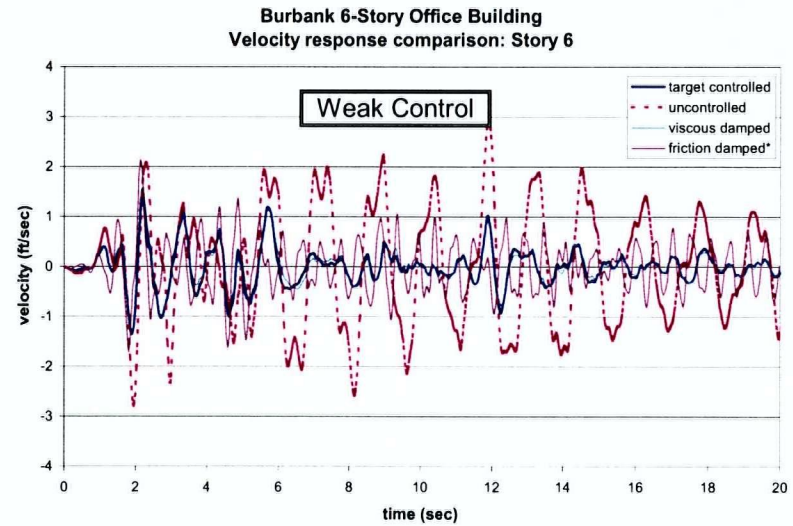
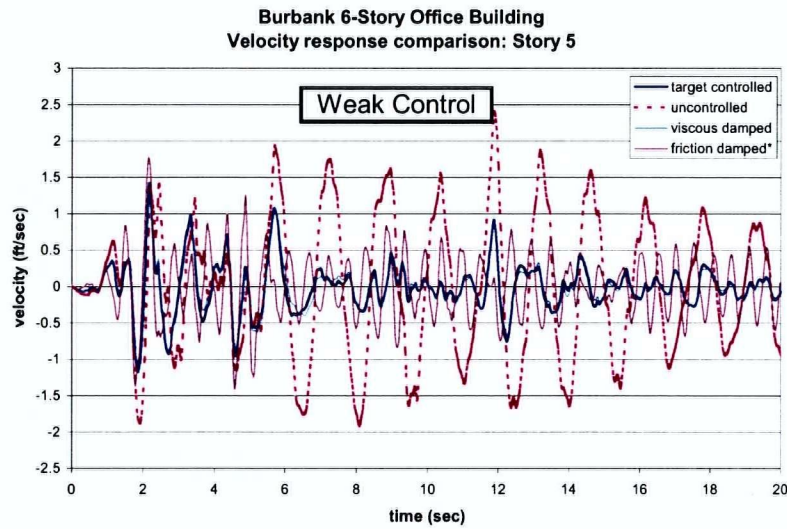


Figure 6.11. Undamped and “weak” controlled response data obtained for the Burbank 6-story office building. Time history velocity response data was obtained from modal superposition procedure in MATLAB using El Centro N00E earthquake input data for all except the friction damped structure whose response was determined using ADINA.

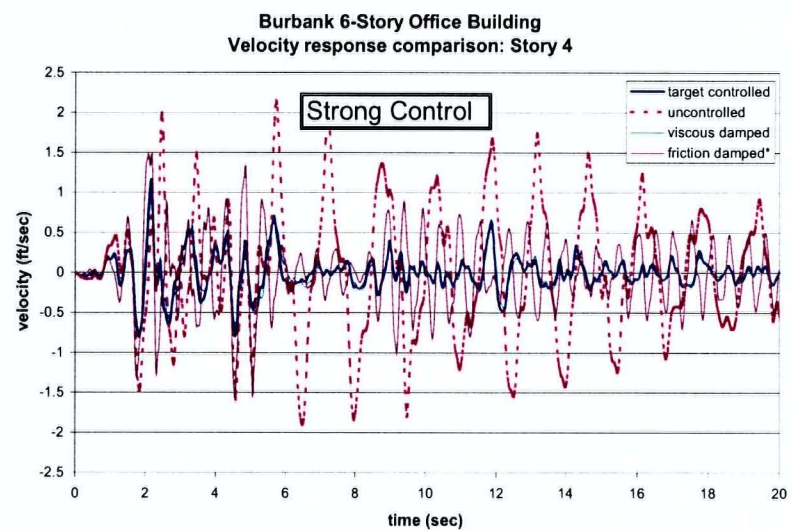
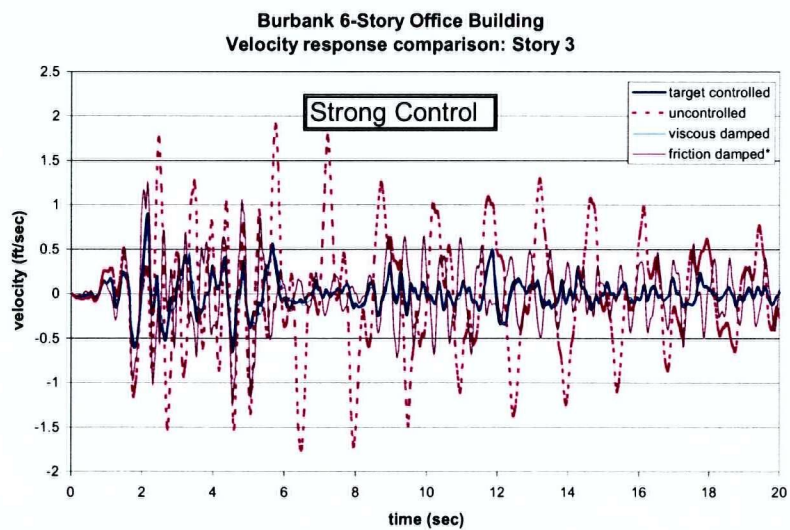
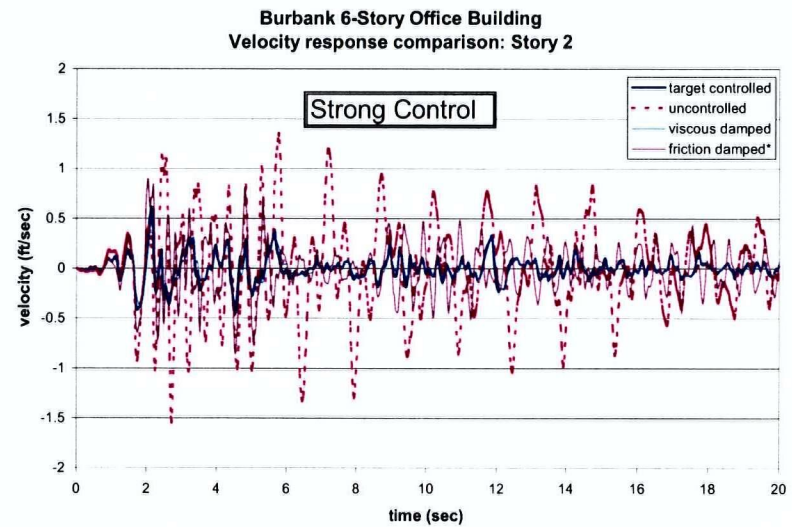
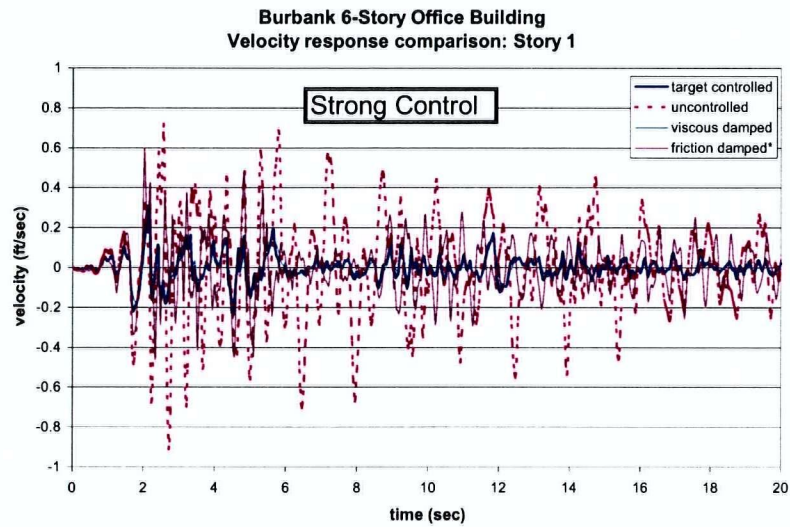


Figure 6.12. Undamped and “strong” controlled response data obtained for the Burbank 6-story office building. (continued next page)

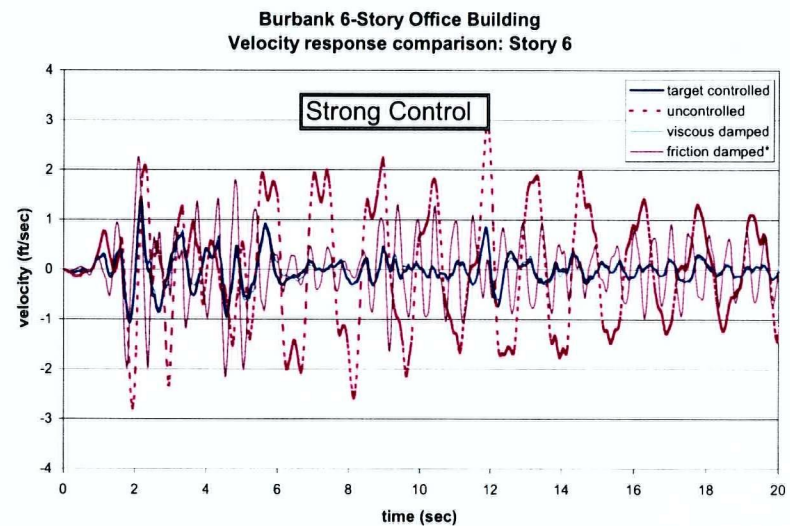
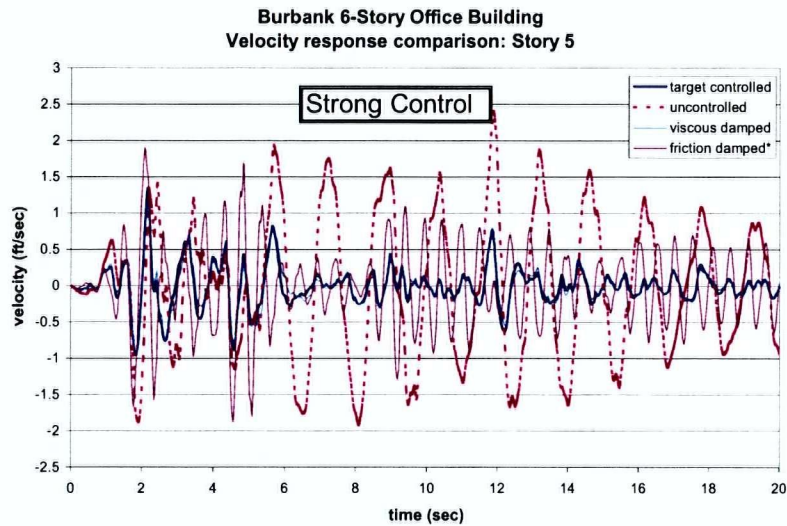


Figure 6.12. Undamped and “strong” controlled displacement response data obtained for the Burbank 6-story office building. Uncontrolled, Target controlled and Viscous Damped time histories were obtained using modal superposition procedure implemented in MATLAB, while the Friction Damped response was obtained using a non-linear time history analysis in ADINA. Note that the friction damped procedure leads to a noticeable offset in the displacement response after approximately 4 seconds. Note that only the first 20 seconds of response are shown to provide sufficient scale to distinguish the different waveforms.

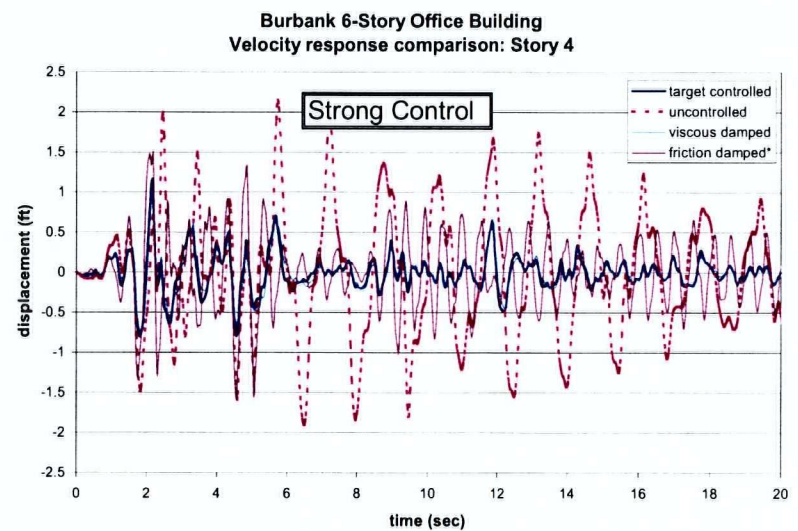
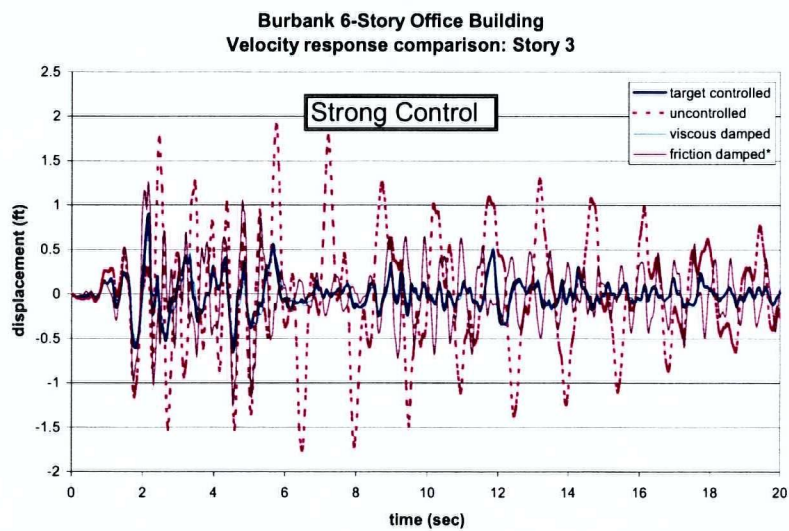
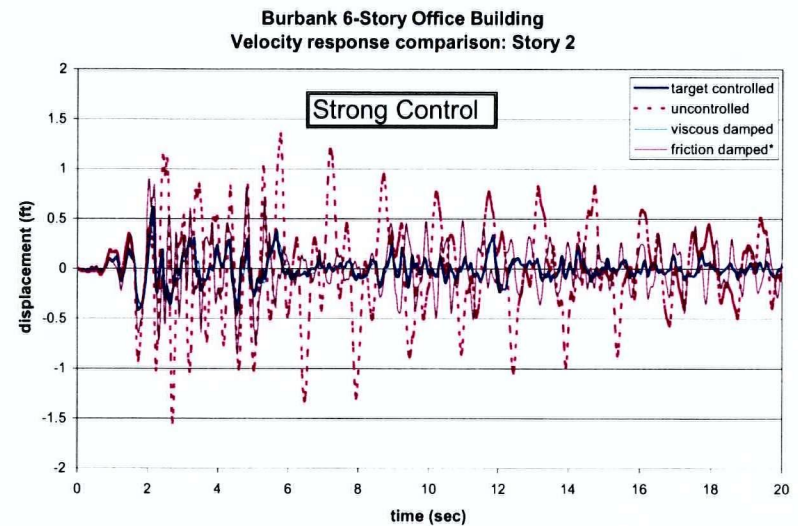
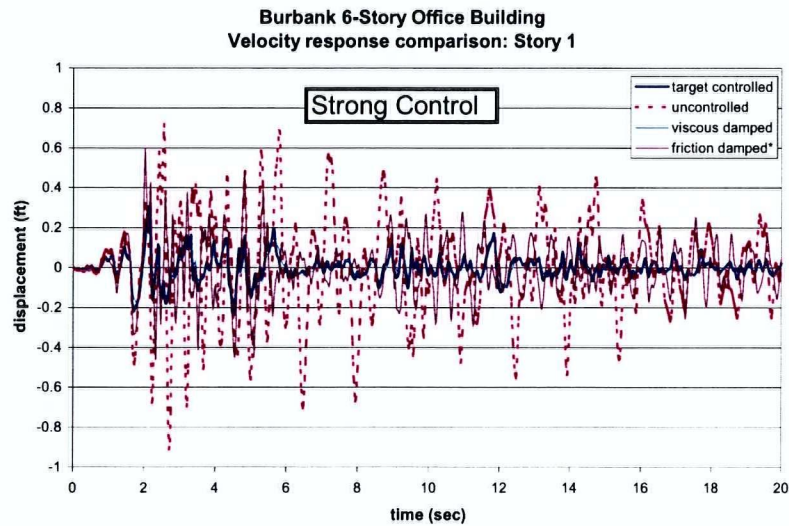


Figure 6.13. Undamped and controlled response data obtained for the Burbank 6-story office building. (Continued next page)

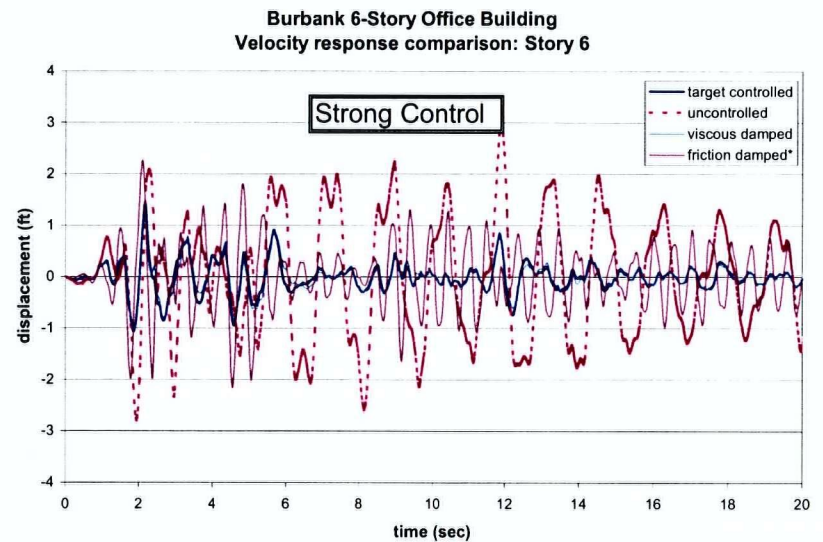
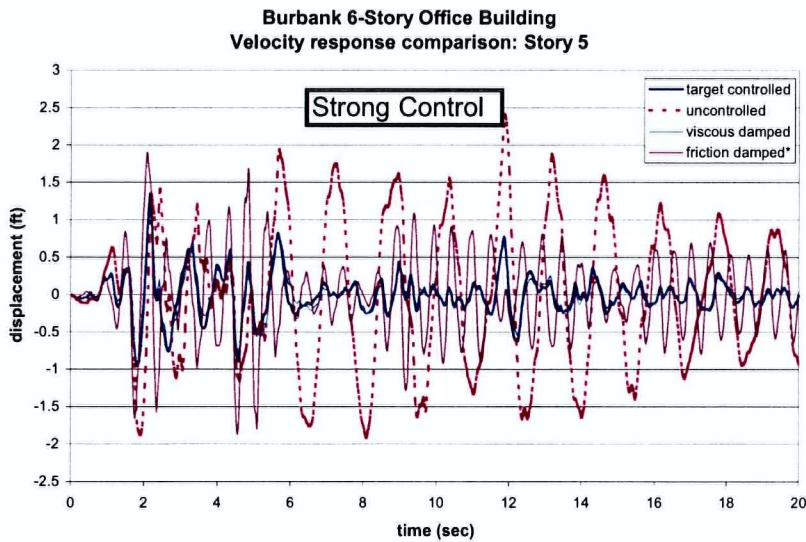


Figure 6.13. Undamped and “strong” controlled velocity response data obtained for the Burbank 6-story office building. Uncontrolled, Target Controlled and Viscous Damped response data was obtained from modal superposition procedure implemented in MATLAB. Friction Damped response data was obtained using non-linear time history analysis implemented in ADINA.

Table 6.7. Comparison of control performance – “Weak” control.

Variable	Without Dampers	Response				Performance: % of uncontrolled response			Comparison	
		Target Control		Visc Damp	Fric Damp	Target	Achieved Visc	Achieved Fric	Visc/Target	Fric/Target
	max x _u	Respm	max x	max x _t	max x _f	(%)	(%)	(%)	(Δ%)	(Δ%)
x ₁	0.085	0.034	0.034	0.040	0.050	40%	47%	59%	18%	47%
x ₂	0.182	0.073	0.072	0.086	0.102	40%	47%	56%	18%	40%
x ₃	0.284	0.114	0.115	0.135	0.144	40%	48%	51%	19%	26%
x ₄	0.381	0.154	0.155	0.181	0.168	41%	47%	44%	17%	9%
x ₅	0.484	0.192	0.190	0.220	0.183	39%	45%	38%	15%	-4%
x ₆	0.579	0.222	0.216	0.246	0.197	37%	43%	34%	11%	-12%
v ₁	0.904	0.318	0.322	0.302	0.574	36%	33%	63%	-5%	80%
v ₂	1.533	0.613	0.657	0.611	1.161	43%	40%	76%	0%	89%
v ₃	1.904	0.885	0.983	0.903	1.680	52%	47%	88%	2%	90%
v ₄	2.135	1.137	1.251	1.119	1.712	59%	52%	80%	-2%	51%
v ₅	2.406	1.389	1.420	1.259	1.778	59%	52%	74%	-9%	28%
v ₆	2.995	1.648	1.546	1.362	2.135	52%	45%	71%	-17%	30%

Table 6.8. Comparison of control performance – “Strong” control.

Variable	Without Dampers max x _u	Response				Performance: % of uncontrolled response			Comparison	
		Target Control		Visc Damp	Fric Damp	Target	Achieved Visc	Achieved Fric	Visc/Target	Fric/Target
		Respm	max x	max x _t	max x _f	(%)	(%)	(%)	(Δ%)	(Δ%)
x ₁	0.085	0.025	0.029	0.032	0.048	34%	38%	56%	30%	94%
x ₂	0.182	0.052	0.059	0.068	0.102	32%	37%	56%	30%	96%
x ₃	0.284	0.082	0.088	0.106	0.154	31%	37%	54%	30%	87%
x ₄	0.381	0.111	0.113	0.141	0.189	30%	37%	50%	27%	70%
x ₅	0.484	0.138	0.136	0.171	0.210	28%	35%	43%	24%	52%
x ₆	0.579	0.159	0.152	0.191	0.220	26%	33%	38%	20%	38%
v ₁	0.904	0.271	0.301	0.261	0.601	33%	29%	66%	-3%	122%
v ₂	1.533	0.544	0.611	0.528	0.898	40%	34%	59%	-3%	65%
v ₃	1.904	0.835	0.901	0.792	1.265	47%	42%	66%	-5%	52%
v ₄	2.135	1.125	1.164	1.011	1.592	54%	47%	75%	-10%	41%
v ₅	2.406	1.402	1.347	1.173	1.908	56%	49%	79%	-16%	36%
v ₆	2.995	1.643	1.451	1.273	2.264	48%	43%	76%	-23%	38%

The objectives of this example are to take the analysis one step further than with the plane frame analysis in Section 6.2 and demonstrate that the method proposed can be utilised to provide estimates of viscous damping coefficients and friction damper slip loads in a complex and irregular structure. The example chosen incorporates

- two simultaneous input directions,
- irregular damper locations, and
- a reduced number of modes used in spectral analysis

During the Magnitude 6.1 Loma Prieta earthquake (October 17, 1989) this structure suffered some damage limited to light cracking of the narrow, transverse shear walls. Many non-structural items not designed to resist earthquake motions suffered damage, including several exhaust fan fume hoods at the roof level that were thrown from their supports.

The building is supported by spread footings. Initial modelling of this structure by engineers at H.J. Dengenkolb (1991) neglected the flexibility of the structure and concentrated the deformability at the foundation level. Modelling of the structure as part of this work confirmed that the concrete structure is very stiff and the observed response periods of 0.36 seconds in the longitudinal direction and 0.57 seconds in the transverse direction are most likely the result of foundation deformability as the vibration periods measured in the lateral and longitudinal directions could only be obtained by introducing soil springs. The soil spring stiffness that was found to provide a match with the measured periods when combined with the estimated stiffness of the structural elements produced a response in the structure that that was dominated by the deformation of the foundation with very little deformation of the structure itself.

Although this mode of response may be common among such concrete structures, the small deformations observed in the structure itself indicated that dampers in the structure would not likely be activated in even a strong earthquake. This realization is instructive in that it highlights the point that not all structures are candidates for damper systems.

Although desirable, it is not necessary that the structure correspond to an actual existing structure. Subsequently, the actual building model was abandoned, and a new model of a hypothetical structure was generated. This hypothetical structure model was constructed with a similar geometry and mass but having a fixed base. It was further assumed that the floors act as rigid diaphragms. The original rocking periods were matched by providing stiffness

characteristic of much more flexible members than the original structure. Admittedly, the structural model used no longer corresponds to that of the structural system of the original structure, however, it was felt that this would not distract from the original objective of demonstrating the mathematical procedure for designing damper systems. The results presented here do not apply to the original structure studied by Dengenkolb (1991).

6.3.1 Structural Modeling

The state vector for the structure was chosen to be:

$$x = [x_1 \ x_2 \ x_3 \ x_4 \ x_5 \ x_6 \ y_1 \ y_2 \ y_3 \ y_4 \ y_5 \ y_6 \ r_1 \ r_2 \ r_3 \ r_4 \ r_5 \ r_6 \dots \ \dot{x}_1 \ \dot{x}_2 \ \dot{x}_3 \ \dot{x}_4 \ \dot{x}_5 \ \dot{x}_6 \ \dot{y}_1 \ \dot{y}_2 \ \dot{y}_3 \ \dot{y}_4 \ \dot{y}_5 \ \dot{y}_6 \ \dot{r}_1 \ \dot{r}_2 \ \dot{r}_3 \ \dot{r}_4 \ \dot{r}_5 \ \dot{r}_6]^T \quad (6.43)$$

where x corresponds to the transverse deflection, y the longitudinal deflection and r the rotation about the chosen model point. Figure 6.14 illustrates the extraction of the 18-DOF model based on the given structure. Each lumped mass represents the translational (X-transverse and Y-longitudinal) and Z-rotational inertia of the floor diaphragm. The transverse and torsional stiffness is represented by the column elements shown in the figure. The mass and stiffness coefficients for each story are summarized in the following Table 6.9. Computations were carried out in imperial units.

Table 6.9. 18 DOF structure story mass and stiffness parameters: Imperial units

Story	Height (ft)	Mass		Stiffness		
		Translational (kslugs)	Rotational (kslug-ft ²)	Transverse (kips/ft)	Longitudinal (kips/ft)	Torsional (kip-ft/rad)
1	16.00	36	10310	175285	198910	2.095E+08
2	12.50	49	62630	235385	254757	2.682E+08
3	12.50	49	52846	235385	254757	2.682E+08
4	12.50	49	52846	235385	254757	2.682E+08
5	12.50	49	52846	235385	254757	2.682E+08
6	12.50	40	52261	235385	254757	2.682E+08

The effect of the eccentricity appears in the value of the rotational inertia of the second story mass corresponding to the third floor diaphragm. The rotational inertia at the second story is higher than that at stories 3, 4 and 5 due to the chosen model point lying 33' (9m) from the

centroid of this diaphragm. In addition, the eccentricity gives rise to off-diagonal stiffness terms that account for the torsional moments generated with an imposed shear in the second story. The following equation illustrates the 18x18 stiffness in imperial units derived from the stiffness parameters above:

$$\mathbf{K} = \begin{bmatrix}
 410671 & -235385 & 0 & 0 & 0 & 0 & 0 & 0 & 0 & 0 \\
 -235385 & 470771 & -235385 & 0 & 0 & 0 & 0 & 0 & 0 & 0 \\
 0 & -235385 & 470771 & -235385 & 0 & 0 & 0 & 0 & 0 & 0 \\
 0 & 0 & -235385 & 470771 & -235385 & 0 & 0 & 0 & 0 & 0 \\
 0 & 0 & 0 & -235385 & 470771 & -235385 & 0 & 0 & 0 & 0 \\
 0 & 0 & 0 & 0 & -235385 & 235385 & 0 & 0 & 0 & 0 \\
 0 & 0 & 0 & 0 & 0 & 0 & 453667 & -254757 & 0 & 0 \\
 0 & 0 & 0 & 0 & 0 & 0 & -254757 & 509514 & -254757 & 0 \\
 0 & 0 & 0 & 0 & 0 & 0 & 0 & -254757 & 509514 & 0 \\
 0 & 0 & 0 & 0 & 0 & 0 & 0 & 0 & -254757 & 0 \\
 0 & 0 & 0 & 0 & 0 & 0 & 0 & 0 & 0 & 0 \\
 0 & 0 & 0 & 0 & 0 & 0 & 0 & 0 & 0 & 0 \\
 0 & 0 & 0 & 0 & 0 & 0 & 0 & 0 & 0 & 0 \\
 -7767718 & 7767718 & 0 & 0 & 0 & 0 & 0 & 0 & 0 & 0 \\
 0 & 0 & 0 & 0 & 0 & 0 & 0 & 0 & 0 & 0 \\
 0 & 0 & 0 & 0 & 0 & 0 & 0 & 0 & 0 & 0 \\
 0 & 0 & 0 & 0 & 0 & 0 & 0 & 0 & 0 & 0 \\
 0 & 0 & 0 & 0 & 0 & 0 & 0 & 0 & 0 & 0 \\
 0 & 0 & 0 & 0 & 0 & 0 & 0 & 0 & 0 & 0 \\
 \dots & -254757 & 0 & 0 & 0 & 0 & 0 & 0 & 0 & 0 \\
 509514 & -254757 & 0 & 0 & 0 & 0 & 0 & 0 & 0 & 0 \\
 -254757 & 509514 & -254757 & 0 & 0 & 0 & 0 & 0 & 0 & 0 \\
 0 & -254757 & 254757 & 0 & 0 & 0 & 0 & 0 & 0 & 0 \\
 0 & 0 & 0 & 477765000 & -268219000 & 0 & 0 & 0 & 0 & 0 \\
 0 & 0 & 0 & -268219000 & 792772701 & -268219000 & 0 & 0 & 0 & 0 \\
 0 & 0 & 0 & 0 & -268219000 & 536438000 & -268219000 & 0 & 0 & 0 \\
 0 & 0 & 0 & 0 & 0 & -268219000 & 536438000 & -268219000 & 0 & 0 \\
 0 & 0 & 0 & 0 & 0 & 0 & -268219000 & 536438000 & -268219000 & -268219000 \\
 0 & 0 & 0 & 0 & 0 & 0 & 0 & -268219000 & 268219000 & 268219000
 \end{bmatrix} \quad (6.44)$$

The frequencies corresponding to the periods of vibration of the original structure are

1. Transverse/Torsional Rocking 1.75Hz
2. Longitudinal Rocking 2.78Hz

The stiffness values above were selected to yield a structure with similar longitudinal and transverse-torsional fundamental periods. The periods obtained from an undamped modal analysis and the associated mode descriptor are presented in the following Table 6.10, where “XT-n” represents the nth transverse-torsional mode, “Y-n” represents the nth longitudinal mode

and “X-n” the nth transverse mode. The first two fundamental transverse-torsional and longitudinal mode frequencies, XT-1 and L-1 respectively correspond well to those identified in the original structure.

Table 6.10. 18 DOF structure modal analysis results

Mode No.	Model Structure (Fixed Base)		Original Structure
	Frequency (Hz)	Mode Description	Frequency (Hz)
1	1.79	XT-1	1.75
2	2.74	L-1	2.78
3	2.97	XT-2	
4	6.99	XT-3	
5	8.19	XT-4	
6	8.26	L-2	
7	11.59	XT-5	
8	13.02	XT-6	
9	13.52	L-3	
10	15.59	XT-7	
11	17.56	XT-8	
12	17.94	L-4	
13	18.62	XT-9	
14	20.71	XT-10	
15	21.04	L-5	
16	22.60	XT-11	
17	22.64	L-6	
18	30.74	XT-12	

The damping inherent in the structure was assumed to be approximately 2% in first two modes. The mass and stiffness proportional factors respectively α and β were set at

$$\alpha=0.34$$

$$\beta=0.001 \quad (6.45)$$

to provide this nominal level of damping. The chosen coefficients yield 2% of critical damping at 2.0 Hz and at 4.4Hz with minimum damping of 1.84% at 2.9Hz, corresponding to the third mode, XT-2. Above 4.4Hz the inherent damping level rises steadily to 9.7% at 30.7 Hz corresponding to the highest mode.

For the assessment it was opted to compare results incorporating the first 2, 4, 8 and the full 18 modes in the modal combination.

The excitation was chosen to be the well known Imperial Valley El Centro record with N00E acting in the transverse (X) direction and the S90W record acting in the longitudinal (Y) direction. No vertical excitation was incorporated into the analysis.

The Q matrix was chosen to have the mass and stiffness matrices on the main diagonal such that the first term in the LQ performance index (Equation 5.6) corresponds to the sum of potential and kinetic energy. The R matrix was set to the identity matrix multiplied by a factor (R_{factor}). This single variable was used to provide a means of adjusting the level of control.

Although it has not been highlighted in previous discussion, one of the key features of casting the design problem into the structural control form is that the strength of the control can be adjusted with a single parameter, in this case R_{factor} , rather than dealing individually with potentially dozens of dampers. The control problem formulation considers the dynamic characteristics of the structure awhile the RSA analysis considers the effect of the excitation on each of the individual dampers. Therefore the procedure transforms the design problem in to one that is much easier to handle.

The designer still has to determine which damper locations are both reasonable and practical. To make this choice requires the knowledge of the architecture and function of the structure and the occupants, present and future.

Three damper configurations were chosen.

Configuration 1: comprises 23 dampers in total: one in one bay in each of all four sides from the base to the top. (See Figure 6.15)

Configuration 2: has 3 dampers in total at the base, two acting in the longitudinal direction and one acting between the base and the second story at the open end of the structure. (See Figure 6.16)

Configuration 3: uses 17 dampers in total: one in each bay of each end acting in the transverse direction (11) and one in one bay per story on one side only of the structure acting in the longitudinal direction (6). (See Figure 6.17)

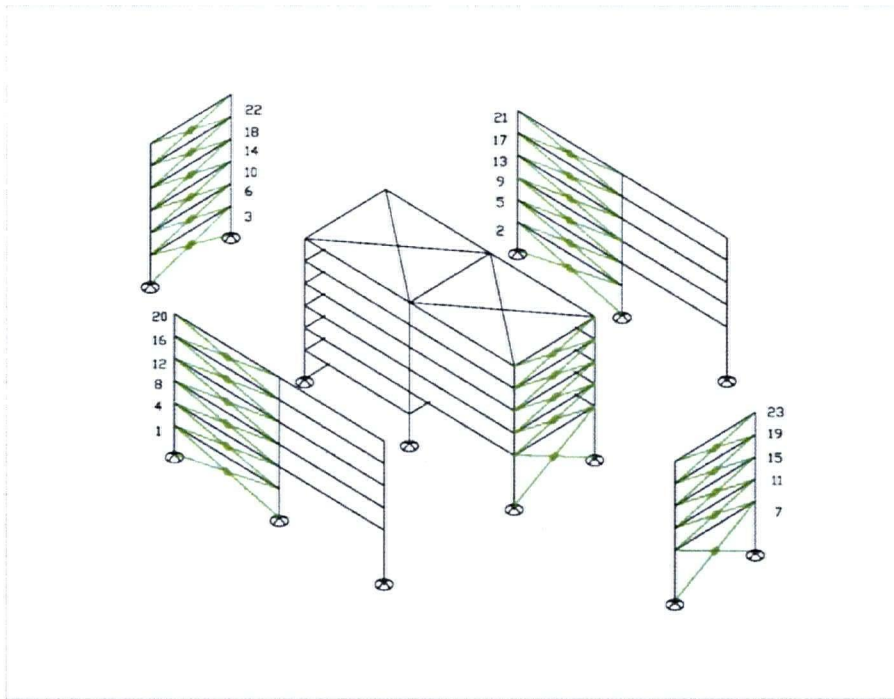


Figure 6.15. Damper Configuration 1 (23 dampers). The numbers identify the damper order in the observer matrix and the output.

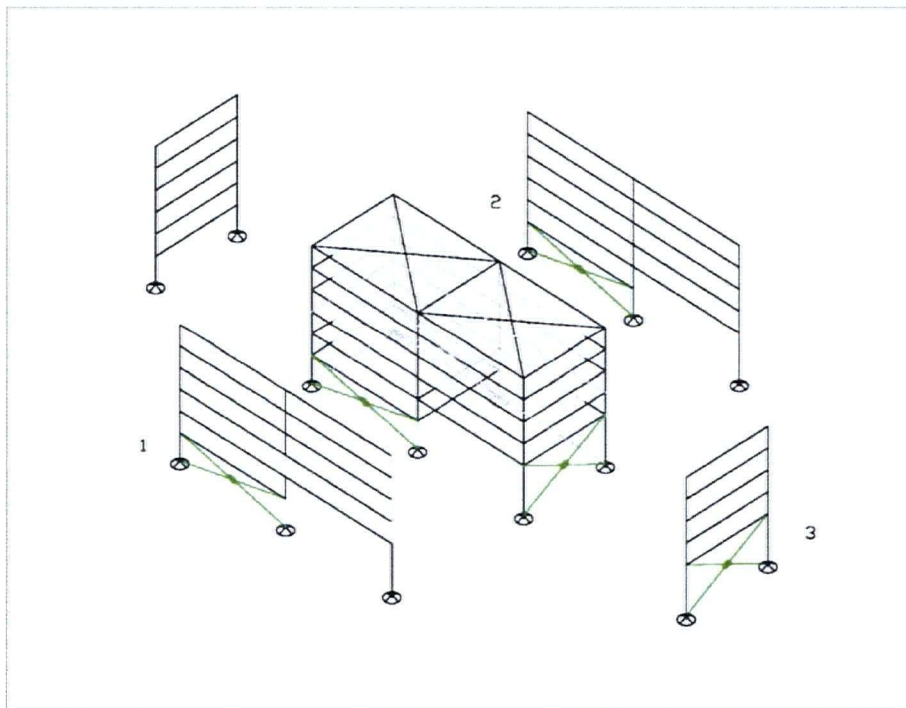


Figure 6.16. Damper Configuration 2 (3 dampers). The numbers identify the damper order in the observer matrix and the output.

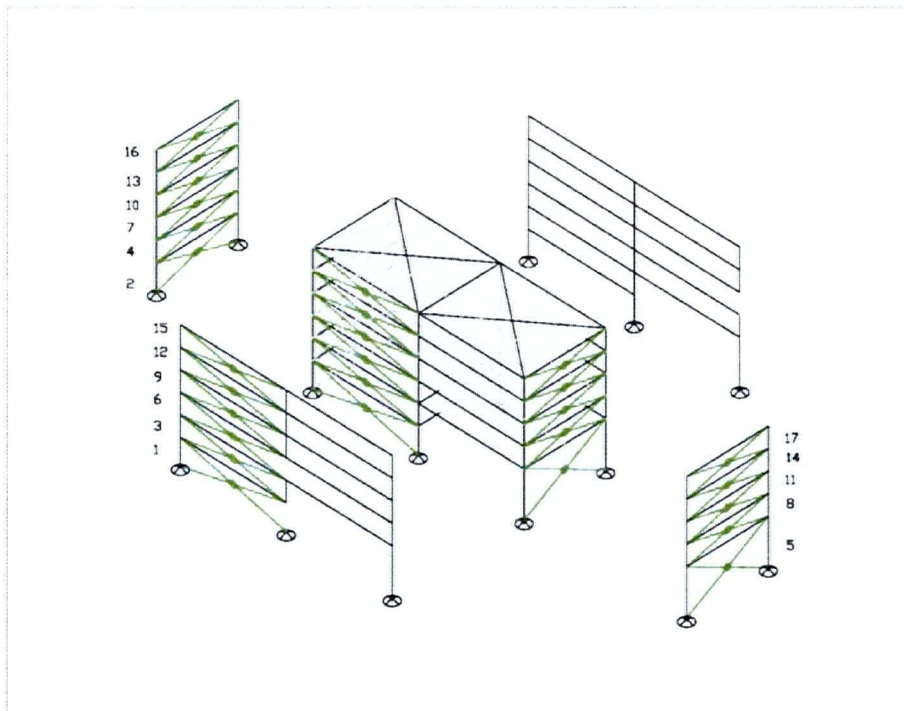


Figure 6.17. Damper Configuration 3 (17 dampers). The numbers identify the damper order in the observer matrix and the output.

6.3.1.1 Configuration 1

Configuration 1, illustrated in Figure 6.15, was chosen as a likely first-choice damping scenario. This configuration has a drawback in that it requires a large number of dampers. In a retrofit situation, each damper installation would bear not only direct construction costs associated with supply and installation of the dampers themselves including removal and reconstruction of architectural finishes, but also indirect costs associated with disruption to existing tenants. Therefore it is understood that this large number of dampers is not necessarily the most cost effective choice in every structure.

Except for the first story there are 4 dampers per story, but only 3 degrees of freedom, therefore one of the dampers is redundant. The practical implication of this redundancy is that the 23×23 CC^T matrix is rank deficient due to linear dependence and cannot be inverted. Rather than to directly invert the CC^T matrix $C^{-1} = C^T(CC^T)^{-1}$, the Moore-Penrose pseudo-inverse was used. For systems that are not redundant, the Moore-Penrose pseudo-inverse coincides with the method derived for use here and provides an even distribution of damping.

6.3.1.2 Configuration 2

Configuration 2, illustrated in Figure 6.16, was chosen as an example of a minimal control strategy in which only 3 dampers are utilised. The dampers are kept in the lowest stories to minimise the direct and indirect construction costs. The savings that may be realized by this choice of system must be compared against the performance. Although Configuration 2 is a very inefficient implementation of the control, it was selected to illustrate how the solution will react to a set of dampers that cannot adequately reproduce the intended control action derived in terms of the full state gain matrix.

In a practical application, however, the acceptability of such a control system depends strongly on the level of damping necessary to achieve the performance requirements. If this system can be shown to meet all performance requirements, it would be advantageous due to the small number of locations in the structure affected.

6.3.1.3 Configuration 3

Configuration 3, illustrated in Figure 6.17, utilises a reduced number of dampers distributed along the height. This unsymmetrical distribution is one that may not be considered at first by a designer. However, because the number of dampers is reduced, it would provide significant cost savings. Providing that all performance objectives could be met it would be preferable to Configuration 1.

6.3.2 Formulation of the Control Problem: Observer Matrices

The different damper systems analysed were described by the observer (damper location) matrices for each chosen configuration. The right hand half (non-zero part) of the observer matrices, C_R are given as follows in imperial units:

Table 6.11 Damper configuration 1, comparison of response obtained with various levels of control

(a)

Rfactor=0.00005

Location-Direction	State Vector - (ft,rad)		
	Uncontrolled	Controlled	% U/C
1-X-disp	0.035	0.013	
2-X-disp	0.152	0.030	
3-X-disp	0.172	0.037	
4-X-disp	0.187	0.042	
5-X-disp	0.197	0.047	
6-X-disp	0.201	0.049	24%
1-Y-disp	0.027	0.013	
2-Y-disp	0.048	0.023	
3-Y-disp	0.065	0.031	
4-Y-disp	0.079	0.037	
5-Y-disp	0.088	0.042	
6-Y-disp	0.093	0.044	47%
1-R-disp	0.002	0.000	
2-R-disp	0.003	0.001	
3-R-disp	0.004	0.001	
4-R-disp	0.004	0.001	
5-R-disp	0.004	0.001	
6-R-disp	0.005	0.001	27%
1-X-vel	0.438	0.251	
2-X-vel	1.645	0.480	
3-X-vel	1.869	0.598	
4-X-vel	2.044	0.705	
5-X-vel	2.164	0.784	
6-X-vel	2.221	0.824	
1-Y-vel	0.462	0.175	
2-Y-vel	0.802	0.305	
3-Y-vel	1.094	0.415	
4-Y-vel	1.325	0.502	
5-Y-vel	1.482	0.563	
6-Y-vel	1.555	0.592	
1-R-vel	0.018	0.006	
2-R-vel	0.032	0.011	
3-R-vel	0.039	0.015	
4-R-vel	0.045	0.017	
5-R-vel	0.049	0.019	
6-R-vel	0.052	0.020	

Rfactor=0.00005

Damper	Damper Horizontal Displacement (ft)		
	Uncontrolled	Controlled	% U/C
1	0.051	0.016	32%
2	0.051	0.016	32%
3	0.031	0.020	64%
4	0.039	0.013	32%
5	0.039	0.013	32%
6	0.025	0.015	60%
7	0.347	0.070	20%
8	0.024	0.010	41%
9	0.024	0.010	41%
10	0.038	0.021	56%
11	0.056	0.013	24%
12	0.019	0.010	51%
13	0.019	0.010	51%
14	0.032	0.022	69%
15	0.043	0.019	44%
16	0.013	0.006	44%
17	0.013	0.006	44%
18	0.023	0.013	55%
19	0.030	0.009	31%
20	0.007	0.004	60%
21	0.007	0.004	60%
22	0.012	0.009	77%
23	0.015	0.008	56%

(b)

Rfactor=0.0001

Location-Direction	State Vector - (ft,rad)		
	Uncontrolled	Controlled	% U/C
1-X-disp	0.035	0.012	
2-X-disp	0.152	0.038	
3-X-disp	0.172	0.044	
4-X-disp	0.187	0.048	
5-X-disp	0.197	0.052	
6-X-disp	0.201	0.053	26%
1-Y-disp	0.027	0.014	
2-Y-disp	0.048	0.025	
3-Y-disp	0.065	0.034	
4-Y-disp	0.079	0.041	
5-Y-disp	0.088	0.046	
6-Y-disp	0.093	0.048	52%
1-R-disp	0.002	0.001	
2-R-disp	0.003	0.001	
3-R-disp	0.004	0.001	
4-R-disp	0.004	0.001	
5-R-disp	0.004	0.001	
6-R-disp	0.005	0.001	31%
1-X-vel	0.438	0.237	
2-X-vel	1.645	0.524	
3-X-vel	1.869	0.627	
4-X-vel	2.044	0.718	
5-X-vel	2.164	0.788	
6-X-vel	2.221	0.823	
1-Y-vel	0.462	0.177	
2-Y-vel	0.802	0.308	
3-Y-vel	1.094	0.420	
4-Y-vel	1.325	0.508	
5-Y-vel	1.482	0.570	
6-Y-vel	1.555	0.599	
1-R-vel	0.018	0.007	
2-R-vel	0.032	0.012	
3-R-vel	0.039	0.015	
4-R-vel	0.045	0.018	
5-R-vel	0.049	0.020	
6-R-vel	0.052	0.021	

Rfactor=0.0001

Damper	Damper Horizontal Displacement (ft)		
	Uncontrolled	Controlled	% U/C
1	0.051	0.019	37%
2	0.051	0.019	37%
3	0.031	0.019	59%
4	0.039	0.014	37%
5	0.039	0.014	37%
6	0.025	0.014	56%
7	0.347	0.091	26%
8	0.024	0.011	46%
9	0.024	0.011	46%
10	0.038	0.020	54%
11	0.056	0.017	31%
12	0.019	0.010	51%
13	0.019	0.010	51%
14	0.032	0.019	61%
15	0.043	0.017	40%
16	0.013	0.006	47%
17	0.013	0.006	47%
18	0.023	0.013	55%
19	0.030	0.010	34%
20	0.007	0.003	49%
21	0.007	0.003	49%
22	0.012	0.007	55%
23	0.015	0.006	37%

Table 6.11 (continued)

(c)

Rfactor=0.0002

Location-Direction	State Vector - (ft.rad)		
	Uncontrolled	Controlled	% U/C
1-X-disp	0.035	0.013	
2-X-disp	0.152	0.047	
3-X-disp	0.172	0.053	
4-X-disp	0.187	0.058	
5-X-disp	0.197	0.061	
6-X-disp	0.201	0.063	31%
1-Y-disp	0.027	0.015	
2-Y-disp	0.048	0.027	
3-Y-disp	0.065	0.036	
4-Y-disp	0.079	0.044	
5-Y-disp	0.088	0.049	
6-Y-disp	0.093	0.052	56%
1-R-disp	0.002	0.001	
2-R-disp	0.003	0.001	
3-R-disp	0.004	0.001	
4-R-disp	0.004	0.001	
5-R-disp	0.004	0.002	
6-R-disp	0.005	0.002	36%
1-X-vel	0.438	0.231	
2-X-vel	1.645	0.561	
3-X-vel	1.869	0.661	
4-X-vel	2.044	0.748	
5-X-vel	2.164	0.814	
6-X-vel	2.221	0.847	
1-Y-vel	0.462	0.179	
2-Y-vel	0.802	0.312	
3-Y-vel	1.094	0.425	
4-Y-vel	1.325	0.515	
5-Y-vel	1.482	0.576	
6-Y-vel	1.555	0.606	
1-R-vel	0.018	0.007	
2-R-vel	0.032	0.012	
3-R-vel	0.039	0.015	
4-R-vel	0.045	0.018	
5-R-vel	0.049	0.021	
6-R-vel	0.052	0.022	

Rfactor=0.0002

Damper	Damper Horizontal Displacement (ft)		
	Uncontrolled	Controlled	% U/C
1	0.051	0.021	41%
2	0.051	0.021	41%
3	0.031	0.018	56%
4	0.039	0.016	41%
5	0.039	0.016	41%
6	0.025	0.013	53%
7	0.347	0.110	32%
8	0.024	0.012	50%
9	0.024	0.012	50%
10	0.038	0.021	54%
11	0.056	0.020	36%
12	0.019	0.010	51%
13	0.019	0.010	51%
14	0.032	0.018	56%
15	0.043	0.017	38%
16	0.013	0.007	51%
17	0.013	0.007	51%
18	0.023	0.013	57%
19	0.030	0.011	39%
20	0.007	0.003	51%
21	0.007	0.003	51%
22	0.012	0.007	55%
23	0.015	0.006	39%

(d)

Rfactor=0.0004

Location-Direction	State Vector - (ft.rad)		
	Uncontrolled	Controlled	% U/C
1-X-disp	0.035	0.014	
2-X-disp	0.152	0.056	
3-X-disp	0.172	0.063	
4-X-disp	0.187	0.069	
5-X-disp	0.197	0.073	
6-X-disp	0.201	0.075	37%
1-Y-disp	0.027	0.016	
2-Y-disp	0.048	0.028	
3-Y-disp	0.065	0.039	
4-Y-disp	0.079	0.047	
5-Y-disp	0.088	0.053	
6-Y-disp	0.093	0.055	60%
1-R-disp	0.002	0.001	
2-R-disp	0.003	0.001	
3-R-disp	0.004	0.001	
4-R-disp	0.004	0.002	
5-R-disp	0.004	0.002	
6-R-disp	0.005	0.002	40%
1-X-vel	0.438	0.231	
2-X-vel	1.645	0.599	
3-X-vel	1.869	0.700	
4-X-vel	2.044	0.786	
5-X-vel	2.164	0.850	
6-X-vel	2.221	0.883	
1-Y-vel	0.462	0.207	
2-Y-vel	0.802	0.359	
3-Y-vel	1.094	0.490	
4-Y-vel	1.325	0.593	
5-Y-vel	1.482	0.663	
6-Y-vel	1.555	0.696	
1-R-vel	0.018	0.007	
2-R-vel	0.032	0.012	
3-R-vel	0.039	0.016	
4-R-vel	0.045	0.019	
5-R-vel	0.049	0.021	
6-R-vel	0.052	0.023	

Rfactor=0.0004

Damper	Damper Horizontal Displacement (ft)		
	Uncontrolled	Controlled	% U/C
1	0.051	0.023	46%
2	0.051	0.023	46%
3	0.031	0.018	56%
4	0.039	0.018	45%
5	0.039	0.018	45%
6	0.025	0.013	54%
7	0.347	0.130	37%
8	0.024	0.013	54%
9	0.024	0.013	54%
10	0.038	0.022	57%
11	0.056	0.023	40%
12	0.019	0.010	54%
13	0.019	0.010	54%
14	0.032	0.018	57%
15	0.043	0.018	41%
16	0.013	0.007	55%
17	0.013	0.007	55%
18	0.023	0.013	58%
19	0.030	0.013	42%
20	0.007	0.004	54%
21	0.007	0.004	54%
22	0.012	0.007	58%
23	0.015	0.006	43%

Table 6.11 (a) (b) (c) and (d) contain summary tables for the expected response and the brace slip/yield force estimated for all 23 dampers of Configuration 1. Control levels corresponding to $R_{factor} = 0.00005, 0.0001, 0.0002$ and 0.0004 . Using $R_{factor} = 0.00005$ led to a reduction of peak displacement under the given earthquake to 24% transverse, 47% longitudinal and 27% torsional compared to the uncontrolled case. Displacements observed at the damper locations ranged from 20% to 77% of displacements observed without control. The weakest control attempted with $R_{factor} = 0.0004$ yielded peak reductions to 37% transverse, 60% longitudinal and 40% torsional compared to the uncontrolled case. Observed displacements ranged from 37% to 58% of valued observed without control.

In general it was observed that elements of the state vector are attenuated to a higher degree with lower values of R_{factor} . This is evident by comparing the displacements and velocities at the top stories. The observed displacements observed by the dampers, however do not follow this trend. Larger drifts are observed in the upper stories with the highest level of control.

The controlled and uncontrolled poles found during the initial analysis are plotted in Figure 6.18 with R_{factor} values ranging from 0.00005 to 0.0004 for comparison. Because a design spectrum has not been established, the modes were combined based on the spectral values established directly from the input time histories. Response quantities were then established by SRSS modal combination. With the stronger control, the poles the corresponding to the fundamental modes of vibration shift further from the origin indicating that higher damping is resulting from the introduction of the control.

Subsequently, the observed SRSS envelope velocities and control forces were established and the ratio of corresponding quantities used to establish the viscous damping coefficients. Figure 6.19 shows the distribution of the viscous dampers for Configuration 1. The damping coefficient is indicated both numerically and graphically through the line weight of the damper and the diameter of the circle. In general it was observed that the larger dampers were found near the base and in the large open bay at the end of the building. The distribution of dampers in the longitudinal direction was found to be quite uniform with damping coefficients in the base stories of 2370 kip-s/ft increasing to 2860 kip-s/ft in the third story and then dropping to 1880 kip-s/ft in the top story. In the lateral direction the maximum values were found in the second and third stories, 2380 kip-s/ft and 2680 kip-s/ft dropping to 1250 kip-s/ft and 1370 kip-s/ft at the top story.

6.3.3.2 Configuration 1 Damper Stiffness and Friction Damper Slip Loads

For Configuration 1, Figure 6.20 illustrates the ideal (infinitely stiff brace slip loads determined for the structure corresponding to the damper distribution shown in Figure 6.19. As in the first part of Example 1, the braces were assumed to be stiff, and the slip or yield force of the corresponding friction damper was set at $\pi/4$ of the peak control force. The distributions of slip loads showed a variation much greater than that of the viscous damping coefficients. The slip load at the base in the longitudinal direction was 404 kips dropping to 81 kips in the top story. In the transverse direction at the end without the open bay the slip load at the base was found to be 436 kips dropping to 142 kips at the top story. The open bay requires a significantly higher slip load than any other bay in the structure with a slip load of 974 kips. The story above, the third story had a slip load of 471 kips and above that the slip loads diminish to 133 kips at the top.

The influence of the brace stiffness is an important consideration that was discussed in Chapter 5. As derived in Chapter 5, the friction damper slip loads in each of the proposed dampers can be evaluated by matching the peak cycle energy dissipation of the viscous and the friction/hysteretic damper. In doing so, the stiffness attributed to the brace, including the brace stiffness, connection stiffness and accounting for any unwanted compliance of the bracing system, needs to be accounted for.

The energy balance leads to the expression for friction slip load, F_f

$$F_f = \frac{K_h d}{2} \left(1 - \sqrt{1 - \frac{\pi F_v}{K_h d}} \right) \quad (6.50)$$

where F_f is the slip load, $F_v = u_{max}$ is the max control (damper) force and $d = d_{max}$ is the story drift that the damper is subjected to. The variables F_f and F_v , due to the way in which the model has been set up, respectively represent the horizontal components of the friction and viscous damper force for the peak cycle. The variable K_h represents the horizontal stiffness of the brace and d represents the horizontal displacement corresponding to the peak cycle. In the limit as the value of K_h approaches infinity, F_f approaches $\frac{\pi F_v}{4}$, consistent with previous assumptions.

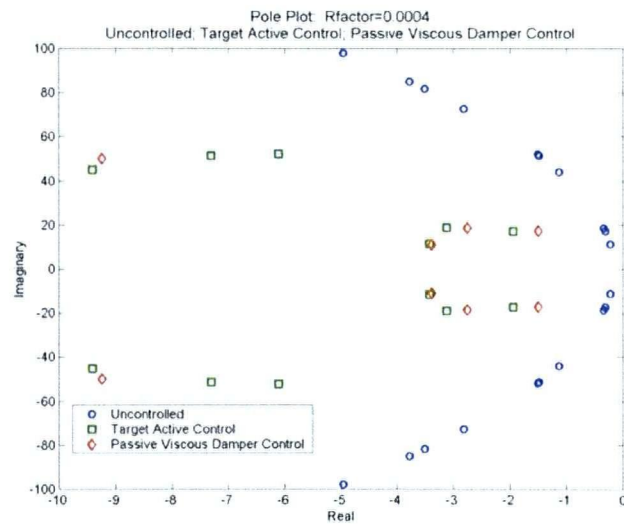
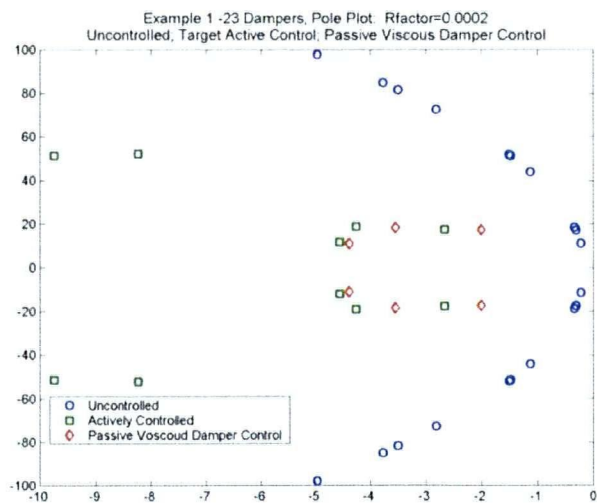
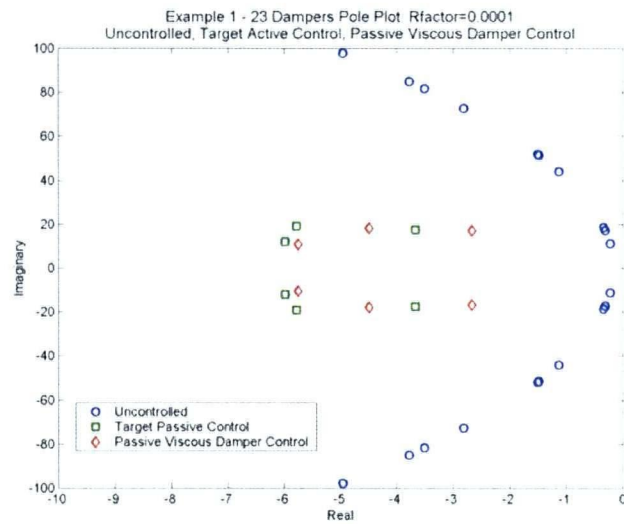
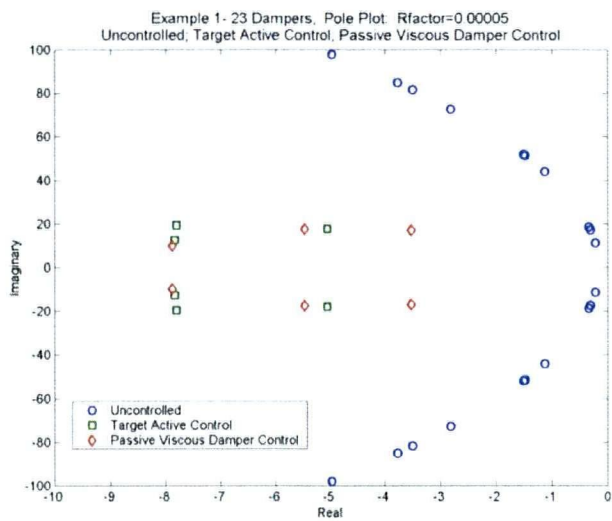


Figure 6.18. Comparison of Pole Locations – 4 different control strengths.

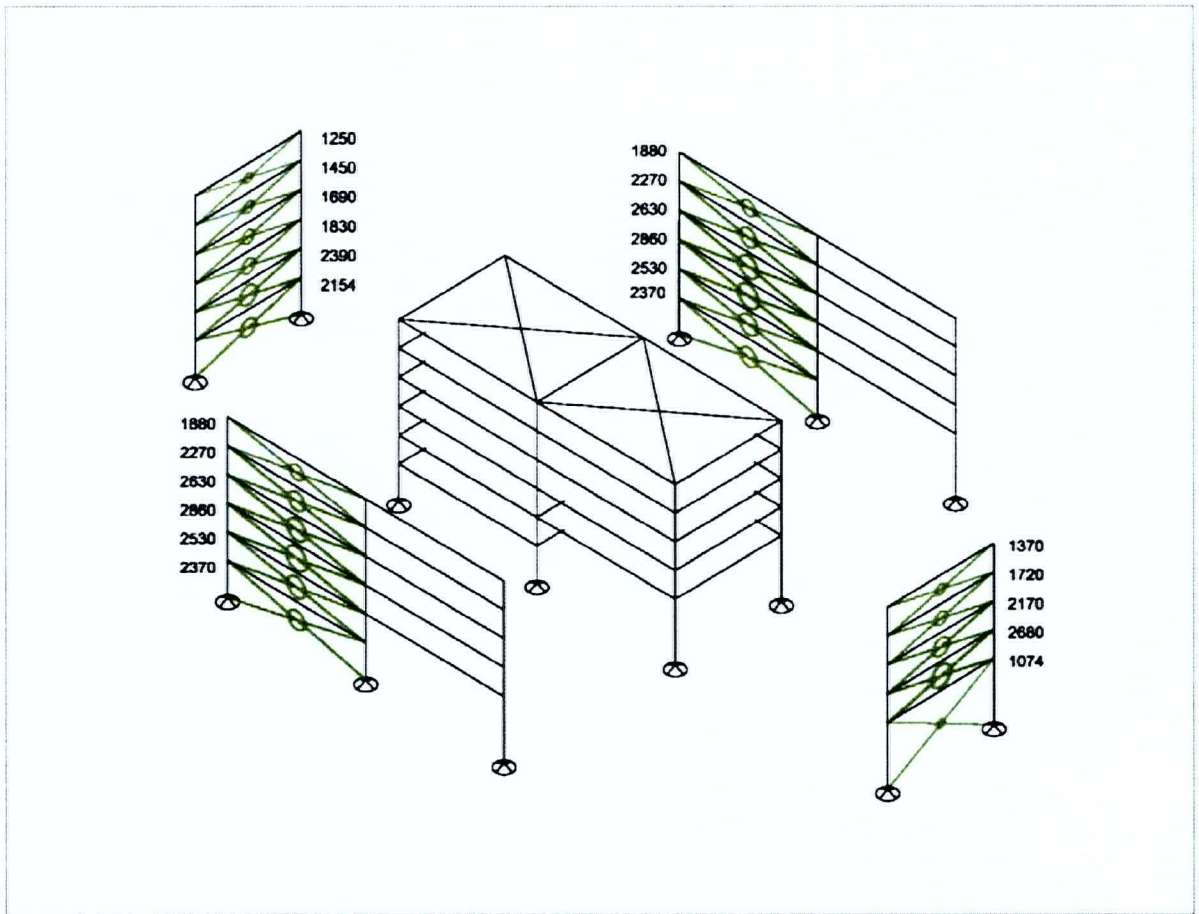


Figure 6.19. Configuration 1 viscous damping coefficients in kip-sec/ft corresponding to Rfactor = 0.00005.

For a value to exist, however, K_h must be greater than or equal to the quantity $\frac{\pi F_v}{d}$. If

$$K_h = \frac{\pi F_v}{d} \text{ then this implies that } F_f = \frac{\pi F_v}{2}.$$

These later expressions are important as they provides an upper limit to the slip force corresponding lower limit on the brace stiffness. The following Figure 6.21 relates the friction slip force to the brace stiffness ratio.

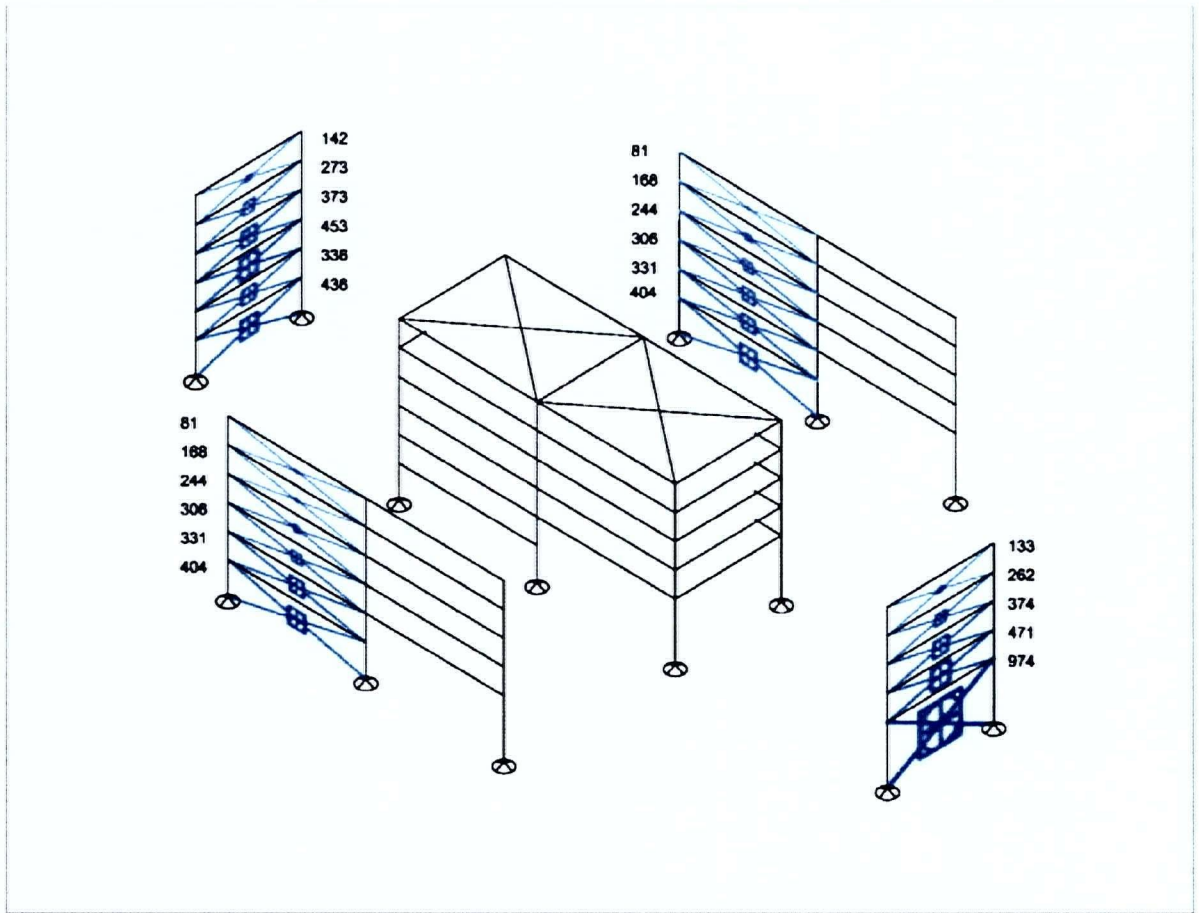


Figure 6.20. Configuration 1: ideal friction damper slip loads in kips for $R_{factor}=0.00005$.

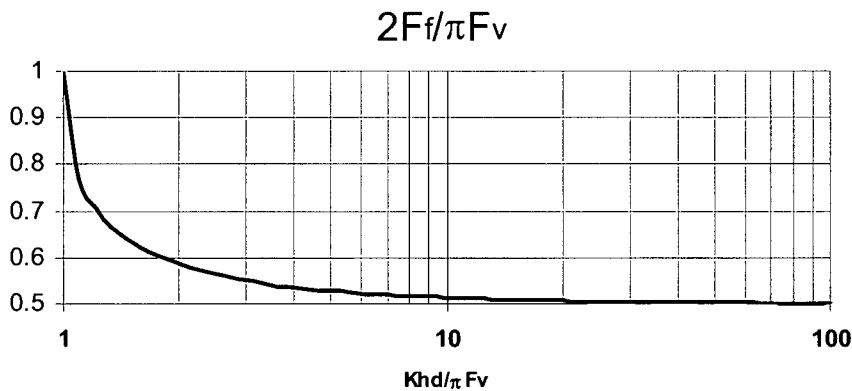


Figure 6.21. Variation of slip force with brace stiffness.

In interpreting the above chart it is necessary to keep in mind that, although the level of viscous damping is dependant on the structure parameters (and the desired control strength), the suitability of the friction damper depends on the magnitude of the excitation. If the earthquake is smaller by half, then the value of F_v is expected to be smaller by half and d is expected to be smaller by half. Therefore, the brace stiffness ratio along the x-axis would remain the same, however, the slip/yield load would be higher than desired by a factor of 2. Similarly, if the earthquake excitation were larger by a factor of 2, the slip/yield load would be half of the desired level. Fortunately, experience has shown that particularly for stiffly braced structures, the response is relatively insensitive to a slip/yield load that is too high while the structure would be more sensitive to a slip load that is too low and would fail to satisfy the desired design criteria. It is therefore desirable to be above the line in the figure and undesirable to fall below it.

In this example however it is noted that the deflections of the uncontrolled and particularly the controlled structures are quite small when compared to the story height, indicating that very stiff bracing will be required to achieve the target control. Assuming initially that two long shallowly sloped diagonal braces will be inserted in the frame in each of the indicated bays, the above equations can be used to establish the minimum brace areas assuming steel and the minimum slip loads associated with chosen brace cross-sectional areas.

Table 6.12 (a) to (d) contains the detailed computation of the brace dimensions for each level of control. It is assumed that in all bays shown, rather than using X-braces, greater efficiency could be realised by using chevron braces. Brace lengths and angles are computed based on this assumption. No allowance has been made for mechanical slop in connections. With the

strongest control, the combination of high control forces, up to 600kips, and small displacements resulted in the need for very stiff braces. Minimum cross sectional areas assumed to be steel ranged from 36 to 83 square inches in all bays. For the sake of the assessment an axial brace stiffness corresponding to a cross-sectional area of 100 square inches was selected. The horizontal force required at the open end is 1240 kips assumed to be carried by two braces.

Table 6.12. Configuration 1 comparison of friction damper design considering brace flexibility.

(a)

Rfactor=0.00005

Damper	Hcomp Fv tot (kip)	Hcomp d (ft)	Brace L= (ft)	Brace Angle (rad)	Number of Braces	Hcomp Fv/brace (kip)	Min As= (in ²)	Choose As= (in ²)	Hcomp Kh= (kip/ft)	Hcomp Ff= (kip)	Hcomp Ff/Fv	Brace Ff (kip)	Brace Stress (ksi)
1	515	0.016	36.7	0.451	2	257	75	100	66232	269	1.047	299	3.0
2	515	0.016	36.7	0.451	2	257	75	100	66232	269	1.047	299	3.0
3	556	0.020	30.1	0.560	2	278	60	100	71504	268	0.964	316	3.2
4	421	0.013	35.3	0.362	2	211	71	100	74347	215	1.022	230	2.3
5	421	0.013	35.3	0.362	2	211	71	100	74347	215	1.022	230	2.3
6	428	0.015	28.4	0.362	2	214	50	100	92383	197	0.918	210	2.1
7	1240	0.070	38.2	0.841	2	620	80	100	34879	670	1.081	1005	10.1
8	390	0.010	35.3	0.362	2	195	82	100	74347	216	1.107	231	2.3
9	390	0.010	35.3	0.362	2	195	82	100	74347	216	1.107	231	2.3
10	577	0.021	28.4	0.456	2	288	50	100	85172	265	0.919	295	3.0
11	600	0.013	28.4	0.456	2	300	83	100	85172	333	1.108	370	3.7
12	311	0.010	35.3	0.362	2	156	67	100	74347	155	0.998	166	1.7
13	311	0.010	35.3	0.362	2	156	67	100	74347	155	0.998	166	1.7
14	475	0.022	28.4	0.456	2	237	40	100	85172	210	0.886	234	2.3
15	476	0.019	28.4	0.456	2	238	46	100	85172	216	0.906	240	2.4
16	214	0.006	35.3	0.362	2	107	78	100	74347	115	1.069	122	1.2
17	214	0.006	35.3	0.362	2	107	78	100	74347	115	1.069	122	1.2
18	348	0.013	28.4	0.456	2	174	51	100	85172	161	0.924	179	1.8
19	334	0.009	28.4	0.456	2	167	67	100	85172	167	0.997	186	1.9
20	103	0.004	35.3	0.362	2	51	56	100	74347	48	0.943	52	0.5
21	103	0.004	35.3	0.362	2	51	56	100	74347	48	0.943	52	0.5
22	181	0.009	28.4	0.456	2	91	36	100	85172	79	0.874	88	0.9
23	169	0.008	28.4	0.456	2	84	38	100	85172	74	0.877	83	0.8

(b)

Rfactor=0.0001

Damper	Hcomp Fv tot (kip)	Hcomp d (ft)	Brace L= (ft)	Brace Angle (rad)	Number of Braces	Hcomp Fv/brace (kip)	Min As= (in ²)	Choose As= (in ²)	Hcomp Kh= (kip/ft)	Hcomp Ff= (kip)	Hcomp Ff/Fv	Brace Ff (kip)	Brace Stress (ksi)
1	408	0.016	36.7	0.451	2	204	59	90	59609	203	0.992	225	2.5
2	408	0.016	36.7	0.451	2	204	59	90	59609	203	0.992	225	2.5
3	403	0.020	30.1	0.560	2	202	44	90	64353	185	0.915	218	2.4
4	322	0.013	35.3	0.362	2	161	54	90	66912	155	0.965	166	1.8
5	322	0.013	35.3	0.362	2	161	54	90	66912	155	0.965	166	1.8
6	296	0.015	28.4	0.362	2	148	34	90	83144	130	0.879	139	1.5
7	1019	0.070	38.2	0.841	2	509	65	90	31391	525	1.031	788	8.8
8	299	0.010	35.3	0.362	2	150	63	90	66912	152	1.016	163	1.8
9	299	0.010	35.3	0.362	2	150	63	90	66912	152	1.016	163	1.8
10	461	0.021	28.4	0.534	2	231	43	90	70474	211	0.913	245	2.7
11	412	0.013	28.4	0.534	2	206	62	90	70474	207	1.006	241	2.7
12	239	0.010	35.3	0.362	2	120	52	90	66912	114	0.950	121	1.3
13	239	0.010	35.3	0.362	2	120	52	90	66912	114	0.950	121	1.3
14	379	0.022	28.4	0.534	2	190	35	90	70474	167	0.881	194	2.2
15	336	0.019	28.4	0.534	2	168	35	90	70474	148	0.883	172	1.9
16	166	0.006	35.3	0.362	2	83	60	90	66912	83	0.998	88	1.0
17	166	0.006	35.3	0.362	2	83	60	90	66912	83	0.998	88	1.0
18	282	0.013	28.4	0.534	2	141	45	90	70474	129	0.919	150	1.7
19	243	0.009	28.4	0.534	2	121	53	90	70474	116	0.957	135	1.5
20	80	0.004	35.3	0.362	2	40	43	90	66912	37	0.913	39	0.4
21	80	0.004	35.3	0.362	2	40	43	90	66912	37	0.913	39	0.4
22	149	0.009	28.4	0.534	2	74	32	90	70474	65	0.873	75	0.8
23	126	0.008	28.4	0.534	2	63	31	90	70474	55	0.867	64	0.7

Table 6.12. (continued)

(c)

Rfactor=0.0002

Damper	Hcomp Fv tot (kip)	Hcomp d (ft)	Brace L= (ft)	Brace Angle (rad)	Number of Braces -	Hcomp Fv/brace (kip)	Min As= (in ²)	Choose As= (in ²)	Hcomp Kh= (kip/ft)	Hcomp Ff= (kip)	Hcomp Ff/Fv -	Brace Ff (kip)	Brace Stress (ksi)
1	312	0.019	36.7	0.451	2	156	39	60	39739	154	0.990	172	2.9
2	312	0.019	36.7	0.451	2	156	39	60	39739	154	0.990	172	2.9
3	280	0.019	30.1	0.560	2	140	33	60	42902	132	0.941	156	2.6
4	240	0.014	35.3	0.362	2	120	35	60	44608	115	0.958	123	2.0
5	240	0.014	35.3	0.362	2	120	35	60	44608	115	0.958	123	2.0
6	201	0.014	28.4	0.362	2	101	25	60	55430	90	0.890	96	1.6
7	854	0.091	38.2	0.841	2	427	42	60	20927	434	1.017	651	10.9
8	223	0.011	35.3	0.362	2	112	42	60	44608	114	1.020	122	2.0
9	223	0.011	35.3	0.362	2	112	42	60	44608	114	1.020	122	2.0
10	362	0.020	28.4	0.534	2	181	36	60	46983	174	0.959	202	3.4
11	286	0.017	28.4	0.534	2	143	34	60	46983	135	0.944	157	2.6
12	179	0.010	35.3	0.362	2	89	39	60	44608	88	0.983	94	1.6
13	179	0.010	35.3	0.362	2	89	39	60	44608	88	0.983	94	1.6
14	296	0.019	28.4	0.534	2	148	31	60	46983	137	0.924	159	2.6
15	236	0.017	28.4	0.534	2	118	27	60	46983	106	0.903	124	2.1
16	124	0.006	35.3	0.362	2	62	42	60	44608	63	1.010	67	1.1
17	124	0.006	35.3	0.362	2	62	42	60	44608	63	1.010	67	1.1
18	217	0.013	28.4	0.534	2	109	35	60	46983	103	0.953	120	2.0
19	172	0.010	28.4	0.534	2	86	34	60	46983	82	0.949	95	1.6
20	60	0.003	35.3	0.362	2	30	40	60	44608	30	0.994	32	0.5
21	60	0.003	35.3	0.362	2	30	40	60	44608	30	0.994	32	0.5
22	114	0.007	28.4	0.534	2	57	35	60	46983	54	0.953	63	1.1
23	92	0.006	28.4	0.534	2	46	33	60	46983	43	0.943	50	0.8

(d)

Rfactor=0.0004

Damper	Hcomp Fv tot (kip)	Hcomp d (ft)	Brace L= (ft)	Brace Angle (rad)	Number of Braces -	Hcomp Fv/brace (kip)	Min As= (in ²)	Choose As= (in ²)	Hcomp Kh= (kip/ft)	Hcomp Ff= (kip)	Hcomp Ff/Fv -	Brace Ff (kip)	Brace Stress (ksi)
1	234	0.021	36.7	0.451	2	117	27	40	26493	117	0.995	130	3.2
2	234	0.021	36.7	0.451	2	117	27	40	26493	117	0.995	130	3.2
3	191	0.018	30.1	0.560	2	95	24	40	28602	91	0.959	108	2.7
4	178	0.016	35.3	0.362	2	89	24	40	29739	85	0.958	91	2.3
5	178	0.016	35.3	0.362	2	89	24	40	29739	85	0.958	91	2.3
6	136	0.013	28.4	0.362	2	68	18	40	36953	61	0.899	65	1.6
7	766	0.110	38.2	0.841	2	383	31	40	13951	411	1.072	616	15.4
8	163	0.012	35.3	0.362	2	82	29	40	29739	84	1.023	89	2.2
9	163	0.012	35.3	0.362	2	82	29	40	29739	84	1.023	89	2.2
10	274	0.021	28.4	0.534	2	137	27	40	31322	136	0.995	158	4.0
11	211	0.020	28.4	0.534	2	106	21	40	31322	99	0.934	115	2.9
12	131	0.010	35.3	0.362	2	65	28	40	29739	67	1.018	71	1.8
13	131	0.010	35.3	0.362	2	65	28	40	29739	67	1.018	71	1.8
14	223	0.018	28.4	0.534	2	112	25	40	31322	109	0.976	127	3.2
15	174	0.017	28.4	0.534	2	87	21	40	31322	81	0.931	94	2.3
16	91	0.007	35.3	0.362	2	45	28	40	29739	46	1.017	49	1.2
17	91	0.007	35.3	0.362	2	45	28	40	29739	46	1.017	49	1.2
18	162	0.013	28.4	0.534	2	81	25	40	31322	79	0.976	92	2.3
19	125	0.011	28.4	0.534	2	63	22	40	31322	59	0.941	68	1.7
20	44	0.003	35.3	0.362	2	22	28	40	29739	22	1.018	24	0.6
21	44	0.003	35.3	0.362	2	22	28	40	29739	22	1.018	24	0.6
22	84	0.007	28.4	0.534	2	42	26	40	31322	42	0.983	48	1.2
23	66	0.006	28.4	0.534	2	33	23	40	31322	31	0.950	37	0.9

Depending on the design criteria, one may conclude that the large cross sectional areas necessary to achieve the strongest level of control may be unworkable and opt for a lesser level of control.

6.3.4 Results: Configuration 2

6.3.4.1 Control Design

With the second damper configuration, the value of R_{factor} was adjusted until top story displacement was reduced to approximately the same performance level as with Configuration 1. Table 6.13 contains envelope estimates of the state vector and the story drifts for $R_{factor} = 0.000015$. The top story displacement in the transverse direction was computed to be 24% of that of the uncontrolled structure, 45% of that of the longitudinal deformation and 29% of that of the uncontrolled torsional displacement. This compares to 24%, 47% and 27% of the transverse torsional and longitudinal displacement of the top story of Configuration 1. While the overall performance appeared similar, the observed damper displacements were somewhat larger ranging from 37% to 69% of the uncontrolled displacements as compared to the 20% to 70% range for Configuration 1.

Viscous damping coefficients, illustrated in Figure 6.22 were 5490 kip-s/ft in the longitudinal direction and 1215 kip-s/ft in the open bay of the loading dock. The dampers in the longitudinal direction are about double of the largest found for Configuration 1. At the open end bay, the viscous damping coefficient compares favourably with the 1074 kip-s/ft determined in Configuration 1, larger by approximately 13%.

The friction damper slip loads determined are shown in Figure 6.23. The slip loads in the longitudinal direction were found to be 1819 kips, more than four times that determined in Configuration 1. In the open bay of the loading dock, the slip load was determined to be 1458 kips, approximately 50% larger than that determined for the same location in Configuration 1.

Following the same procedure as used in the previous example, properties of chevron bracing sufficient to activate the friction dampers was considered. The detailed calculation is contained in Table 6.14. It was determined that the minimum stiffness of the longitudinal braces corresponds to two steel members having cross-sectional area of 255 square inches. The minimum stiffness of the brace in the open end-bay was found to correspond to a two-member chevron brace having cross-sectional area of 91 square inches.

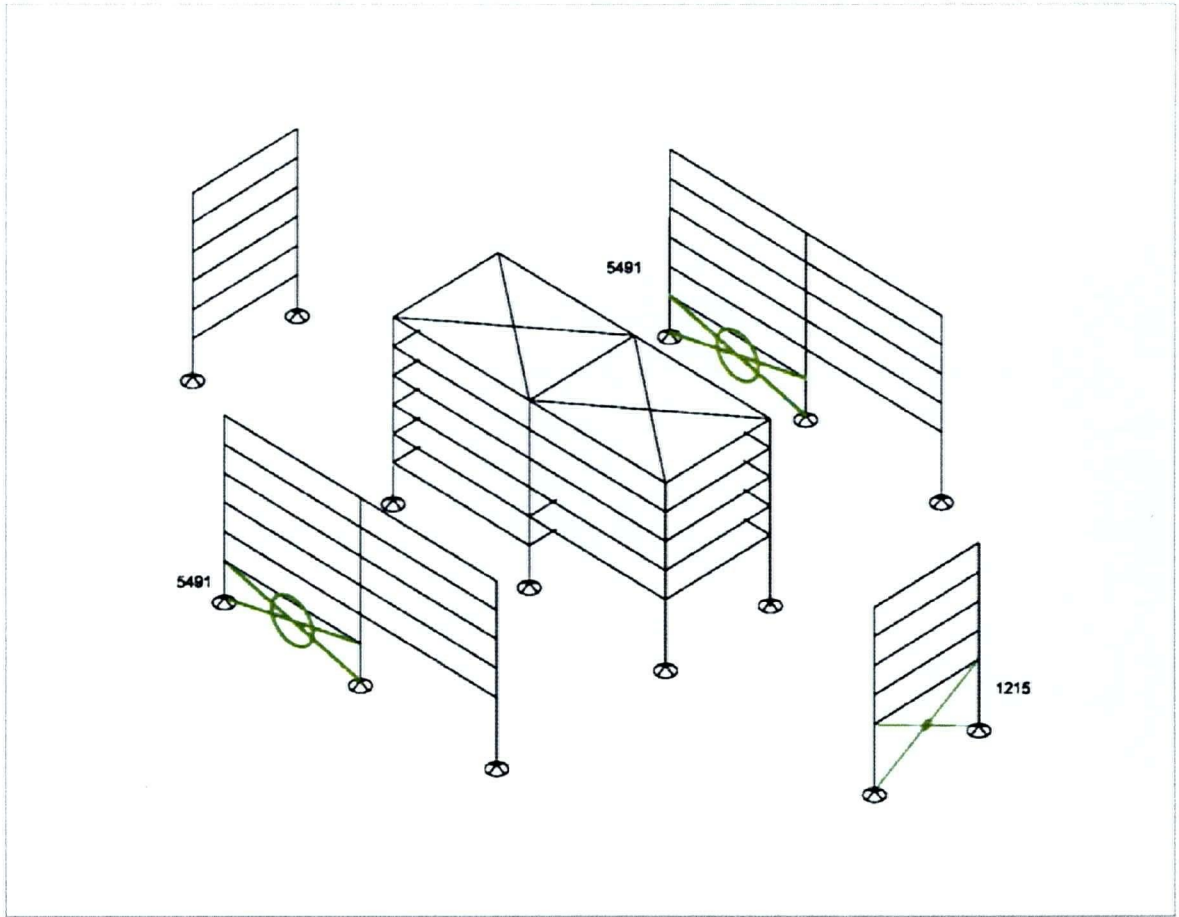


Figure 6.22. Configuration 2 viscous damping coefficients in kip-sec/ft for Rfactor = 0.000015.

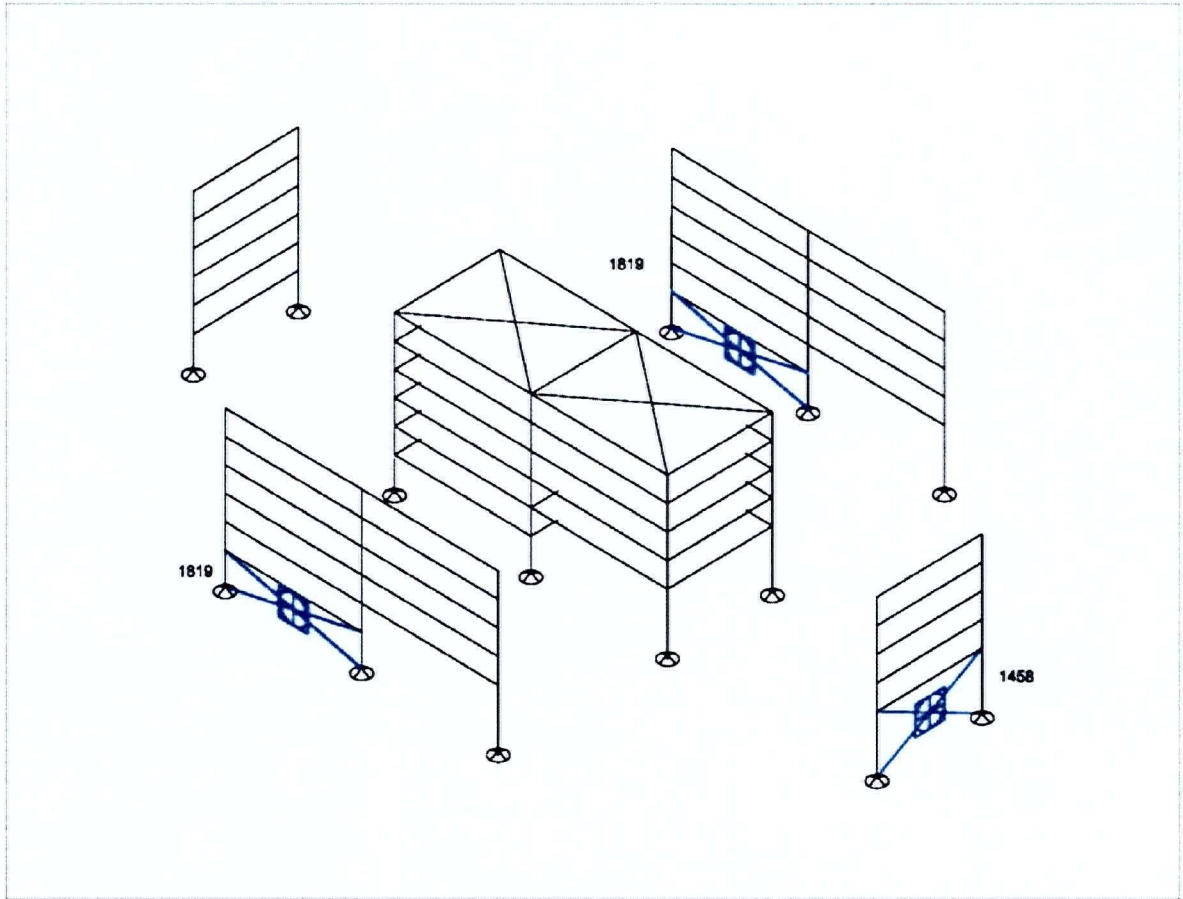


Figure 6.23. Configuration 2 – friction damping slip loads in kips for Rfactor=0.000015.

Table 6.13. Configuration 2 comparison of controlled and uncontrolled response with Rfactor=0.000015.

Rfactor=0.000015				Rfactor=0.000015			
Location-Direction	State Vector - (ft,rad)			Ext Wall Drift	Damper Horizontal Displacement (ft)		
	Uncontrolled	Controlled	% U/C		Uncontrolled	Controlled	% U/C
1-X-disp	0.035	0.013		1	0.051	0.022	42%
2-X-disp	0.152	0.039		2	0.051	0.022	42%
3-X-disp	0.172	0.042		3	0.031	0.022	70%
4-X-disp	0.187	0.045		4	0.039	0.014	37%
5-X-disp	0.197	0.048		5	0.039	0.014	37%
6-X-disp	0.201	0.050	25%	6	0.025	0.015	59%
1-Y-disp	0.027	0.017		7	0.347	0.091	26%
2-Y-disp	0.048	0.024		8	0.024	0.012	50%
3-Y-disp	0.065	0.031		9	0.024	0.012	50%
4-Y-disp	0.079	0.036		10	0.038	0.026	69%
5-Y-disp	0.088	0.040		11	0.056	0.024	44%
6-Y-disp	0.093	0.042	45%	12	0.019	0.010	51%
1-R-disp	0.002	0.001		13	0.019	0.010	51%
2-R-disp	0.003	0.001		14	0.032	0.022	69%
3-R-disp	0.004	0.001		15	0.043	0.019	44%
4-R-disp	0.004	0.001		16	0.013	0.007	52%
5-R-disp	0.004	0.001		17	0.013	0.007	52%
6-R-disp	0.005	0.001	29%	18	0.023	0.016	69%
1-X-vel	0.438	0.266		19	0.030	0.014	47%
2-X-vel	1.645	0.649		20	0.007	0.004	55%
3-X-vel	1.869	0.701		21	0.007	0.004	55%
4-X-vel	2.044	0.763		22	0.012	0.008	71%
5-X-vel	2.164	0.817		23	0.015	0.008	51%
6-X-vel	2.221	0.852					
1-Y-vel	0.462	0.275					
2-Y-vel	0.802	0.357					
3-Y-vel	1.094	0.445					
4-Y-vel	1.325	0.521					
5-Y-vel	1.482	0.582					
6-Y-vel	1.555	0.615					
1-R-vel	0.018	0.010					
2-R-vel	0.032	0.015					
3-R-vel	0.039	0.017					
4-R-vel	0.045	0.019					
5-R-vel	0.049	0.022					
6-R-vel	0.052	0.023					

Table 6.14. Configuration 2 comparison of friction damper design considering brace flexibility.

Rfactor=0.000015													
Damper	Hcomp Fv tot (kip)	Hcomp d (ft)	Brace L= (ft)	Brace Angle (rad)	Number of Braces	Hcomp Fv/brace (kip)	Min As= (in^2)	Choose As= (in^2)	Hcomp Kh= (kip/ft)	Hcomp Ff= (kip)	Hcomp Ff/Fv	Brace Ff (kip)	Brace Stresss (ksi)
1	2316	0.022	36.7	0.451	2	1158	255	300	198695	1310	1.131	1456	4.9
2	2316	0.022	36.7	0.451	2	1158	255	300	198695	1310	1.131	1456	4.9
3	1857	0.091	38.2	0.841	2	929	91	300	104636	795	0.857	1193	4.0

6.3.5 Results: Configuration 3

As with the design of the control with Configuration 1, the control design for the Configuration 3 damper arrangement proceeded with the selection of $R_{factor} = 0.00005$. Table 6.15 contains the envelope values obtained for the response of the state vector and the observed displacements of the dampers. The top story transverse, longitudinal torsional response was found to be 21%, 43% and 24%, compared to the 24%, 47% and 27% obtained for Configuration 1. The drifts in each of the bays were computed to range from 22% to 41%, with a few exceptions, comparable to that obtained for Configuration 1.

The viscous damping coefficients determined are shown in Figure 6.24. In the transverse direction viscous damping coefficients were found to be quite similar to those obtained with the full 23 dampers. In the longitudinal direction, the damping coefficients were found to be larger by approximately 33%.

Friction damping coefficients found for Configuration 3 are shown in Figure 6.25. Similar to the viscous damping coefficients, transverse direction slip loads agreed with those determined with Configuration 1 to within 5%. Slip loads in the longitudinal direction are higher by 52% at the base and varying to 37% higher at the top story when compared with Configuration 1 slip loads.

The calculation of brace slip loads including brace flexibility is shown in Table 6.16. As expected, the minimum brace stiffness in the transverse direction is similar to that of Configuration 1. In the longitudinal direction, however, the minimum brace stiffnesses was larger by 52% at the base to 36% at the top consistent with the increase in slip load.

6.3.6 Notes on Modal Combinations

Much of the modal superposition and response spectral analysis for this structure was done with a reduced number of modes. In this computation, the uncontrolled response to the El Centro N00E and S90W records were applied in the transverse and longitudinal directions, respectively. In Table 6.17 the magnitudes of the uncontrolled response envelopes are compared with 2, 4, 8 and the full 18 modes included in the analysis. The results indicate that including 8 out of 18 modes is able to reproduce the response to a high degree of accuracy. Displacements were computed with a slightly greater degree of precision than velocities.

Table 6.15. Configuration 2 comparison of controlled and uncontrolled response with Rfactor=0.000015.

Rfactor=0.00005

Location-Direction	State Vector - (ft,rad)		
	Uncontrolled	Controlled	% U/C
1-X-disp	0.035	0.009	
2-X-disp	0.152	0.032	
3-X-disp	0.172	0.036	
4-X-disp	0.187	0.039	
5-X-disp	0.197	0.042	
6-X-disp	0.201	0.043	21%
1-Y-disp	0.027	0.012	
2-Y-disp	0.048	0.021	
3-Y-disp	0.065	0.028	
4-Y-disp	0.079	0.034	
5-Y-disp	0.088	0.038	
6-Y-disp	0.093	0.040	43%
1-R-disp	0.002	0.000	
2-R-disp	0.003	0.001	
3-R-disp	0.004	0.001	
4-R-disp	0.004	0.001	
5-R-disp	0.004	0.001	
6-R-disp	0.005	0.001	24%
1-X-vel	0.438	0.181	
2-X-vel	1.645	0.487	
3-X-vel	1.869	0.548	
4-X-vel	2.044	0.601	
5-X-vel	2.164	0.646	
6-X-vel	2.221	0.673	
1-Y-vel	0.462	0.165	
2-Y-vel	0.802	0.285	
3-Y-vel	1.094	0.387	
4-Y-vel	1.325	0.467	
5-Y-vel	1.482	0.523	
6-Y-vel	1.555	0.549	
1-R-vel	0.018	0.006	
2-R-vel	0.032	0.011	
3-R-vel	0.039	0.013	
4-R-vel	0.045	0.015	
5-R-vel	0.049	0.017	
6-R-vel	0.052	0.018	

Rfactor=0.00005

Ext Wall Drift	Damper Horizontal Displacement (ft)		
	Uncontrolled	Controlled	% U/C
1	0.051	0.016	31%
2	0.051	0.015	30%
3	0.031	0.012	39%
4	0.039	0.012	31%
5	0.039	0.012	30%
6	0.025	0.009	37%
7	0.347	0.076	22%
8	0.024	0.009	36%
9	0.024	0.009	38%
10	0.038	0.015	40%
11	0.056	0.012	22%
12	0.019	0.007	36%
13	0.019	0.007	39%
14	0.032	0.013	40%
15	0.043	0.010	23%
16	0.013	0.005	37%
17	0.013	0.005	39%
18	0.023	0.009	41%
19	0.030	0.007	25%
20	0.007	0.002	37%
21	0.007	0.003	38%
22	0.012	0.005	41%
23	0.015	0.004	26%

Table 6.16. Configuration 3 comparison of friction damper design considering brace flexibility.

Rfactor=0.00005

Damper	Hcomp Fv tot (kip)	Hcomp d (ft)	Brace L= (ft)	Brace Angle (rad)	Number of Braces -	Hcomp Fv/brace (kip)	Min As= (in^2)	Choose As= (in^2)	Hcomp Kh= (kip/ft)	Hcomp Ff= (kip)	Hcomp Ff/Fv -	Brace Ff (kip)	Brace Stresss (ksi)
1	785	0.016	36.7	0.451	2	392	118	150	99348	421	1.074	468	3.1
2	574	0.012	30.1	0.560	2	287	104	150	107256	290	1.012	342	2.3
3	629	0.012	35.3	0.362	2	315	111	150	111521	327	1.039	350	2.3
4	441	0.009	28.4	0.456	2	220	88	100	85172	258	1.171	287	2.9
5	1247	0.076	38.2	0.841	2	623	74	100	34879	648	1.039	971	9.7
6	544	0.009	35.3	0.362	2	272	132	150	111521	317	1.167	339	2.3
7	605	0.015	28.4	0.456	2	303	73	100	85172	314	1.037	349	3.5
8	615	0.012	28.4	0.456	2	307	93	100	85172	382	1.241	425	4.3
9	433	0.007	35.3	0.362	2	217	131	150	111521	250	1.157	268	1.8
10	497	0.013	28.4	0.456	2	249	72	100	85172	256	1.028	285	2.8
11	490	0.010	28.4	0.456	2	245	89	100	85172	290	1.186	323	3.2
12	297	0.005	35.3	0.362	2	149	128	150	111521	169	1.137	181	1.2
13	364	0.009	28.4	0.460	2	182	72	100	84778	187	1.030	209	2.1
14	344	0.007	28.4	0.456	2	172	86	100	85172	196	1.141	219	2.2
15	140	0.002	35.3	0.362	2	70	124	150	111521	78	1.107	83	0.6
16	189	0.005	28.4	0.456	2	94	71	100	85172	96	1.021	107	1.1
17	174	0.004	28.4	0.456	2	87	82	100	85172	96	1.105	107	1.1

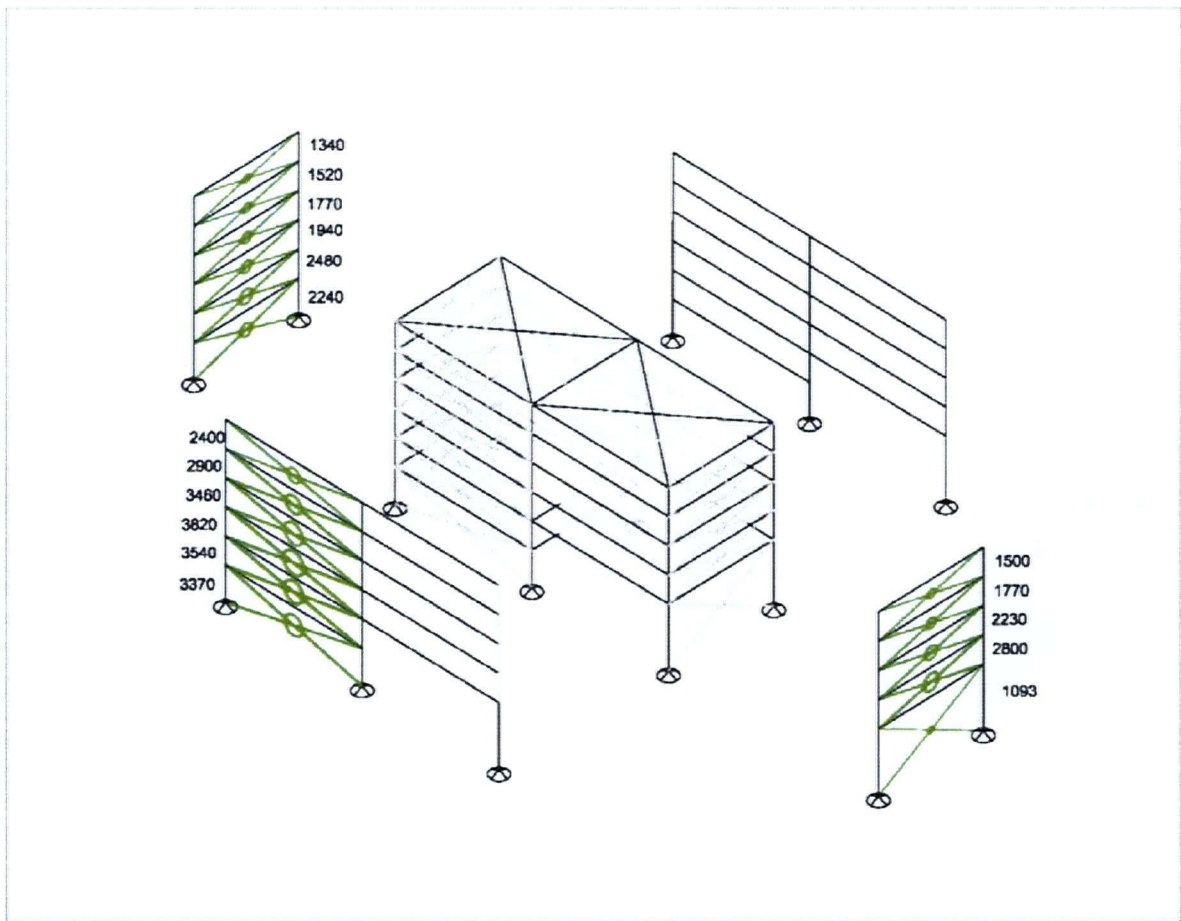


Figure 6.24. Configuration 3 viscous damping coefficients in kip-sec/ft for $R_{factor} = 0.00005$.

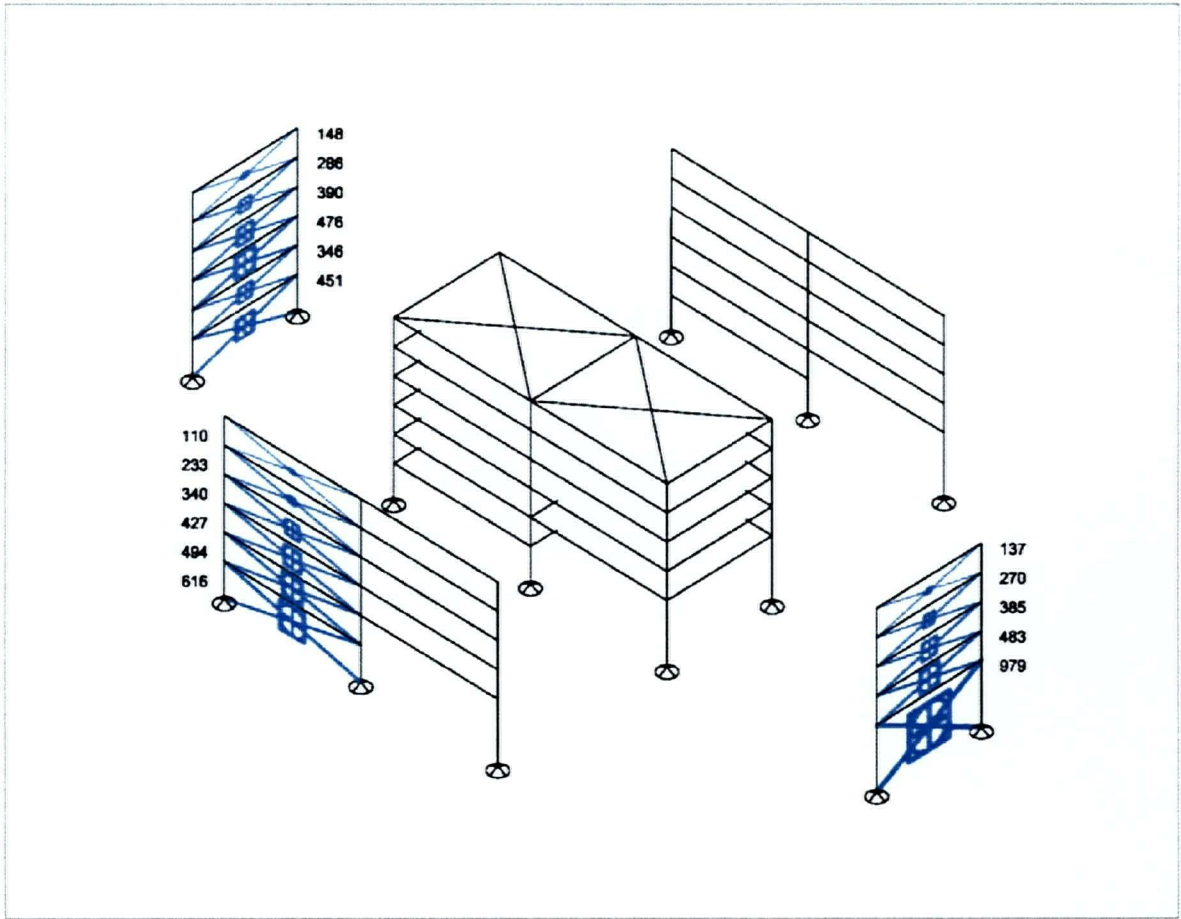


Figure 6.25. Configuration 3 – friction damping slip loads in kips for $R_{factor}=0.00005$.

Table 6.17. Comparison of envelope state vector computed using a reduced number of modes.

Uncontrolled Response State Vector							
DOF	Number of modes included in analysis				Comparison		
	2	4	8	18	2/18	4/18	8/18
x1	0.0311	0.0344	0.0345	0.0345	90.1%	99.7%	100.0%
x2	0.1513	0.1521	0.1521	0.1521	99.5%	100.0%	100.0%
x3	0.1699	0.1716	0.1716	0.1716	99.0%	100.0%	100.0%
x4	0.184	0.1867	0.1867	0.1867	98.6%	100.0%	100.0%
x5	0.1933	0.1967	0.1967	0.1967	98.3%	100.0%	100.0%
x6	0.1975	0.2013	0.2013	0.2013	98.1%	100.0%	100.0%
y1	0.0274	0.0274	0.0274	0.0274	100.0%	100.0%	100.0%
y2	0.0477	0.0477	0.0477	0.0477	100.0%	100.0%	100.0%
y3	0.0652	0.0652	0.0653	0.0653	99.8%	99.8%	100.0%
y4	0.0791	0.0791	0.0791	0.0791	100.0%	100.0%	100.0%
y5	0.0884	0.0884	0.0884	0.0884	100.0%	100.0%	100.0%
y6	0.0927	0.0927	0.0927	0.0927	100.0%	100.0%	100.0%
r1	0.0017	0.0017	0.0017	0.0017	100.0%	100.0%	100.0%
r2	0.003	0.003	0.003	0.0030	100.0%	100.0%	100.0%
r3	0.0035	0.0035	0.0035	0.0035	100.0%	100.0%	100.0%
r4	0.0039	0.004	0.004	0.0040	97.5%	100.0%	100.0%
r5	0.0042	0.0043	0.0043	0.0043	97.7%	100.0%	100.0%
r6	0.0043	0.0045	0.0045	0.0045	95.6%	100.0%	100.0%
dx1	0.3329	0.4176	0.4381	0.4382	76.0%	95.3%	100.0%
dx2	1.6196	1.6411	1.6453	1.6453	98.4%	99.7%	100.0%
dx3	1.8186	1.8665	1.869	1.8690	97.3%	99.9%	100.0%
dx4	1.9699	2.0439	2.0441	2.0441	96.4%	100.0%	100.0%
dx5	2.0695	2.1633	2.1642	2.1642	95.6%	100.0%	100.0%
dx6	2.1148	2.2183	2.2213	2.2213	95.2%	99.9%	100.0%
dy1	0.4596	0.4596	0.4616	0.4619	99.5%	99.5%	99.9%
dy2	0.7992	0.7992	0.8015	0.8016	99.7%	99.7%	100.0%
dy3	1.0933	1.0933	1.0943	1.0943	99.9%	99.9%	100.0%
dy4	1.3252	1.3252	1.3252	1.3253	100.0%	100.0%	100.0%
dy5	1.4817	1.4817	1.4821	1.4821	100.0%	100.0%	100.0%
dy6	1.5539	1.5539	1.555	1.5551	99.9%	99.9%	100.0%
dr1	0.0178	0.0181	0.0181	0.0181	98.3%	100.0%	100.0%
dr2	0.0317	0.032	0.0321	0.0321	98.8%	99.7%	100.0%
dr3	0.0373	0.039	0.0391	0.0391	95.4%	99.7%	100.0%
dr4	0.0416	0.045	0.045	0.0450	92.4%	100.0%	100.0%
dr5	0.0446	0.0494	0.0494	0.0494	90.3%	100.0%	100.0%
dr6	0.0461	0.0516	0.0517	0.0517	89.2%	99.8%	100.0%

6.4 General Discussion

In this chapter, three examples of structures of increasing complexity were used to illustrate the practical application of the proposed control theory based methodology for designing viscous and friction dampers in structures. Each was used to illustrate different properties of the process.

The first example was the same 4-story uniform shear structure used to examine the extension of the SDOF transfer function based method to the MDOF structure. This structure was used to link to previous work by providing a comparison to the results obtained using the transfer function procedure and also the results obtained using the level set programming technique. By

applying the control theory based methodology to this structure, it was possible to examine the differences between the various methods and gain a better understanding of the strengths of each.

The second example structure was extracted from an existing flexible steel moment resisting frame structure located in the Los Angeles area. The primary purpose of this example was to illustrate the capability with which the viscous and friction damped structures could replicate the target active control in a realistic structure.

In the final example, a complex, 18DOF asymmetrical structure with coupled lateral and torsional modes was analysed. This example was used to illustrate how the proposed control theory based method could be used to deal with a more complex structural system.

6.4.1 4-Story Structure

For illustrative purposes, two control levels termed “weak” and “strong” were used. The stronger control, as expected, resulted in smaller displacements, but at the expense of higher control forces. While a simple displacement based performance function was used, it was also recognised that an evaluation of the performance of the structure would eventually have to include an assessment of force demands on all structural elements. Higher control forces place higher demands on some members.

Considering the design problem in terms of story drifts, it was illustrated that the frequency characteristics of the design earthquake (either El Centro or San Fernando) strongly influence the selection of viscous and friction damping coefficients.

The passive system could match the performance of the “weak” target control nearly exactly and the “strong” control reasonably well. The ability to match the target active control performance was found to diminish as the strength of the control increased.

Given a flexible brace, it was shown that an optimal slip load distribution could be found that is capable of producing minimum displacement by dissipating the maximum energy. This optimal slip load compared favourably to those slip loads found by the other methods (LSP and the extended transfer function method), but did not provide a precise match. The key advantage with the control theory based method is that one need not target the minimum drift. The results obtained with each of the earthquakes illustrated that for one event, San Fernando, only a weak control was necessary to keep within the drift ratio limit set as the performance criteria, while

with El Centro input, a significantly stronger control was necessary to keep within the same acceptable performance criteria. This demonstrated that the control theory based method allows greater flexibility in design by allowing the designer to select a control strength that meets specified performance criteria. This is an advantage over using the minimum drift, as targeted in the transfer function method, because it allows for economical implementation of the control. This would be an advantage, particularly when there is an advantage in limiting the control force demands on the structure.

6.4.2 Burbank 6-Story Structure

A “weak” and a “strong” control were utilised to illustrate the control capability. The damping associated with the fundamental mode with the “weak” and “strong” control had damping ratios of 35% and 50% respectively. These damping ratios might be considered to be quite high, but are indicative of the level of damping with which superior structural performance can be obtained with viscous and friction dampers.

Comparison of the time history response illustrates a remarkable resemblance between the active and the passive viscous damper response. The friction-damped structure, however, was shown to have a strikingly different character of response containing higher frequency components and often peak response exceeding the target considerably, particularly in the early stages of the earthquake. The results suggest that while the passive viscous damped structure is a reasonably faithful approximation of the target active control, the difference in character of the friction damped structure reduces its ability to match peak values for the highly damped structures considered in this example.

The difference in the control capability of the “strong” and “weak” control was examined and it was shown that both the passive viscous dampers and the passive friction dampers were, in general, not as effective as the fully active controller in reducing the peak deformations, with the friction dampers being significantly less effective than the target control. These results suggest that the designer should be aware of the reduced effectiveness with each step moving away from the active control and perhaps overshoot the active control strength somewhat so as to end up with a friction damped structure whose response remains within prescribed performance limits.

6.4.3 18 DOF Eccentric Building Structure

The main purpose of this structural example was to use a more complex structure that would allow one to investigate different damper configurations. Three different configurations were chosen; a full 23 damper system with dampers in each story around the perimeter of the structure; a minimal 3 damper system with dampers contained only within the lowest story; and finally a 17 damper asymmetrical arrangement that could represent a practical response to constraints on the retrofit design.

The full 23 damper system and the 17 damper system were found to have quite similar performance, with the latter being more efficient in the utilisation of space and material. The latter distribution is one that would not likely be chosen by an automatic algorithm, but due to non-structural considerations that may include architectural considerations or cost constraints, is one that may be considered more desirable.

Friction dampers were considered in terms of both the required slip load and the minimum brace cross-sectional area to activate the dampers in the given structure. It was found that the brace areas necessary to activate the friction dampers were quite large. This should not be surprising since the structure on which the investigation was based is a stiff reinforced concrete structure.

The design philosophy has been up to this point that the damper system should be able to keep the structural deformations to a level that the primary structural system remains elastic. With such a stiff structure, it was shown that very substantial (stiff) braces are necessary to provide the ability to control it. The brace stiffness necessary to provide effective damping at small deformations could perhaps be judged to be too high to be practical, and perhaps unnecessary. In this case, the designer might opt to use different performance criteria in which the control system would only respond in an optimal manner when larger deformations occur after the primary structure has sustained some damage. This is a vastly more complex performance criteria than considered within the scope of this thesis and, but one for consideration in further practical studies.

Chapter 7: Summary, Conclusions and Recommendations

7.1 Summary

7.1.1 General

The studies that comprise this thesis were motivated by the need for a method of designing optimally damped structures for earthquake and other external loads. While the focus was on friction/hysteretic dampers, the design of viscous dampers was also included to provide a more complete treatment of the control problem, and to provide a theoretical basis for the design of friction/hysteretic dampers.

Experience has shown that vastly improved structural performance can be obtained with active and semi-active control systems. But this performance comes at the price of increased reliance on complex equipment. Both active and semi-active systems require sensors and actuators, and, in the case of an active control, the provision of significant amounts of energy from an external source. Passive systems, on the other hand, which include viscous, friction and hysteretic dampers, act as self-contained sensors and actuators, and consequently are much simpler and more reliable systems.

The goal of this thesis was to find practical methods of determining optimal damper sizes for structures subjected to earthquake loads. In the case of multi-degree of freedom structures, optimal damper sizing includes the determination of the optimal distribution of dampers. It was assumed that the friction dampers are supported by braces that have some flexibility. Brace flexibility is an undesirable characteristic as it degrades the effectiveness of the damper.

7.1.2 SDOF Structures

The research began with the investigation of the response of single degree of freedom viscous and friction damped structures subjected to sinusoidal and white noise excitations. Semi-active “off-on” friction dampers were also included in the discussion. Viscous damped structures are linear and closed form analytical solutions exist. These were developed conveniently using Laplace transform techniques. Friction damped structures, being non-linear, do not have

analytical solutions. However, an iterative analytical energy balance approach was developed to determine the frequency response of a friction damped structure with a flexible brace.

Given a SDOF structure with a viscous damper in a flexible brace, it was shown that the viscous damper leading to minimum drift depends on the frequency content of the excitation measured with respect to the frequencies of the structure, those frequencies being the fully braced and unbraced natural frequencies. Similarly, friction damped structures depend on the frequency content of the excitation and also on its magnitude.

A design method was proposed based on the transfer function normalized with respect to the magnitude of the excitation and the frequency of the structure. The transfer function was shown to provide a convenient basis to evaluate the response of the structure to a variety of significant loadings and also provide a basis for understanding the expected outcome of design changes such as increased stiffness, mass and damper strength.

The proposed optimization procedure was based on the computation of the root mean square story drift. The RMS drift was computed from the PSD of the response, which in turn was obtained from the product of the PSD of the excitation and the established transfer function associated with a particular size of damper. It is assumed in this process that the peak response is proportional to the RMS response such that the minimization of the RMS response corresponds to the minimization of the peak response. It is also assumed that the excitation results in steady state response.

The families of transfer functions associated with increasing viscous damper sizes were shown to transition from a curve having a peak at the unbraced natural frequency where the damping force generated is insignificant, to one with a peak at the braced natural frequency when the damping coefficient is so high that essentially no damper deformation results. The same characteristic family of curves was also shown for friction-damped structures.

Establishing the character of these transfer functions was an important step because it provided a framework for the families of transfer functions and set limits on the frequency characteristics of input for which a damper (either viscous or friction) would be useful. A high frequency structure, or one with the bulk of the excitation below the unbraced natural frequency would benefit most from a rigidly connected brace. A low frequency structure, or one with the bulk of the excitation above the braced natural frequency would benefit most from not having any brace or damper connected at all. Only if the excitation includes response between these two

frequencies would a non-trivial solution exist for the optimal damper. Structures subjected to these excitations do benefit from the optimization of slip load or viscous damping coefficient. This is presumed to be true for the majority of structures subjected to earthquake loads.

It was found that the analytically determined set of transfer functions for sinusoidal input were not capable of reproducing the drift vs slip load for structures subjected to white-noise excitation.

Consequently, response time history data was extracted from SDOF structure numerical models having various damper sizes and brace stiffness parameters subjected to sinusoidal and white noise excitations. These data were then used to build up families of transfer functions representing the response of the friction damped structures in the frequency domain. These data sets were expressed in terms of non-dimensional variables to facilitate their application to a variety of structures.

Utilising each of the transfer functions in turn, the RMS displacements could be determined rapidly by computing the integral of the product of the PSD of the input and the response transfer functions for each slip load or damping coefficient. The slip load or damping coefficient that leads to the minimum response is considered optimal. The shape of the curve expressing maximum inter-story drift vs. slip load was found to be relatively flat near its minimum indicating that the structure response is relatively insensitive to the precise value of the slip load.

Transfer function curves for the semi-active “off-on” friction damped structure were also determined numerically. The family of curves clearly indicated that an optimal slip load does not exist for this semi-active control system, as was confirmed by numerical simulation.

7.1.3 MDOF Structures

It was recognised that multi-degree of freedom structures have a very complex response, but often can be represented by the response of a single dominant mode. Initially, the extension of the SDOF design methodology to MDOF structures was considered.

Level set programming, an optimization tool, was used to study the optimal slip loads in a uniform 4-story structure. The LSP results were used to understand the optimal distribution of slip loads as well as provide a point of comparison for the structure under consideration.

Using the SDOF transfer functions established in the first part of this study, the base slip load was established then distributed according to the predetermined distribution. Based on an

assumed distribution involving the fundamental mode shape and the story shears, and guided by the LSP results, the friction damper slip loads above the base story were estimated. It was shown that it was possible to obtain reasonable estimates of optimal slip load using the extended SDOF procedure, providing an overall calibration constant was included. It was recognised that this procedure is limited to MDOF structures that possesses a regular construction, respond primarily in a single identifiable mode, and whose slip load distribution is well understood. While these assumptions may be a valid for some structures, it was recognised that this procedure would not be applicable to a general structural systems. Consequently an alternative procedure was sought. The theory of modern structural control, with its formulation based on the state-space description of the equations of motion, was proposed as a basis for the design of dampers at predetermined locations within a general structural system. The well-known LQ control algorithm provides a means of computing the time independent active control gain matrix, whose gains describe force components proportional to displacements and velocities that lead to an optimal control of the structure. By linking the state-space formulation of the equations of motion with a response spectral analysis, a method was provided for rapidly determining a set of passive dampers that provide a performance that is comparable to the fully active control.

The procedure investigated at this stage is embodied in the following general steps:

- 1 Formulate the system dynamics in state space form
- 2 Establish the target (active) control by solving for the LQ control problem for full state or observer gain matrix
- 3 Using the controlled system as a target, perform a state-space response spectral analysis to establish envelope damper velocities, displacements and full state control forces
- 4 Use the above to estimate the viscous damper coefficients and subsequently the friction damper slip loads
- 5 Evaluate the performance of the structure with established performance criteria. If necessary re-estimate more appropriate control parameters and repeat steps 2 through 5 until the structure performs as required.

Once locations for dampers have been selected, the proposed design method was used to determine the passive viscous damping coefficients that approximate the optimal active control.

After establishing these viscous damping coefficients, by matching peak cycle energy dissipation, the corresponding friction damper slip loads were then established. The theoretical derivation of the procedures necessary to compute the viscous and friction damper parameters was provided, followed by several illustrative examples.

The general control theory based method excluded the consideration of flexible braces. Therefore it did not target an absolute minimum response of the structure having friction dampers and flexible braces, as did the SDOF procedure. But, it was shown that an absolute minimum response could be found by increasing the strength of the control to the point at which the peak cycle energy of the ideal viscous damper could only just be provided by the combination of friction damper and flexible brace. While it was found that the optimal slip loads predicted in this way did not reproduce the same slip load distribution as found using LSP, the general slip force magnitudes were comparable. It was observed that the performance index of the control theory based method and the objective function used by the LSP search algorithm differed slightly.

The MDOF procedure was developed based on the time independent LQ control algorithm. While this was desirable in this case for its simplicity, many alternative control algorithms exist, including instantaneous optimal control, and H_∞ control (Soong, 1989b).

7.2 Conclusions

7.2.1 General

The work undertaken as part of this research achieved the primary objective of providing methodologies for the design of damping systems to improve the performance of structures in earthquakes. The transfer function based SDOF method provided insight into the response of structures with viscous and friction dampers. The control theory based method developed for MDOF structures overcame many of the deficiencies of the transfer function method. While the strength of the control depends on the control parameters, the control theory based method could effectively be used to satisfy performance criteria in a rapid assessment.

7.2.2 SDOF Structures

For the SDOF structures “optimal” was defined as the structural system that led to the minimum drift. The optimization was based on a search for the minimum RMS drift, computed by combining response transfer functions with the PSD functions representing the excitation. The family of viscous damped transfer functions could be solved analytically, and their solution provided some insight into the optimization problem. However, the transfer functions for the friction damper, being a non-linear element, are not defined. The transfer functions for the friction damped system are not unique but depend on the magnitude and frequency content of the excitation. It was found that analytically derived curves for sinusoidal response were not able to provide accurate predictions of the optimal friction damping slip loads in structures when subjected to white noise or earthquake excitations. However, transfer functions derived numerically based on the non-linear response time history data using white noise input were found to provide accurate optimal slip load predictions.

7.2.3 MDOF Structures

In extending of the SDOF transfer function based optimization procedure to a MDOF structure, it was necessary to represent the structure using a single mode (the fundamental mode). It was also necessary to provide an estimate of the optimal distribution of the slip loads. An expression was proposed based on the drift mode shape and the shear forces in each story that was in general agreement with the optimal slip load distributions determined using the LSP trial and error procedure. It was also found that in order to replicate the results determined by LSP, calibration coefficients are necessary. It was therefore concluded that the need to provide slip force distributions and calibration coefficients restrict the applicability of the method to regular structure forms that have been studied in detail.

To overcome these difficulties a more general procedure was developed that is applicable to a structure with any number of dampers. The LQ control was used to provide an optimal target for the design of passive viscous dampers at pre-selected locations in a general MDOF structure. Using the peak cycle energy dissipation, corresponding friction damper slip loads could be set, providing the flexibility in the brace was not too great.

The proposed design procedure within which the control based design procedure is to be implemented provides the designer with the ability to rapidly search for the control parameters

that are consistent with the design objectives. The passive damping coefficients, viscous or friction, are a function of the excitation. The response induced by the excitation is used when attempting to determine the passive ideal viscous damping coefficients and again when determining the corresponding friction damper slip loads. Response spectral analysis derived for application with non-classically damped structural systems in state space form enables the rapid evaluation of these response quantities. The use of peak cycle force matching was found to result in a passive control system with comparable performance to the target active system, but the ability to match the target control degrades as the strength of the active system increases.

Corresponding friction dampers, evaluated based on matching the energy dissipated in the peak cycle approached the performance of the target control system, but did not fully achieve the target. While the peak cycle energy matching procedure provides a good estimate, it is necessary for the designer to keep in mind that the final friction damped system will not be as effective as the target. Therefore it is necessary for the designer to overshoot the performance with the target system.

It was found that the flexibility of the brace served to limit the capability of the friction damped structure. Minimum brace stiffness was related to the deformations imposed on the brace/damper by the structure and the necessary peak cycle energy dissipation. A critical level of control was determined defined as the level of deformations for which the flexible brace deformation would just limit the ability of the damper to develop the required slip load and dissipate the peak cycle energy equivalent to the viscous damper. This slip force corresponds to the overall optimal slip load leading to minimum deflection as previously considered.

Comparing the results obtained by LSP to those obtained by the control theory based method showed that while the distribution of slip loads differed somewhat, the absolute values of the obtained slip loads were in reasonably good agreement. While a substantial calibration coefficient was necessary with the extended SDOF procedure, with the control theory based method a calibration factor appeared to be unnecessary. It is therefore concluded that the control theory based method provides reasonable and useful results.

By the three examples presented, the MDOF damper design methodology was shown to be useful in dealing with more complex structures. Techniques were provided to deal with both over specified systems (more dampers than degrees of freedom in the structure) and under specified systems (fewer dampers than degrees of freedom in the structure) with reasonable

results. The ability to test alternative configurations of dampers provides the designer with an important tool for responding to design constraints and for reducing costs.

The MDOF procedure proposed provides for more flexibility in the design process; providing the designer with the ability to experiment with different damper configurations and rapidly check their performance. Response spectral analysis is much more efficient than time history analysis because it provides estimates of the peak response quantities directly using the design spectrum. The expense of doing extensive non-linear time history analysis is avoided in the initial design stages, permitting the designer to investigate variations in the damper configuration. This is expected to result in better and more efficient designs of the control systems.

7.3 Recommendations

During the course of this study, several topics were identified as potential areas for further investigation. The following sections highlight the areas where further work could be directed.

7.3.1 SDOF Structures

7.3.1.1 Steady State vs. Transient Response

The assessment methodology presented for SDOF structures was based on the steady state response to sinusoidal excitations and the stationary response to white noise excitations.

Transient and non-stationary response may in some cases influence the choice of optimal slip load. Further work is recommended to clarify for which structures and excitations transient and non-stationary response plays a role, and how it influences the choice of optimal dampers.

7.3.1.2 RMS vs. Peak Response

The proposed optimization procedure was based on the assumption that the peak response is proportional to the RMS response. A better understanding of the relationship between peak and RMS responses would be helpful in interpreting the results of the SDOF procedure. It is therefore recommended to consider a study of the relationship between peak and RMS response.

7.3.1.3 Hysteretic vs. Friction Dampers

Hysteretic dampers have been considered to be extensions of friction dampers, however this simplification does not reflect the true character of hysteretic response. Hysteretic material

exhibits a multi-level memory effect that may have a significant influence on the energy dissipation. Subsequently, inability to fully model the salient characteristics of a hysteretic device may lead to inaccuracies when applying the design methodology. It is therefore recommended that further work be carried out on hysteretic systems.

7.3.2 MDOF Structures

7.3.2.1 Input Spectra for State-Space RSA

In order to carry out the design of structures with the state-space response spectral analysis procedures developed in this thesis, input design spectra are necessary. While the lack of such spectra was sidestepped by using spectral ordinates derived directly from particular input earthquake records, it is recommended to consider developing uniform hazard response spectra and/or design spectra cast in the 3-D form presented. Appendix C contains a collection of 3-D spectra obtained for a number of sample records.

The state-space modal combination procedure included “Sine” and “Cosine” component surfaces. It is observed that by using the two spectra surfaces, the spectra are able to provide more information about the excitation characteristics than contained in the form of response spectra commonly in use. Simplifying the analysis such that a single surface could be used would be preferable.

Investigation of 3-D response spectra may provide an improved understanding of the ability of earthquakes to excite heavily damped structures. While it is not known if significant new information is included in spectra of this form, it is suggested that looking at earthquakes using these spectra may provide more information related to the site, or the source of earthquakes in general for which the structure is to be designed.

7.3.2.2 Investigate Alternative Modal Combination Procedures

The work presented herein relied heavily on a modal combination technique adapted from the SRSS procedure. This procedure was used here for its simplicity rather than for its accuracy. Alternative procedures, such as the CQC modal combination procedure, for example, are preferred in practice. It is recommended that consideration be given to the study of modal analysis procedures in the state-space formulation of structural dynamics. Particular attention needs to be paid to the transition from sub-critical to super-critical damping. Zhou, Yu and

Dong, (2004) have recently developed the CCQC method for the analysis of non-classically damped systems.

7.3.2.3 Investigate Alternative Control Algorithms

The work presented here was based on the time independent LQ control algorithm. The current trend in structural control is to utilise more advanced control techniques such as instantaneous optimal control and H_∞ control. It is recommended that research be undertaken into the application of more advanced control techniques that can potentially provide a control with a measure of optimality that is more in line with the structural performance objectives.

7.3.2.4 Investigate Optimal Design of Viscous Dampers with Flexible Brace

The SDOF investigation led to a simple result whereby the optimal performance of the linear viscous damped structure under a white noise excitation was obtained by selecting a damper which together with the brace has a response time constant equal to that of the structure. An investigation should be carried out to establish whether a similar simple result exists for a general MDOF structure.

7.4 Thesis Contributions

The main contribution of this thesis was the proposal of design methods for the design of dampers at pre-selected locations in SDOF and MDOF structures. For SDOF structures the proposed procedure entails the prediction of RMS drift response using a set of transfer functions established for the purpose. For MDOF structures a general method based on the LQ control problem was derived. A key feature of this work was the explicit consideration of the flexibility of the brace(s) that connects the damper(s) to the structure. With these two methods, the structural designer has new tools with which to size viscous, friction or hysteretic dampers in structures subjected to seismic and other loads.

7.4.1 SDOF Structures

With the SDOF design method, a key contribution was the provision of design curves for viscous damped structures; friction damped structures under sinusoidal excitation; friction damped structures under white noise excitation and “off-on” semi-active friction dampers. These sets of curves were provided in a non-dimensional form allowing for their use with any SDOF

structure/excitation combination. Using these curves together with the PSD of the input excitation, the designer can rapidly compute the expected deformations of the damped structure and subsequently determine the optimal damper size.

7.4.2 MDOF Structures

Extensive studies of the optimal slip loads in a uniform 4-story shear structure using LSP provided an understanding of the optimal slip load distributions using various objective functions and earthquake excitations. This study also provided benchmark optimal slip loads with which to test the proposed design methodologies. The LSP investigation also highlighted that the slip load distribution leading to optimal performance is not always unique, but depends on the structure and the excitation.

The key contribution of this thesis in connection with general MDOF structures is the proposal of a method for the design of dampers using the LQ control as a basis. The proposed method provides a rapid means of determining the optimal damper sizes at pre-selected locations in the structure by using a response spectrum analysis derived for the state space form of the equations of motion of the structure. The RSA procedure uses the damped mode shapes and can be applied to non-classically damped structures with high damping. The methods derived are particularly well suited to incorporating a small number of dampers in a large finite element model.

Modal combination procedures in the state-space form enable both supercritically and subcritically damped modes to be incorporated in the analysis. Using such analysis methods will enable design engineers to consider structures with much higher damping and this is expected to result in structures that are more resistant to dynamic loads.

References

- Abdel-Rohman, M. and Leipholz, H.H.E. (1979a) "A General Approach to Active Structural Control" Proceedings Of ASCE Journal of the Eng. Mech. Div., Vol. 105, No. EM6, Dec. 1979, pp. 1007-1023
- Abdel-Rohman, M. and Leipholz, H.H.E. (1979b) "Automatic Active Control of Structures" Proceedings of ASCE Journal of the Eng. Mech. Div., Vol. 106, 1980
- Abdel-Rohman, M. and Leipholz, H.H.E., Quintana, V.H. (1979c) "Design of Reduced Order Observers for Structural Control Systems" Structural Control, H.H.E Leipholz, Ed., IUTAM, 1980
- Abdel-Rohman, M. (1985) "Feasibility of Active Control of Tall Buildings" Structural Control, Proceedings of the Second International Symposium on Structural Control, University of Waterloo, July 15-17, 1985, Ed. H.H.E. Leipholz, Martinus Nijhoff
- ADINA (2002) 900 Node ADINA v8.0 software plus program documentation, © 1994-2002 ADINA R&D Inc.
- Akbay, Z. and Aktan H.M. (1991) "Actively Regulated Friction Slip Braces" 6th Canadian Conference on Earthquake Engineering, Toronto, pp. 367-374
- Aiken I.D. and Kelly, J.M. (1990) "Earthquake Simulator Testing and Analytical Studies of Two Energy-Absorbing Systems for Multistory Structures", Report No. UCB/EERC-90/03, University of California, Berkeley, CA
- Architectural Record, Sept. 1971, pp.155-158
- Bakhtavar, M.S., Ventura, C.E. and Prion, H.G.L. (2000) "Seismic Behaviour and Computer Modelling of Low-Rise Steel Frame Structures" Earthquake Engineering Research Facility Technical Report No. 00-01, July 2000
- Backe, W., Forster, I. (1985) "Fluid Technical Unit for Active Control of Deformations", Structural Control, Proceedings of the Second International Symposium on Structural Control, University of Waterloo, July 15-17, 1985, Ed. H.H.E. Leipholz, Martinus Nijhoff
- Bouten, H., Meyr, H. (1985) "Control Design for ADC-Girder" Structural Control, Proceedings of the Second International Symposium on Structural Control, University of Waterloo, July 15-17, 1985, Ed. H.H.E. Leipholz, Martinus Nijhoff
- Building Seismic Safety Council (2000) NHERP Recommended Provisions for Seismic Regulations for New Buildings and Other Structures Part 1: Provisions (FEMA 368), Prepared by the Building Seismic Safety Council for the Federal Emergency Management Agency, Washington D.C.

- Carotti, A., De Miranda, M. and Turei, E. (1985) "An Active Protection System for Wind Induced Vibrations of Pipeline Suspension Bridges" Structural Control, Proceedings of the Second International Symposium on Structural Control, University of Waterloo, July 15-17, 1985, Ed. H.H.E. Leipholtz, Martinus Nijhoff
- Caughey T.K. and Stumpf, H.J. (1969) "Transient Response of a Dynamic System Under Random Excitation" Transactions of the ASME Journal of Applied Mechanics, December 1969, pp. 563-566.
- Chang, J.C.H. and Soong, T.T. (1979) "The Use of Aerodynamic Appendages for Tall Building Control" Structural Control, H.H.E Leipholtz, Ed., IUTAM, 1980
- Chen, C. and Chen, G. (2002) "Non-linear Control of a 20-story Steel Building with Active Piezoelectric Friction Dampers" Structural Engineering and Mechanics, Vol. 14, No. 1, pp. 21-38.
- Cheng, F. and Pantelides, C. (1988) "Optimal Placement of Actuators for Structural Control" Tech. Rep. NCCER-88-0037 1988. National Center for Earthquake Engineering Research, State University of New York, Buffalo. N.Y.
- Chowdhury, A.H., Iwuchukwu, M.D., Garske, J.J. (1985) "The Past and Future of Seismic Effectiveness of Tuned Mass Dampers" Structural Control, Proceedings of the Second International Symposium on Structural Control, University of Waterloo, July 15-17, 1985, Ed. H.H.E. Leipholtz, Martinus Nijhoff
- Ciampi, V., Arcangeli, M. and Fertilo, R. (1991a) "Dissipative Bracings for Seismic Protection of Buildings" International Meeting on Earthquake Protection of Buildings" Ancona, June 6/8, pp. 87-100/D.
- Ciampi, V. (1991b) "Use of Energy Dissipating Devices, Based on Yielding of Steel for Earthquake Protection of Structures" International Meeting on Earthquake Protection of Buildings, Ancona, June 6/8, pp. 41-58/D.
- Constantinou, M.C., Soong, T.T. and Dargush, G.F. (1996) "Passive Energy Dissipation Systems for Structural Design and Retrofit" Course Notes for the course sponsored by the National Center for Earthquake Engineering Research and the National Science Foundation, Seattle, Washington, September 12-14.
- Curtis, A.R.D., Nelson, P.A., Elliott, S.J. (1985) "Active Minimalization of Vibrational Energy in Periodically Excited Structures" Structural Control, Proceedings of the Second International Symposium on Structural Control, University of Waterloo, July 15-17, 1985, Ed. H.H.E. Leipholtz, Martinus Nijhoff
- Dehghanyar, T.J., Masri, S.F., Miller, R.K., and Caughey, T.K. (1985) "On-line Parameter control of Non-linear Flexible Structures" Structural Control, Proceedings of the Second International Symposium on Structural Control, University of Waterloo, July 15-17, 1985, Ed. H.H.E. Leipholtz, Martinus Nijhoff

- H.K. Dengenkolb Associates (1991) "Effects of the Loma Prieta Earthquake on the Veterans Administration Palo Alto Medical Center", October 4, 1991.
- Domke, H. (1985) "Increase in Efficiency and Reliability of load bearing Members by Active Deformation Control" Structural Control, Proceedings of the Second International Symposium on Structural Control, University of Waterloo, July 15-17, 1985, Ed. H.H.E. Leipholz, Martinus Nijhoff
- Dowdell, D.J. and Cherry, S. (1994a) "Semi Active Friction Dampers for Seismic Response Control of Structures" Proceedings of the Fifth U.S. National Conference on Earthquake Engineering, Chicago, IL.
- Dowdell, D.J. and Cherry, S. (1994b) "Structural control Using Semi-active Friction Dampers" Proceedings of the First World Conference on Structural Control, 3-5 August, Los Angeles, California. pp. FA1-59-58.
- Dowdell, D.J. and Cherry, S. (1994c) "Optimal Seismic Response Control of Friction Damped Structures," 10th European Conference on Earthquake Engineering, (ed. Duma), Balkema, Rotterdam, pp. 2051-2056.
- Dowdell, D.J. Leipholz, H.H.E., Topper, T. (1988) "Fatigue Life Prediction for Discrete Strain Markov Processes" International Journal of Fatigue, Vol. 10, No. 4, October, pp. 227-236.
- Dowdell, D.J., Leipholz, H.H.E., Topper, T. (1989) "Experimental Verification of Fatigue Life Predictions for Discrete Strain Markov Processes" International Journal of Fatigue, Vol. 11, No. 1, January, pp.19-28.
- Filiatrault, A. and Cherry, S. (1985) "Final Report - Performance Evaluation of Friction Damped Braced Steel Frames under Simulated Earthquake Loads" Submitted to Department of Supply and Services Canada, November.
- Filiatrault, A., and Cherry, S. (1988) "Seismic Design of Friction Damped Braced Steel Plane Frames by Energy Methods" Report UBC EERL-88-01
- Filiatrault, A., and Cherry, S. (1990) "A simplified Seismic Design Procedure for Friction Damped Structures" Proc. of the 4th US National Conference on Earthquake Engineering, Palm Springs, CA. Vol. 3. pp. 479-488.
- Filiatrault, A. (1991) "Friction Damping in Aseismic Design of Buildings: The Canadian Experience" International Meeting on Earthquake Protection of Buildings, Ancona, June 6/8, 1991.
- Feng, M.Q., Shinozuka, M., and Fujii, S. (1993) "Friction-Controllable Sliding Isolation System" Journal of Engineering Mechanics, Vol. 119, No. 9, Sept., 1993 pp. 1845-1864.
- Fujita, S., Satomoto, K., Yokozawa, O., Shimoda, I., Masami, M., Nagai, K. and Kimoto, K. (1994) "Fundamental Study on Vibration Attenuation Systems for High Rise Buildings" First World Conference on Structural Control, Los Angeles, California, pp. FP-25 -34.

Gasparini, D.A. and Vanmarcke, E.H. (1976) "Simulated Earthquake Motions Compatible with Prescribed Response Spectra" Report No. 2, Evaluation of Seismic Safety of Buildings, Massachusetts Institute of Technology Department of Civil Engineering, Publication No. R76-4.

Grigorian, C.E., Yang, T.S. and Popov, E.P. (1993) "Slotted Bolted Connection Energy Dissipators" Earthquake Spectra, Vol. 9, No. 3

Haftka, R.H., Martinovic, Z.N., Hallauer, W.L., Schamel, G. (1985) "The Effect of Small Structural Changes on Optimized Active Control Systems" Structural Control, Proceedings of the Second International Symposium on Structural Control, University of Waterloo, July 15-17, 1985, Ed. H.H.E. Leipholtz, Martinus Nijhoff

Hagedorn, P. (1985) "On a New Concept of Active Vibration Damping of Elastic Structures" Structural Control, Proceedings of the Second International Symposium on Structural Control, University of Waterloo, July 15-17, 1985, Ed. H.H.E. Leipholtz, Martinus Nijhoff

Hanson, R.D. and Soong, T.T. (2001) "Seismic Design with Supplemental Energy Dissipation Devices", EERI Engineering Monograph 8.

Hirsch, G., Huffmann, G. and Klein-Tebbe, A. (1988) "Semi-Active Control of Earthquake Induced Oscillations of Structures" Proceedings of the 9th World Conference on Earthquake Engineering, Tokyo-Kyoto, Japan, Vol. VIII, pp.483-488.

Hirsch, G. (1985) "Practical Experiences in Passive Vibration Control of Chimneys (Conclusions from Wind Tunnel and Full Scale Tests)" Structural Control, Proceedings of the Second International Symposium on Structural Control, University of Waterloo, July 15-17, 1985, Ed. H.H.E. Leipholtz, Martinus Nijhoff

Housner, G.W., Soong, T.T., Masri, S.F. (1994) "Second Generation of Active Structural Control in Civil Engineering" First World Conference on Structural Control, Los Angeles California, pp. Panel-3-18

Inaudi, J.A., Kelly, J.M. (1993) "Minimum Variance Control of Base Isolated Floors" Journal of Structural Engineering, ASCE, Vol. 119, No. 2, Feb., 1993, pp 438-453.

Kelly, J.M. (1979) "Control Devices for Earthquake Resistant Design" Structural Control, H.H.E. Leipholtz, Ed., IUTAM, 1980

Kelly, J.M. and Aiken, I.D. (1991) "Earthquake Simulator Testing of Energy Absorbing Systems for Multistory Structures" International Meeting on Earthquake Protection of Buildings, Ancona, June 6/8

Klein, R.E., and Sali, H. (1979) "The Time Optimal Control of Wind Induced Structural Vibrations using Active Appendage" Structural Control, H.H.E. Leipholtz, Ed., IUTAM, 1980

Klein, R.E. and Healy, M.D. (1985) "Semi-Active Control of Wind Induced Oscillations in Structures" Structural Control, Proceedings of the Second International Symposium on Structural Control, University of Waterloo, July 15-17, 1985, Ed. H.H.E. Leipholtz, Martinus Nijhoff

Kobori, T., Kanayama, H. and Kumagata, S. (1988) "A Proposal of New Anti-Seismic Structure with Active Seismic Response Control System - Dynamic intelligent Building" Proceedings of the 9th World Conference on Earthquake Engineering, Tokyo-Kyoto, Japan, Vol. VIII, pp.465-470.

Kobori, T. (1999) "Mission and Perspective Towards Future Structural Control Research," Proceedings of the Second World Conference on Structural Control, Kyoto, Japan, VI pp.25-34

Kobori, T. (1994) "Future Direction on Research and Development of Seismic-Response-Contolled Structure" First World Conference on Structural Control, Los Angeles CA, USA. pp. Panel-19 - Panel-31.

Kreyszig, E., 1983, Advanced Engineering Mathematics, 5th Edition, Wiley, pp. 830-837, 842-846

Lund, R.A. (1979) "Active Damping of Large Structures in Winds" Structural Control, H.H.E Leipholz, Ed., IUTAM, 1980.

Leipholz, H.H.E. and Abdel Rohman, M. (1986) Control of Structures, Martinus Nijhoff

Masri, S.F., Bekey, G.A. and Udawadia, F.E. (1979) "On-Line Pulse Control of Tall Buildings" Structural Control, H.H.E Leipholz, Ed., IUTAM, 1980

MathWorks Inc. (1999) MATLAB R11 v.5.3.0 program plus documentmation, © 1984-1999, The MathWorks Inc.

McNamara, R.J. (1977) "Tuned Mass Dampers for Buildings" Journal of the Structural Division, Proceedings of ASCE, Vol. 103, No. ST9, Feb. 1977.

Medeot, R. (1991) "Experimental Testing and Design of Aseismic Devices" International Meeting on Earthquake Protection of Buildings, Ancona, June 6/8, 1991.

Meirovitch, L. and Oz, H. (1979) "Active Control of Structures by Modal Synthesis" in Structural Control, H.H.E Leipholz, Ed., IUTAM, 1980

Meirovitch, L. (1990) Dynamics and Control of Structures, John Wiley and Sons

Modi, V.J., Welt, F. and Seto, M.L. (1995) "Control of Wind Induced Instabilities Through Application of Nutation Dampers: A Brief Overview", Engineering Structures, Vol. 17, No. 9, pp. 626-638.

Modi, V.J., and Munshi, S.R. (1998) "An Efficient Liquid Sloshing Damper for Vibration Control" Journal of Fluids and Structures, Vol. 12, pp. 1055-1071, 1998.

Naeim, F. (1989) The Seismic Design Handbook, Van Nostrand Reinhold

Niwa, N., Kobori, T., Takahashi, M., Hatada, T., Kurino, H., Tagami, J. (1995) "Passive Seismic Response Controlled High-Rise Building with High Damping Device" Earthquake Engineering and Structural Dynamics, Vol. 24, pp.655-671.

- Pall, A.S., and Marsh, C. (1982) "Response of Friction Damped Braced Frames" J. Struct. Division ASCE 108 (ST6), pp. 1313-1323
- Pall, A.S. (1984) "Response of Friction Damped Buildings" Proc. of the 8th World Conference on Earthquake Engineering, San Francisco, Vol. V., pp. 1007-1014.
- Pall, A.S., Verganelakis, V., and Marsh, C. (1987) "Friction Dampers for Seismic Control of Concordia University Library Building" Proceedings of the 5th Canadian Conference on Earthquake Engineering, pp. 191-200.
- Pall, A.S. (1989) "Friction-Dampers for Economic Seismic Design", Seismic Engineering Research and Practice, eds. Charles A. Kircher and Anil K. Chopra, ASCE pp. 159-168.
- Pall A.S., Venezia, S., Proulx, P., and Pall, R. (1993) "Friction Dampers for Seismic Control of Canadian Space Agency Headquarters" Earthquake Spectra 9(3). pp. 547-557.
- Patten, W.N., He, Q., Kuo, C.C., Liu, L. and Sack, R.L. (1994) "Suppression of Vehicle Induced Bridge Vibration Via Hydraulic Semiactive Vibration Dampers (SAVD)" First World Conference on Structural Control, 3-5 August, Los Angeles, California, pp. FA1-30-38.
- Patten, W.N. Kuo, C.C., He, Q., Liu, L. and Sack R.L. (1994b) "Seismic Structural Control via Hydraulic Semiactive Vibration Dampers (SAVD)" First World Conference on Structural Control, 3-5 August, Los Angeles, CA, USA. pp. FA2-83 -89.
- Pekau, O.A. and Guimond, R. (1991) "Controlling Seismic Response of Eccentric Structures by Friction Dampers" Earthquake Engineering and Structural Dynamics, Vol. 20, pp. 505-521.
- Petersen, N.R. (1979) "Design of Large Scale Tuned Mass Dampers" Structural Control, H.H.E Leipholtz, Ed., IUTAM, 1980. pp. 581 - 596.
- Polak, E., Pister, K.S. and Ray, D. (1976) "Optimal Design of Framed Structures Subjected to Earthquakes" Engineering Optimization, Vol. 2, pp.65-71.
- Reinhorn, A.M., Manolis, G.D., and Wen C.Y. (1985) "An On-line Control Algorithm for Inelastic Structures" Structural Control, Proceedings of the Second International Symposium on Structural Control, University of Waterloo, July 15-17, 1985, Ed. H.H.E. Leipholtz, Martinus Nijhoff
- Reinhorn, A.M., Riley, M.A. (1994) "Control of Bridge Vibrations with Hybrid Devices" First World Conference on Structural Control, 3-5 August, Los Angeles, California
- Reinhorn, A.M., Gluk, N., Gluk, J. and Levy, R. (1988) "Optimal Design of Supplemental Dampers for Control of Structures" 11th European Conference on Earthquake Engineering © 1998 Balkema, Rotterdam
- Riley, M.A., Reinhorn, A.M., Nagarajaiah, S., Subramaniam, R. (1994) "Control Algorithms for Structures with Hybrid Isolation Systems" Proceedings of the Fifth U.S. National Conference on Earthquake Engineering, EERI, Chicago, IL. pp 981-990

Rakheja, S. and Sankar, S. (1985) "Vibration and Shock Isolation Performance of a Semi-Active "On-Off" Damper" Transactions of the ASME, Journal of Vibration, Acoustics, Stress and Reliability in Design, Vol. 107, Oct. 1985, pp. 398-403

Sack, R.L., Kuo, C.C., Wu, H.C. and Patten, W.N. (1994) "Seismic Motion Control via Semiactive Hydraulic Actuators" Proceedings of the Fifth U.S. National Conference on Earthquake Engineering, Chicago, IL.

Sage, A.P. and White, C.C. (1977) Optimum Systems Control, Second Edition, Prentice Hall

Sakamoto, M., Kobori, T., Yamada, T., and Takahashi, M. (1994) "Practical Applications of Active and Hybrid Response Control Systems and Their Verifications by Earthquake and Strong Wind Observations" First World Conference on Structural Control, Los Angeles California, pp. WP2-90-99.

Samali, B., Yang, J.N., and Yeh, C.T. (1985) "Active Tendon Control System for Wind Excited Tall Building" Structural Control, Proceedings of the Second International Symposium on Structural Control, University of Waterloo, July 15-17, 1985, Ed. H.H.E. Leipholz, Martinus Nijhoff

Scholl, R. (1988) "Brace Dampers: An Alternative Structural System for Improving the Earthquake Performance of Buildings" Proceedings of the Eighth World Conference on Earthquake Engineering, San Francisco, CA. pp. 1015-1022.

Scott, Richard (2001) In the Wake of Tacoma, Suspension Bridges and the Quest for Aerodynamic Stability, American Society of Civil Engineers Press.

Shinozuka, M., Samaras, E. and Paliou, C. (1985) "Active Control of Floating Structures" Structural Control, Proceedings of the Second International Symposium on Structural Control, University of Waterloo, July 15-17, 1985, Ed. H.H.E. Leipholz, Martinus Nijhoff

Soong, T.T., Reinhorn, A.M., and Jang, J.N. (1985) "A Standardized Model for Structural Control Experiments and Some Experimental Results" Structural Control, Proceedings of the Second International Symposium on Structural Control, University of Waterloo, July 15-17, 1985, Ed. H.H.E. Leipholz, Martinus Nijhoff

Soong, T.T. (1988) "State of the Art Review Active Structural Control in Civil Engineering" Eng. Struct. Vol. 10, April. pp. 73 - 83

Soong, T.T. (1989) Active Control of Structures, Longman Scientific and Technical.

Soong, T.T., Masri, S., and Housner, G.W. (1991) "An Overview of Active Structural Control under Seismic Loads", Earthquake Spectra, Vol 7, No. 3., 1991, pp. 483-505.

Soong, T.T. (1999) "Structural Control, Impact on Structural Research in General", Proceedings of the Second World Conference on Structural Control, Kyoto, Japan, VI pp5-14.

- Stafford, F.B. and Masri, S.F. (1984) "Development of a Pulse Rocket for Earthquake Excitation of Structures" Proceedings of the Eight World Conference on Earthquake Engineering, San Francisco, CA, Vol. V. pp. 23-30.
- Sun, L.M., Fujino, Y., and Koga, K. (1995) "A Model of Tuned Liquid Damper for Suppressing Pitching Motions of Structures" Earthquake Engineering and Structural Dynamics, Vol. 24, pp. 625-636.
- Suzuki, T., Kageyama, M., Nobata, A., Inaba, S., Yoshida, O. (1994) "Active Vibration Control System Installed in a High-Rise Building" First World Conference on Structural Control, Los Angeles CA, USA. FP3-3 - FP3-11.
- Symans, M.D. and Constantino, M.C. (1996) "Semi-active Control of Earthquake Induced Vibration" Proceedings of the 11th World Conference on Earthquake Engineering, Acapulco, Mexico
- Sztrimbely, W.M. (1985) "Discontinuous Pulse Control of Longitudinal Vibrations within a Train Consist", Structural Control, Proceedings of the Second International Symposium on Structural Control, University of Waterloo, July 15-17, 1985, Ed. H.H.E. Leipholtz, Martinus Nijhoff
- Teramoto, T., Kitamura, H., Araki, K., Takada, K. (1988) "Application of Friction Damper to Highrise Buildings" 13th Congress of the International Association for Bridge and Structural Engineering, Helsinki, June 6-10
- Tremblay R., and Stierner, S.F. (1993) "Energy Dissipation Through Friction Bolted Connections in Concentrically Braced Steel Frames" ATC-17-1 Seminar on Seismic Isolation, Passive Energy Dissipation and Active Control, San Francisco, California, pp. 557-568.
- Tremblay, R. (1994) "Seismic behavior and design of friction concentrically braced frames for steel buildings", University of British Columbia, Ph.D. Thesis
- Vulcano, A. (1991) "Nonlinear Seismic Response of Damped Braced Frames" International Meeting on Earthquake Protection of Buildings, Ancona, June 6/8
- Weaver, H. Joseph (1983) Applications of Discrete and Continuous Fourier Analysis, Wiley Interscience.
- Wen, Y.K., and Shinozuka, M. (1994) "Cost-Effectiveness Issues in Active Structural Control" First World Conference on Structural Control, Los Angeles CA, USA. pp. FA3-19-28.
- Yamamoto, M. and Aizawa, S. (1994) "Control Effects of Active Mass Damper System Installed on Actual Buildings" First World Conference on Structural Control, Los Angeles CA, USA. pp. FP1-13-22.
- Yang, J.N., Akbarpour, A. and Ghaemmaghami, P. (1987) "New Optimal Control Algorithms for Structural Control" Journal of Engineering Mechanics, Vol. 113, No. 9, September, pp. 1369-1386.

- Yang, J.N., Danieliens, A., and Liu, S.C. (1991) "Aseismic Hybrid Control Systems for Building Structures" *Journal of Engineering Mechanics*, Vol. 117, No. 4, April, pp. 836-853.
- Yao, J.T.P. (1979) "Identification and Control of Structural Damage" *Structural Control*, H.H.E Leipholtz, Ed., IUTAM
- Yao, J.T.P. (1972) "Concept of Structural Control" *ASCE Journal of the Structural Division*, Vol. 98, pp. 1567-1574
- Yassien, H.A. (1994) "A Level Set Global Optimization Method for Nonlinear Engineering Problems" University of British Columbia PhD Thesis, and "LSP4 - A Demonstration Level Set Programming Tool For Global Optimization" program documentation obtained from author.
- Yue, C., Butsen, T. and Hendrick, J.K. (1989) "Alternative Control Laws for Automotive Active Suspensions" *Transactions of the ASME, Journal of Dynamic Systems, Measurement and Control*, Vol. 111, June, 1989, pp. 286-291.
- Zayas, V.A. and Low, S.S. (1989) "Earthquake Resistant Design using Friction Pendulum Connections" *Seismic Engineering Research and Practice*, eds. Charles A. Kircher and Anil K. Chopra, ASCE 1989, pp.149-158.
- Zhou, X.Y., Yu, R.F. and Dong, L. (2004) "The Complex Complete-Quadratic-Combination (CCQC) Method for Seismic Responses of Non-Classically Damped Linear MDOF System", 13th World Conference on Earthquake Engineering, Vancouver. No. 848
- Zuk, W. (1979) "The Past and Future of Active Structural Control Systems" *Structural Control*, H.H.E Leipholtz, Ed., IUTAM, 1980

Appendix A:

Solution of the Riccati Matrix

Appendix A: Solution of the Ricatti Matrix

A.1 The Time Variant vs the Time Invariant Ricatti Matrix

Chapter 2 developed the concepts of the Linear Quadratic Regulator problem and presented 3 methods for deriving the time independent Ricatti matrix as an intermediate step in determining the optimal gains. In this Appendix, the theoretical background is presented and an example is presented that illustrates the process of the solution of the Ricatti matrix. The form of the Ricatti matrix considered here in its time dependent form is

$$\dot{P}(t) + P(t)A - \frac{1}{2}P(t)BR^{-1}B^T + A^T P(t) + 2Q = 0, \quad P(t_f) = 0 \quad (\text{A.1})$$

The matrix A describes the dynamic properties of the structure, and B the influence of the control force. The matrices Q and R are the chosen weighting matrices that define the performance index (Equation 2.6, Chapter 2, with $H=0$). The Ricatti matrix, is used to determine the gain matrix, G , describing the feedback coefficients as follows

$$G(t) = -\frac{1}{2}R^{-1}B^T P(t). \quad (\text{A.2})$$

The gain matrix is time dependent if the Ricatti matrix is, and constant if the Ricatti matrix is time invariant.

By the exclusion of the excitation from Equation A.1 above, the Ricatti matrix is incapable of responding to the excitation, and therefore this implies that the time varying nature of the Ricatti matrix is independent of the excitation and depends only on the arbitrary choice of t_f .

Therefore it can be observed that the time varying character of the Ricatti matrix is of little practical value to the case of a structure subjected to an unknown excitation. The condition $P(t_f) = 0$ in Equation A.1 simply provides an initial assumption for the solution of the Ricatti matrix. Experience shows that under backward integration, the values of the Ricatti matrix rapidly approach stationary values. Based on the structure shown in Figure A.1, Figure A.2 shows a graph each of the 16 terms of a 4x4 matrix evolving under backward integration.

While backward integration of the Ricatti matrix may, at times, provide a convenient method for establishing the time independent Ricatti matrix coefficients, the stationary or time-independent

Ricatti matrix can be obtained directly without the need for backward integration through the solution of the time dependant Ricatti equation:

$$PA - \frac{1}{2}PBR^{-1}B^T P + A^T P + 2Q = 0 \quad (\text{A.3})$$

While the derivation of the optimal control gains do not consider the external excitation, optimality has been demonstrated for the case that the external excitation is a zero mean white noise process (Sage and White (1977)).

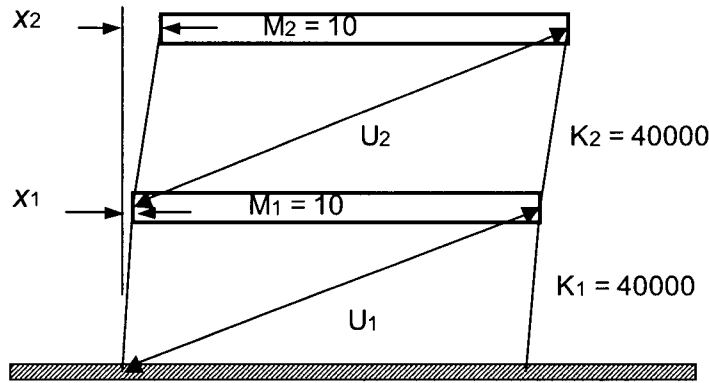


Figure A.1. 2DOF structure used to illustrate the solution of the time varying Ricatti matrix.

A.2 Linearized Solution of the Ricatti matrix

The solution of the time dependant Ricatti matrix under backward integration has been observed to be prone to numerical instabilities. Meirovitch offers a method for reducing the non-linear matrix equation to a linear equation that avoids potential numerical instabilities and helps to explain an algorithm (Potters algorithm) by which the Ricatti Matrix can be obtained directly without integration.

Consider that the Ricatti matrix $P(t)$ is given by the following product

$$P(t) = E(t)F^{-1}(t) \quad (\text{A.4})$$

The value of $\dot{P}(t)$ is given by the chain rule

$$\dot{P}(t) = \dot{E}(t)F^{-1}(t) + E(t)\dot{F}^{-1}(t) \quad (\text{A.5})$$

observing that

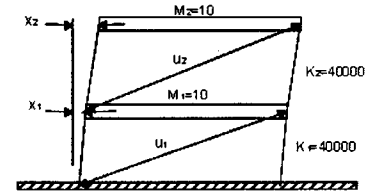
$$F^{-1}(t)F(t) = I \quad (\text{A.6})$$

Reconstruction of the Riccati Matrix
by backward integration

$$Q = \begin{bmatrix} 1 & -0.5 & 0 & 0 \\ -0.5 & 1 & 0 & 0 \\ 0 & 0 & 10 & 0 \\ 0 & 0 & 0 & 10 \end{bmatrix}$$

$$R = \begin{bmatrix} 0.001 & 0 \\ 0 & 0.001 \end{bmatrix}$$

Structure:



P =

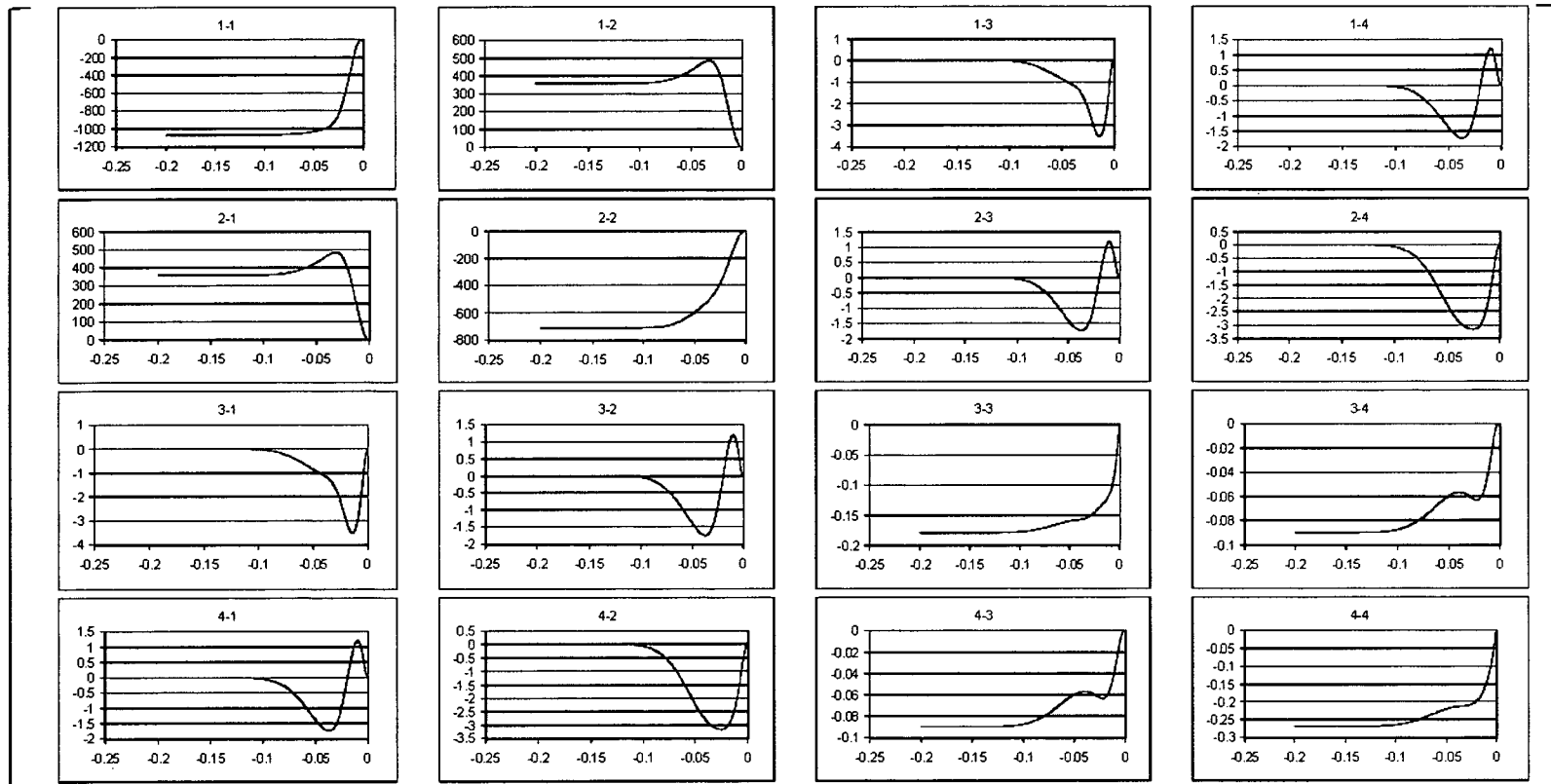


Figure A.2. Computation of the Riccati matrix by backward integration.

and after differentiating both sides of Equation A.6 with respect to time

$$\dot{F}^{-1}(t)F(t) + F^{-1}(t)\dot{F}(t) = 0 \quad (\text{A.7})$$

it follows that

$$\dot{F}^{-1}(t) = -F^{-1}(t)\dot{F}(t)F^{-1}(t) \quad (\text{A.8})$$

so that when substituted into Equation A.5 yields the expanded expression

$$\dot{P}(t) = \dot{E}(t)F^{-1}(t) - E(t)F^{-1}(t)\dot{F}(t)F^{-1}(t) \quad (\text{A.9})$$

By substituting Equations A.4 and A.9 into Equation A.1, the following equation is obtained

$$\begin{aligned} \dot{E}(t)F^{-1}(t) - E(t)F^{-1}(t)\dot{F}(t)F^{-1}(t) + E(t)F^{-1}(t)A - \frac{1}{2}E(t)F^{-1}(t)BR^{-1}B^T \\ + A^T E(t)F^{-1}(t) + 2Q = 0 \end{aligned} \quad (\text{A.10})$$

Multiplying on the right by $F(t)$, the following expression is obtained

$$\begin{aligned} \dot{E}(t) - E(t)F^{-1}(t)\dot{F}(t) + E(t)F^{-1}(t)AF(t) - \frac{1}{2}E(t)F^{-1}(t)BR^{-1}B^T F(t) \\ + A^T E(t) + 2QF(t) = 0 \end{aligned} \quad (\text{A.11})$$

Assuming that

$$\dot{E}(t) = -A^T E(t) - 2QF(t) \quad (\text{A.12})$$

and then substituting Equation A.12 in Equation A.11 and pre-multiplying by $(EF^{-1})^{-1}$ yields the following expression for $\dot{F}(t)$

$$\dot{F}(t) = -\frac{1}{2}BR^{-1}B^T E(t) + AF(t) \quad (\text{A.13})$$

Equations A.12 and A.13 can be written as the single step ordinary differential equation with constant coefficients

$$\begin{bmatrix} \dot{E}(t) \\ \dot{F}(t) \end{bmatrix} = \begin{bmatrix} -A^T & -2Q \\ -\frac{1}{2}BR^{-1}B^T & A \end{bmatrix} \begin{bmatrix} E(t) \\ F(t) \end{bmatrix} \quad (\text{A.14})$$

The expanded matrix can be evaluated using backward integration. By partitioning this matrix, the Ricatti matrix at any time can be evaluated by substituting into Equation A.4.

A.3 Potter's Algorithm

Backwards integration is a time consuming process whose success is dependent on the chosen integration time step. It is possible to directly find the time independent values of the Ricatti

matrix using a method called Potter's algorithm described in Meirovitch(1990). With Potter's algorithm we attempt to solve for the steady state values of the Ricatti matrix. Because the performance index used differs slightly from that used by Meirovitch, the method is re-derived here following the steps given by Meirovitch.

Using a constant Ricatti matrix in place of the time varying one derived above gives a constant set of feedback gains with which a near optimal control can be implemented.

In the steady state solution, the matrix $\dot{P}(t) \Rightarrow 0$ therefore the matrix Ricatti equation reduces to Equation A.3.

Consider the matrix

$$W = \frac{1}{2}BR^{-1}B^T P - A \quad (\text{A.15})$$

and write the (right) eigenvalue problem associated with W in the form

$$WF = FJ \quad (\text{A.16})$$

where F is the matrix of columns of eigenvectors and J is the diagonal matrix of eigenvalues.

Combining Equation A.3 and A.16 one can write an equation for PWF

$$PWF = 2QF + A^T PF = PFJ \quad (\text{A.17})$$

one can also write an expression for WF directly from Equation A.15

$$WF = \frac{1}{2}BR^{-1}B^T PF - AF = FJ \quad (\text{A.18})$$

Substituting $PF=E$, into Equation A.17 yields

$$A^T E + 2QF = EJ \quad (\text{A.19})$$

and Equations A.18 and A.19 can be combined in an equation similar to equation A.14.

$$\begin{bmatrix} A^T & 2Q \\ \frac{1}{2}BR^{-1}B^T & -A \end{bmatrix} \begin{bmatrix} E \\ F \end{bmatrix} = \begin{bmatrix} E \\ F \end{bmatrix} [J] \quad (\text{A.20})$$

or more simply as

$$[M] \begin{bmatrix} E \\ F \end{bmatrix} = \begin{bmatrix} E \\ F \end{bmatrix} [J] \quad (\text{A.21})$$

Equation A.21 is an eigenvalue problem containing $4n$ eigenvalues and associated eigenvectors. Of that only $2n$ are required to define matrices E and F . Therefore it is necessary to determine which eigenvalues are necessary to retain and discard the remainder. The eigenvalues of M that

need to be retained are those with positive real parts since these lead to convergence under backward integration. Retaining these $2n$ associated eigenvectors one can compile the square matrices E and F and subsequently compute the Ricatti matrix as

$$P = EF^{-1}, \quad (\text{A.22})$$

the time invariant version of Equation A.4.

In summary, to apply Potters algorithm the following steps are necessary:

1. Generate the $4n \times 4n$ matrix $\begin{bmatrix} A^T & 2Q \\ \frac{1}{2}BR^{-1}B^T & -A \end{bmatrix}$
2. Extract the (right) eigenvalues and eigenvectors
3. For each positive eigenvalue, compile the eigenvectors
4. Partition the eigenvectors into $2n$ square E and F matrices
5. compute $P = EF^{-1}$

A.4 Example Solution of the Time Invariant Ricatti Matrix

Given a 4-story uniform shear structure pictured in Figure A.3, the equations of motion can be written in the form

$$M\ddot{x} + C\dot{x} + Kx + Bu = -Lg(t) \quad (\text{A.23})$$

by defining the following mass, stiffness and damping matrices

$$M = \begin{bmatrix} 10 & 0 & 0 & 0 \\ 0 & 10 & 0 & 0 \\ 0 & 0 & 10 & 0 \\ 0 & 0 & 0 & 10 \end{bmatrix} \quad (\text{A.24})$$

$$K = \begin{bmatrix} 2400 & -1200 & 0 & 0 \\ -1200 & 2400 & -1200 & 0 \\ 0 & -1200 & 2400 & -1200 \\ 0 & 0 & -1200 & 1200 \end{bmatrix} \quad (\text{A.25})$$

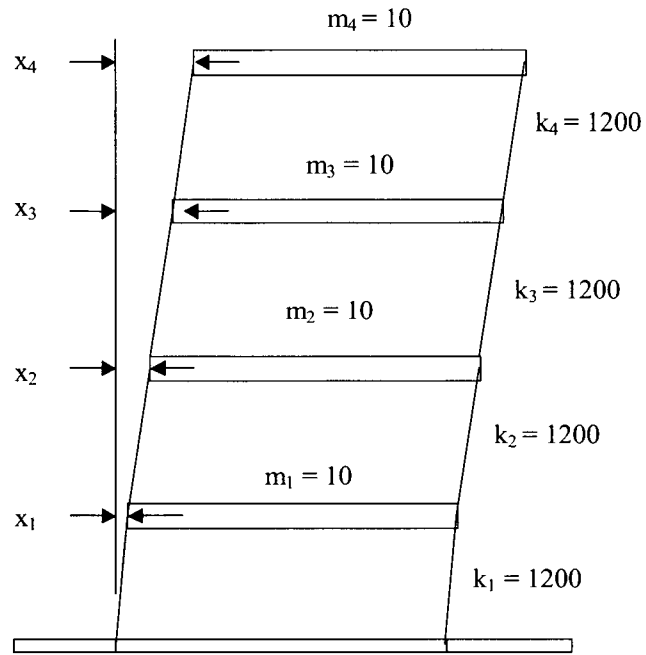


Figure A.3. 4-Story regular moment frame structure.

$$C = \begin{bmatrix} 13 & -6 & 0 & 0 \\ -6 & 13 & -6 & 0 \\ 0 & -6 & 13 & -6 \\ 0 & 0 & -6 & 7 \end{bmatrix} \quad (\text{A.26})$$

the state-space representation of the equation of motion can be expressed in the form

$$\dot{\bar{x}} = A\bar{x} + Bu + \bar{L}g(t) \quad (\text{A.27})$$

where \bar{x} is the state vector defined as

$$\bar{x} = \begin{bmatrix} x \\ \dot{x} \end{bmatrix} \quad (\text{A.28})$$

by defining the following matrices

$$A = \begin{bmatrix} 0 & I \\ -M^{-1}K & -M^{-1}C \end{bmatrix} = \begin{bmatrix} 0 & 0 & 0 & 0 & 1 & 0 & 0 & 0 \\ 0 & 0 & 0 & 0 & 0 & 1 & 0 & 0 \\ 0 & 0 & 0 & 0 & 0 & 0 & 1 & 0 \\ 0 & 0 & 0 & 0 & 0 & 0 & 0 & 1 \\ -1.3 & 0.6 & 0 & 0 & -240 & 120 & 0 & 0 \\ -0.6 & -1.3 & 0.6 & 0 & 120 & -240 & 120 & 0 \\ 0 & 0.6 & -1.3 & 0.6 & 0 & 120 & -240 & 120 \\ 0 & 0 & 0.6 & -0.7 & 0 & 0 & 120 & -120 \end{bmatrix} \quad (\text{A.29})$$

$$B = \begin{bmatrix} 0 & 0 & 0 & 0 \\ 0 & 0 & 0 & 0 \\ 0 & 0 & 0 & 0 \\ 0 & 0 & 0 & 0 \\ -0.1 & 0.1 & 0 & 0 \\ 0 & -0.1 & 0.1 & 0 \\ 0 & 0 & -0.1 & 0.1 \\ 0 & 0 & 0 & -0.1 \end{bmatrix} \quad (\text{A.30})$$

find the control that minimizes the performance function defined by

$$J = \frac{1}{2} \int_{t_0}^{t_f} [\bar{x}^T(t)Q\bar{x}(t) + \bar{u}^T(t)R\bar{u}(t)] dt \quad (\text{A.31})$$

where

$$Q = \begin{bmatrix} 1200 & 0 & 0 & 0 & & & & \\ 0 & 1200 & 0 & 0 & & & & \\ 0 & 0 & 1200 & 0 & & & & \\ 0 & 0 & 0 & 1200 & & & & \\ & & & & 10 & 0 & 0 & 0 \\ & & & & 0 & 10 & 0 & 0 \\ & & 0 & & 0 & 0 & 10 & 0 \\ & & & & 0 & 0 & 0 & 10 \end{bmatrix} \quad (\text{A.32})$$

$$R = 0.1I = \begin{bmatrix} 0.1 & 0 & 0 & 0 \\ 0 & 0.1 & 0 & 0 \\ 0 & 0 & 0.1 & 0 \\ 0 & 0 & 0 & 0.1 \end{bmatrix} \quad (\text{A.33})$$

Determining the gain matrix G such that

$$\bar{u}(t) = G\bar{x}(t) \quad (\text{A.34})$$

satisfies the optimality condition bringing the structure to the zero-state in the absence of an external disturbance $g(t)$.

Find the Ricatti matrix by

- i) Direct backward integration
- ii) Potter's algorithm

Verify that the structure is stable under the applied control by examining the system poles and discuss the significance of the results obtained.

A.4.1 Solution

In order to establish the gain matrix we must first evaluate the Ricatti matrix. First, presuming that at a final time t_f were defined in the problem, the time varying evolution of the Ricatti matrix is obtained. Then, utilizing Potter's algorithm the steady state value of the Ricatti matrix is determined directly.

A.4.1.1 Reverse Integration

The non-linear differential equation describing the evolution of the Ricatti equation is as follows:

$$\dot{P}(t) = -2Q - P(t)A - A^T P(t) + \frac{1}{2}P(t)BR^{-1}B^T P(t) \quad (\text{A.35})$$

Assuming that at t_f the Ricatti matrix is an 8×8 matrix of zeros, backward integration can proceed as follows: Presuming that the time step is short enough to permit the assumption of constant velocity, then

$$P_{n+1} = P_n - \dot{P}\Delta t \quad (\text{A.36})$$

Applying this algorithm with a sufficiently short time step and a sufficiently large n , the steady state will be reached. Since plotting all 64 elements of the Ricatti matrix is too onerous, only selected values are plotted in the graphs of Figure A.4.

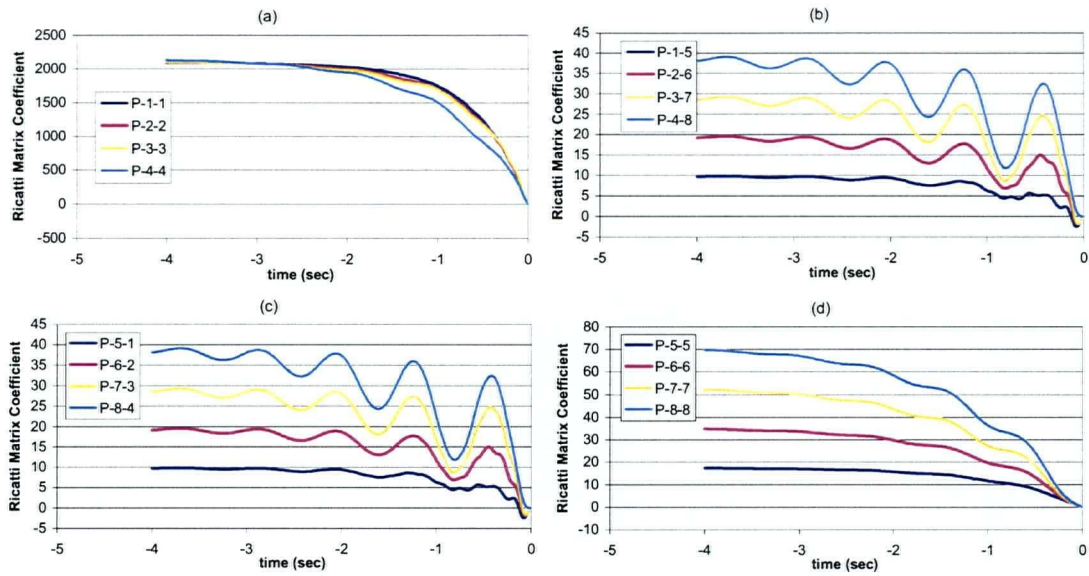


Figure A.4. Evolution of Riccati matrix main diagonal terms under backward integration.

The final (steady-state) value of the Riccati matrix is given as follows:

$$P = \begin{bmatrix} 2095.2 & 28.0 & 10.0 & 5.6 & 9.8 & 9.6 & 9.5 & 9.5 \\ 28.0 & 2105.2 & 33.5 & 15.6 & 9.6 & 19.3 & 19.1 & 19.0 \\ 10.0 & 33.5 & 2110.9 & 43.6 & 9.5 & 19.1 & 28.2 & 28.6 \\ 5.6 & 15.6 & 43.6 & 2138.7 & 9.5 & 19.0 & 28.6 & 38.4 \\ 9.8 & 9.6 & 9.5 & 9.5 & 17.4 & 17.5 & 17.5 & 17.4 \\ 9.6 & 19.3 & 19.1 & 19.0 & 17.5 & 34.9 & 35.0 & 34.9 \\ 9.5 & 19.1 & 28.8 & 28.6 & 17.5 & 35.0 & 52.3 & 52.4 \\ 9.5 & 19.0 & 28.6 & 38.4 & 17.4 & 34.9 & 52.4 & 69.9 \end{bmatrix} \quad (\text{A.37})$$

Substituting this matrix into the matrix Riccati equation verifies that the equation is satisfied.

The gain matrix is determined by

$$G = -\frac{1}{2} R^{-1} B^T P \quad (\text{A.38})$$

Substitution of the Riccati matrix and the R and B matrices into this equation yields the associated gain matrix

$$G = \begin{bmatrix} 4.894 & 4.812 & 4.756 & 4.728 & 8.712 & 8.762 & 8.738 & 8.717 \\ -0.083 & 4.839 & 4.784 & 4.756 & 0.049 & 8.689 & 8.740 & 8.738 \\ -0.056 & -0.111 & 4.839 & 4.812 & -0.024 & 0.028 & 8.869 & 8.762 \\ -0.028 & -0.056 & -0.083 & 4.895 & -0.021 & -0.028 & 0.049 & 8.712 \end{bmatrix} \quad (\text{A.39})$$

The stability of the control can be checked by examining the poles of the system

$$\dot{\bar{x}} = (A + BG)\bar{x} \quad (\text{A.40})$$

as discussed in Chapter 2, the poles of the system are simply the eigenvalues of the matrix $A+BG$. For the given system the following eigenvalues are obtained

$$\lambda_{(A+BG)} = \begin{bmatrix} -1.5376 + 20.5423i \\ -1.5376 - 20.5423i \\ -1.1855 + 16.7562i \\ -1.1855 - 16.7562i \\ -0.7879 + 10.9488i \\ -0.7879 - 10.9488i \\ -0.5228 + 3.8035i \\ -0.5228 - 3.8035i \end{bmatrix} \quad (\text{A.41})$$

which all fall in the left hand plane (have negative real parts). Therefore, under the action of the control force given by the gain matrix, the structure is stable. By comparison, the original poles of the uncontrolled structure are given as follows

$$\lambda_{(A)} = \begin{bmatrix} -1.1096 + 20.5577i \\ -1.1096 - 20.5577i \\ -0.7542 + 16.7662i \\ -0.7542 - 16.7662i \\ -0.3500 + 10.9489i \\ -0.3500 - 10.9489i \\ -0.0862 + 3.8035i \\ -0.0862 - 3.8035i \end{bmatrix} \quad (\text{A.42})$$

The action of the control force is to shift the poles toward the real axis and further along the negative real axis

A.4.1.2 Potter's Algorithm

Potter's algorithm is derived in Chapter 2. With Potter's algorithm the matrix

$$M = \begin{bmatrix} -A^T & -2Q \\ -\frac{1}{2}BR^{-1}B^T & A \end{bmatrix} \quad (\text{A.43})$$

is constructed. The eigenvalues and eigenvectors are evaluated and the ones with positive real parts are retained. Based on the values above, the retained eigenvalues are evaluated to be

$$\lambda^+_{(M)} = \begin{bmatrix} -1.538 + 20.542i \\ -1.538 - 20.542i \\ -1.186 + 16.756i \\ -1.186 - 16.756i \\ -0.789 + 10.949i \\ -0.789 - 10.949i \\ -0.532 + 3.832i \\ -0.532 - 3.832i \end{bmatrix} \quad (\text{A.44})$$

and associated eigenvectors are defined by the following

$$\phi^+_{(M)} = \begin{bmatrix} E \\ F \end{bmatrix} \quad (\text{A.45})$$

and enumerated as follows

$$E = \begin{bmatrix} 0.368 - 0.218i & 0.368 + 0.218i & -0.078 - 0.651i & -0.078 + 0.651i & -0.481 - 0.315i & -0.481 + 0.315i & -0.114 - 0.189i & -0.114 + 0.189i \\ -0.565 + 0.334i & -0.565 - 0.334i & 0.027 + 0.226i & 0.027 - 0.226i & -0.481 - 0.314i & -0.481 + 0.314i & -0.214 - 0.355i & -0.214 + 0.355i \\ 0.497 - 0.293i & 0.497 + 0.293i & 0.693 + 0.572i & 0.693 - 0.572i & 0 & 0 & -0.289 - 0.479i & -0.289 + 0.479i \\ -0.196 + 0.116i & -0.196 - 0.116i & -0.052 - 0.425i & -0.052 + 0.425i & 0.481 + 0.315i & 0.481 - 0.315i & -0.328 - 0.545i & -0.328 + 0.545i \\ -0.011 - 0.018i & -0.011 + 0.018i & -0.039 + 0.005i & -0.039 - 0.005i & -0.030 + 0.043i & -0.030 - 0.043i & -0.052 + 0.022i & -0.052 - 0.022i \\ 0.017 + 0.027i & 0.017 - 0.027i & 0.013 - 0.002i & 0.013 + 0.002i & -0.030 + 0.043i & -0.030 - 0.043i & -0.098 + 0.041i & -0.098 - 0.041i \\ -0.015 - 0.023i & -0.015 + 0.023i & 0.034 - 0.004i & 0.034 + 0.004i & 0 & 0 & -0.133 + 0.055i & -0.133 - 0.055i \\ 0.006 + 0.009i & 0.006 - 0.009i & -0.025 + 0.003i & -0.025 - 0.003i & 0.030 - 0.043i & 0.030 + 0.043i & -0.151 + 0.063i & -0.151 - 0.063i \end{bmatrix} \quad (\text{A.46})$$

$$F = \begin{bmatrix} 0.182 - 0.101i & 0.182 + 0.101i & -0.027 - 0.314i & -0.027 + 0.314i & -0.220 - 0.160i & -0.220 + 0.160i & -0.039 - 0.092i & -0.039 + 0.092i \\ -0.279 + 0.154i & -0.279 - 0.154i & 0.009 + 0.109i & 0.009 - 0.109i & -0.220 - 0.160i & -0.220 + 0.160i & -0.073 - 0.173i & -0.073 + 0.173i \\ 0.245 - 0.136i & 0.245 + 0.136i & 0.024 + 0.277i & 0.024 - 0.277i & 0 & 0 & -0.099 - 0.233i & -0.099 + 0.233i \\ -0.097 + 0.054i & -0.097 - 0.054i & -0.018 - 0.205i & -0.018 + 0.205i & 0.220 + 0.160i & 0.220 - 0.160i & -0.112 - 0.265i & -0.112 + 0.265i \\ -2.346 - 3.581i & -2.346 + 3.581i & -5.236 + 0.828i & -5.236 - 0.828i & -1.581 + 2.529i & -1.581 - 2.529i & -0.332 + 0.373i & -0.332 - 0.373i \\ 3.594 + 5.487i & 3.594 - 5.487i & 1.819 - 0.288i & 1.819 + 0.288i & -1.581 + 2.529i & -1.581 - 2.529i & -0.624 + 0.373i & -0.624 - 0.373i \\ -3.161 - 4.825i & -3.161 + 4.825i & 4.605 - 0.728i & 4.605 + 0.728i & 0 & 0 & -0.841 + 0.503i & -0.841 - 0.503i \\ 1.248 + 1.906i & 1.248 - 1.906i & -3.418 + 0.541i & -3.418 - 0.541i & 1.581 - 2.529i & 1.581 + 2.529i & -0.957 + 0.572i & -0.957 - 0.572i \end{bmatrix} \quad (\text{A.47})$$

The Ricatti matrix is evaluated as

$$P = EF^{-1} \quad (\text{A.48})$$

yielding

$$P = \begin{bmatrix} 2098.5 & 33.0 & 15.2 & 10.2 & 9.9 & 9.9 & 9.8 & 9.8 \\ 33.0 & 2113.7 & 43.3 & 25.4 & 9.9 & 19.7 & 19.7 & 19.6 \\ 15.2 & 43.3 & 2123.9 & 58.4 & 9.8 & 19.7 & 29.5 & 29.5 \\ 10.2 & 25.4 & 58.4 & 2156.9 & 9.8 & 19.6 & 29.5 & 34.4 \\ 9.9 & 9.9 & 9.8 & 9.8 & 17.6 & 17.8 & 17.9 & 17.9 \\ 9.9 & 19.7 & 19.7 & 19.6 & 17.8 & 35.5 & 35.7 & 35.8 \\ 9.8 & 19.7 & 29.5 & 29.5 & 17.9 & 35.7 & 53.4 & 53.6 \\ 9.8 & 19.6 & 29.5 & 39.4 & 17.9 & 35.8 & 53.6 & 71.2 \end{bmatrix} \quad (\text{A.49})$$

The Ricatti matrix is nearly exactly the same as that obtained using backward integration. The resulting gain matrix and its stable damping effect on the structure have already been shown

A.5 Significance of the Results

The preceding numerical example illustrates the steps required to obtain the gain matrix associated with the optimal active control of the structure. The optimal solution is dependant on the choices of the Q and R matrices. The Q matrix represents the weighting placed on the response of the structure while the R matrix represents the weighting placed on the control effort. With the Q matrix, a simple diagonal form was chosen with the portion related to displacements weighted by stiffness and the portion related to velocities weighted by mass. The R -matrix is chosen as proportional to an identity matrix indicating that even weighting is placed at each damper location. The ratio of the Q to the R matrix controls the strength of the control and as chosen, the control strength is governed by the choice of a single factor modifying the R matrix. In this way the design problem is simplified by reducing the number of choices to a manageable number.

The poles of the uncontrolled structure contain both real and imaginary parts, located nearer the imaginary axis than the real. This is indicative of a lightly damped structure. The controlled structure pushes the poles to the left with increasing ratio of Q to R .

While more involved numerically, Potter's algorithm was able to directly compute the time invariant Ricatti matrix directly. It was found that more than about 400 time steps of backward integration was required to retain reasonable accuracy, entailing approximately 3×10^6 floating point operations. Potter's algorithm, on the other hand achieved the same result in about 143,000

floating point operations, about 20 times faster. One of the problems with the backward integration scheme is that the length of the time step is sensitive to the highest frequencies included in the system dynamics. The presence of high frequencies is apparent from the roughness of the curves describing the evolution of some of the terms in the Ricatti matrix. It is therefore apparent that significant numerical advantage is derived from using Potter's algorithm.

Appendix B:
Performance Index Study

Appendix B: Performance Index Study

B.1 Control Structure

The LQ regulator control based on the minimization of the quadratic performance index

$$J = \int_{t_0}^{t_f} (x^T Q x + u^T R u) dt \quad (\text{B.1})$$

after solution of the optimization problem leads to the equation for the full state gain

$$G = -\frac{1}{2} R^{-1} B^T P \quad (\text{B.2})$$

The validity of this expression was investigated numerically by using a perturbation technique. The value of G was varied through multiplication by a constant and the value of the integral of Equation B.1 was computed. Three artificial time histories, shown in Figure B.1 were used. The structure used was a 6-story uniform shear structure having mass and stiffness given as follows:

$$k = \begin{bmatrix} 2400 & -1200 & 0 & 0 & 0 & 0 \\ -1200 & 2400 & -1200 & 0 & 0 & 0 \\ 0 & -1200 & 2400 & -1200 & 0 & 0 \\ 0 & 0 & -1200 & 2400 & -1200 & 0 \\ 0 & 0 & 0 & -1200 & 2400 & -1200 \\ 0 & 0 & 0 & 0 & -1200 & 1200 \end{bmatrix} \quad (\text{B.3})$$

$$m = \begin{bmatrix} 10 & 0 & 0 & 0 & 0 & 0 \\ 0 & 10 & 0 & 0 & 0 & 0 \\ 0 & 0 & 10 & 0 & 0 & 0 \\ 0 & 0 & 0 & 10 & 0 & 0 \\ 0 & 0 & 0 & 0 & 10 & 0 \\ 0 & 0 & 0 & 0 & 0 & 10 \end{bmatrix} \quad (\text{B.4})$$

and

$$c = \begin{bmatrix} 13 & -6 & 0 & 0 & 0 & 0 \\ -6 & 13 & -6 & 0 & 0 & 0 \\ 0 & -6 & 13 & -6 & 0 & 0 \\ 0 & 0 & -6 & 13 & -6 & 0 \\ 0 & 0 & 0 & -6 & 13 & -6 \\ 0 & 0 & 0 & 0 & -6 & 7 \end{bmatrix} \quad (\text{B.5})$$

The control parameters were taken to be

$$Q = \begin{bmatrix} 2400 & -1200 & 0 & 0 & 0 & 0 & 0 & 0 & 0 & 0 & 0 & 0 \\ -1200 & 2400 & -1200 & 0 & 0 & 0 & 0 & 0 & 0 & 0 & 0 & 0 \\ 0 & -1200 & 2400 & -1200 & 0 & 0 & 0 & 0 & 0 & 0 & 0 & 0 \\ 0 & 0 & -1200 & 2400 & -1200 & 0 & 0 & 0 & 0 & 0 & 0 & 0 \\ 0 & 0 & 0 & -1200 & 2400 & -1200 & 0 & 0 & 0 & 0 & 0 & 0 \\ 0 & 0 & 0 & 0 & -1200 & 1200 & 0 & 0 & 0 & 0 & 0 & 0 \\ 0 & 0 & 0 & 0 & 0 & 0 & 10 & 0 & 0 & 0 & 0 & 0 \\ 0 & 0 & 0 & 0 & 0 & 0 & 0 & 10 & 0 & 0 & 0 & 0 \\ 0 & 0 & 0 & 0 & 0 & 0 & 0 & 0 & 10 & 0 & 0 & 0 \\ 0 & 0 & 0 & 0 & 0 & 0 & 0 & 0 & 0 & 10 & 0 & 0 \\ 0 & 0 & 0 & 0 & 0 & 0 & 0 & 0 & 0 & 0 & 10 & 0 \\ 0 & 0 & 0 & 0 & 0 & 0 & 0 & 0 & 0 & 0 & 0 & 10 \end{bmatrix} \quad (\text{B.6})$$

and

$$R = \begin{bmatrix} 0.02 & 0 & 0 & 0 & 0 & 0 \\ 0 & 0.02 & 0 & 0 & 0 & 0 \\ 0 & 0 & 0.02 & 0 & 0 & 0 \\ 0 & 0 & 0 & 0.02 & 0 & 0 \\ 0 & 0 & 0 & 0 & 0.02 & 0 \\ 0 & 0 & & & & 0.02 \end{bmatrix} \quad (\text{B.7})$$

The control problem was solved and the full state gain matrix was obtained. Presuming dampers at every story, the observer matrix was

$$C = \begin{bmatrix} 0 & 0 & 0 & 0 & 0 & 0 \\ 0 & 0 & 0 & 0 & 0 & 0 \\ 0 & 0 & 0 & 0 & 0 & 0 \\ 0 & 0 & 0 & 0 & 0 & 0 \\ 0 & 0 & 0 & 0 & 0 & 0 \\ 0 & 0 & 0 & 0 & 0 & 0 \\ 1 & 0 & 0 & 0 & 0 & 0 \\ -1 & 1 & 0 & 0 & 0 & 0 \\ 0 & -1 & 1 & 0 & 0 & 0 \\ 0 & 0 & -1 & 1 & 0 & 0 \\ 0 & 0 & 0 & -1 & 1 & 0 \\ 0 & 0 & 0 & 0 & -1 & 1 \end{bmatrix} \quad (\text{B.8})$$

and the fully populated observer feedback matrix was computed using the formula

$$G_2 = GC^T(CC^T)^{-1} \quad (\text{B.9})$$

The truncated observer matrix was extracted from the observer feedback matrix as follows

$$G_3 = \text{diag}(G_2) \quad (\text{B.10})$$

each of the three gain matrices were scaled and individually incorporated into the structural model. The input time histories were each applied and the performance index evaluated.

B.2 Findings

Averages of the performance indices obtained are plotted in Figure B.2. It was found that at a scale factor of unity, the full state gain matrix gave rise to the minimum performance index. With the observer feedback, however the minimum of the performance index was found for a scale factor between 1 and 2, and for the truncated feedback, the scale factor leading to the minimum performance index was found to be approximately 5.

B.3 Conclusions

It is concluded that

- 1) the expression for optimal full state gain matrix, Equation B.2 does give rise to the minimum performance index;
- 2) the fully populated square observer feedback matrix is a close approximation to the full state feedback with an absolute minimum at a scale factor of between 1 and 2
- 3) the truncated feedback provides a weak control. Comparable performance levels would only result if the gain matrix is scaled up by a factor of about 5.

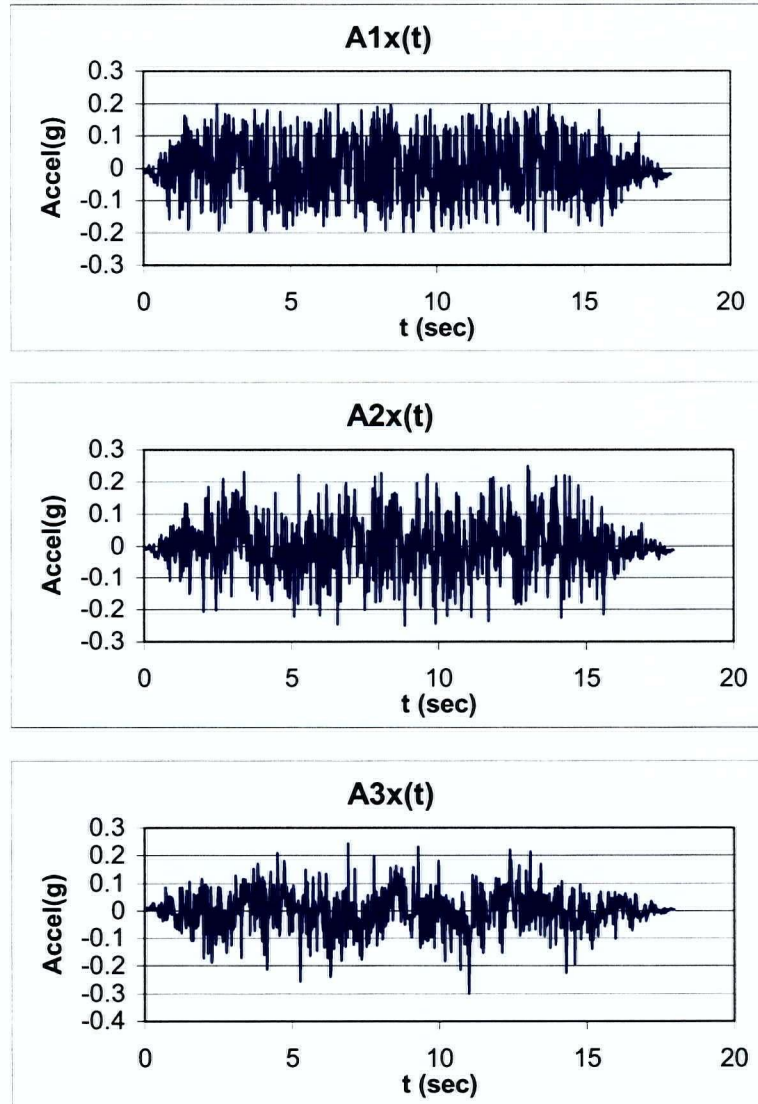


Figure B.1. Three artificial time histories used to simulate control response. Artificial time histories were generated using the program Simquake, Gasparini and Vanmarke (1976)

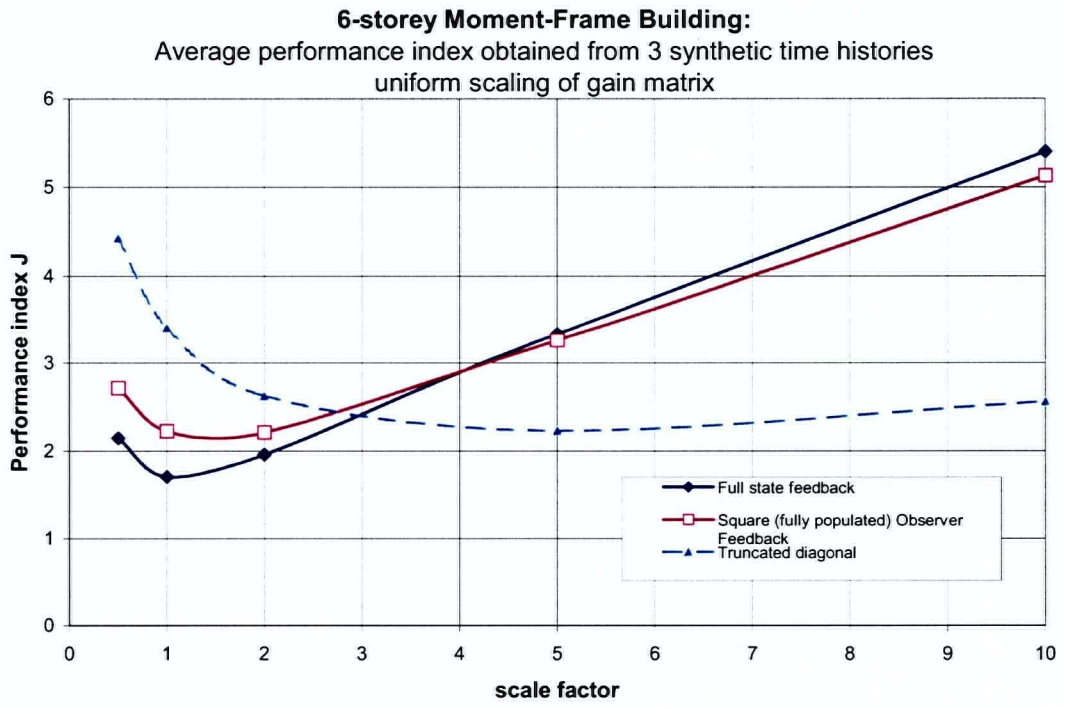


Figure B.2. Values of performance index obtained for (1) Full state feedback; (2) Observer feedback, and (3) Truncated observer feedback.

Appendix C:

3-D Response Spectra

Appendix C: 3-D Response Spectra

C.1 Background

Response spectral analysis (RSA) is the process of combining mode response components in order to estimate envelope values of the earthquake response of the structure. In a classical RSA, the mode shapes and frequencies are extracted from an undamped modal analysis. The damping relating to each mode is determined in the assessment through the choice of the response spectra curve. The response spectra curve provides the peak amplitude expected for a single degree of freedom structure with the selected damping having varying frequencies (or periods) over the practical range of structural frequencies (or periods) to be expected. A family of response spectra curves exists for varying damping values.

Multi-degree of freedom structures, by nature, possess multiple mode shapes, associated frequencies and damping coefficients. Associated with each mode is a participation factor that quantifies the level to which the excitation can excite the particular mode. In a classical RSA damping is presumed not to affect the mode shapes. If this is the case analysis using the suite of response spectra curves is acceptable. Normally, the response spectrum curve is chosen to correspond to the damping in the first few contributing modes.

The relative contributions of each mode are determined as a product of the spectral ordinate and the participation factor. Typically, high frequency modes are not excited as much by earthquake excitation and receive a low participation factor.

The more rigorous derivation of the equations of motion for the non-classically damped structure in state space form given in Chapter 5 has shown that the general relationship is more complex requiring two general functions of period and damping as a basis. The assumption that undamped mode shapes provide a sufficient basis for the assessment of a particular structure is not true in general, particularly for structures with discrete dampers whose mode shapes are strongly affected by the local effects of the dampers. Therefore the procedure developed in Chapter 5 differs in many ways from the classical procedure described above.

Basing the modal analysis on the state-space description of the equations of motion, the modal combination proceeds on the basis of the damped mode shapes, frequencies and participation factors.

Identifying that the integrals in Equation 5.51 repeated below in Equation C.1 provide the time history response of a structure with a pair of poles given by $(\zeta, \pm \omega)$

$$\begin{aligned} S^C(t) &= \int_0^t e^{\zeta(t-\tau)} \cos(\omega(t-\tau)) \ddot{x}_g(\tau) d\tau \\ S^S(t) &= \int_0^t e^{\zeta(t-\tau)} \sin(\omega(t-\tau)) \ddot{x}_g(\tau) d\tau \end{aligned} \quad (C.1)$$

The absolute maxima of each of the above functions

$$\begin{aligned} S_{\max}^C(\zeta, \omega) &= \max(|S^C(t)|) = \max\left(\left|\int_0^t e^{\zeta(t-\tau)} \cos(\omega(t-\tau)) \ddot{x}_g(\tau) d\tau\right|\right) \\ S_{\max}^S(\zeta, \omega) &= \max(|S^S(t)|) = \max\left(\left|\int_0^t e^{\zeta(t-\tau)} \sin(\omega(t-\tau)) \ddot{x}_g(\tau) d\tau\right|\right) \end{aligned} \quad (C.2)$$

express the envelope response functions to be used in the RSA.

Several earthquakes were investigated and their 3-D Sine and Cosine response spectra were evaluated. The earthquakes are listed in Table C.1. Log Plots of the spectra appear in Figures C.1 (a) and (b) through C.8 (a) and (b).

C.2 General Observations

The plots obtained for the Sine and Cosine curves all have the same basic shape. The real coefficient corresponds to the damping, ζ , while the positive or negative imaginary coefficient corresponds to the response frequency, ω . The units of the response for acceleration input correspond to velocity as seen from the integration with respect to time in Equations C.1 and C.2. All graphs display a hump for small real coefficient, corresponding to a lightly damped structure, which decreases substantially with increasing ζ . After the hump, both Sine and Cosine surfaces drop to zero. However for small imaginary coefficients the Cosine surfaces reaches a plateau, while the Sine surface drop to zero. Other than for frequencies below the

hump, the character of the surfaces is very similar, but not identical. Individual curves display many “spikes”. It is interesting to note that the ridges associated with each spike subside and get smoother on lines running parallel to the Real (ζ) axis.

Traditional response spectra are part of the surfaces presented. Figure C.9 illustrates the relationship of the pole locations in the real and imaginary plane corresponding to particular damping coefficients. The curve traced along $\zeta=0$ corresponds to the undamped spectra while the curve traced along $\omega=0$ corresponds to both critical and super-critical damping. For critical and Super-critical damping, only the Cosine curve contributes to the response as the Sine curve is equal to zero along $\omega=0$.

The earthquakes chosen have different characteristics. The two records used in the bulk of the example analyses are given in Figures C.1 and C.2. Whereas El Centro displays several smooth spikes and ridges, The San Fernando displays one prominent peak and ridge. The response for the San-Fernando record is influenced by a single story structure, and subsequently, the dominant peak may be a result of its local influence. Hachinohe, Figure C.3, is a long duration soil record. Four distinct and well-separated spikes are displayed, the first of which has an imaginary coefficient of about 7, corresponding to an undamped frequency of just over 1 Hz. UCSC Los Gatos Presentation Centre is a near field rock motion influenced a the name implies by a structure. Several low rounded spikes and one dominant spike are observed. The dominant spike corresponds to a frequency of about 4Hz. The Ofunato Bochi record is a long duration record on rock. This record shows a cluster of high frequency spikes with the highest corresponding to about 5Hz. Further inferences are left to the reader.

C.3 Conclusions and Recommendations

It is suggested that the information in this format provides a more complete tool for the analysis of structures and also for the characterization of earthquakes. Individual earthquake records characterized by these surfaces may provide additional information not apparent when using the traditional 5% damped spectra curves. This study is outside the scope of this thesis.

Application of the RSA technique in design requires a different sort of input. Characterization of a design event requires a curve that represents a typical or an envelope curve (surface) that captures the characteristics of an event or events associated with the performance criteria.

Uniform hazard spectra are often derived for such a purpose using the 5% damped structure as a basis. It would be useful to extend such hazard assessments to cover the whole range of structural inputs such that structures with low and high damping, and more importantly structures containing modes with both low and high damping can be analysed and designed.

Table C.1: Selected Earthquakes for Evaluation of 3-D State-Space Response Spectra

Earthquake	Date	Magnitude	Record Site	Epicentral Dist	Record Type	Component	Site characteristics
IMPERIAL VALLEY EARTHQUAKE	May 18, 1940	6.5	EL CENTRO	11.3	Corrected	0 90 UP	Commonly used record
SAN FERNANDO EARTHQUAKE	February 9, 1971		LAKE HUGHES, ARRAY STATION 12	24.3	Corrected	N21E	one storey building Commonly used record
TOKACHI-OKI EARTHQUAKE	May 16, 1968	7.9	HACHINOHE HARBOUR	187	Corrected	NS EW UD	Long Duration Soil Record
LOMA PRIETA EARTHQUAKE	October 18, 1989	-	LOS GATOS PRESENTATION CENTER	-	Corrected	0 90 UP	Near Fault motion on Rock
MIYAGI-OKI EARTHQUAKE	June 12, 1978	7.4	OFUNATO BOCHI RECORD	116	Corrected	41 131 UP	Long Duration Rock Record
OLYMPIA EARTHQUAKE	April 13, 1949	-	SEATTLE ARMY BASE RECORD	47	Corrected	182 272 UP	GROUND LEVEL 1 STORY BLDG. Long Duration Soil Record
NORTHRIDGE EARTHQUAKE	January 17, 1994	-	SYLMAR CONVERTER STATION RECORD	-	Corrected	0 90 UP	Near Fault Motion on Soil
KERN COUNTY, CA EARTHQUAKE	July 21, 1952	7.2	TAFT LINCOLN SCHOOL TUNNEL RECORD	41.45	Corrected	21 111 UP	Commonly used record

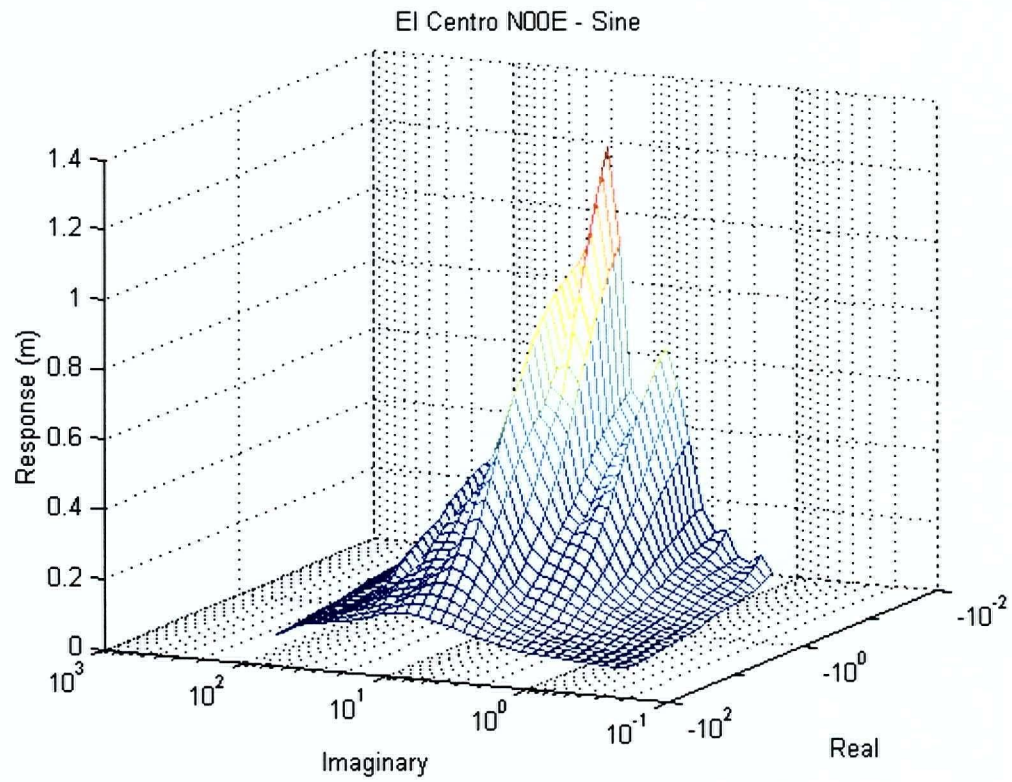
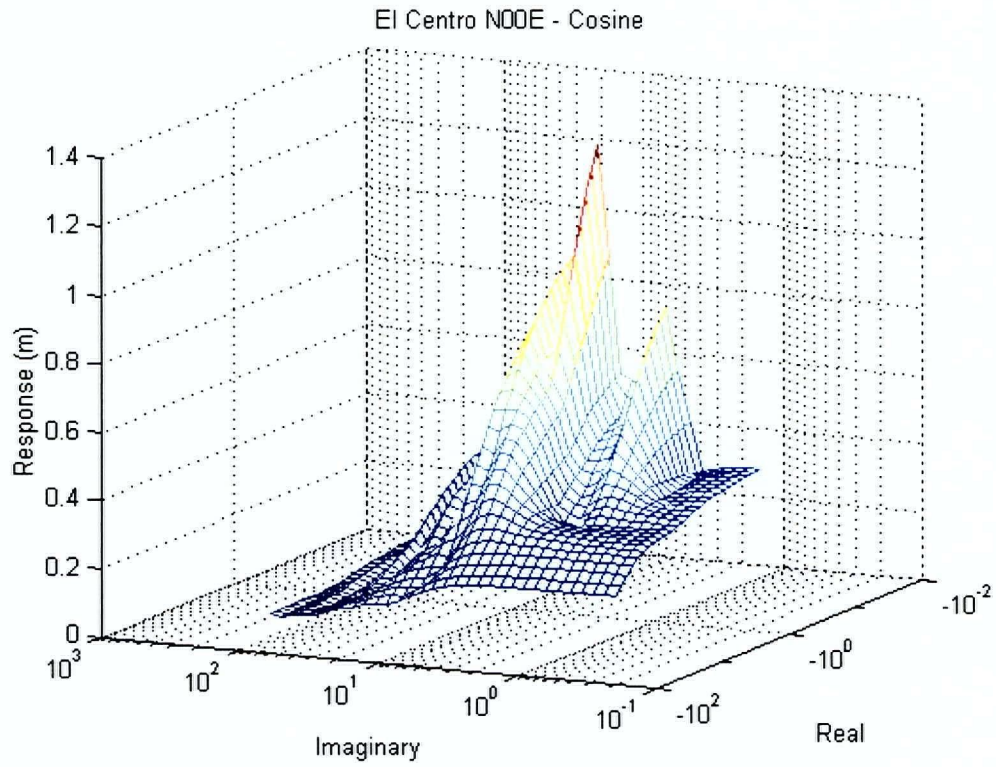


Figure C.1. El Centro N00E.

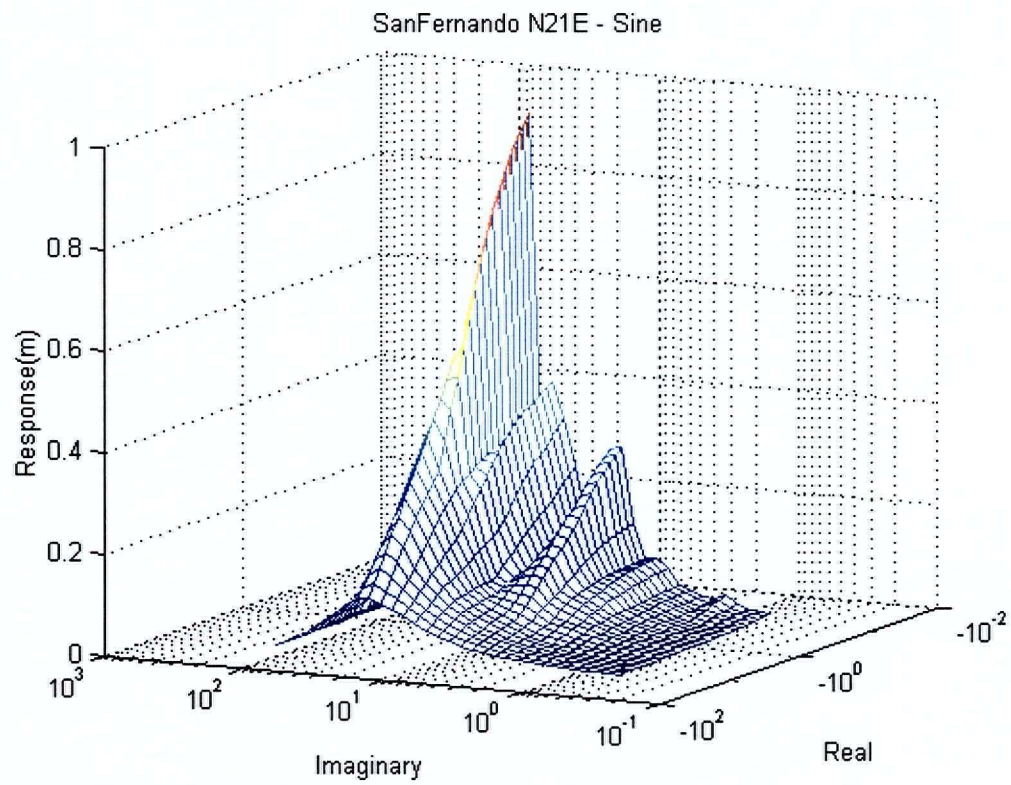
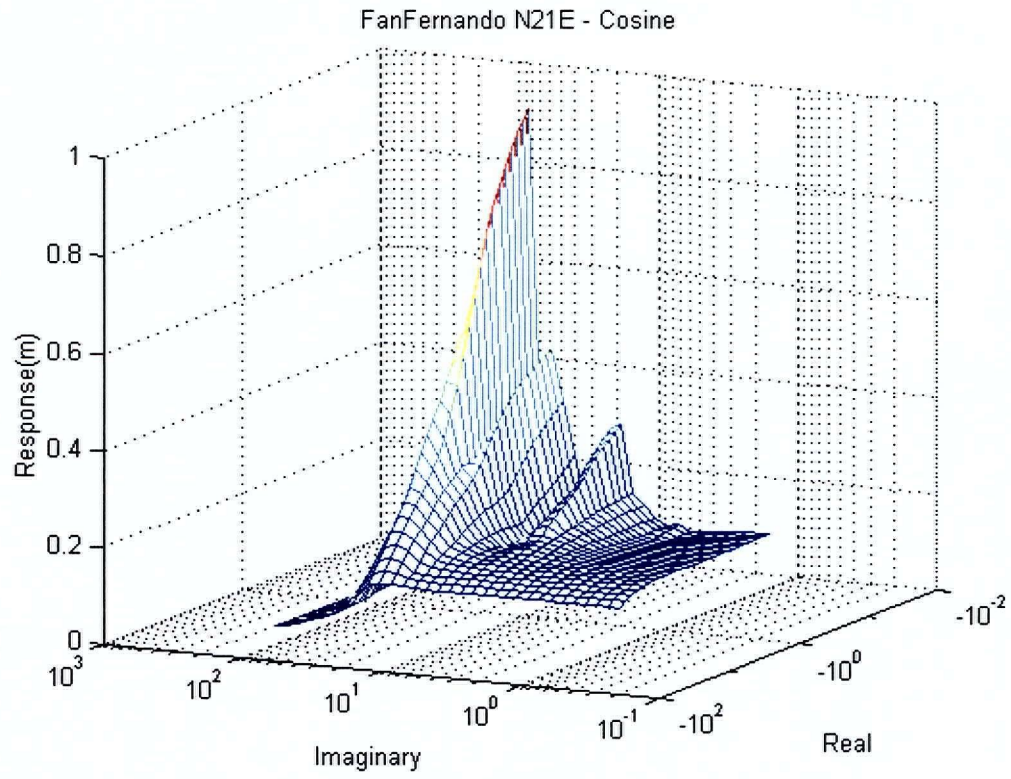


Figure C.2. San Fernando N21E.

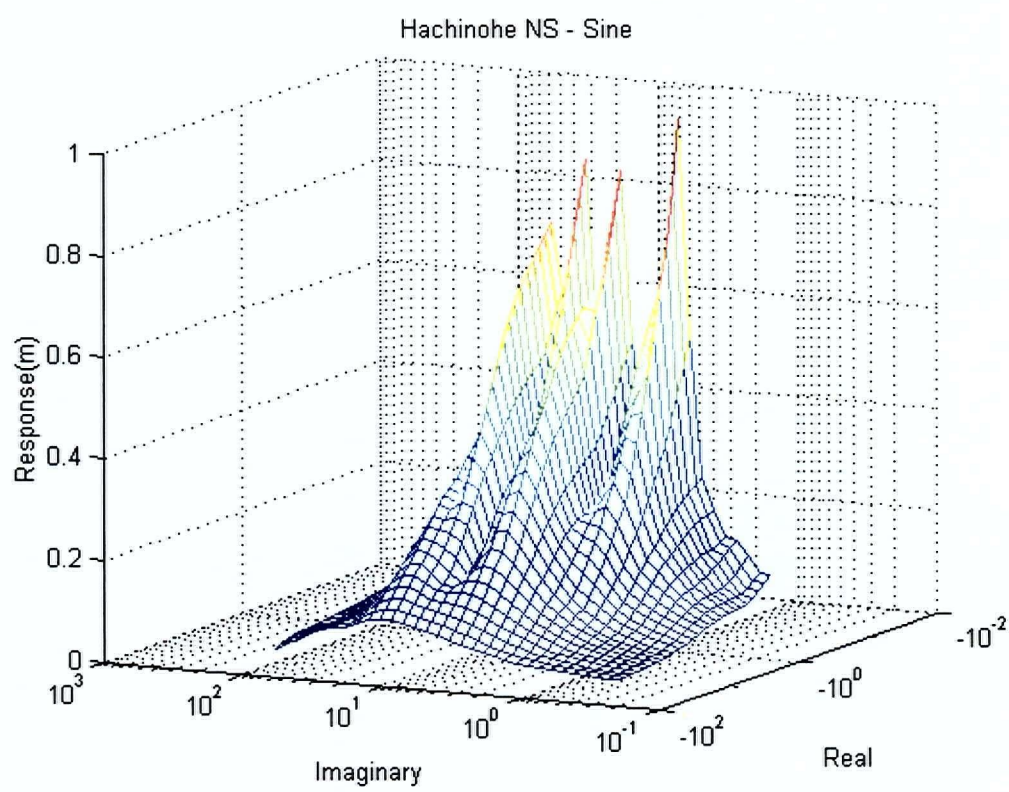
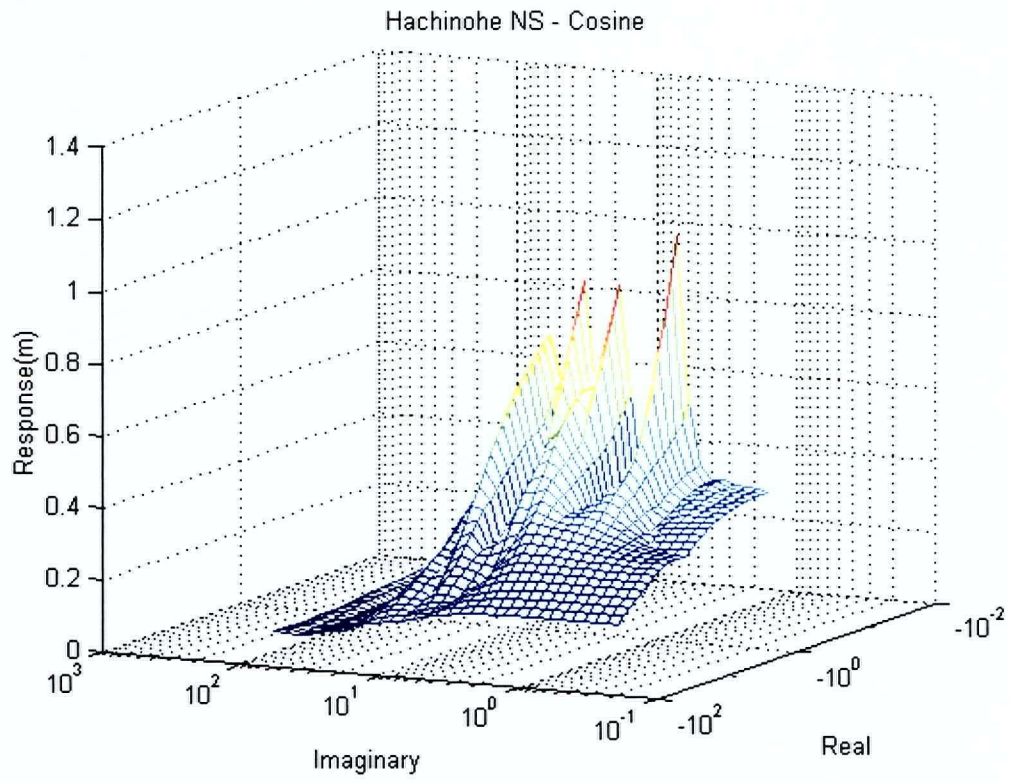


Figure C.3. Hachinohe Harbour NS record.

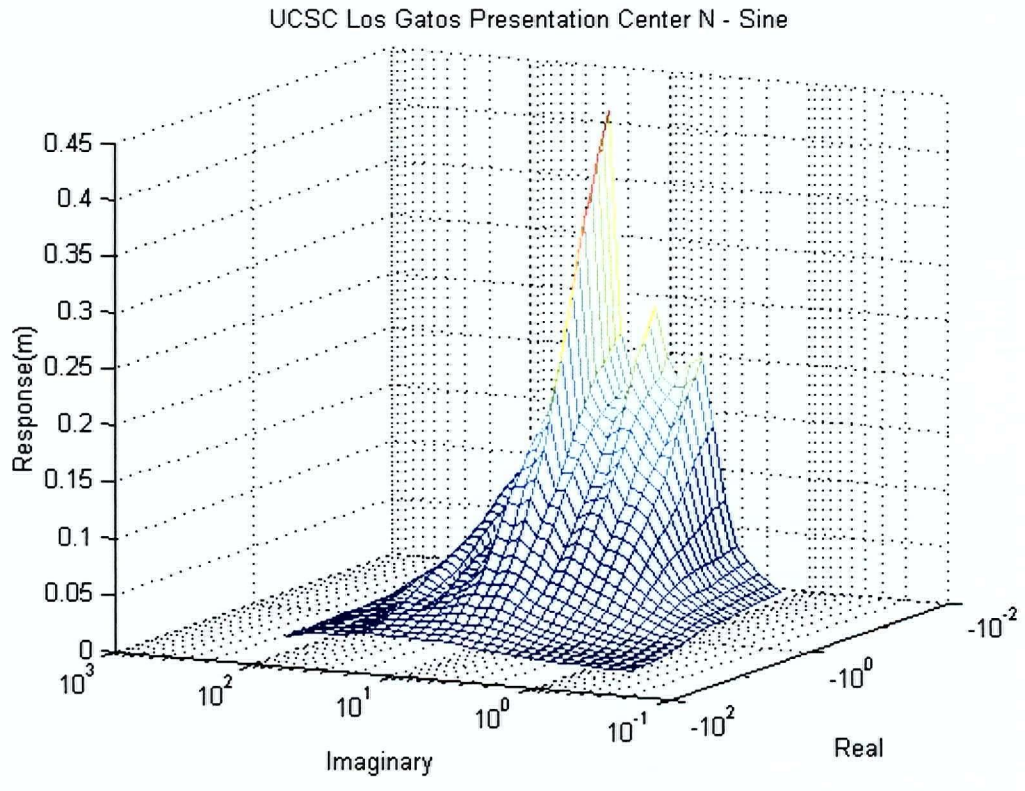
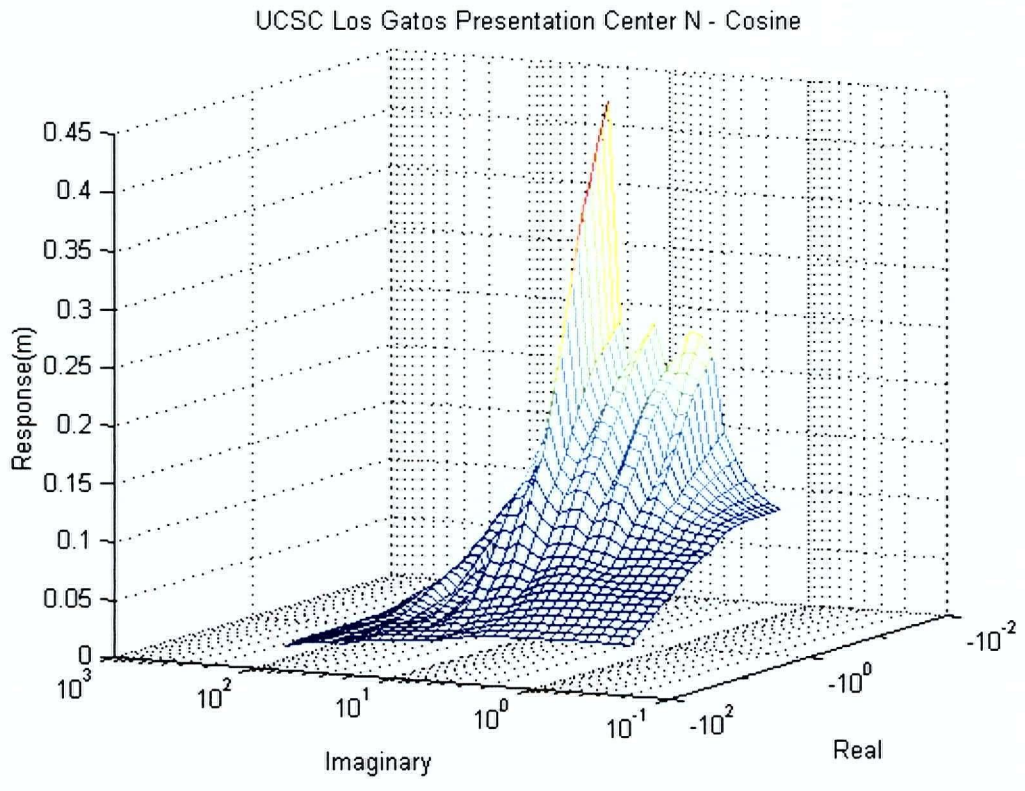


Figure C.4. UCSC Los Gatos Presentation Center record.

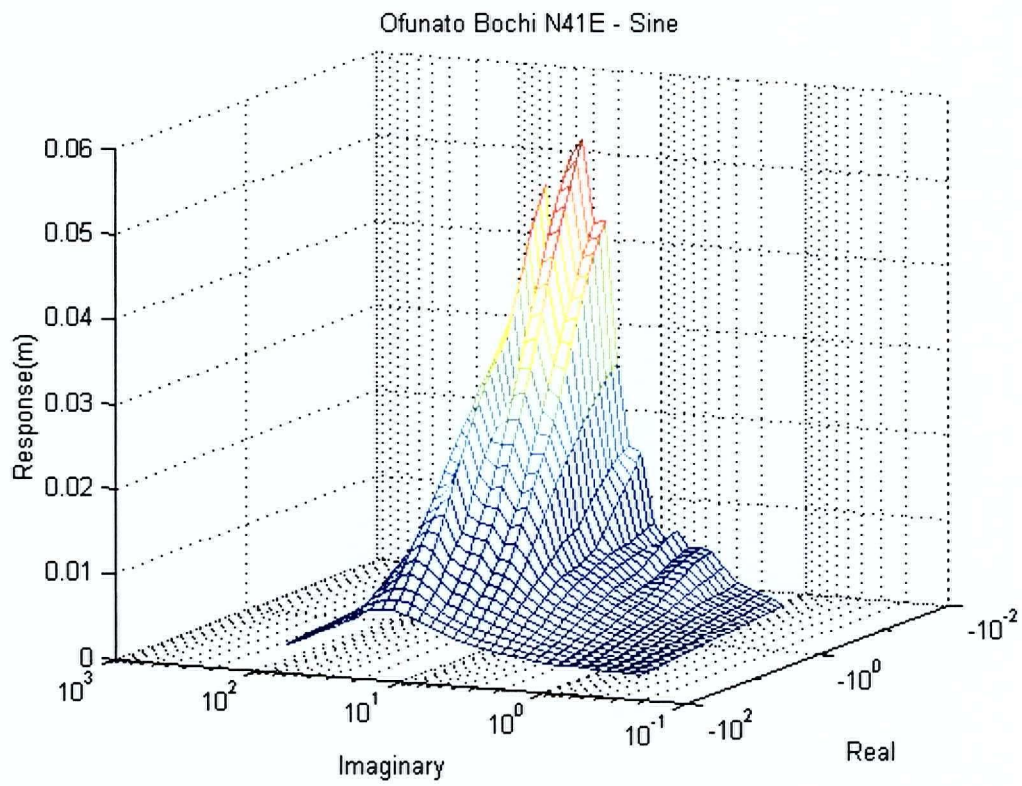
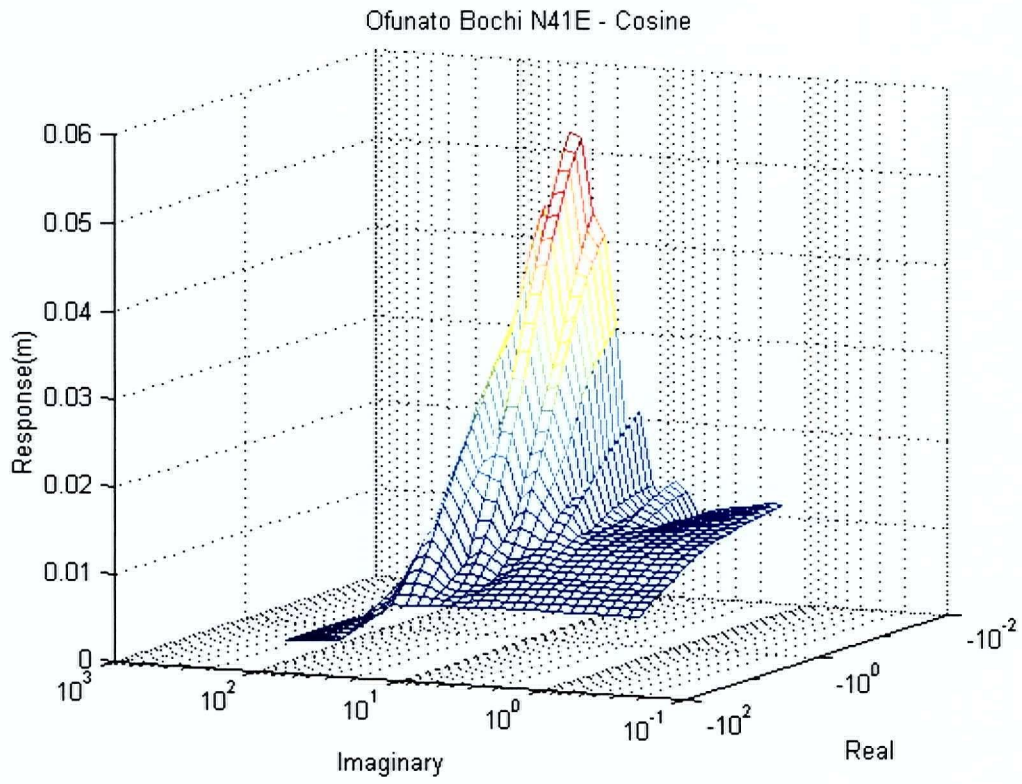


Figure C.5. Ofunato Bochi N41E record.

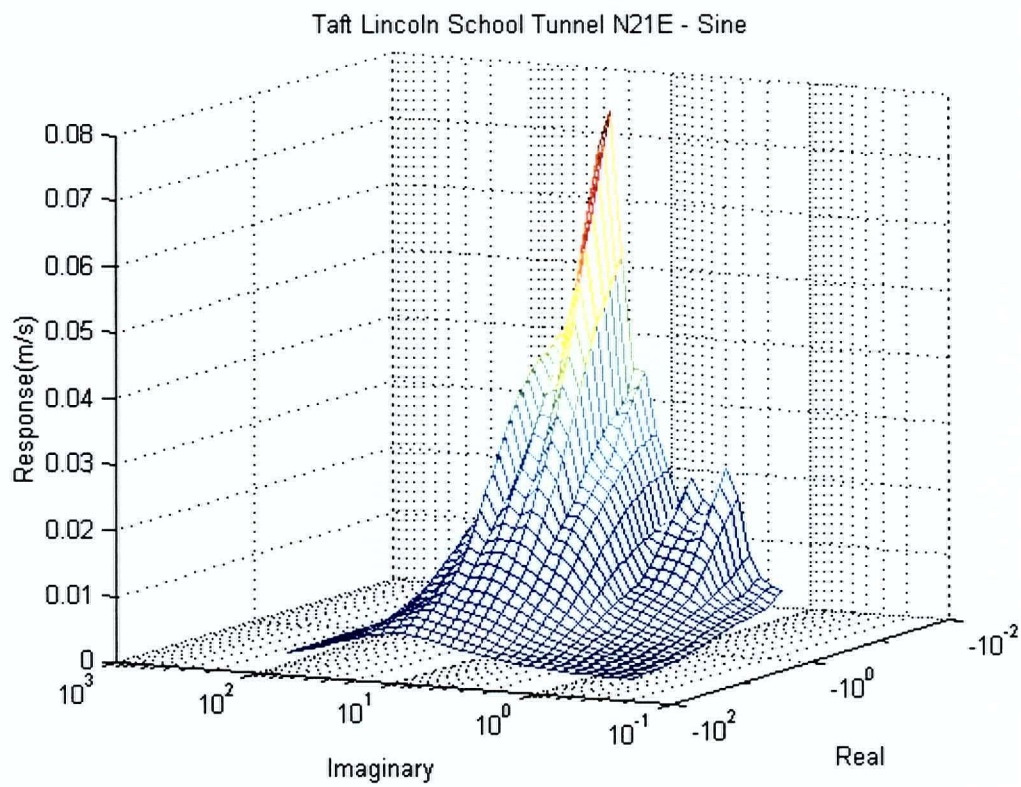
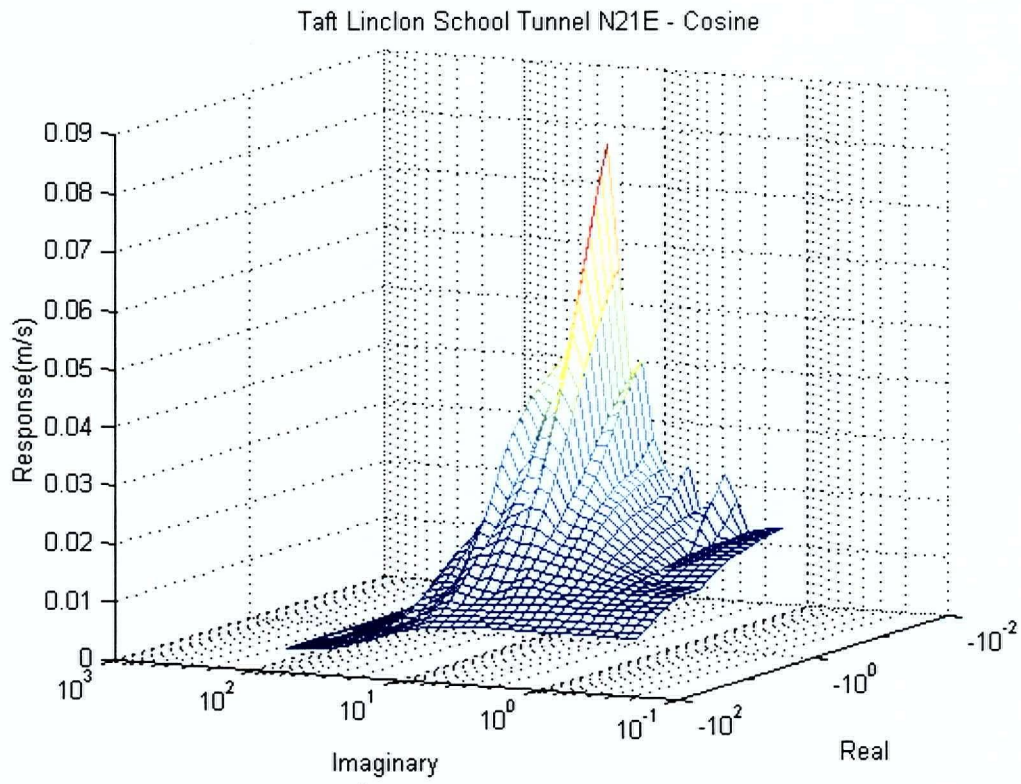


Figure C.6. Taft 21.

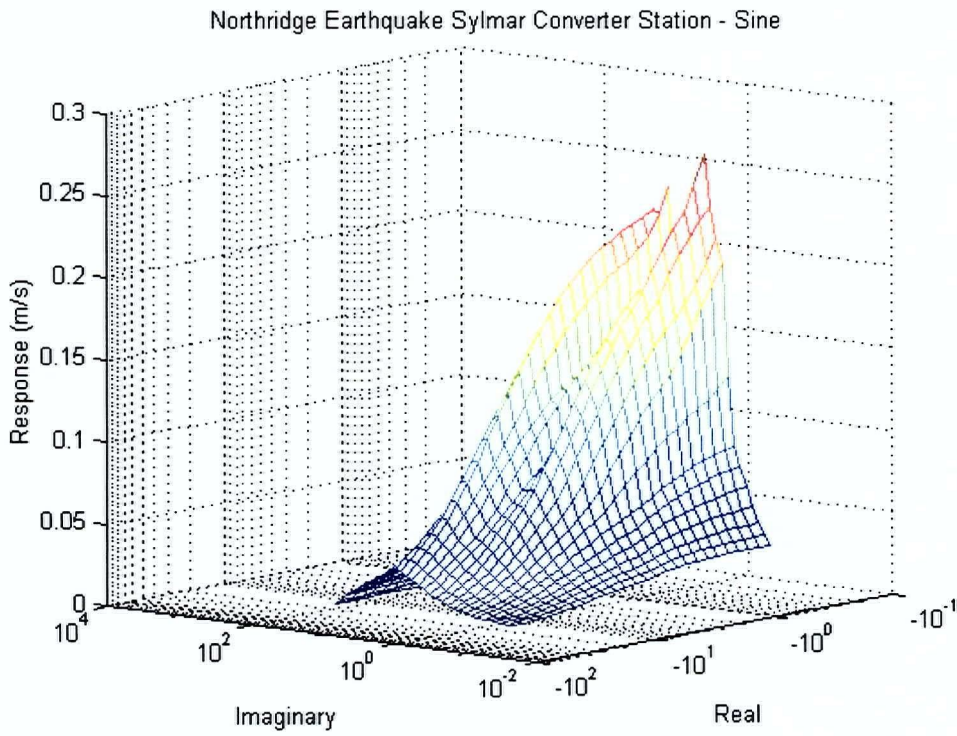
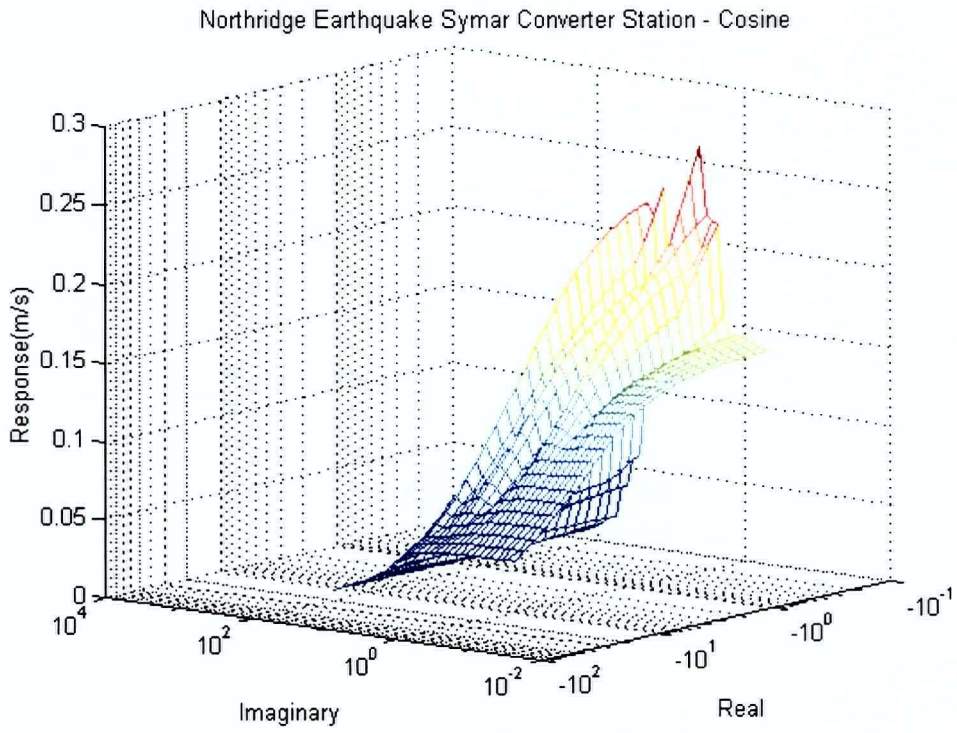


Figure C.7. Sylmar 00.

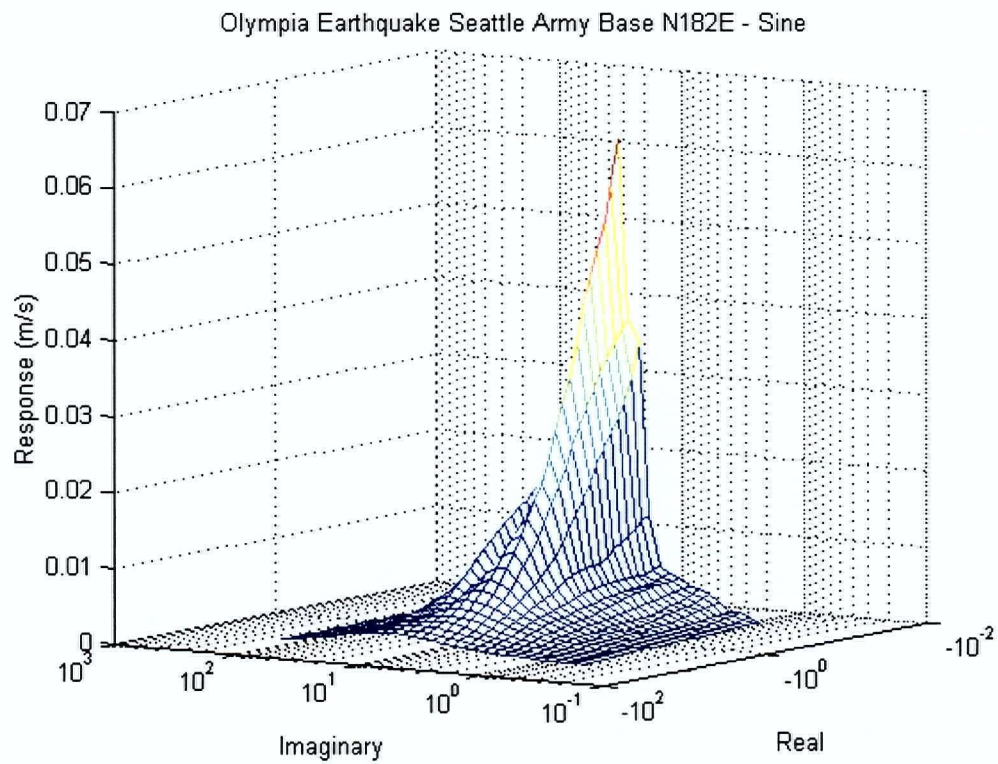
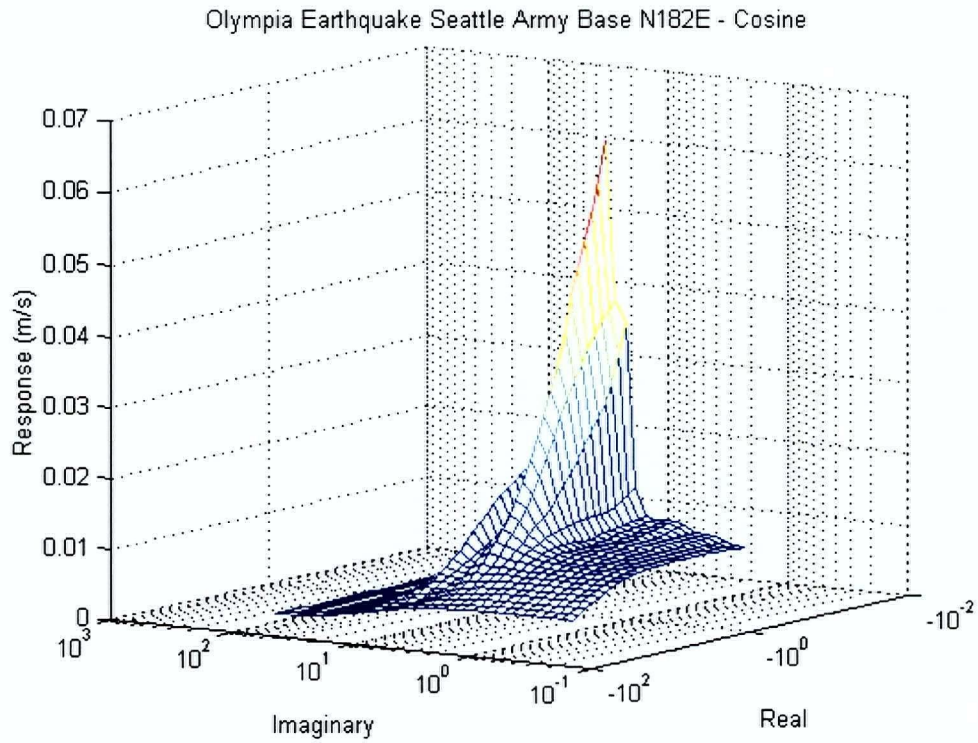


Figure C.8. Olympia Seattle Army Base record 182.

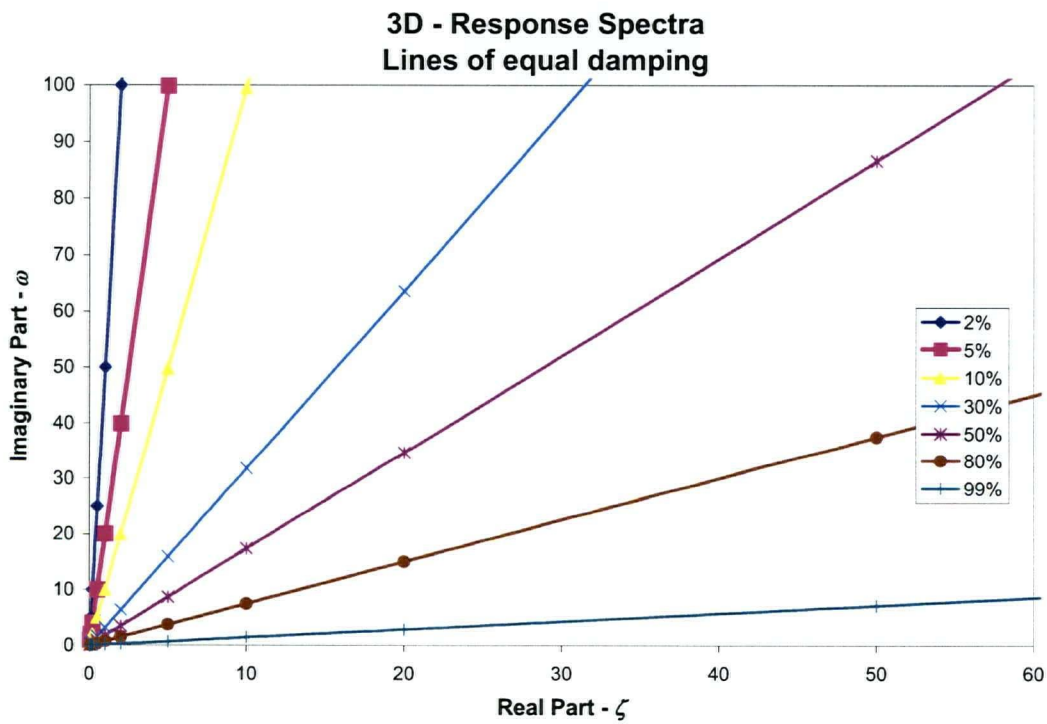
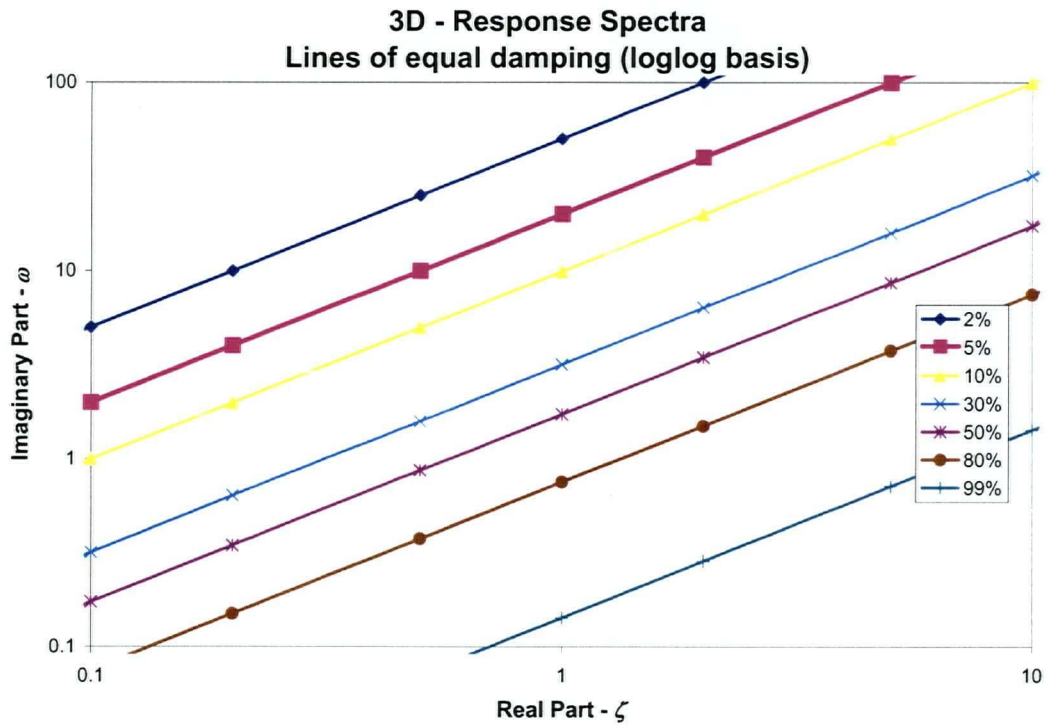


Figure C.9. Relationship of traditional response spectra to the 3-D spectra.

Appendix D:

MathCad Worksheet: 4-Story Structure Transfer Function

Transfer Functions of Multi-DOF Structures: Uniform 4-Story Structure

The following is the mathematical derivation of the transfer functions of the 4-story structure used as an example to evaluate the slip load distribution. The theoretical derivation of transfer functions is provided as background information. Transfer functions are derived for both displacements and also for story drifts. Frequencies and participation factors are compared. In addition, a comparison is made between the full MDOF transfer function and the first mode model of the MDOF structure for the first story drift transfer function.

First: define the mass, stiffness, damping and excitation distribution matrices in their usual form:

$$M := \begin{pmatrix} 1 & 0 & 0 & 0 \\ 0 & 1 & 0 & 0 \\ 0 & 0 & 1 & 0 \\ 0 & 0 & 0 & 1 \end{pmatrix} \quad K := \begin{pmatrix} 2400 & -1200 & 0 & 0 \\ -1200 & 2400 & -1200 & 0 \\ 0 & -1200 & 2400 & -1200 \\ 0 & 0 & -1200 & 1200 \end{pmatrix}$$

$$C := \begin{pmatrix} 3.33 & -1.66 & 0 & 0 \\ -1.66 & 3.33 & -1.66 & 0 \\ 0 & -1.66 & 3.33 & -1.66 \\ 0 & 0 & -1.66 & 1.66 \end{pmatrix} \quad L := \begin{pmatrix} 1 \\ 1 \\ 1 \\ 1 \end{pmatrix}$$

Next define the transformation matrices to convert from displacement to drift form:

$$T := \begin{pmatrix} 1 & 0 & 0 & 0 \\ 1 & 1 & 0 & 0 \\ 1 & 1 & 1 & 0 \\ 1 & 1 & 1 & 1 \end{pmatrix} \quad T^{-1} = \begin{pmatrix} 1 & 0 & 0 & 0 \\ -1 & 1 & 0 & 0 \\ 0 & -1 & 1 & 0 \\ 0 & 0 & -1 & 1 \end{pmatrix}$$

Where $d = \text{inv}(T) x$ and $x = Td$. This is illustrated by the following two examples which verify that the transformation relates displacements to story drifts

$$x := \begin{pmatrix} 1 \\ 2 \\ 3 \\ 3.5 \end{pmatrix} \quad T^{-1} \cdot x = \begin{pmatrix} 1 \\ 1 \\ 1 \\ 0.5 \end{pmatrix} \quad d := \begin{pmatrix} 1 \\ 1 \\ 1 \\ 0.5 \end{pmatrix} \quad T \cdot d = \begin{pmatrix} 1 \\ 2 \\ 3 \\ 3.5 \end{pmatrix}$$

The Transfer functions are complex functions of frequency. To proceed we need to define the complex j and the range of frequencies to use in plotting.

Define: $j := \sqrt{-1}$

For

$$k := 0..495$$

choose

$$\omega_k := 1.0 + .2 \cdot k$$

Starting with the Laplace transform of the usual differential equation of motion:

$$M \cdot s^2 \cdot X + C \cdot s \cdot X + K \cdot X + M \cdot L \cdot A = 0$$

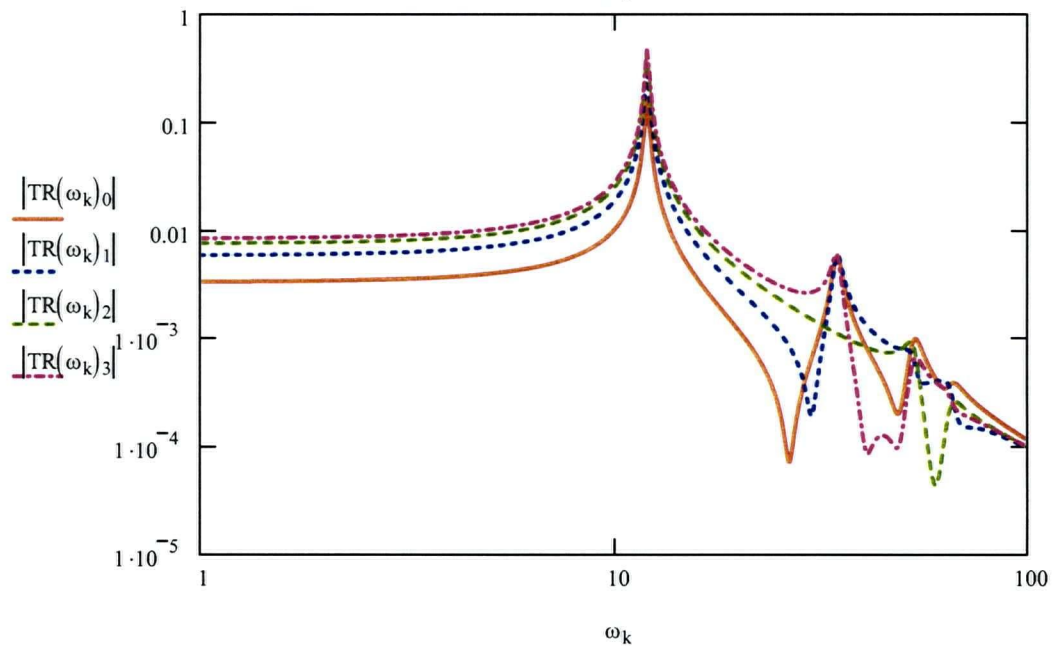
The solution for the transformed variable $X = L(x)$ is upon substitution of $s=j\omega$:

$$X = \left[(-M \cdot \omega^2 + i \cdot C \cdot \omega + K)^{-1} \right] \cdot M \cdot L \cdot A$$

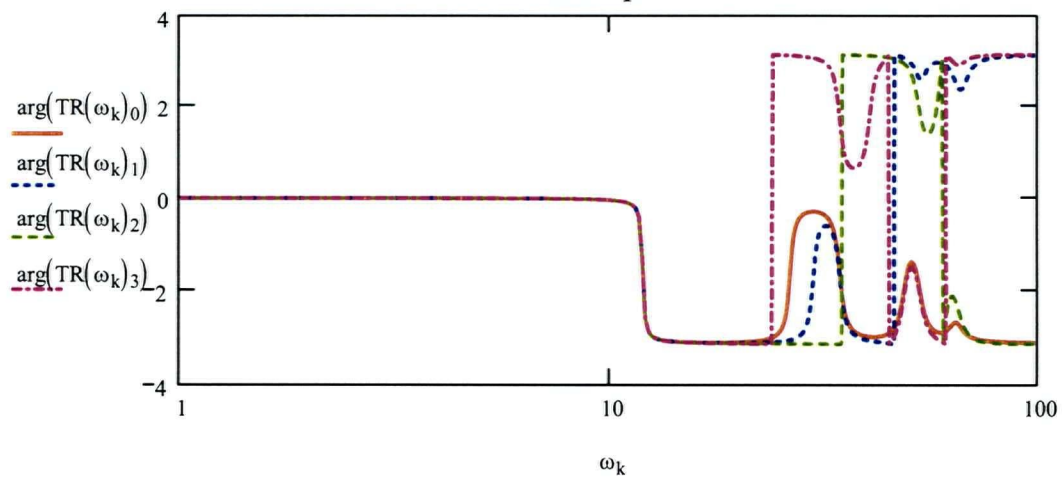
The set of 4 transfer functions corresponding to each story are:

$$TR(\omega) := (-M \cdot \omega^2 + j \cdot C \cdot \omega + K)^{-1} \cdot M \cdot L$$

Gain plot



Phase plot



To find transfer functions for variable D rather than X, start with the usual Laplace transform

$$M \cdot s^2 \cdot X + C \cdot s \cdot X + K \cdot X + M \cdot L \cdot A = 0$$

Substitute TD for X

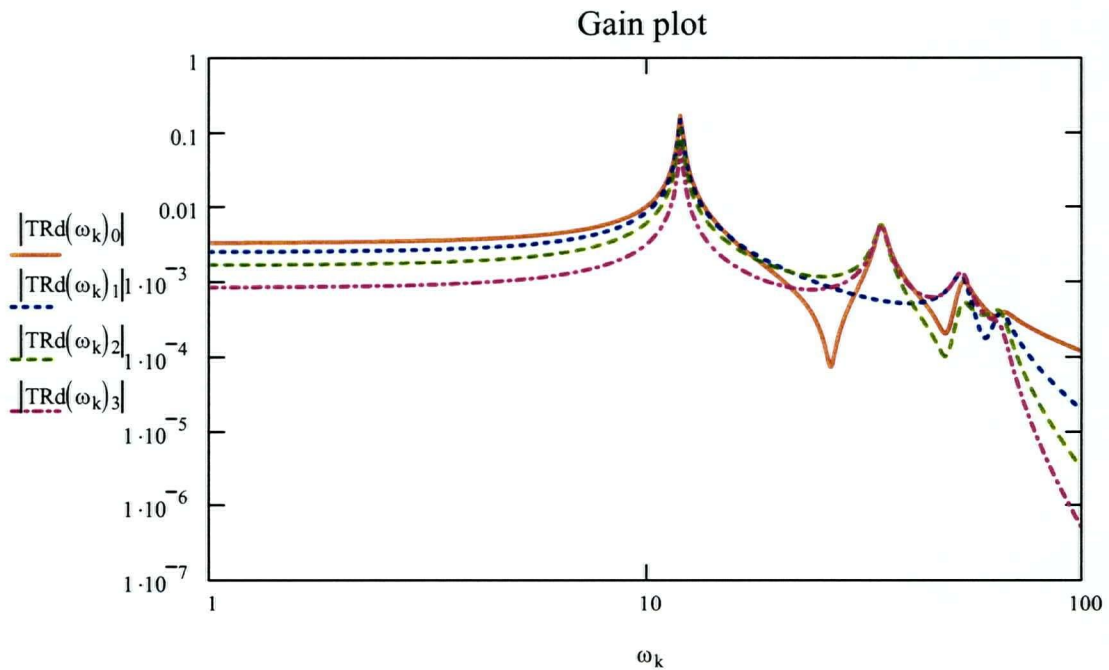
$$M \cdot T \cdot s^2 \cdot D + C \cdot T \cdot s \cdot D + K \cdot T \cdot D + M \cdot L \cdot A = 0$$

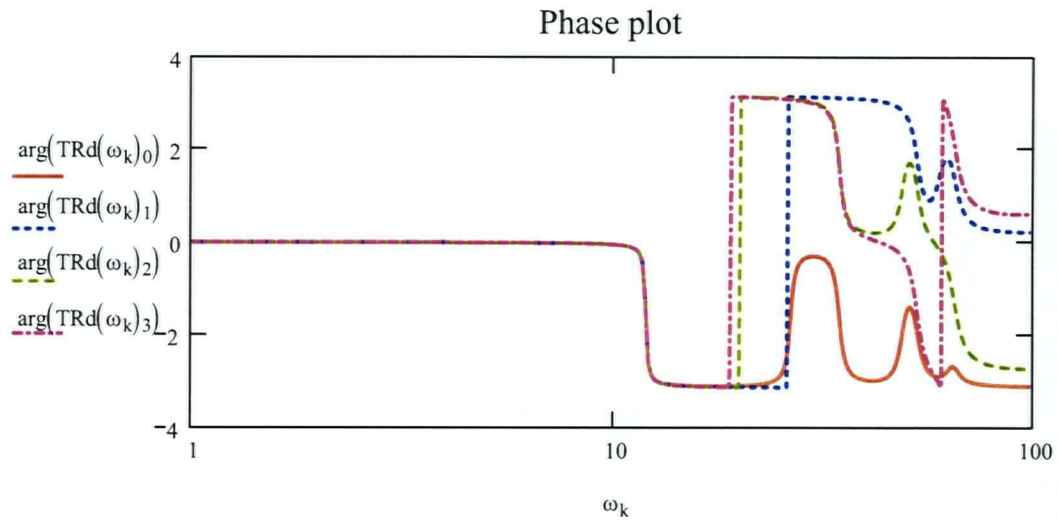
Solve for D and substitute $j\omega$ for s

$$D = \left[\left(-M \cdot T \cdot \omega^2 + j \cdot C \cdot T \cdot \omega + K \cdot T \right)^{-1} \right] \cdot M \cdot L \cdot A$$

As before, define the transfer functions at each story level

$$\text{TRd}(\omega) := \left(-M \cdot T \cdot \omega^2 + j \cdot C \cdot T \cdot \omega + K \cdot T \right)^{-1} \cdot M \cdot L$$





The above 4-DOF system can be reduced to a set of SDOF orthonormal systems by using the eigenvalues and eigenvectors. The modal analysis for the structure in the displacement variables and in the drift variables follows.

With displacement variables the response frequencies are found to be

$$f_x := \text{sort}(\text{eigenvals}(M^{-1} \cdot K)) \quad f_x = \begin{pmatrix} 144.738 \\ 1.2 \times 10^3 \\ 2.817 \times 10^3 \\ 4.239 \times 10^3 \end{pmatrix} \quad \leftarrow \text{minimum value}$$

$$\omega_0 := \sqrt{f_x_0} \quad \omega_0 = 12.031$$

$$\omega_1 := \sqrt{f_x_1} \quad \omega_1 = 34.641 \quad (\text{checked from graph})$$

$$\omega_2 := \sqrt{f_x_2} \quad \omega_2 = 53.073$$

$$\omega_3 := \sqrt{f_x_3} \quad \omega_3 = 65.104$$

Repeating the same process but using the inter-story drift variables leads to the same eigenvalues

$$f_d := \text{sort}(\text{eigenvals}[(M \cdot T)^{-1} \cdot K \cdot T]) \quad f_d = \begin{pmatrix} 144.738 \\ 1.2 \times 10^3 \\ 2.817 \times 10^3 \\ 4.239 \times 10^3 \end{pmatrix} \quad \leftarrow \text{minimum value}$$

$$\omega_0 := \sqrt{f_d_0} \quad \omega_0 = 12.031$$

$$\omega_1 := \sqrt{f_d_1} \quad \omega_1 = 34.641 \quad (\text{checked from graph})$$

$$\begin{aligned}\omega_2 &:= \sqrt{fd_2} & \omega_2 &= 53.073 \\ \omega_3 &:= \sqrt{fd_3} & \omega_3 &= 65.104\end{aligned}$$

For each case show that the eigenvectors associated with each set of variables are equivalent.

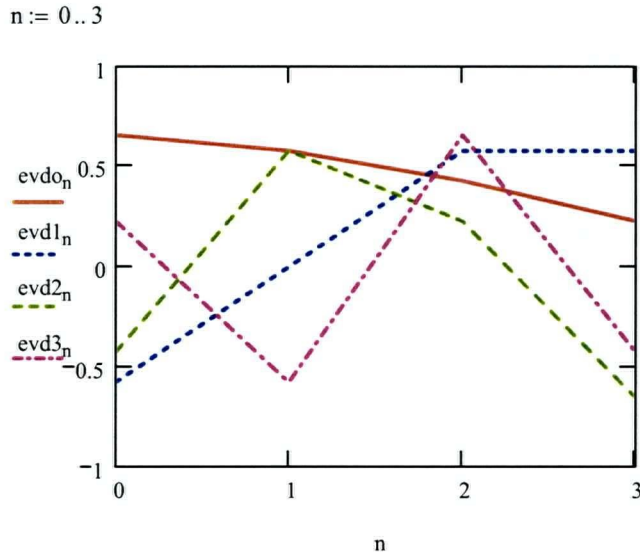
Check first mode:

$$\begin{aligned}\text{evdo} &:= \text{eigenvec}\left[(M \cdot T)^{-1} \cdot K \cdot T, \omega_1\right] = \begin{pmatrix} 0.657 \\ 0.577 \\ 0.429 \\ 0.228 \end{pmatrix} \\ \text{evxo} &:= \text{eigenvec}\left(M^{-1} \cdot K, \omega_1^2\right) = \begin{pmatrix} 0.228 \\ 0.429 \\ 0.577 \\ 0.657 \end{pmatrix} & \frac{\text{evxo}_0}{\text{evdo}_0} \cdot T \cdot \text{evdo} &= \begin{pmatrix} 0.228 \\ 0.429 \\ 0.577 \\ 0.657 \end{pmatrix} & \text{(Checks)}\end{aligned}$$

Determine the remaining eigenvectors:

$$\begin{aligned}\text{evd1} &:= \text{eigenvec}\left[(M \cdot T)^{-1} \cdot K \cdot T, \omega_1^2\right] & \text{evx1} &:= \text{eigenvec}\left(M^{-1} \cdot K, \omega_1^2\right) \\ \text{evd1} &= \begin{pmatrix} -0.577 \\ 0 \\ 0.577 \\ 0.577 \end{pmatrix} & \text{evx1} &= \begin{pmatrix} -0.577 \\ -0.577 \\ 0 \\ 0.577 \end{pmatrix} \\ \text{evd2} &:= \text{eigenvec}\left[(M \cdot T)^{-1} \cdot K \cdot T, \omega_2^2\right] & \text{evx2} &:= \text{eigenvec}\left(M^{-1} \cdot K, \omega_2^2\right) \\ \text{evd2} &= \begin{pmatrix} -0.429 \\ 0.577 \\ 0.228 \\ -0.657 \end{pmatrix} & \text{evx2} &= \begin{pmatrix} -0.657 \\ 0.228 \\ 0.577 \\ -0.429 \end{pmatrix} \\ \text{evd3} &:= \text{eigenvec}\left[(M \cdot T)^{-1} \cdot K \cdot T, \omega_3^2\right] & \text{evx3} &:= \text{eigenvec}\left(M^{-1} \cdot K, \omega_3^2\right) \\ \text{evd3} &= \begin{pmatrix} 0.228 \\ -0.577 \\ 0.657 \\ -0.429 \end{pmatrix} & \text{evx3} &= \begin{pmatrix} 0.429 \\ -0.657 \\ 0.577 \\ -0.228 \end{pmatrix}\end{aligned}$$

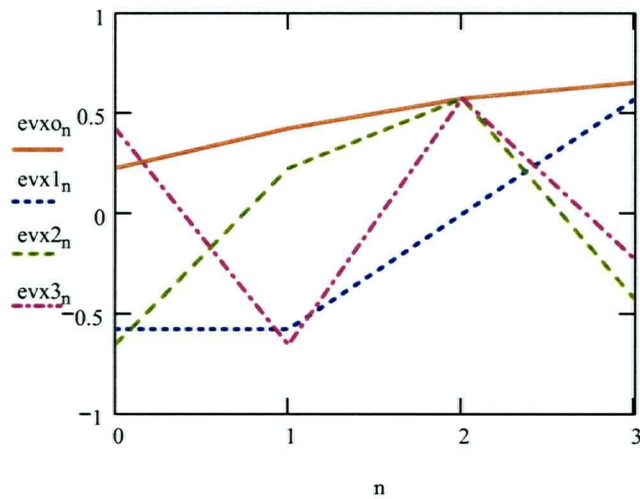
Plot the eigenvectors



$$\phi_d := \begin{pmatrix} \text{evdo}_0 & \text{evd1}_0 & \text{evd2}_0 & \text{evd3}_0 \\ \text{evdo}_1 & \text{evd1}_1 & \text{evd2}_1 & \text{evd3}_1 \\ \text{evdo}_2 & \text{evd1}_2 & \text{evd2}_2 & \text{evd3}_2 \\ \text{evdo}_3 & \text{evd1}_3 & \text{evd2}_3 & \text{evd3}_3 \end{pmatrix}$$

<---Inter-story Drift Mode Shapes

$$\phi_d^T \cdot T^{-1} \cdot M \cdot T \cdot L = \begin{pmatrix} 1.89 \\ 0.577 \\ -0.28 \\ -0.121 \end{pmatrix}$$



$$\phi := \begin{pmatrix} \text{evxo}_0 & \text{evx1}_0 & \text{evx2}_0 & \text{evx3}_0 \\ \text{evxo}_1 & \text{evx1}_1 & \text{evx2}_1 & \text{evx3}_1 \\ \text{evxo}_2 & \text{evx1}_2 & \text{evx2}_2 & \text{evx3}_2 \\ \text{evxo}_3 & \text{evx1}_3 & \text{evx2}_3 & \text{evx3}_3 \end{pmatrix}$$

<---Displ't Mode Shapes

$$\phi^T \cdot M \cdot L = \begin{pmatrix} 1.89 \\ -0.577 \\ -0.28 \\ 0.121 \end{pmatrix}$$

Determine an equivalent SDOF dynamic system:

Equivalent modal Mass:

$$m_0 := \text{evdo}^T \cdot T^{-1} \cdot M \cdot T \cdot \text{evdo} \quad m_0 = 1$$

$$m_1 := \text{evd1}^T \cdot T^{-1} \cdot M \cdot T \cdot \text{evd1} \quad m_1 = 1$$

$$m_2 := \text{evd2}^T \cdot T^{-1} \cdot M \cdot T \cdot \text{evd2} \quad m_2 = 1$$

From drift mode shapes

$m3 := \text{evd3}^T \cdot T^{-1} \cdot M \cdot T \cdot \text{evd3}$	$m3 = 1$	$m0 + m1 + m2 + m3 = 4$
$m_{x0} := \text{evx0}^T \cdot M \cdot \text{evx0}$	$m_{x0} = 1$	
$m_{x1} := \text{evx1}^T \cdot M \cdot \text{evx1}$	$m_{x1} = 1$	From displ mode shapes
$m_{x2} := \text{evx2}^T \cdot M \cdot \text{evx2}$	$m_{x2} = 1$	
$m_{x3} := \text{evx3}^T \cdot M \cdot \text{evx3}$	$m_{x3} = 1$	$m_{x0} + m_{x1} + m_{x2} + m_{x3} = 4$

Equivalent load:

$p0 := \text{evd0}^T \cdot T^{-1} \cdot M \cdot L$	$p0 = 0.657$		Modal Participation Factors
$p1 := \text{evd1}^T \cdot T^{-1} \cdot M \cdot L$	$p1 = -0.577$		$m0^{-1} \cdot p0 = 0.657$
$p2 := \text{evd2}^T \cdot T^{-1} \cdot M \cdot L$	$p2 = -0.429$	From drift mode shapes	$m1^{-1} \cdot p1 = -0.577$
$p3 := \text{evd3}^T \cdot T^{-1} \cdot M \cdot L$	$p3 = 0.228$		$m2^{-1} \cdot p2 = -0.429$
$p_{x0} := \text{evx0}^T \cdot M \cdot L$	$p_{x0} = 1.89$		$m3^{-1} \cdot p3 = 0.228$
$p_{x1} := \text{evx1}^T \cdot M \cdot L$	$p_{x1} = -0.577$	From displ mode shapes	$m_{x0}^{-1} \cdot p_{x0} = 1.89$
$p_{x2} := \text{evx2}^T \cdot M \cdot L$	$p_{x2} = -0.28$		$m_{x1}^{-1} \cdot p_{x1} = -0.577$
$p_{x3} := \text{evx3}^T \cdot M \cdot L$	$p_{x3} = 0.121$		$m_{x2}^{-1} \cdot p_{x2} = -0.28$
			$m_{x3}^{-1} \cdot p_{x3} = 0.121$

note: the first mode displacement participation factor is about 3 times the participation factor of the second mode. Therefore, we can neglect higher modes with some degree of confidence. The same cannot be said for the story drifts

Evaluate Rayleigh damping in each of the modes using story drifts

$$C_d := \phi_d^T \cdot T^{-1} \cdot M^{-1} \cdot C \cdot T \cdot \phi_d$$

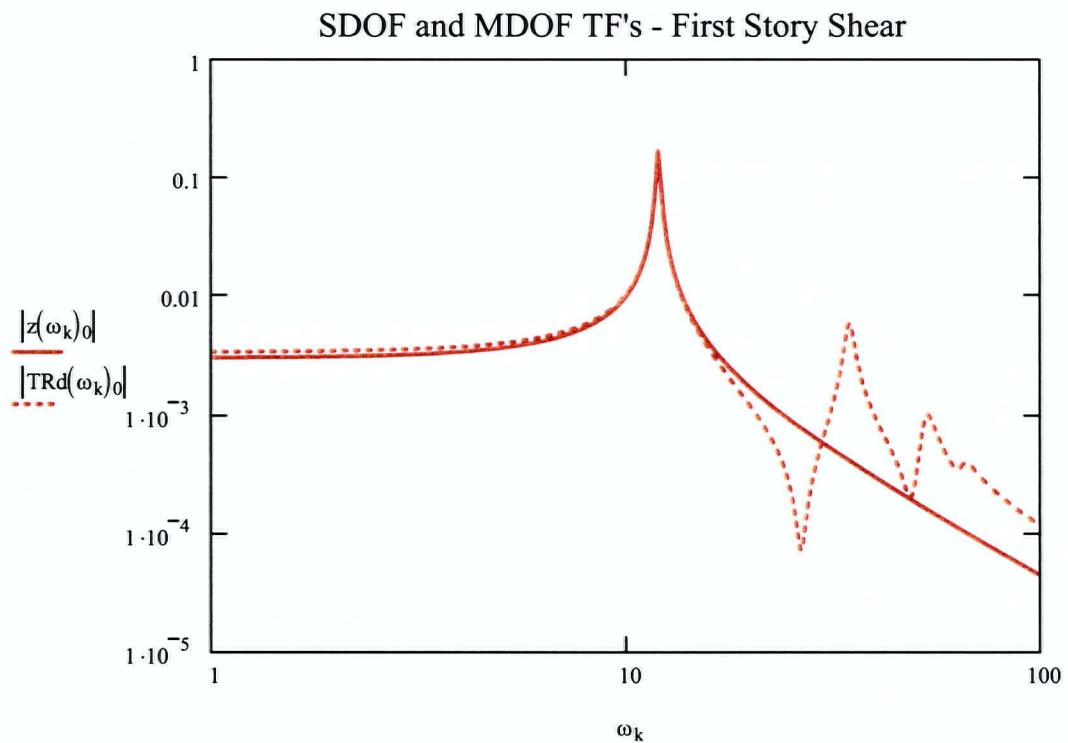
$$C_d = \begin{pmatrix} 0.206 & -1.316 \times 10^{-3} & 6.378 \times 10^{-4} & 2.766 \times 10^{-4} \\ -0.011 & 1.667 & 1.615 \times 10^{-3} & 7.005 \times 10^{-4} \\ 0.012 & 3.791 \times 10^{-3} & 3.905 & -7.965 \times 10^{-4} \\ 8.101 \times 10^{-3} & 2.474 \times 10^{-3} & -1.199 \times 10^{-3} & 5.873 \end{pmatrix}$$

$$\frac{C_{d_{0,0}}}{\omega_0} = 0.01712$$

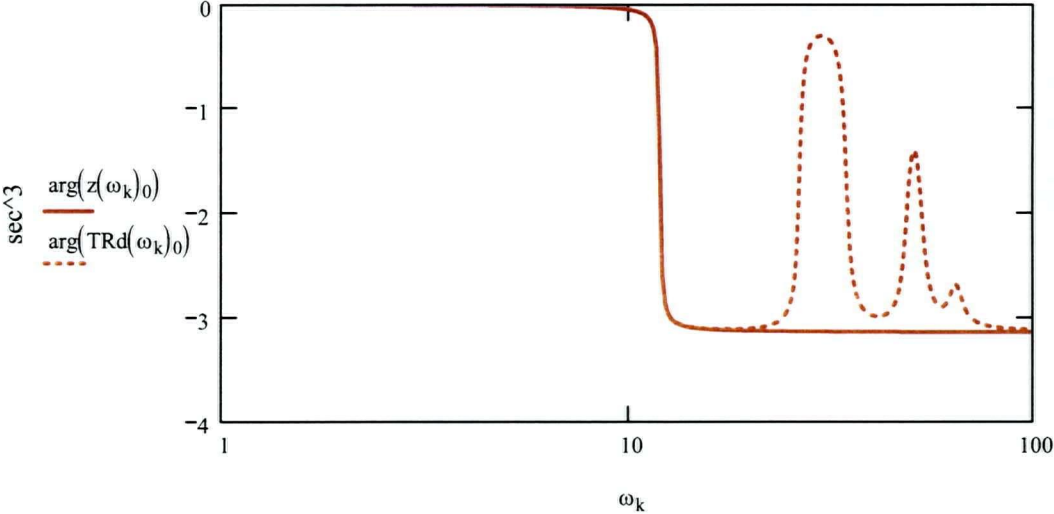
Determine SDOF first mode transfer function for first story drift using story drift variables. functions

$$z(\omega) := \left[\omega^2 \cdot (-1) + j \cdot C_{d_{0,0}} \cdot \omega + \omega_0^2 \right]^{-1} \cdot |p_0| \cdot |m_0^{-1}| \cdot \text{evdo}$$

Compare SDOF and MDOF transfer functions at each story:



SDOF and MDOF TF's - First Story Shear



Appendix E:
Band Limited Gaussian White Noise

Appendix E: Band Limited Gaussian White Noise

E.1 White Noise

In Chapter 3 a procedure for determining a white noise time history process was described.

Since the distribution is only approximately Normal, an assessment of the fit was undertaken to verify the ability of the method to provide results that fit the normal distribution.

The procedure is as follows:

1. Generate two random numbers a and b on the interval $(0,1)$ with uniform distribution
2. Evaluate the formula $x = \cos(\pi a)\sqrt{-2\ln(b)}$

The distribution for the resulting random number, x , has zero mean, standard deviation 1 and the resulting distribution closely resembles a Normal curve.

Figure E.1 shows a segment of the time history function generated using the above procedure. Figure E.2(a) and (b) show plots of the cumulative probability distribution and the associated PDF associated with the time history. The results illustrate that the procedure produces a white noise function that is sufficiently close to the normal distribution for the purposes of the work in this investigation.

It is apparent from the fit of the data to the ideal normal curves, the approximate procedure is an accurate reproduction of the true normal distribution

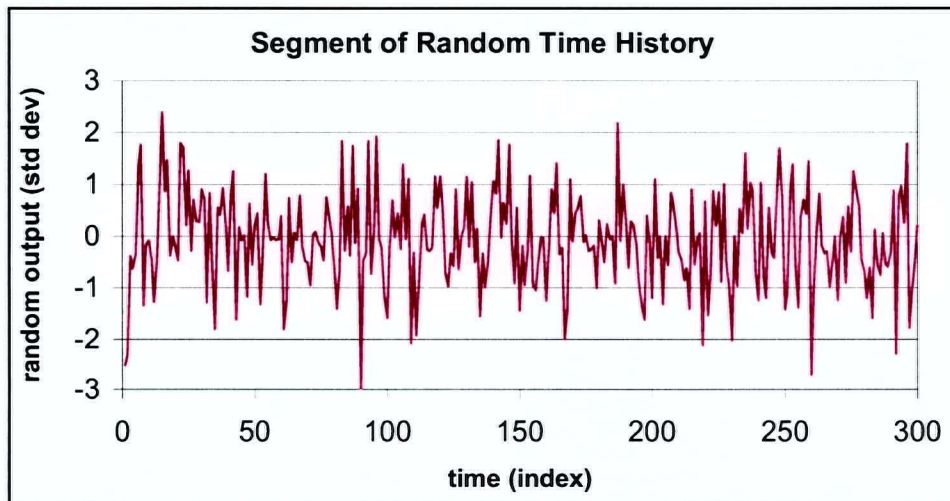


Figure E.1. Segment of random time history.

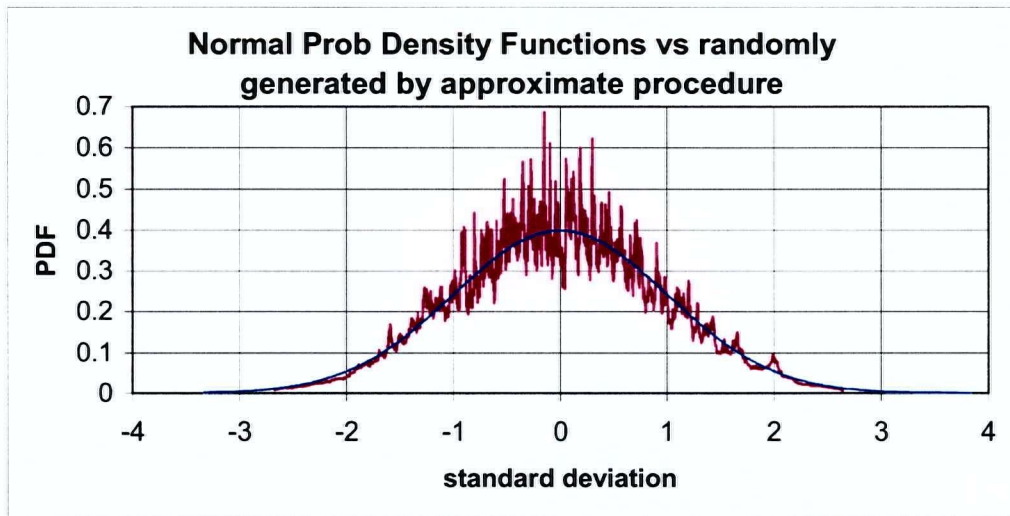


Figure E.2. Probability density function and smoothed randomly generated PDF.

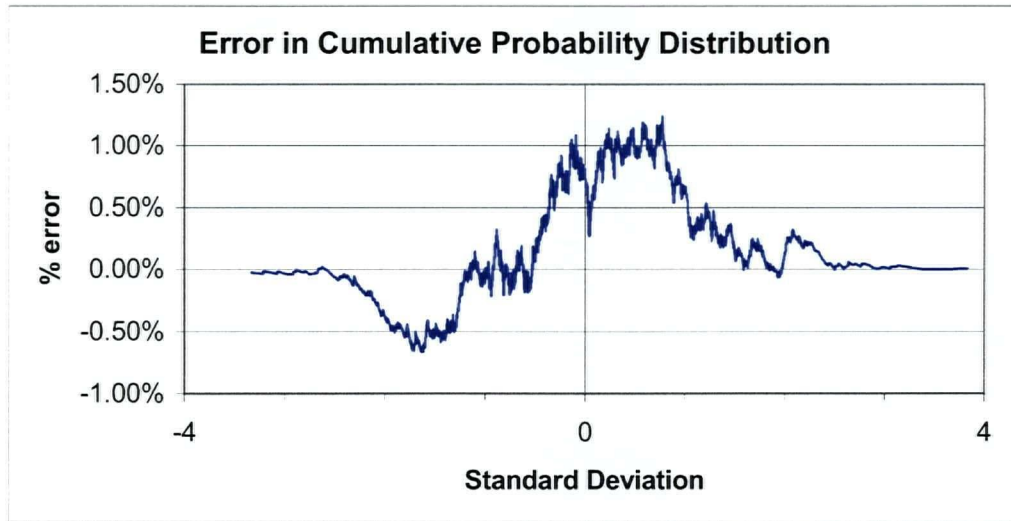


Figure E.3. Error in cumulative probability distribution. (% of full scale)

E.2 Alternate Band Limited White Noise Procedure

The procedure used above produces a white noise whose energy band is limited to the Nyquist frequency associated with the time step of the time history. The frequency content of the time history can be more tightly controlled by using the following procedure:

- 1) step 1 select time step and set of frequencies
- 2) step 2 generate and scale amplitude of sinusoid at each selected frequency and offset by random phase shift
- 3) step 3 superimpose all component sinusoids to produce final signal

This method is more cumbersome in that it requires significantly more computational effort than the previously described method. It also results in a periodic function when the lowest frequency considered has a period less than half of the duration of the record.

Appendix F

Level Set Programming and Optimal Slip Load Distribution in MDOF Structures

Appendix F: Level Set Programming and Optimal Slip Load Distribution in MDOF Structures

F.1 Level Set Programming

Level Set Programming (LSP) is an optimization procedure, developed by Yassien (1994), that is capable of handling problems where the function or its derivatives are discontinuous, have steep or infinite gradients or possess “fuzzy” objective functions. The work described in this section constitutes an investigation into the optimal slip loads in a 4-story shear structure with uniform mass and stiffness distribution. With the results of this investigation it was attempted to find a general rule by which the slip loads can be proportioned. Only the uniform shear structure was considered, therefore generality applicability of the results obtained is limited to this structure. The control systems considered include the passive friction damped (CSFD) and the semi-active off-on control system.

F.1.1 Objective Functions, Level Sets and Scatter Plots

The LSP optimization procedure constitutes a search for a set of parameters, in this case representing slip loads of the dampers in the chosen 4-story structure, that lead to the minimum response as measured by an “objective function.” Objective functions are functions chosen to measure the response. In the control theory presented in Chapter 2, the response was measured using a performance index. The two terms, for the purposes of this investigation are synonymous. Objective functions evaluate to a single real valued number, which represents the magnitude of the response experienced by the structure. The minimisation of the objective function corresponds to the optimal performance of the structure and the set of dampers required to achieve it.

The level set programming method provides an alternative to gradient methods commonly used to establish minimum values of performance functions. As indicated gradient methods break down if the objective function to be determined or its differentials are discontinuous, steep or “fuzzy” in the region of interest.

The LSP method does not require gradients to be computed and is therefore less prone to numerical instabilities. The method is based on the concept of a “level set” and on random sampling of the performance function with randomly chosen input variables $x_1, x_2 \dots x_n$. For a selected level L , the level set is the set of randomly selected input variables that lead to an objective function $f(x_1, x_2 \dots x_n)$ that satisfies the relation

$$f(x_1, x_2 \dots x_n) \leq L \quad (\text{F.1})$$

For a function $f(x_1, x_2 \dots x_n)$ that has a single global minimum

$$f_{\min} = f(x_1^*, x_2^* \dots x_n^*). \quad (\text{F.2})$$

It can be said that as L approaches the value of f_{\min} , the variance of each of the input variables satisfying the level-set will approach zero. The search for f_{\min} continues until the range of each of the input variables within the level set is acceptably small.

The search space is the n -dimensional hypercube with each dimension corresponding to initial search space of each input variable. In this case $n = 4$ and the hypercube is 4-dimensional. A level set is typically comprised of 60 points $(x_1, x_2 \dots x_n)$, comprised of sets of input variables in the hypercube for which the objective function satisfies Equation F.1. For each point evaluated (whether or not it is found to be a member of the level set) it is required to perform a time history simulation and subsequently evaluate the objective function based on the time-history output.

Within the search space, input variables are chosen having a uniform distribution. However, because the level set is restricted to functions that are less than L , as L is lowered, the points in the hypercube will begin to form a cluster. The shape of the scatter plot satisfying the level set can be viewed to get some understanding of the shape of the objective function by the shape and location of the level set point cluster.

Because random sampling of the input variables is being utilised, random sampling over the entire search space is not practical when the level set is restricted to a small cluster. It is therefore required to reduce the search ranges as the search progresses to avoid unnecessary function evaluations and expedite the search process. This procedure is built into the LSP search algorithm.

The chief drawback of LSP is that it often requires a large number of evaluations of the objective function to find the optimum. Consequently LSP is a computationally intensive, time consuming process.

F.2 Problem Formulation

Figure F.1 illustrates the 4 DOF uniform shear structure model used in the following investigation. Formulated in terms of inter-story drift, the governing equation of motion of the structure is as follows

$$\begin{aligned}
 \begin{bmatrix} \ddot{d}_1 \\ \ddot{d}_2 \\ \ddot{d}_3 \\ \ddot{d}_4 \end{bmatrix} &= \begin{bmatrix} -k & k & 0 & 0 \\ m & m & 0 & 0 \\ k & -2k & k & 0 \\ 0 & m & m & k \\ 0 & 0 & m & -2k \end{bmatrix} \begin{bmatrix} d_1 \\ d_2 \\ d_3 \\ d_4 \end{bmatrix} + \begin{bmatrix} -c & c & 0 & 0 \\ m & m & 0 & 0 \\ c & -2c & c & 0 \\ m & m & m & 0 \\ 0 & c & -2c & c \\ 0 & m & m & m \\ 0 & 0 & c & -2c \\ 0 & 0 & m & m \end{bmatrix} \begin{bmatrix} \dot{d}_1 \\ \dot{d}_2 \\ \dot{d}_3 \\ \dot{d}_4 \end{bmatrix} \\
 &+ \begin{bmatrix} -a_g \\ 0 \\ 0 \\ 0 \end{bmatrix} + \begin{bmatrix} -1 & 1 & 0 & 0 \\ m & m & 0 & 0 \\ 1 & -2 & 1 & 0 \\ m & m & m & 0 \\ 0 & 1 & -2 & 1 \\ m & m & m & m \\ 0 & 0 & 1 & -2 \\ 0 & 0 & m & m \end{bmatrix} \begin{bmatrix} u_1 \\ u_2 \\ u_3 \\ u_4 \end{bmatrix}
 \end{aligned} \tag{F.3}$$

where $d_i(t)$ are the inter-story drifts at the specified story and k , c and m are the stiffness, damping and mass of each story and $a_g(t)$ is the horizontal ground acceleration. The variables $u_i(t)$ represent the reaction of the friction damper/brace device connected between story i and story $i-1$. Note that the inherent damping of the structure in this case is proportional to the stiffness matrix.

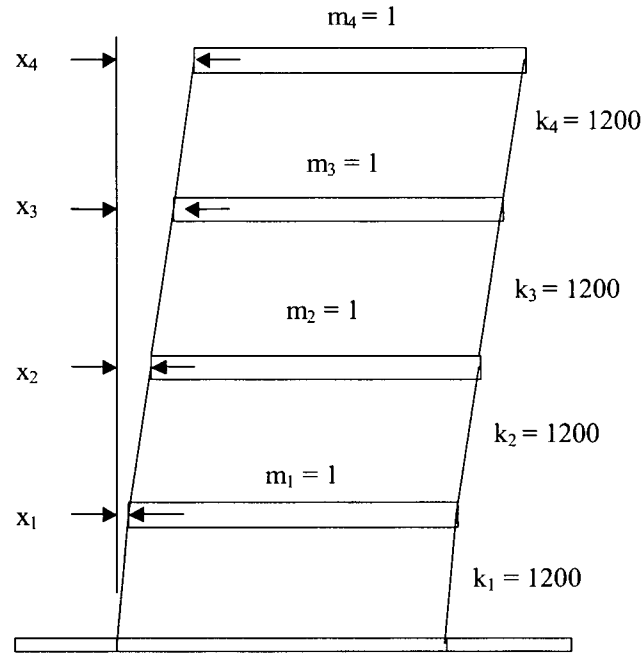


Figure F.1. 4-Story regular moment frame structure.

F.2.1 Coordinate Transformations

Coordinate transformations are useful to cast the dynamic problem in terms of variables that are meaningful. Instead of \hat{x} , say that it is preferable to express the equation of motion in terms of vector \hat{d} , representing inter-story drift, where the relationship between the two is given as

$$T\hat{d} = \hat{x} \quad (\text{F.4})$$

The matrix T is an appropriate square and invertible transformation matrix. The hats above the variables \hat{d} and \hat{x} are used to indicate that these are $n \times 1$ vectors representing displacements, rather than $2n \times 1$ vectors used to represent system states which include both displacements and velocities.

Applying the transformation to the variables in the usual second-order equation of motion yields the following equation:

$$MT\ddot{\hat{d}} + CT\dot{\hat{d}} + KT\hat{d} + Bu = -L\ddot{x}_g \quad (\text{F.5})$$

and the new system of equations is expressed in terms of the transformed system variables. In the above equation, symmetry is not preserved. To preserve symmetry, one may choose to pre-multiply by T^{-1} , yielding

$$T^{-1}MT\ddot{\hat{d}} + T^{-1}CT\dot{\hat{d}} + T^{-1}KT\hat{d} + T^{-1}Bu = -T^{-1}L\ddot{x}_g \quad (\text{F.6})$$

where $M^* = T^{-1}MT$, $C^* = T^{-1}CT$ and $K^* = T^{-1}KT$ can be used as new symmetrical mass, damping and stiffness matrices. Substituting the above in Equation F.6 yields the revised state-space equation

$$\begin{bmatrix} \dot{\hat{d}} \\ \dot{\hat{d}} \end{bmatrix} = \begin{bmatrix} 0 & I \\ -T^{-1}M^{-1}KT & -T^{-1}M^{-1}CT \end{bmatrix} \begin{bmatrix} \hat{d} \\ \dot{\hat{d}} \end{bmatrix} + \begin{bmatrix} 0 \\ -T^{-1}M^{-1}\tilde{B} \end{bmatrix} u + \begin{bmatrix} 0 \\ -T^{-1}\tilde{L} \end{bmatrix} \ddot{x}_g$$

or

$$\dot{d} = A^*d + B^*u + L^*\ddot{x}_g$$

where d represents the new transformed state variables.

Equation F.6 represents a shift in both the system variables and the forces used to evaluate the response. With the given structure choosing T as the lower triangular matrix

$$T = \begin{bmatrix} 1 & 0 & 0 & 0 \\ 1 & 1 & 0 & 0 \\ 1 & 1 & 1 & 0 \\ 1 & 1 & 1 & 1 \end{bmatrix} \quad (\text{F.8})$$

the transformation of Equation F.5 represents the transformation to inter-story drift. Rather than choosing to multiply by T^{-1} , which does not transform system forces into a natural form, the matrix T^T was used to put the equation of motion into story drift-shear form, yielding

$$T^TMT\ddot{\hat{d}} + T^TCT\dot{\hat{d}} + T^TKT\hat{d} + T^TBu = -T^TL\ddot{x}_g. \quad (\text{F.9})$$

The right hand term of Equation F.9 represents the shear force distribution under earthquake excitation. In expanded form the right hand term becomes

$$-T^TL\ddot{x}_g = \begin{bmatrix} 1 & 1 & 1 & 1 \\ 0 & 1 & 1 & 1 \\ 0 & 0 & 1 & 1 \\ 0 & 0 & 0 & 1 \end{bmatrix} \begin{bmatrix} 1 \\ 1 \\ 1 \\ 1 \end{bmatrix} \ddot{x}_g = \begin{bmatrix} 4 \\ 3 \\ 2 \\ 1 \end{bmatrix} \ddot{x}_g \quad (\text{F.10})$$

and the mass and stiffness matrices, respectively

$$T^T MT = \begin{bmatrix} 4m & 3m & 2m & m \\ 3m & 3m & 2m & m \\ 2m & 2m & 2m & m \\ m & m & m & m \end{bmatrix}, \quad (F.11)$$

$$T^T KT = \begin{bmatrix} k & 0 & 0 & 0 \\ 0 & k & 0 & 0 \\ 0 & 0 & k & 0 \\ 0 & 0 & 0 & k \end{bmatrix}$$

where $m = m_1 = m_2 = m_3 = m_4$ and $k = k_1 = k_2 = k_3 = k_4$.

F.2.2 Objective Functions

Two objective functions were used. The first, the total energy integral was defined as

$$O_E = \frac{1}{2} \int_{t=0}^{t_f} \left\{ \begin{bmatrix} d_1 & d_2 & d_3 & d_4 \end{bmatrix} \begin{bmatrix} k & 0 & 0 & 0 \\ 0 & k & 0 & 0 \\ 0 & 0 & k & 0 \\ 0 & 0 & 0 & k \end{bmatrix} \begin{bmatrix} d_1 \\ d_2 \\ d_3 \\ d_4 \end{bmatrix} \right. \quad (F.12)$$

$$\left. + \begin{bmatrix} \dot{d}_1 & \dot{d}_2 & \dot{d}_3 & \dot{d}_4 \end{bmatrix} \begin{bmatrix} 4m & 3m & 2m & m \\ 3m & 3m & 2m & m \\ 2m & 2m & 2m & m \\ m & m & m & m \end{bmatrix} \begin{bmatrix} \dot{d}_1 \\ \dot{d}_2 \\ \dot{d}_3 \\ \dot{d}_4 \end{bmatrix} + \begin{bmatrix} e_1 & e_2 & e_3 & e_4 \end{bmatrix} \begin{bmatrix} \alpha k & 0 & 0 & 0 \\ 0 & \alpha k & 0 & 0 \\ 0 & 0 & \alpha k & 0 \\ 0 & 0 & 0 & \alpha k \end{bmatrix} \begin{bmatrix} e_1 \\ e_2 \\ e_3 \\ e_4 \end{bmatrix} \right\} dt$$

and

$$O_{RMS(d)} = \max_i \left[\sqrt{\frac{1}{t_f} \int_{t=0}^{t_f} d_i^2 dt} \right], \quad i = 1, 2, 3, 4 \quad (F.13)$$

The total energy integral objective function corresponds most closely to the Strain-Energy-Area (SEA) performance function used by Filiatrault and Cherry (1990), and is equivalent to the Linear Quadratic performance index with the weighting matrix Q as defined in terms of story drift and shear, but excluding the R matrix term related to the control effort. It is reasonable to neglect R due to the fact that the slip loads u_c are not varied as a function of time.

The maximum story drift was chosen for its direct correspondence to the objective of reducing the displacements.

F.2.3 Excitation

Three excitations were considered

- impulse input – initial story drift velocity of 1 in all stories at $t=0$
- white-noise input – randomly sampled normally distributed base acceleration impulses having zero mean and standard deviation = 1.
- earthquake acceleration – two earthquakes were used, “El Centro” (May 18, 1940 Imperial Valley EQ, El Centro component N00E record) and “San Fernando” (Feb 9, 1971 Lake Hughes Array Station 12 component N21E record)

For the earthquake input, the ratio k/m was set equal to 1200 in order to produce a structure with its first mode frequency in a practical range. The unbraced natural period of the structure was 1.91Hz. With brace stiffness ratios of $\alpha = 1, 2, 3$ and 5, braced frequency ratios of the structure were 2.71, 3.32, 3.83 and 4.69 Hz respectively.

Earthquake time histories are plotted in Figures F.2(a) and (b) respectively for the El Centro and the San Fernando records. The normalized Trifunac and Brady integral [see Naeim, (1989)] is also plotted along with the 5% and 95% bounds delimiting the strong motion portion of the record. The input PSD functions for the strong motion portion of the El Centro and San Fernando input records obtained using a 1024 point FFT are shown in Figure F.3. The El Centro record is relatively smooth with a rounded peak occurring in the 1-2 Hz range, while the San-Fernando record has a comparatively sharp double peak occurring in the 4-5 Hz range. It should be noted that with a friction damped structure, the response will be governed by frequencies equal to and greater than the fundamental mode frequency. The fact that the San-Fernando record contains a significant amount of energy above the fundamental mode indicates that this record has more potential to excite higher modes than El Centro.

For impulse and White-noise input analyses, the mass and stiffness were assigned values of unity giving a structure with a fundamental period of about 18 sec. Simulations were comprised of 1000 time steps of 0.02 sec allowing for about 11 cycles of response at the fundamental period. Scaling the time period to correspond to the selected 1.91 Hz structure would indicate that the white noise would correspond to a strong-motion event with duration of about 7.8 seconds of strong motion. In contrast the strong motion duration portion of the El Centro record, calculated using the criterion of Trifunac and Brady was found to be 24 seconds while that for the San

Fernando record was found to be 10 seconds allowing for about 45 and 20 cycles of the fundamental mode respectively.

White noise input was generated using randomly generated points having zero mean and standard deviation of 1. A single time history was used following the reasoning that if the time-history was constantly re-sampled during the progress of the LSP algorithm the LSP sampling algorithm would begin to distil the input by rejecting a large proportion of otherwise valid time histories and in the end make conclusions based on a set of input time histories that do not themselves have characteristics representative of the input set.

Impulse input was defined as an initial story drift velocity of 1 at all stories. With this input, the upper mass would have an initial velocity of 4.

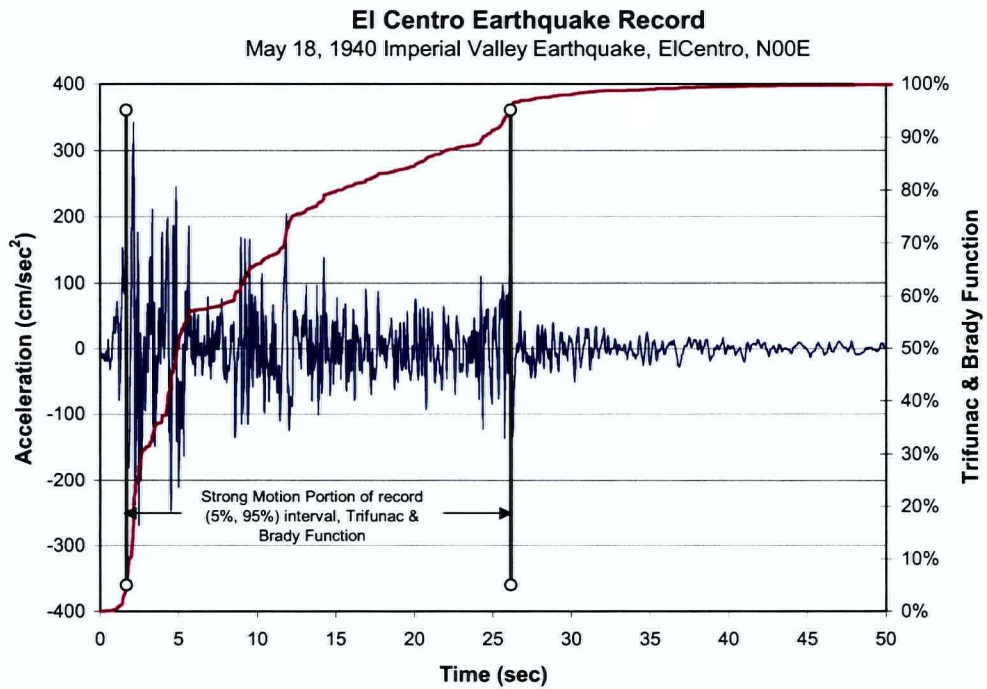
F.2.4 Modeling Considerations

The modelling procedure for the friction dampers follows that presented in Chapter 3. The structure was considered to remain elastic. Integration of the equations of motion was undertaken using a combination of a Runge-Kutta-Nystrom integration technique for a 2nd order system (structural response) and a Runge-Kutta method for a first order system (damper response) (see Kreyszig, 1983).

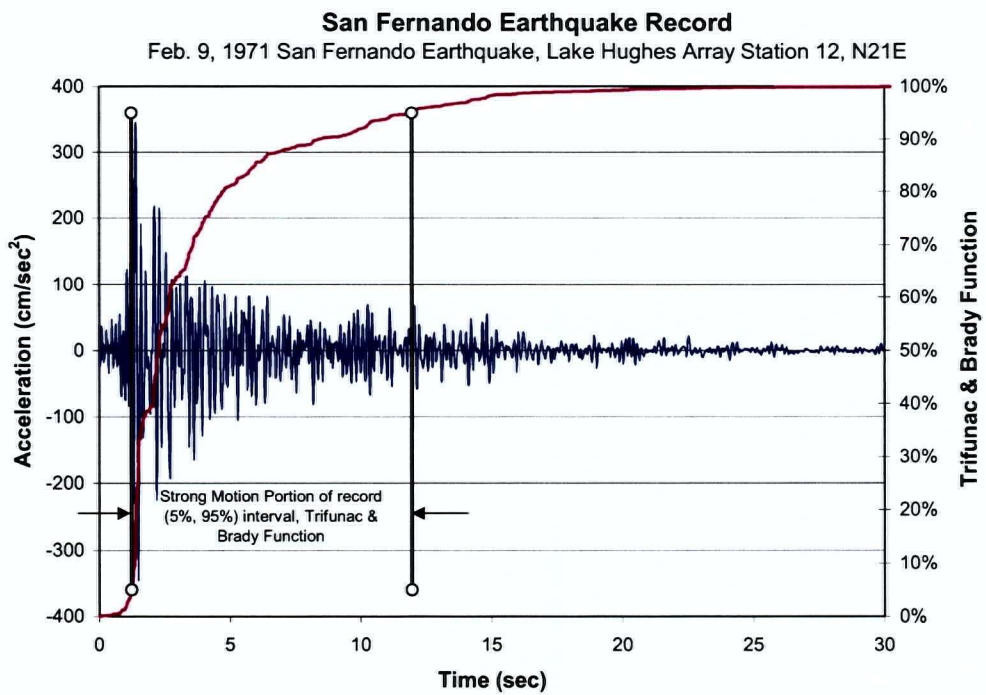
Because the LSP algorithm requires many evaluations of the objective function, each involving a full simulation of the response to a specified input time history, effort was made to streamline the computations. Recognising that it is not required to record the time history response but to simply evaluate the objective function computations were simplified by eliminating the processing involved with recording this data. Also recognising that the absolute value of the objective function is not important, the objective functions were modified as follows:

$$O_E = \sum_{q=1}^r \sum_{i=1}^n \left[kd_i + m \left(\sum_{j=1}^i \dot{d}_j \right)^2 + \alpha ke_i^2 \right], t = t_1, t_2, \dots, t_q, \dots, t_r \quad (\text{F.14})$$

where r indicates the number of time steps over which the response is computed and $t_r = t_f$ the final time step in the computed response.



(a)



(b)

Figure F.2. Earthquake input time histories with identified strong motion duration.

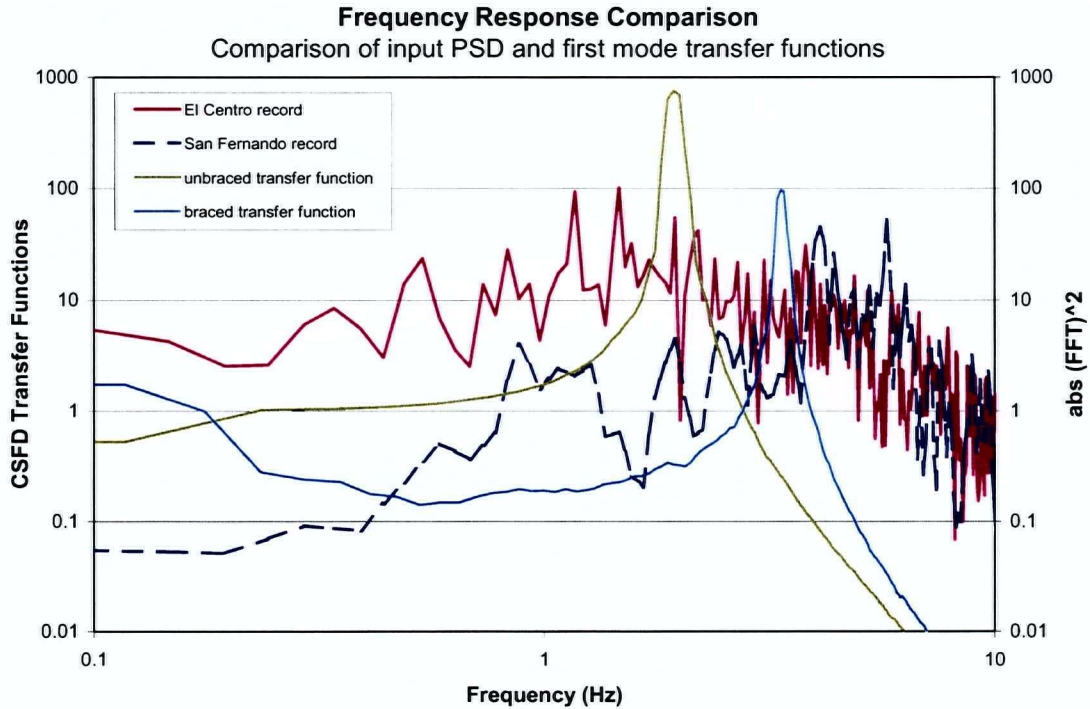


Figure F.3. Comparison of Power Spectral Density functions for the two input time histories. “El Centro” and “San Fernando”.

where the overall sum represents the sum of each time step in the time history and the sum over i represents the sum over each story. The RMS was reduced to the function

$$O_{RMS(d)} = \max_i \left[\sum_{q=1}^r [d_i(t_q)]^p \right], t = t_1, t_2, \dots, t_q, \dots, t_r \quad (F.15)$$

Because of the random nature of the parameter (slip load) selection algorithm, the results are in general not repeatable. Successive trial optimizations using the same deterministic input will not necessarily lead to the same conclusion.

F.2.5 Sample LSP Analysis

F.2.5.1 Example Using El Centro Input – Min RMS Drift

Using El Centro record ground motion input with $\alpha = 2$ as an example, the LSP process is illustrated. The objective function used in this example is the minimization of the maximum RMS displacement. Figure F.4 to Figure F.8 illustrate the evolution of the scatter plot of the retained points within the level set. In these figures the search space is illustrated as a set of 6 2-D projections on the surface of a 4-dimensional hyper-cube and labelled with the selected

variable. Labels at the left and top indicate the dimensions being viewed. One point in 4-dimensional space has 6 projections. Small crosses indicate the projections of the point that lead to the smallest value of the evaluated objective function. Figure F.4 illustrates the uniformly distributed scatter plot of the initial step. The points are randomly distributed within the indicated search range.

Figure F.5 shows the scatter plot of points within the level set after 6 iterations. Note that the density of points indicates locations where the minimum value is more likely to be found. In Figure F.6, particularly for variable $X(1)$ which represents the slip load at the first story, two groupings of points appear to be emerging. The minimum objective function appears in the set that is nearest to the upper limit, in this case nearly 8.0 kN/tonne of story weight. Note the unit structure has mass of 4 tonnes with 1 tonne mass on each of the 4 stories.

Figures F.7 and F.8 show the scatter plots after 13 and 17 iterations. In these plots it is clear that the lowest objective function has a minimum when $X(1)$ is likely above the selected maximum range of 8.0 and also indicates that of the groupings that emerged for the first story slip load, $X(1)$, the set near the upper limit clearly does not contain the absolute minimum. It was later shown that the absolute minimum had $X(1)$ approximately equal to 8.4.

Figure F.9 is a plot that indicates the progress of the iteration. The scale on the right represents the number of function evaluations performed starting with an the initial 120 function evaluations. A total of 3454 function evaluations were required. The scale on the left represents the value of the level set at each iteration. The initial level set was 0.228, but the minimum identified up to iteration 17 was 0.109, less than half of the initial level set. These two numbers indicate that the optimal friction dampers are capable of reducing the RMS drift by about a factor of 2. Looking back at the scatter plots indicates that at an RMS drift of approximately 0.14 about $\frac{3}{4}$ of the optimal performance was obtained after 6 iterations, and at about an RMS drift of 0.12, after 10 iterations the performance improvement was increased to better than $\frac{9}{10}$ of optimal. If these lesser performance improvements provide acceptable performance, the acceptable range of slip force is really quite broad. This is consistent with the relatively flat drift versus slip load curve obtained for the SDOF system.

Clearly, the results obtained in this case show that the distribution of slip load is quite important with a relatively high slip load of 8.4kN/tonne obtained for the lower story to a slip load of 0.5kN/tonne at the top story yielding the optimal performance.

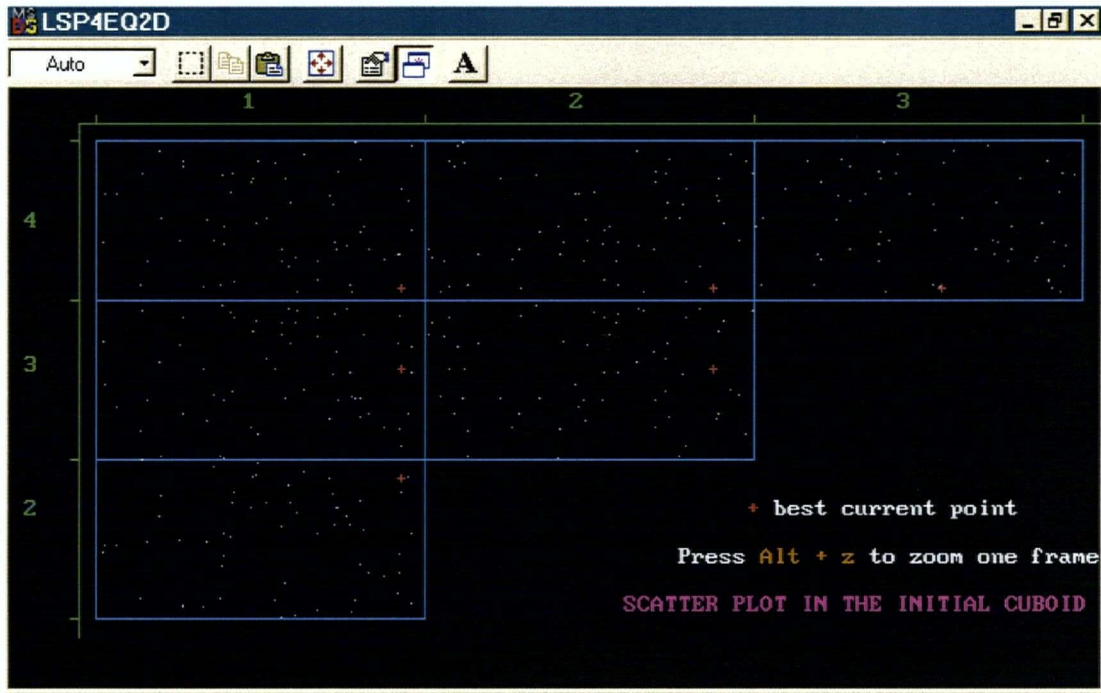


Figure F.4. LSP Initial Distribution Scatter Plot – El Centro record, Objective Function: $\max \text{RMS}(d_i)$.

Initial search space:

- $x(1) - (0, 8)$
- $x(2) - (0, 7)$
- $x(3) - (0, 6)$
- $x(4) - (0, 5)$

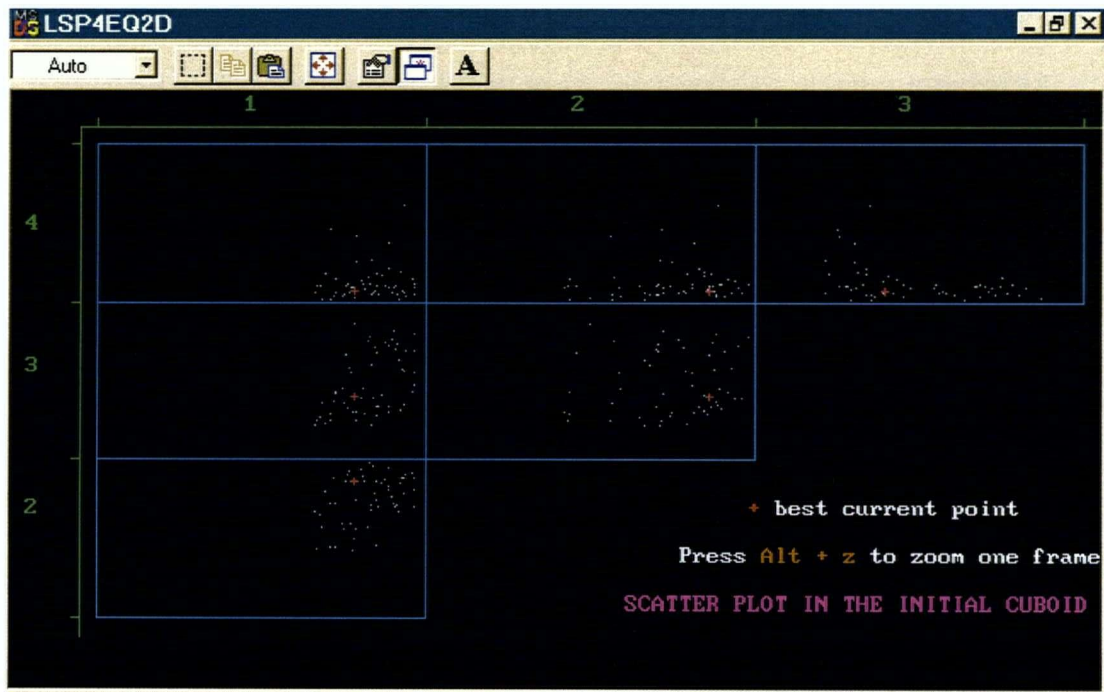


Figure F.5. LSP Iteration 6 – note that the search space is beginning to be reduced substantially.

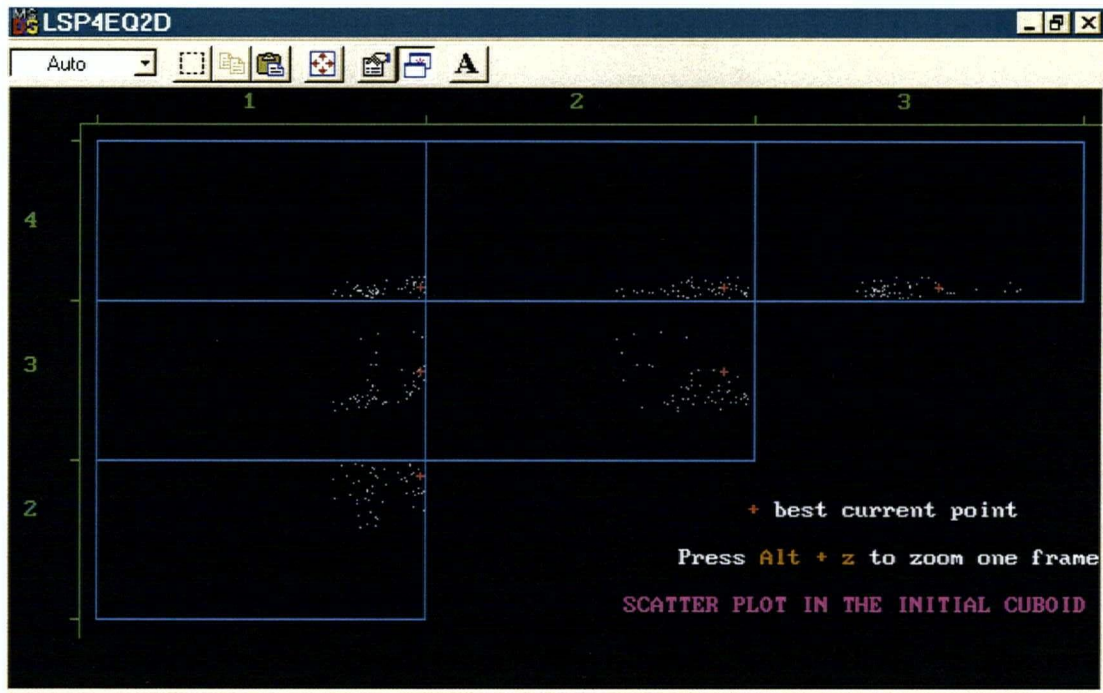


Figure F.6. LSP Iteration 8 – note the appearance of two distinct blobs of data points with different strengths of first-story slip load. The objective of this run was to try to separate them but it appears that the group of points has the lower minimum.

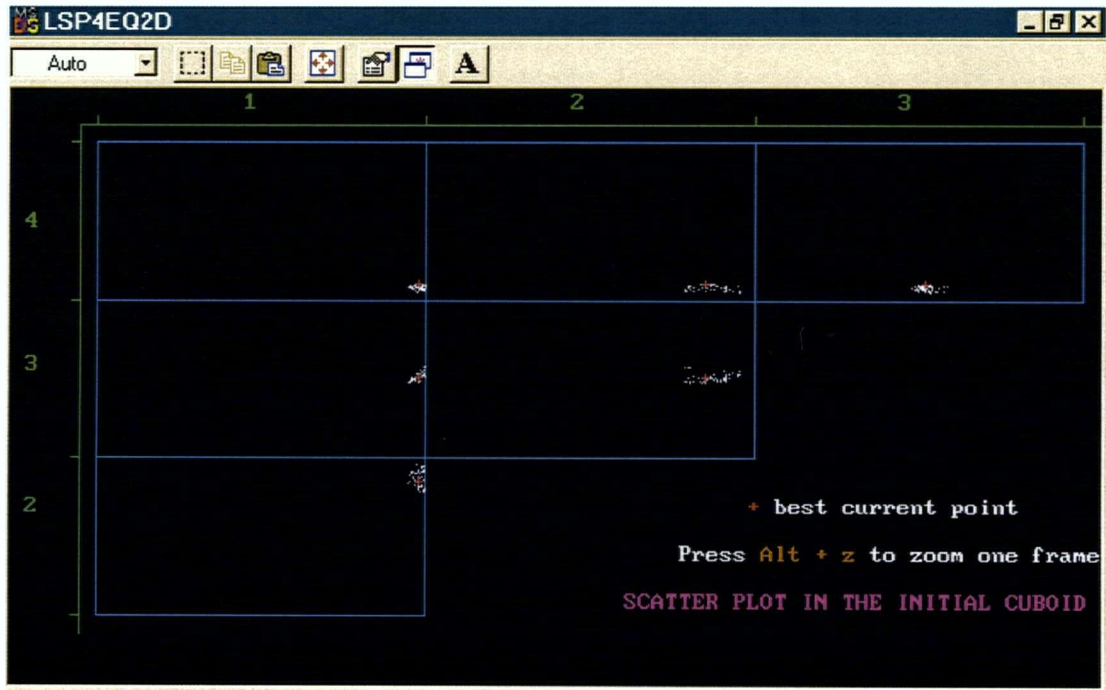


Figure F.7. LSP Iteration 13

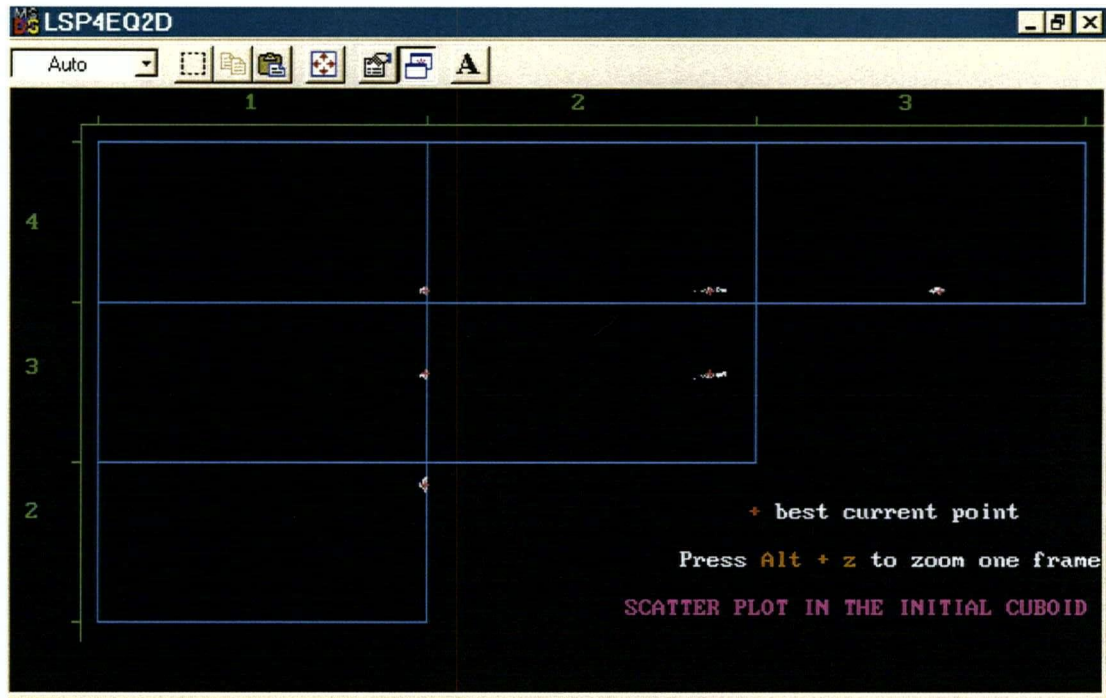


Figure F.8. Convergence – LSP Iteration 17

Note that the crowding of the points against the upper limit of the global search range for $x(1)$ indicated that the global minimum would be found for $x(1) > 8\text{kN/tonne}$

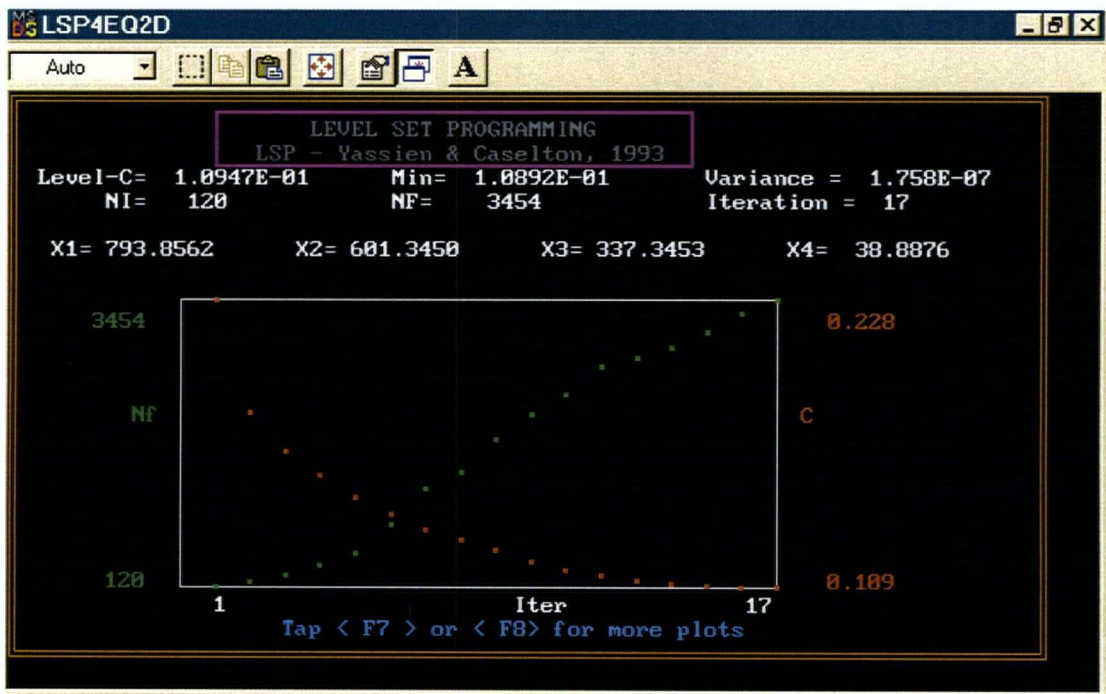


Figure F.9. Optimization progress to iteration 17: Note that output indicates the current optimal slip loads multiplied by a factor of 100. Note that 3454 function evaluations were required in total to this point.

F.2.6 LSP Results

The LSP algorithm was carried out on the indicated load cases using both objective functions where applicable. Where the distributions of points in the scatter plots indicated the likelihood of multiple local minima, the search ranges were refined such that the distribution for each could be obtained.

F.2.6.1 Impulse

Figures F.10 to F.14 show the distributions of slip load obtained for impulse input. Because the RMS drift objective function carries little meaning in this case, only the minimum total energy function was evaluated.

Results for $\alpha=1$ are plotted in Figure F.10. Two local minima were obtained with quite different distributions. The first obtained had the lowest slip load at the base story and the highest at the second while the second point cluster converged to an optimal distribution with a high slip load at the first story and the smallest at the third story.

Results for $\alpha=2$ are plotted in Figure F.11. In this case three clusters were found with nearly identical slip load in the upper stories, again with the overall minimum appearing in the third story. Two clusters shared the same value for the slip load in the bottom story but showed markedly different slip loads in the second story. The remaining set of slip loads had a higher slip load in the first story, but a second story slip load nearest to the lower value.

For $\alpha=3$, results obtained for three identified clusters are plotted in Figure F.12. These results show less agreement, particularly in the upper story where the identified optimal slip loads differ by almost an order of magnitude.

For $\alpha=5$, plotted in Figure F.13, three clusters were also identified, each having nearly identical slip load distribution on the first and fourth stories, but a wide variation on the slip loads at the second and third stories.

The first obtained distribution for each brace stiffness ratio, α , is plotted in Figure F.14. These results indicate that the optimal slip loads generally increase as the brace stiffness ratio increases and that the slip loads in the lower stories are likely to be higher than those in the upper stories, but the overall character does not provide a consistent trend.

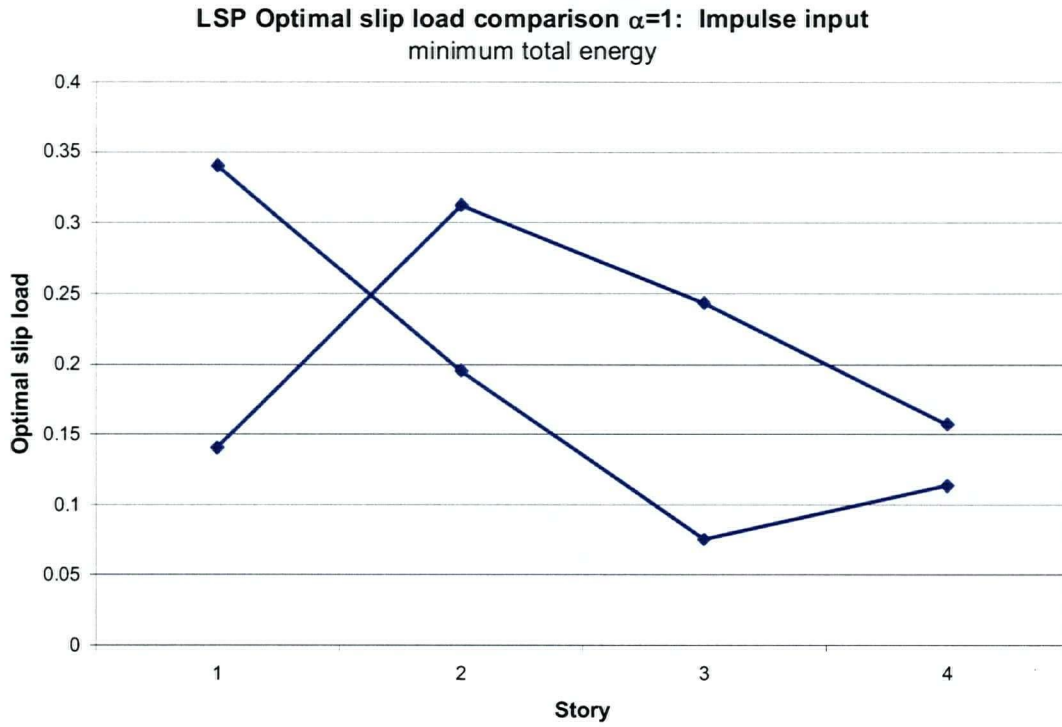


Figure F.10. LSP optimal slip load – Impulse input – minimum total energy, $\alpha=1$.

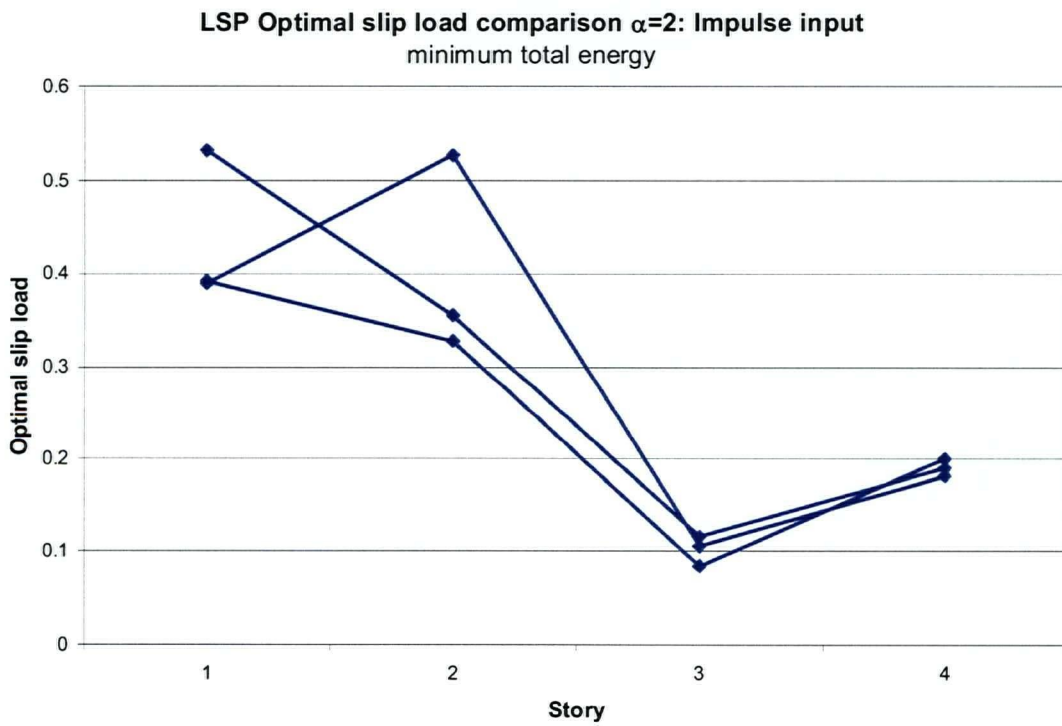


Figure F.11. LSP optimal slip load – Impulse input – minimum total energy, $\alpha=2$.

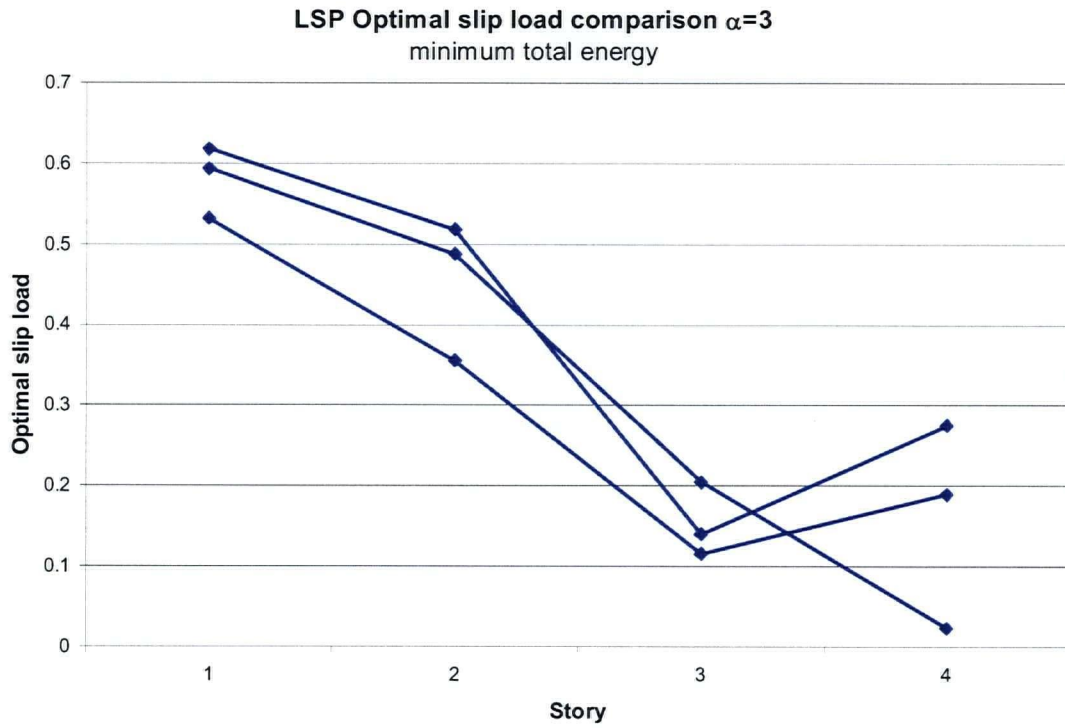


Figure F.12. LSP optimal slip load – Impulse input – minimum total energy, $\alpha=3$.

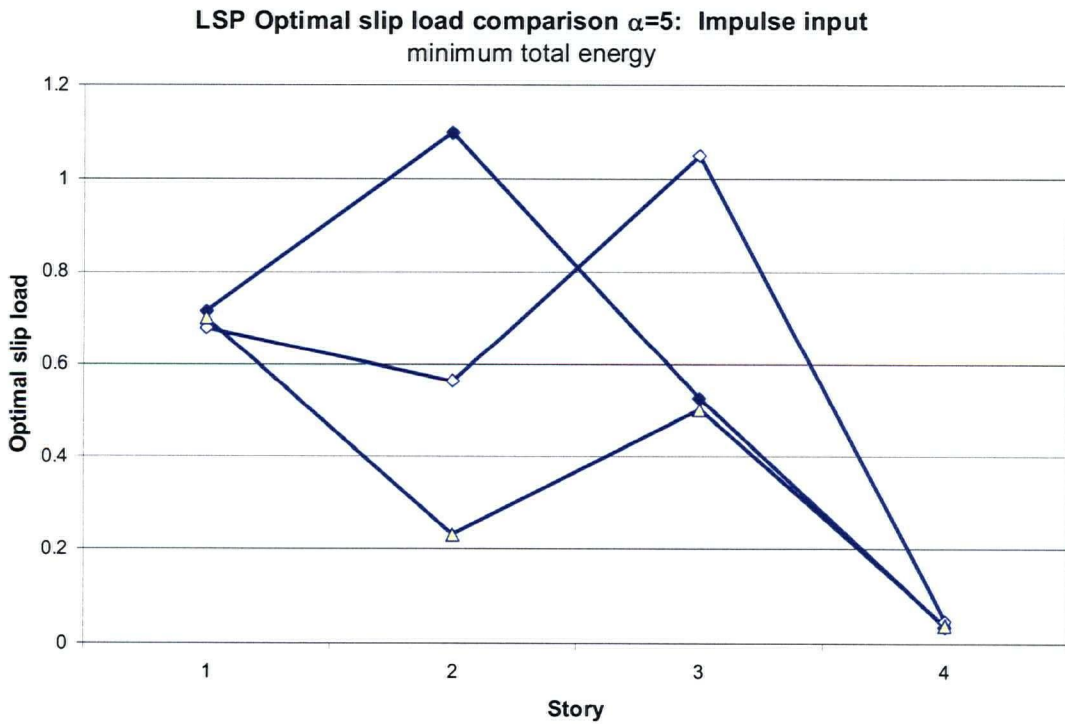


Figure F.13. LSP optimal slip load – Impulse input – minimum total energy, $\alpha=5$.

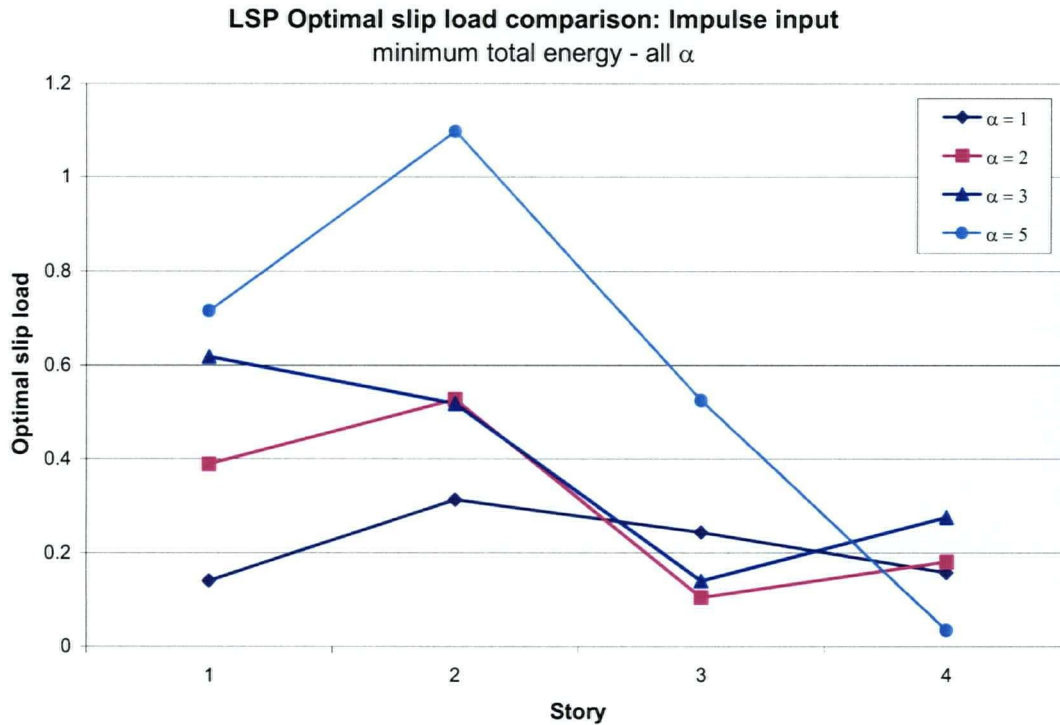


Figure F.14. LSP optimal slip load – impulse input – minimum total energy, comparison of all α .

F.2.6.2 White Noise

Figures F.15 through F.20 deal with the results obtained for white noise input. Figures F.15 to F.19 show the results obtained for increasing brace stiffness ratio for both of the minimum total energy and the minimum RMS drift objective functions. Minimum total energy results are plotted with a solid line while minimum RMS drift results are shown with a dashed line. Unlike the distributions obtained for the impulse functions, the results obtained for white noise input appear to be far more consistent with $\alpha=2$ being the only brace stiffness ratio for which multiple distributions were obtained.

In each case, distributions obtained for the minimum total energy objective function were found to vary over a smaller range than for the min RMS drift objective function, as evidenced by the appearance of a lesser average slope of the solid lines linking the slip load obtained for each story than for the dashed lines.

Figure F.19 compares the optimal slip loads obtained for the minimum total energy objective function with varying brace stiffness ratio. The results obtained indicate that the optimal slip

loads are much higher at the base story than at the top and vary in a nearly linear manner. It is curious that the results for $\alpha=2, 3$ and 5 are grouped apart from the results obtained for $\alpha=1$.

The results obtained using the min RMS drift objective function show a similar trend. While similar levels of slip load were observed for all α in the top story, ranging up to 0.9kN , the resulting optimal slip loads at 3.7 kN in the first story for min RMS drift was more than double the 1.6 kN obtained for the minimum total energy objective function at $\alpha=5$. Neglecting the second set of slip loads obtained for $\alpha=2$, the slip loads obtained for the min RMS story drift objective function for $\alpha=1, 2$ and 3 appear to be grouped while the results obtained for $\alpha=5$ are separated. The results obtained do not appear to have a definite shape and could be said to vary approximately linearly from the base to the top.

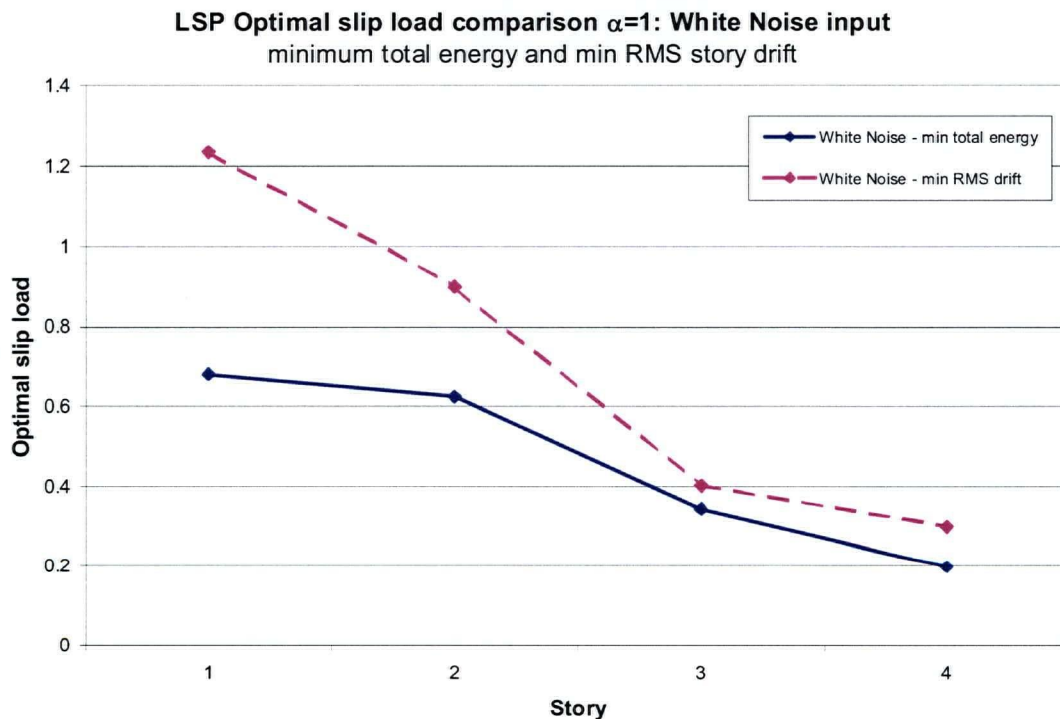


Figure F.15. LSP optimal slip load – white noise input – minimum energy, minimum RMS drift, $\alpha=1$.

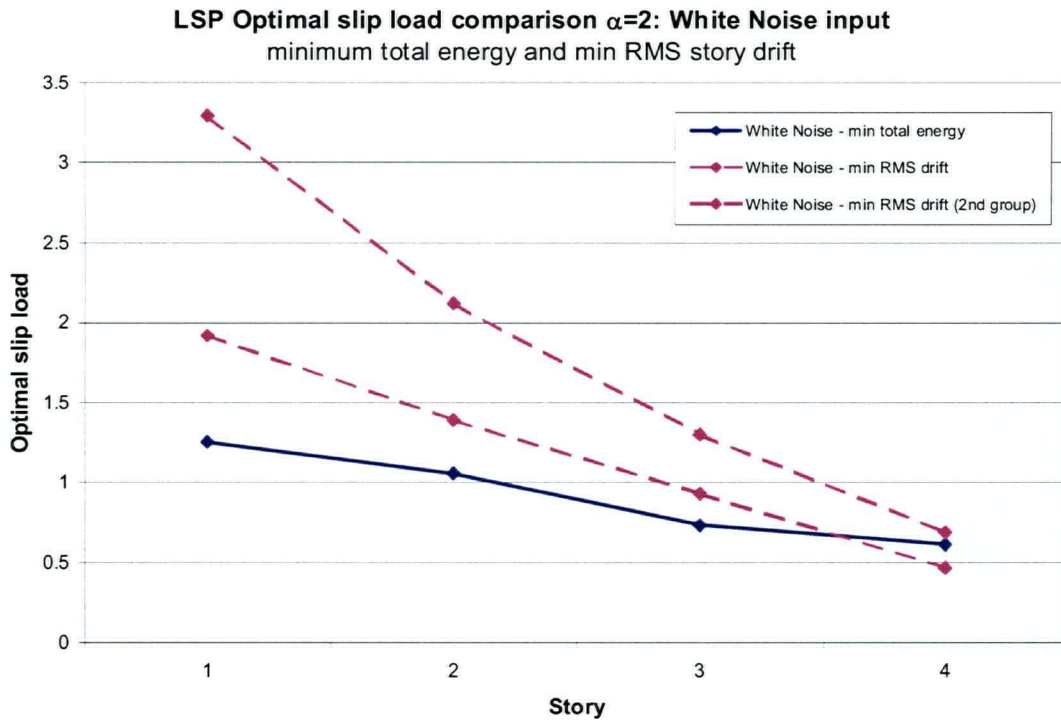


Figure F.16. LSP optimal slip load – white noise input – minimum energy, minimum RMS drift, $\alpha=2$.

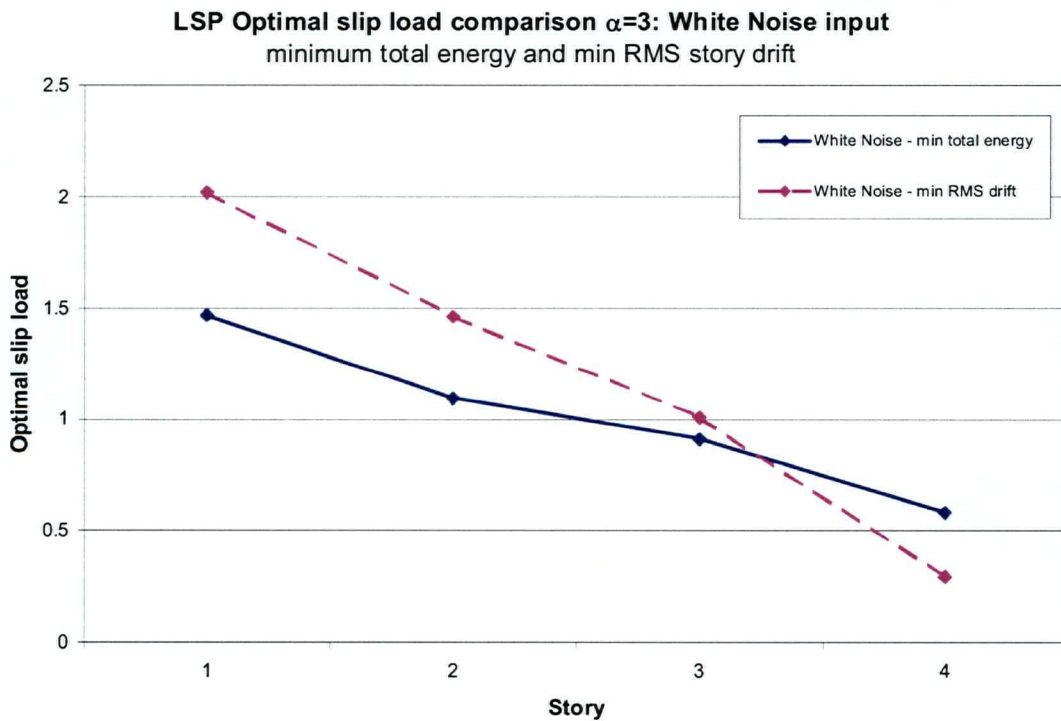


Figure F.17. LSP optimal slip load – white noise input – minimum energy, minimum RMS drift, $\alpha=3$.

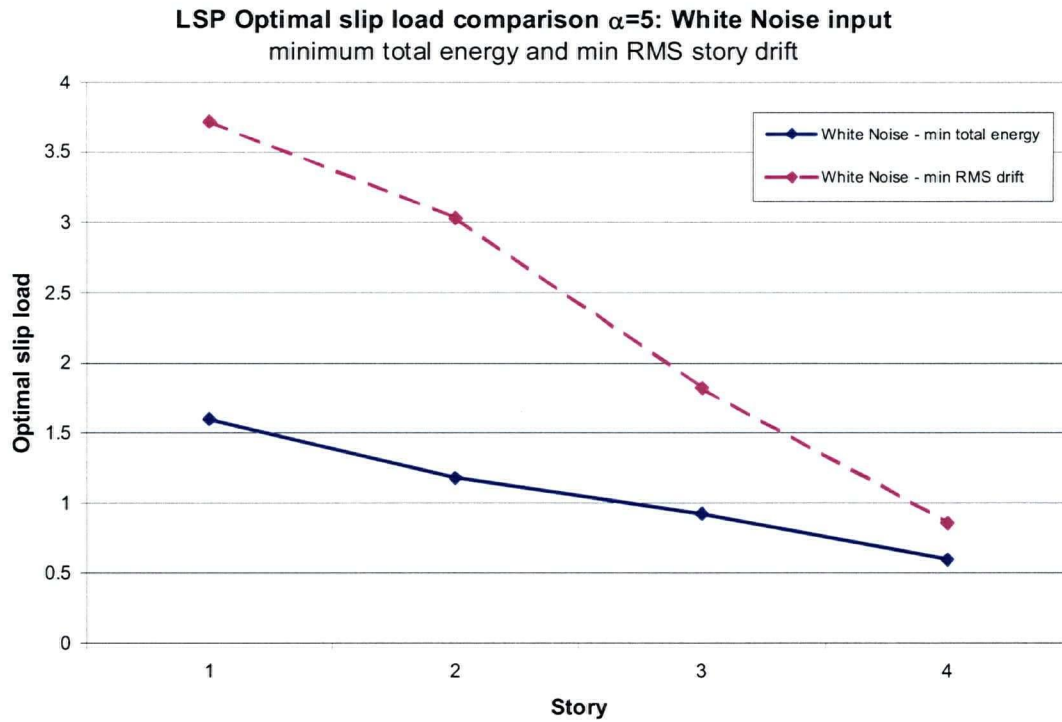


Figure F.18. LSP optimal slip load – white noise input – minimum energy, minimum RMS drift, $\alpha=5$.

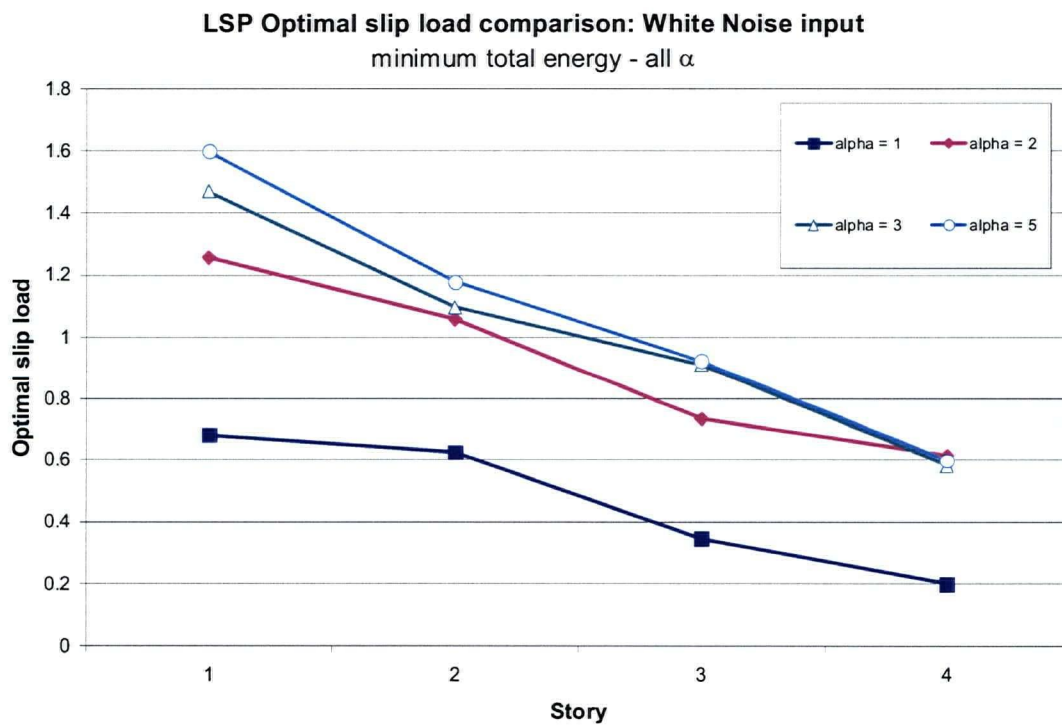


Figure F.19. LSP optimal slip load – white noise input – minimum energy – compare all α .

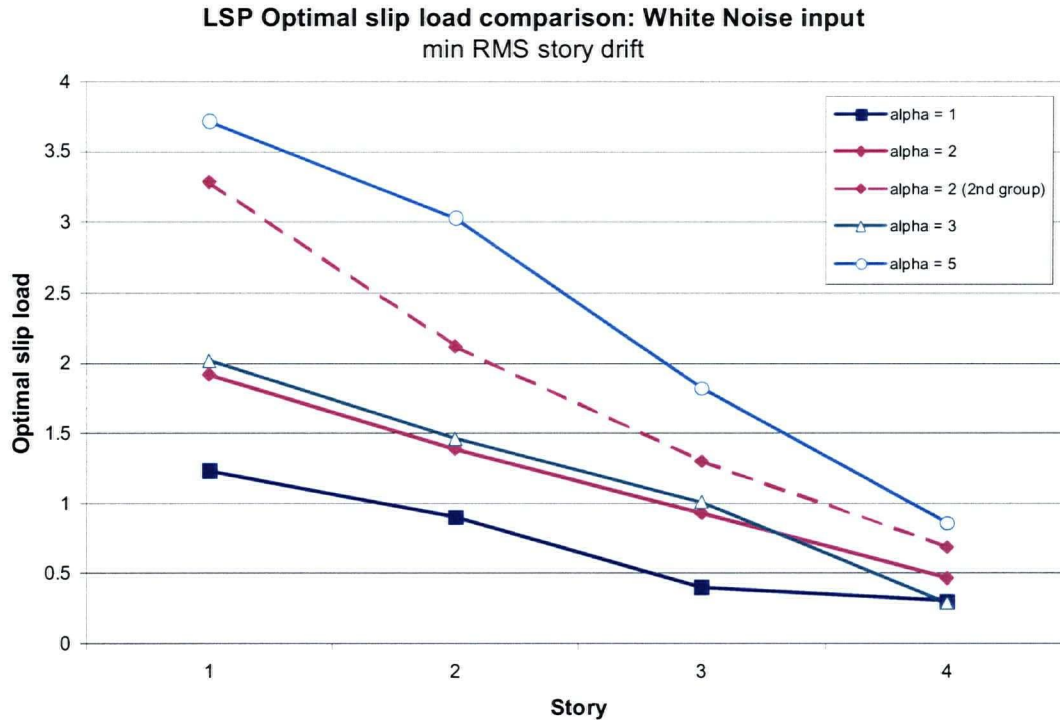


Figure F.20. LSP optimal slip load – white noise input – minimum RMS drift – compare all α .

F.2.6.3 Earthquake

Figure F.21 to F.24 compare the results obtained with earthquake input. As with the white noise input, minimum total energy objective function results are illustrated with solid lines while the obtained min RMS drift objective function results are plotted with dashed lines. El Centro results are plotted with solid diamond markers while results obtained with San Fernando record input are plotted with hollow triangular markers. The optimal slip loads are expressed in terms of kN/tonne of story mass. The total weight of the structure is about 39kN therefore the maximum slip load observed was just over 20% of the total weight of the structure.

For $\alpha = 1$, it is observed that the optimal slip loads for the El Centro input record are significantly higher than the corresponding slip loads for the San Fernando input. As found with the impulse and the white-noise input, the slip loads corresponding to the min RMD drift objective function are significantly higher than for the corresponding minimum total energy and on average show less variation from the base to the top. And, similar to the results obtained for the impulse loading with higher α , the results obtained for the San Fernando input and the

minimum total energy objective function appears to show a great variability. Often the slip load obtained at the fourth story turned out to be greater than the slip load at the third.

Results obtained for $\alpha=2$ did not indicate the existence of clusters, therefore a single set of slip loads was obtained for each objective function and earthquake input combination. The results appear to be typical of the type of results with the highest slip loads corresponding to the min RMS drift objective function; and a somewhat flatter average distribution evidenced with the minimum total energy objective function.

The results obtained for $\alpha = 3$ and $\alpha = 5$ in Figures F.23 and F.24 respectively appear to have much less distinction between the results obtained for the two objective functions, particularly with the El Centro record input whose slip loads appear to follow the same trend. With the San Fernando input the slip loads for the two objective functions follow the typical trend with the min RMS drift objective function yielding somewhat higher slip loads.

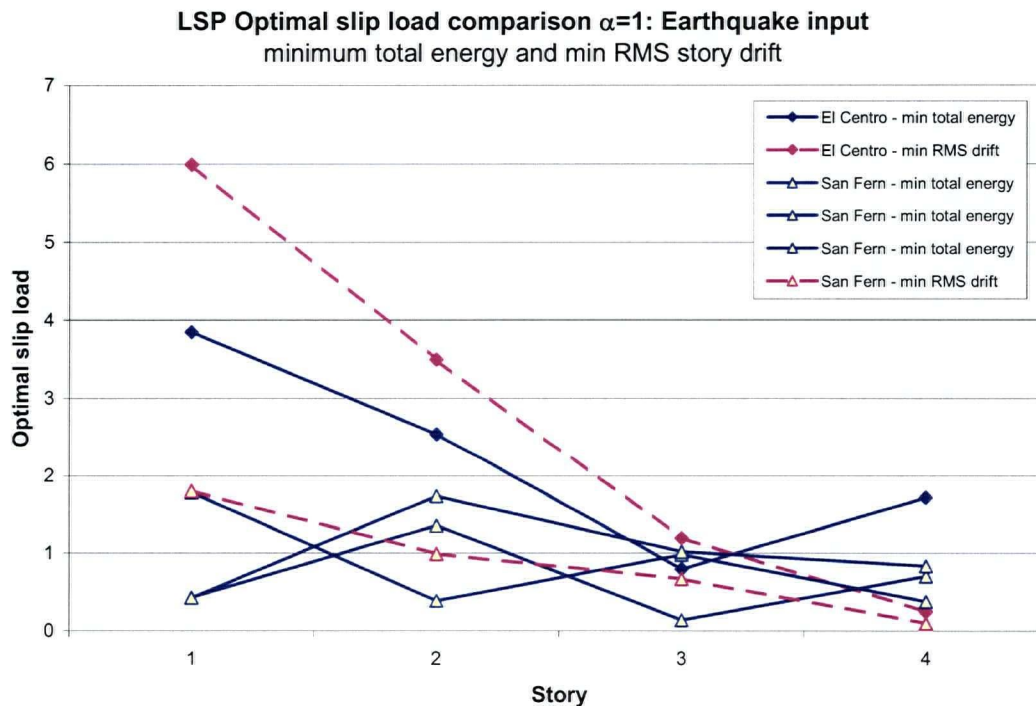


Figure F.21. LSP optimal slip load comparison – earthquake input – min energy, min drift, $\alpha=1$.

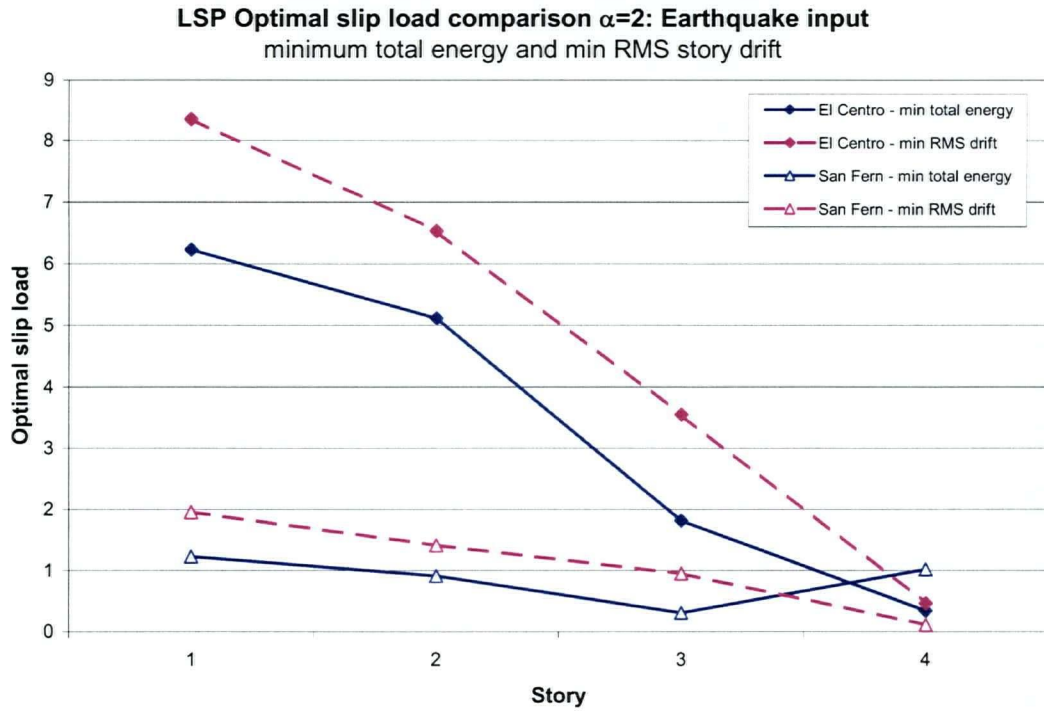


Figure F.22. LSP optimal slip load comparison – earthquake input – min energy, min drift, $\alpha=2$.

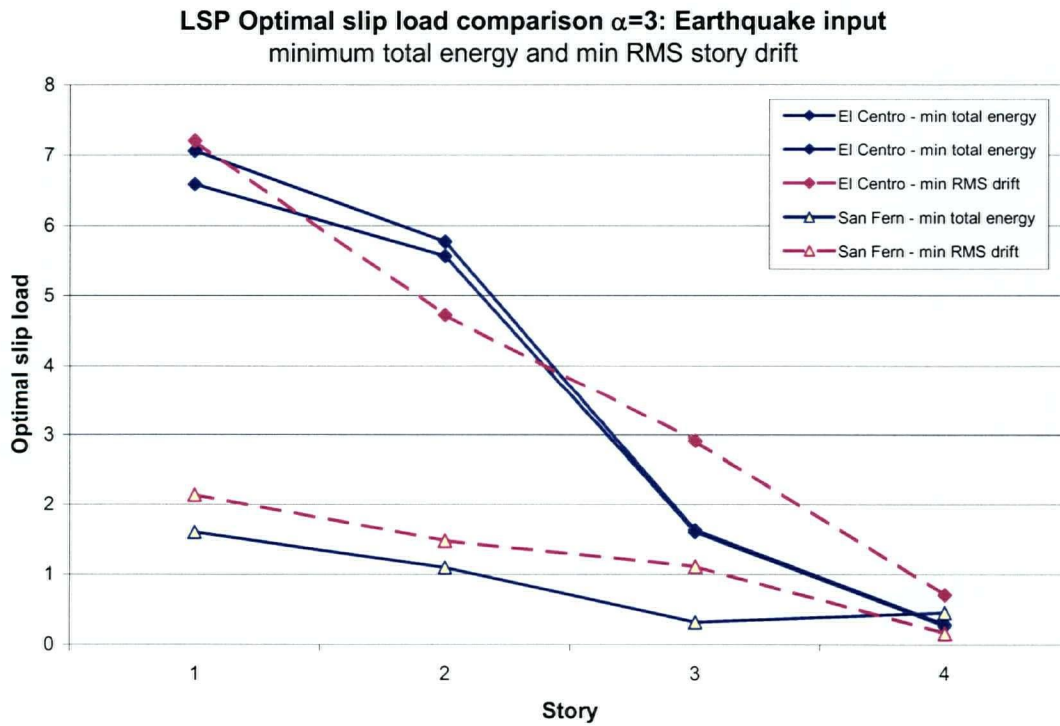


Figure F.23. LSP optimal slip load comparison – earthquake input – min energy, min drift, $\alpha=3$.

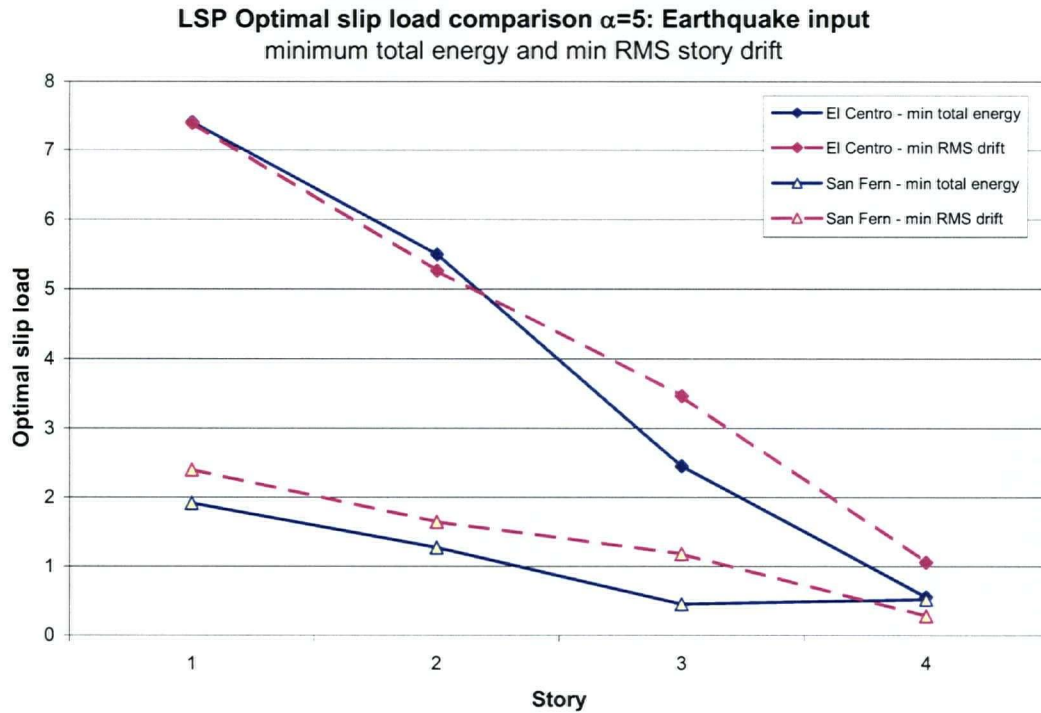


Figure F.24. LSP optimal slip load comparison – earthquake input – min energy, min drift, $\alpha=5$.

F.2.7 Note on Off-On Damped Structures

The LSP procedure was applied to off-on friction damped structures and the following general observations are made. The case with $\alpha = 1$, objective function minimum total energy and input excitation the El Centro record was run. Using an initial search space of $x(1)$ - $x(4)=(0,10)$ the following scatter plot, Figure F.25, was obtained after 8 iterations.

Compared to the scatter plot in Figure F.6, the scatter plot at 8 iterations is distributed over a wider area. This is an indication that the objective function has become quite flat for higher levels of slip load, as recognized with the analysis of the SDOF structure in the previous chapter. The number of function evaluations required to achieve this level set was 2490, significantly more than the approximately 1410 required for 8 iterations of the previous example. Note that the underlying assumption here is that the performance improvement is related to the number of iterations regardless of the objective function.

The slip loads cannot be directly compared to the off-on case because of the flatness of the objective function. The following table compares the results found previously with the ranges determined up to the 8th iteration. The results indicate that the off-on friction damped semi-

active system provides a substantial improvement in the performance of the structure. The slip loads at the lower end of the slip range indicate the minimum values necessary to achieve the given level of performance. These values are more than double the slip loads obtained for the constant slip force friction dampers. This indicates that the off-on semi-active control algorithm is capable of improving the performance of the structure with a given brace stiffness ratio when compared to its CSFD counterpart. However that improvement comes at the price of providing force capacity.

Whereas high slip loads impede the performance of the CSFD, the same is not true for the off-on controller. Similar to the single degree of freedom system, this property enables the structural system to perform optimally for excitations of lesser magnitude than used for the design.

The CSFD will lose its optimality for lesser events. On the other hand, the response for a smaller excitation (assuming similar frequency characteristics) will be smaller, therefore if the objective is simply to protect against large response (accelerations or deflections) as is expected to be the most common case, the lessening of the excitation coupled with the relative insensitivity of the response to the magnitude of the slip loads in the optimal range makes optimal performance unnecessary.

Table F.1. Comparison of the performance of the off-on friction damper controlled structure.

Story	CSFD – Optimal Slip Load after 17 iterations	Off-on Friction Damped Structure Slip Load Range at 8 Iterations at
	$L_{\min}=17.9e3$ (kN/tonne)	$L_{\min}=6.32e3$ (kN/tonne)
1	3.9	$8.1 - 10^*$ (8.5)
2	2.5	$5.6 - 10^*$ (9.7)
3	0.8	$2.8 - 8.2^*$ (5.1)
4	1.7	$0^* - 9.1$ (1.0)

Comparison after 8 iterations using the LSP algorithm with optimal CSFD obtained by carrying the LSP algorithm to completion. The modeled structure is the 4-story uniform structure having $\alpha=1$. The minimum total energy objective function was used. L_{\min} represents the value of the objective function for the slip loads indicated in brackets.

Semi-active control implemented with the off-on controller was found to require significantly higher slip loads to achieve its optimal performance than the optimal CSFD. It was also observed that the performance of the off-on system is relatively insensitive to the precise value

of the slip load, providing the minimum is exceeded. The optimal performance achieved by the off-on system is also superior to the CSFD when measured by the total energy objective function. The chart in Figure F.26 compares the values of the minimum total energy objective functions obtained for various values of brace stiffness ratios with that for the off-on control case. It can be seen on this graph that the off-on semi-active control has the ability to extend the performance significantly such that the performance level obtained was more characteristic of a higher brace stiffness ratio, in this case $\alpha = 3$. This is important as it emphasizes that if the structure that requires retrofit is configured in such a way that a sufficiently high stiffness cannot be provided, the semi-active control algorithm could provide a significant enhancement of the performance.

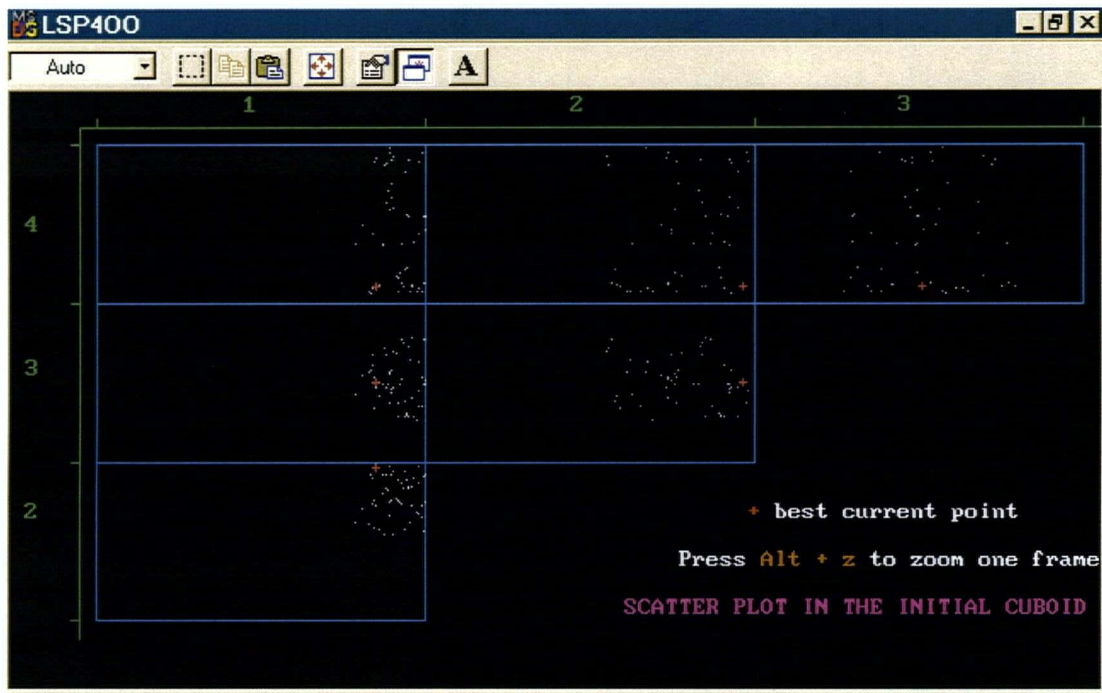


Figure F.25. LSP Scatter plot $\alpha=1$, minimum total energy, El Centro record input. Scatter plot after 8 iterations in initial search space with $x(1)=x(2)=x(3)=x(4)=(0,10)$. Compared to Figure F.8 at 8 iterations, the scatter plot is spread over a wide area. An explanation for this is that the objective function becomes relatively flat and this does not permit the narrowing of the search space and forces the algorithm to undertake a greater number of function evaluations to fill the level set. The total number of function evaluations taken to reach this point was 2490, somewhat higher than that observed in the previous case. The indicated slip loads are much higher than those shown in Figure F.23, indicating that with the off-on algorithm it is best to provide as high a slip load as possible.

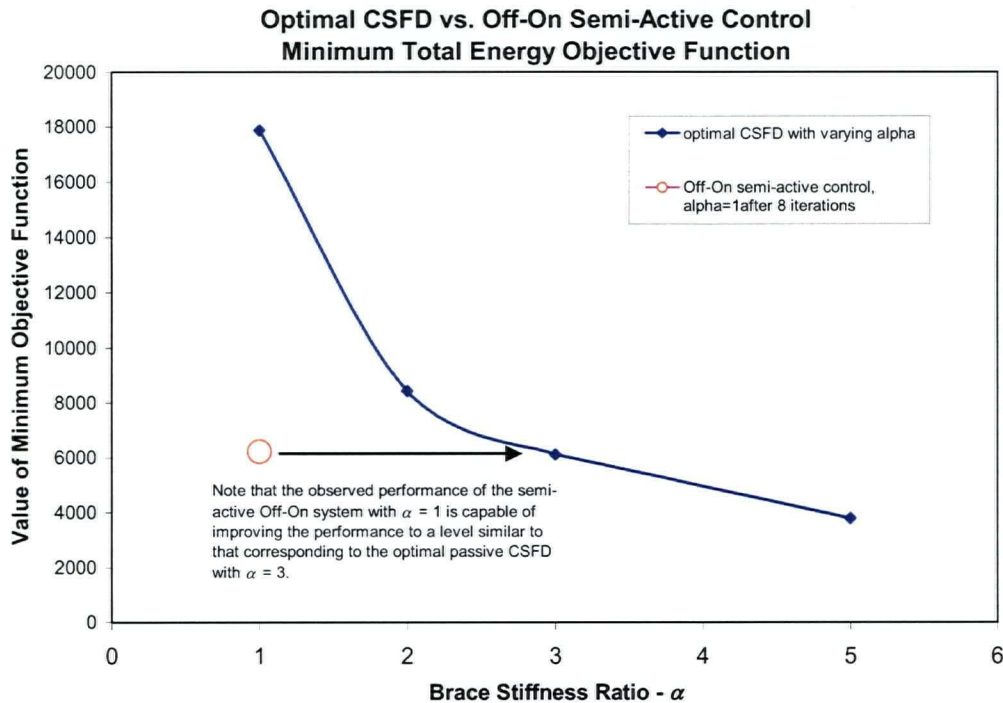


Figure F.26. Comparison of CSFD minimum level set with 8 iterations off-on level set, $\alpha=1$.

F.2.8 General Observations and Implication to Designers

It was generally observed that, in some of the cases cluster of points with nearly identical L_{\min} would emerge. This was most often observed with san Fernando earthquake and white noise input and brace stiffness ratios of $\alpha = 1$ or 2. Variability was also observed for impulse input with all brace stiffnesses. This observation highlights the fact that the objective function defines a rough surface that often leads to several “optimal” distributions. The optimal slip load distribution is not unique, but dependent on the character of the excitation, and the selected objective function. The implication for the designer in designing against earthquake loads is that some understanding of the character of the input excitation for which the structure is to be designed and it’s relationship to that of any particular excitation used to evaluate the design is important.

The PSD of the San Fernando earthquake, Figure F.3, indicates that a significant level of input occurs above the fundamental natural frequency. It is expected that excitation in these frequencies would tend to excite higher modes, and the contribution of these higher modes could be responsible for contributing to the roughness of the objective function.

The off-on semi-active viscous damper was shown to have a positive effect on the control of the 4-story structure but at the expense of significantly higher slip loads. This is consistent with the observations of Dowdell and Cherry (1994a). It is reasonable to expect that the cost of a control system is reduced if the brace stiffness and control force are lower. This supports the conclusion that the value of the semi-active systems in MDOF structures is questionable.